Quantifying the London Specific Component of PM_{10} Oxidative Activity

Prepared for the Department for Environment, Food and Rural Affairs (Defra), the Scottish Executive, the Welsh Assembly Government and the DoE in Northern Ireland

November 2009

Ian S Mudway, Gary Fuller, David Green, Chrissi Dunster and Frank J Kelly

Lung Biology: The Environmental Research Group

MRC-HPA Centre for Environment and Health

King's College London

Title	Quantifying the London Specific Component of PM_{10} Oxidative Activity

Customer	The Department for Environment, Food and Rural Affairs (Defra), the Scottish Executive, the Welsh Assembly Government and the DoE in Northern Ireland

Customer Ref	

File Reference	LUNGBIOLOGY/STUDIES/DEFRA/VCMOP/ COMPARISON OF METHODS FOR THE DETERMINATION OF PARTICULATE OXIDATIVE ACTIVITY.DOC

Report Number	KCLERG/ISM/OPMETHOD/DEFRA1

Lung Biology, Environmental Research Group
MRC-HPA Centre for Environment and Health
King's College London
Franklin-Wilkins Building
150 Stamford St
London SE1 9NH
Tel 020 7848 3895

	Name	Signature	Date
Author	Ian Mudway		November 2009

Reviewed by	Frank J Kelly		November 2009

Approved by	Frank Kelly		November 2009

Table of Contents

Blank page

Glossary

RTLF	Respiratory tract lining fluid
AA	Ascorbate
UA	Urate
GSH	Glutathione (reduced)
GSx	Total glutathione
GSSG	Glutathione disulphide
DTT	Dithiothreitol
DTNB	5,5'-dithiobis-2-nitrobenzoic acid
DTPA	Diethylene triamine pentaacetic acid
OP	oxidative potential
$OP^{AA}/\mu g$	Ascorbate dependant oxidative potential per unit mass
OP^{AA}/m^3	Ascorbate dependent oxidative potential per m^3 sample air
$OP^{GSH}/\mu g$	Ascorbate dependant oxidative potential per unit mass
OP^{GSH}/m^3	Ascorbate dependent oxidative potential per m^3 sample air
H_2O_2	Hydrogen peroxide
$O_2^{\cdot -}$	Superoxide
$^{\cdot}OH$	Hydroxyl radical
EPR	electron paramagnetic resonance
DMPO	5,5-dimethylpyrroline-N-oxide
ICP-MS	Inductively Coupled Plasma Mass Spectroscopy
HPLC-EC	High Pressure Liquid Chromatography with Electrochemical Detection
ROS	Reactive Oxygen Species
RNS	Reactive Nitrogen Species
NFκB	Nuclear Factor kappa B

Study context

The work outlined in this report was performed as part of the King's College London contract "Volatile Correction Model and Oxidative Potential Measurements". This programme is part of DEFRA's "Particle Numbers and Concentration" contract, managed by the National Physical Laboratory.

Overview

Epidemiological studies have consistently demonstrated associations between the mass concentration of ambient particulate matter (PM) and negative impacts on cardio-respiratory health (*Brunekreef and Holgate 2002*). Whilst this observation is consistent across numerous studies, considerable heterogeneity in the PM effect size estimate exists in the literature, even where data sets have been analysed using identical methods (*Bell et al. 2004; Janssen et al. 2002; Katsouyanni et al. 2001; Samet et al. 2000; Zanobetti et al. 2002*). Apart from random variation and differences across study populations, such discrepancies have been argued to reflect the use of imperfect indicators of exposure. Whilst the majority of epidemiological studies make use of ambient PM mass concentration, this measurement ignores PM sources and constituents, and, therefore the biological activity of particles. From a toxicological perspective much of the mass of PM_{10} consists of biologically inert material: sodium chloride, crustal dust, ammonium sulphates and nitrates etc, whilst, the content of relatively low masses of transition metals and organic species are likely to contribute significantly to the health effects reported in the literature. It has therefore been proposed that alternative, more health relevant PM metrics are required.

There is growing scientific consensus that the capacity of inhaled PM to elicit oxidative stress at the air-lung interface may underpin many of the acute and chronic symptoms observed in populations exposed to elevated PM concentrations *(Borm et al 2007; Gilliland et al 1999; Li et al 2002; Kelly 2003; Li et al 2003; Nel 2005; Nel et al 2001; Xia et al 2004*). This potential to drive potentially damaging biological oxidations has been linked to a number of particle characteristics, including composition (*Aust et al, 2002; Squadrito et al, 2001*), size and surface area (*Brown 2001*). In the oxidative stress paradigm, inhaled particles generate oxidative stress through three major pathways:

1. By the direct introduction of oxidizing species into the lung, including redox catalysts such as transition metals (*Aust et al, 2002*) and quinones (*Squadrito et al, 2001*) absorbed onto the particle surface.

2. Via the xenobiotic metabolism of polyaromatic hydrocarbons (PAHs), resulting in their bio-transformation in vivo to quinones and reactive electrophiles through the cytochrome P450, epoxide hydrolase and dihydrodial dehydrogenase pathways (*Bonvallot et al, 2001*)

3. By stimulating inflammatory cells to produce reactive oxygen and nitrogen species (ROS and RNS), either through endotoxin mediated pathways (*Monn et al, 2003*), futile phagocytic processing (*Soukup and Becker, 2001*), or as a secondary consequence of oxidative stress triggered up-regulation of redox sensitive transcription factors such as NFκB that direct the synthesis of pro-inflammatory cytokines (*Bonvallot 2002*).

In light of these observations it has been proposed that a measure of the capacity of PM to oxidise target molecules, its oxidative potential (OP), may potentially serve as a biologically pertinent index of PM toxicity. The use of a toxicity based metric has the advantage that it effectively integrates differences in PM size distribution, surface area and composition into a simple unitary expression. Previously we have quantified PM oxidative potential by examining the capacity of particle suspensions, or water soluble extracts, to oxidise antioxidants from models of human respiratory tract lining fluids (RTLFs), using model PM (carbon black, residual oil fly ashes, silicates - *Zielinski et al 1999),* diesel exhaust PM_{10} (Mudway et al 2004), biomass derived $PM_{2.5}$ (*Mudway et al 2005*), environmental tobacco smoke $PM_{2.5}$ (*Duggan et al 2006*), as well as ambient $PM_{2.5}$ (*Kunzeli et al 2006*), $PM_{0.1\text{-}2.5}$ and $PM_{2.5\text{-}10}$ (*Mudway et al 2005*). In these studies the incubations were performed employing physiological concentrations of the antioxidants ascorbate (AA), urate (UA) and glutathione (GSH), with incubations performed at pertinent antioxidant concentrations, pH7.4 and 37^{o}C to model the reactions likely to occur in vivo when inhaled particles first interact at the air-lung interface. In contrast, other published methods quantify PM oxidative potential either through assessment of direct radical generation by electron paramagnetic resonance (*Shi et al, 2003a*) or via the oxidation of biomolecules such as DNA (*Gilmour et al, 1995; Shi et al, 2006*) or non-physiological target molecules (*Cho et al, 2005).* Whilst all of these assays measure certain aspects of PM OP, the incubation conditions employed are often non-physiological and little is known about how these various endpoints relate to one another. This later point is

important as an uninformed reading of the existing literature may leave the reader with the impression that all these assays are measuring the same thing, whilst in reality each method may display differential sensitivity to various pro-oxidants, or PM size fractions. In addition, these acellular approaches are limited to an assessment of the 'intrinsic' oxidative potential of particles reflecting the concentration of redox active metals, quinone and radicals associated with the particle surface; not latent activity attributable to PAH metabolism or the induction of inflammation.

Part I – Comparison of methodologies for assessing particulate matter oxidative potential

Abstract

Using archived $PM_{2.5}$ and PM_{10} samples from Marylebone Road between July 2004 and Sept 2006 we compared three published methods for the determination of particle oxidative potential. The first two methods quantified antioxidant losses from single or composite antioxidant solutions, while the third measured the oxidation of dithiothreitol (DTT). Water leachable metals were determined by ICP-MS and related to the extent of oxidation observed with each method. Metal contributions to the observed oxidative potentials were further investigated using the metal chelator, diethylene triaminepentaacetic acid (DPTA) in the ascorbate-only model. We observed considerable temporal variation in each of the PM metrics examined in both PM fractions, with evidence of quantitative associations between DDT depletion rates and the glutathione dependent oxidative potential/μg observed in the synthetic RTLF model. Particulate-induced loss of glutathione from the synthetic respiratory tract lining fluid model (RTLF) was not strongly associated with ascorbate loss in the same model, which were of a larger magnitude and correlated with the ascorbate depletion rates (total and metal dependent) observed in the single antioxidant model. PM oxidative activity was associated with Ba, Cu, Mo and Mn water soluble metal concentrations, with Cu particularly predictive of the extent of DTT and GSH oxidation. As the DTT assay has been proposed to be specific for quinones we investigated its apparent association with Cu further, demonstrating that Cu did catalyze the oxidation of DTT and that DTPA inhibited PM-induced DTT depletion. In contrast, co-incubation of DTPA with PM samples in the ascorbate only model decreased the oxidation rate by approximately 60%, implying a non-metal contribution to the loss of this antioxidant. These data demonstrate that ascorbate and thiol dependent oxidative losses are likely to be sensitive to differing panels of pro-oxidants and that the oxidative potential outputs from the synthetic RTLF model provides a similar level of information obtained from a combination of the DTT and ascorbate depletion methods.

Key words: Particulate matter, PM_{10}, $PM_{2.5}$, oxidative potential, ascorbate, glutathione, metals, quinones, dithiothreitol

Figures

Figure 1.9: The degree of association between OP^{GSH}/μg with total, metal dependent and metal independent ascorbate depletion rates established in the single antioxidant model.

Figure 1.10: Dose dependant Cu ($CuSO_4$) and 9,10-phenathroquinone (9,10-PQ) dependent DTT oxidation rates, with and without the addition of DTPA, relative to the particle free control.

Figure 1.11: Ascorbate depletion rates with increasing doses of Cu ($CuSO_4$) and 9,10-phenathroquinone (9,10-PQ) with and without co-incubation with DTPA relative to a particle free control.

Figure 1.12: Rates of DTT and AA oxidation over a range of concentrations with a panel of model and environmental PM samples.

Tables

Table 1.1: Pearson correlation analyses of the measured of PM oxidative activity metrics derived from each of the tested models.

Table1.2: The degree of association between DTT oxidation rates and the concentration of water soluble metals determined in all PM samples, as well as segregated by fraction.

Table 1.3: The degree of association (Pearson correlation) between ascorbate and glutathione dependent oxidative potentials and the concentration of water soluble metals determined in all PM samples, as well as segregated by fraction.

Table 1.4: Correlation matrix for the degree of association between total, metal dependent and independent ascorbate depletion rates with PM aqueous metal concentrations.

Table 1.5: DTT and AA depletion rates (minus background auto-oxidation rates) for representative PM samples at 15 μg/mL, with and without co-incubation with the metal chelator DTPA (200 μM).

Aims

Primary - To investigate the comparability of methods for assessing PM oxidative activity using a panel of environmental $PM_{2.5}$ and PM_{10} samples collected from a busy urban roadside site. ***Secondary –*** To examine the relationship between these measures of PM oxidative potential and PM water soluble metal composition.

Background

The capacity of inhaled particles to elicit oxidative stress at the air-lung interface has been proposed to provide a mechanistic link between PM composition and their capacity to induce inflammation and injury in the lung. This hypothesis implies that much of the toxicity of ambient PM is attributed to their organic radicals, redox catalysts (transition metals and quinones) concentrations and precursor chemicals (polyaromatic hydrocarbons) content which can be metabolised in vivo to redox active compounds. These species are present in relatively low abundance in ambient PM thus much of the mass of PM will contribute little to the observed toxicity. Consequently, it has been argued that particle oxidative potential may represent a better metric of the health impacts of ambient PM than concentration alone. Several groups have developed assays that provide some measure of PM oxidative potential, based on the capacity of particles, or particle extracts to oxidise a range of substrates (proteins, DNA, antioxidants or fluorescent probes), mostly in acellular systems. Whilst all of these assays undoubtedly measure aspects of PM oxidative potential, it is not clear how these assays relate to one another, whether they display differential sensitivity to pro-oxidants, or how prognostic they are for predicting in vivo toxicity. In this study we have examined three of the more commonly employed methods for assessing PM oxidative activity, in order to address the first two of these questions.

In the work presented in this report we have performed a comparison of three of the most common techniques for the assessment of PM oxidative potential, based on:

1. Antioxidant depletion from a complex synthetic RTLF.
2. Antioxidant depletion from a simple synthetic RTLF, with and without metal chelation,
3. Dithiothreitol (DTT) oxidation.

Whilst, antioxidant loss from the RTLF model has been shown to be sensitive to both transition metals and quinones (*Ayres et al, 2008*), the ascorbate depletion assay was developed initially as an assay of trace metal concentrations (Welch et al, 2002), and the

DTT oxidation assay, as a measure of quinone catalysed oxidation (*Kumagai et al, 2002; Cho et al, 2005*). Whilst the ascorbate only model has been shown to be sensitive to quinones (*Roginsky et al, 1999*), the DTT assay is still largely presented in the literature as being quinone specific (*Cho et al, 2005*). In addition to examining the quantitative relationship between PM oxidative potential determined in each of these assays, aqueous metal concentrations were also examined, as an initial step toward understanding the determinants of the observed activity.

Methods

Details of the filter archive: 30 $PM_{2.5}$ and 21 PM_{10} TEOM filters were obtained from the kerbside Marylebone Road site, covering the period June 04 – Sept 06 and March 06 – Sept 06, respectively. On average the $PM_{2.5}$ filters represented collection periods of 18 ± 5 days, whilst the PM_{10} samples were collected on an approximately weekly basis: 8 ± 2 days. Of the 819 day period across which $PM_{2.5}$ filters were recovered, a total of 533 days (65%) were sampled, compared with 87.9% for the PM_{10} filters, which were collected over a shorter interval (182 days). Considering the equivalent period over which both $PM_{2.5}$ and PM_{10} filters were collected 29 – March 06 to the 22-27 – Sept 06, a total of 8 and 21 filters were obtained respectively, covering 79.7 and 87.9% of the sampling period.

Extraction and re-suspension of TEOM filter PM: Individual filters, both PM_{10} and $PM_{2.5}$, were placed in 50 ml falcon tubes containing 2 ml of methanol. The tubes were then vortexed for 10 minutes, before sonication using a MSE Soniprep 150 (23 kHz) generator with a titanium probe at an amplitude of 5 microns for 30 seconds. Samples that yielded oily extracts, which were not readily resuspended by vortexing, underwent physical scraping from the sides of the extraction tubes with plastic pipettes prior to sonication. The methanol extract was then transferred to a second falcon tube and an additional 2 ml of methanol added to the remaining filter prior to a further 10-minute period of vortexing. This second methanol extract was then added to the first, prior to drying down under nitrogen at 35^{o}C. The dried extract was subsequently re-suspended at stock concentrations of 12.56 or 55.6 μg/ml in Chelex100-resin treated ultra-pure water containing 5% HPLC-grade methanol by vortexing for 10 minutes and sonication, as outlined above. Removal of contaminating metals from the water-methanol mixture was achieved by adding 3 g of Chelex-100 resin to100 ml of the solution with stirring over-night at rtp. The resin was removed by vacuum filtration and the purified 5% methanol solution carefully decanted. Prior to use in the resuspension protocol the pH of the water-methanol solution was adjusted to neutrality using Chelex resin treated 1M HCl or 1M NaOH. Once PM samples were resuspended in the solution, the pH of the suspension was checked and where necessary readjusted to 7 as outlined above, prior to use in the incubation protocols.

Measuring PM oxidative activity in the synthetic RTLF model: The oxidative capacity of PM was determined by their ability to oxidize a range of protective antioxidant molecules present at the surface of the lung using a validated in vitro model (*Zielinski et al 1999; Mudway et al 2004*). These incubations were performed at a final particle concentration of 50 μg/ml. Antioxidant solutions contained equimolar concentrations (200 μM) of ascorbate, urate and reduced glutathione. Co-incubations of PM and antioxidants were then performed for 4 hours at 37^{o}C at a pH of 7. At the end of this period, particles were removed by centrifugation (13,000 rpm for 60 minutes, 4^{o}C) prior to determination of the remaining antioxidant concentrations. To ensure intra-assay standardization between experiments control PM samples were also run. These consisted of a particle free control (auto-oxidation), residual oil fly ash; ROFA (positive control) and the inert carbon black particle M120 (negative control). Composition details of these control particles have been published previously (*Zielinski et al 1999; Miller et al 1998*). All incubations were performed in triplicate. Ascorbate and urate were determined using reverse phase high-pressure liquid chromatography with electro-chemical detection in the amperometric mode (Iriyama et al 1984). Reduced and oxidized glutathione were measured using the enzyme recycling method of Tietze modified for use on a plate reader (Baker et al 1990).

Ascorbate and Urate analysis: Fifty μl of the PM supernatant was removed from each incubation tube and added to 50 μl of ice-cold metaphosphoric acid (MPA) and 400 μl of HPLC-grade water to achieve a final acid concentration of 5%. Ascorbate and UA concentrations were then determined simultaneously using reverse phase HPLC with electrochemical detection. Twenty μL aliquots of each sample were injected for analysis using a Gilson model 231 auto-sampler onto a 10 x 150 mm, 5μM C18 column, eluted with 0.2mM K_2HPO_4-H_3PO_4, containing 0.25 mM octanesulphonic acid (pH 2.1) at a flow rate of 1.5 ml/min. An EG&G amperometric electrochemical detector (Jones Chromatography, Hengoed, Wales) was used for detection, with the potential set at 400 mV, a time constant of 5 s, cathodic output and a current sensitivity of 0.5 μA. Sample concentrations were determined against a standard curve containing ascorbic acid (0-25 μM) and uric acid (0-50 μM) (both Sigma) prepared in 5% MPA.

Glutathione analysis: Further aliquots (16.7 μl) of the PM supernatants were diluted into 983.3 μl of 100 mM sodium phosphate buffer, pH 7.5, containing 1 mM EDTA. Standards

containing 0-165 pmol/50 µl GSSG, equivalent to 0-330 pmol/50 µl GSx were also prepared in this buffer. Fifty µl of sample and standard were then transferred to the wells of a microtitre plate prior to the addition of 100 µl of a reaction mixture to achieve final reagent concentration in each well of 0.15 mM DTNB, 0.2 mM NADPH and 1 U of glutathione reductase. Immediately after the addition of the reaction mixture the microtitre plate was transferred to a plate reader (SpectraMAX 190; Molecular Devices) for analysis. The rate of 5-thio-2-nitrobenzoic acid (TNB) formation was then followed by the rate of change in absorbance at 405nm over a 2 min period at 30°C. To determine GSSG concentrations, 5 µl of undiluted 2-vinyl pyridine (Aldrich chemical Co, Poole, UK) was added to 130 µl of the samples and standards, vortexed briefly and incubated at room temperature for 1 h. Samples and standards were then plated out and ran as above. The GSH pool was calculated indirectly by the subtraction of the measured GSSG (x2) from the total glutathione (GSx) concentration.

Deriving expressions of PM_{10} oxidative potential - PM oxidative potential (OP) was determined using the following set of calculations based on the data derived from the synthetic RTLF model. Equations 1.1-1.3 are presented as examples for ascorbate calculations with GSH determined in an identical manner. The percentage AA loss and percentage GSH loss was calculated from the concentration of AA and GSH remaining following PM incubation with the synthetic RTLF relative to particle free controls also incubated for four hours with RTLF.

$$\%\text{AA Loss} = \frac{\text{Sample AA } (\mu\text{M})}{\text{Control 4h Blank AA } (\mu\text{M})} \times 100 \qquad \text{Equation 1.1}$$

This percentage antioxidant depletion was normalized by the final PM concentration used in the RTLF incubations (50 µg mL^{-1}) to yield PM oxidative potential per unit mass: OP^{AA} μg^{-1} and OP^{GSH} μg^{-1}.

$$\frac{OP^{AA}}{ug} = \frac{\%\text{AA Loss}}{50\,(ug\ mL^{-1})} \qquad \text{Equation 1.2}$$

Multiplication of this unit mass metric with the ambient PM concentration (calculated as the extracted PM filter mass, µg, divided by the sampled volume of air, m^3) produced an

oxidative potential metric of PM induced AA and GSH depletion calculated per cubic metric of ambient air: OP^{AA} m^{-3} and OP^{GSH} m^{-3}.

$$\frac{OP^{AA}}{m^3} = \frac{OP^{AA} / \mu g}{[Ambient\ PM](\mu g\ m^{-3})} \qquad \text{Equation 1.3}$$

AA depletion assay: Oxidative activity of selected PM suspensions was also assessed by their capacity to deplete ascorbate-from an ascorbate only model. This approach was also used to investigate the mechanisms driving PM oxidative activity, by the addition of the transition metal chelator DTPA. PM stock solutions were prepared as outlined previously and diluted to a starting concentration of 12.5 μg/ml before incubation with ascorbate. All PM exposures were performed in triplicate in UV 96 well flat-bottomed plates (Greiner bio-one) at a final volume of 200 μl. Exposures were initiated by the addition of 20 μl of a concentrated stock of ascorbate (2 mM) into each well containing 160 μl of PM suspension and 20 μl of Chelex-100 resin treated water, to starting concentrations of 200 μM ascorbate and 10 μg/ml of PM. Immediately prior to the addition of ascorbate to each assay well, the plate was pre-incubated for 10 minutes at 37°C in a plate reader (Spectra Max 190) and during the exposure the plate was maintained at this temperature. Over this period, additional aliquots of each PM sample were also pre-incubated in the presence of 200 μM of DTPA by the addition of 20 μl of 2 mM DTPA (pH7) in Chelex-100 resin treated water.

After addition of ascorbate, the concentration remaining in each well was monitored every 2 min for a period of 2 h by measuring the absorbance at 265 nm. In order to control for the contribution of absorbance of the particles themselves, ascorbate free controls containing 40 μl of Chelex-resin treated water and 160 μl of individual particle stocks were run in parallel on the plate and subtracted from the sample absorbance readings. The rate of ascorbic acid depletion was determined by performing a linear regression through the initial part of a concentration verses time plot using Microcal Software Limited's OriginLab (version 5.0). This was performed for each of the triplicates with the rate of ascorbic acid depletion finally expressed as mean mol/s x 10^{-9} depletion of ascorbate ± standard deviation. From these data three rates, indicative of aspects of the PM oxidative activity could be derived: the total oxidative activity (the rate of ascorbate depletion associated with the sample minus that observed in the appropriate blank), the metal dependant oxidative activity (the fraction of the observed depletion rate that could be

inhibited by co-incubation with an excess of DTPA) and the non-metal dependent oxidative activity (the residual depletion rate following DTPA treatment).

DTT oxidation assay: DTT depletion was based on the published method of Cho et al (*Cho et al 2005*) modified for high throughput analysis using 96 well plates. Briefly, 240 µl aliquots of PM suspensions at 12.5 µg/ml, prepared in Chelex treated water containing 5% methanol, were added to the wells of 96 well plate in triplicate. Particle free blanks were also run on each plate, together with ROFA and London $PM_{2.5-10}$ control samples. Following equilibration of these PM samples and controls to 37^{o}C, 30 µl aliquots of DTT (1 mM, pre-warmed to 37^{o}C) were added together with either 30 µl of Chelex-100 treated water or 30 µl of DPTA (2 mM) after which the plate was briefly mixed. At this time, 0 minutes, 35 µl of the experimental sample was removed from each well using 8 channel pipette and transferred into the wells of a second 96 well microplate each containing 35 µl of a chilled 10% w/v TCA solution. The plate was then tapped, mixed and covered before placing in a fridge (4^{o}C). This procedure was then repeated following incubation at 37^{o}C for 15, 30 and 60 min. At the end of the incubation period 140 µl of 0.4 M Tris buffer, containing 20 mM EDTA pH8.9 was added to the 70 µl of TCA-reacted sample in each well using 8 channel pipette, prior to the addition of 26.7 µl DTNB (1.25 mM prepared in the Tris buffer) reagent. The plate was then mixed in the microplate reader (SpectraMax190) for 5 seconds prior to incubation at 30^{o}C for 5 min after which the absorbance at 412 nm was determined to provide an estimate of the free thiol remaining. The concentration of thiol remaining at each time, minus that observed in the particle free blank was then used to calculate the loss of DTT expressed as nmol/s

ICP-MS analysis of aqueous PM extracts: 1-2 ml of the particle suspensions prepared in Chelex100-resin treated ultra-pure water containing 5% HPLC-grade methanol, as outline previously, were centrifuged 13,000 rpm for 1 h, 4^{o}C to remove particles. To ensure the removal of all particles the resultant supernatant was filtered through an Anotop-0.02µm Whatman filter. 0.9 ml of the filtrate was then added to a further 0.9 ml of Chelex-100 resin treated HPLC-grade water prior to analysis by ICP-MS. Each batch of samples was ran in parallel to a Chelex-water blank, as well as aqueous extracts derived from ROFA and a stock environmental $PM_{2.5-10}$ sample collected from London. The London sample was ran to provide Fe and Cu measurements, as these metals were low abundance in the

aqueous extract obtained from the ROFA sample. Samples were then transferred to the Mass Spectroscopy Unit at King's College for the quantification of Al, As, Ba, Be, Cd, Cu, Fe, Mn, Mo, Ni, Pb, V and Zn by ICP-MS using a ELAN DRC ICP-MS (MSF008). Elemental concentrations were determined with reference to a 4-point standard curve based on a ICP multi element standard solution VI CertiPUR® (Merck, Lot. No. OC529648). All concentrations were corrected for the background elemental concentrations determined in the Chelex-100 resin treated water blank ran in parallel to each batch of samples.

Results

Variability in PM oxidative potential - Both $PM_{2.5}$ and PM_{10} samples displayed considerable temporal variability in their OP, irrespective of which of the methods was employed to establish this parameter. Considering DDT depletion, the greatest rates observed were associated with PM_{10} samples. A similar pattern was observed for both OP^{AA}/μg and OP^{GSH}/μg, although here the contrast between the two size fractions for OP^{GSH}/μg was not significant. The total ascorbate depletion rate was also found to be greatest in PM_{10} samples, though no statistically significant contrasts were observed when these rates were separated into their metal dependent and independent components.

Correlations between different OP methodologies - Overall (based on both $PM_{2.5}$ and PM_{10} samples) DDT depletion was found to correlate with both OP^{AA}/μg and OP^{GSH}/μg, but not with ascorbate depletion rate, measured either as total, metal dependent and metal independent. Notably the association between DTT depletion rate and OP^{GSH}/μg was strongest in the $PM_{2.5}$ fraction, whilst it displayed little association with the OP^{AA}/μg expression. PM OP^{AA}/μg and OP^{GSH}/μg were not associated in either fraction, suggesting that these two measures obtained from the synthetic RTLF model were sensitive to different PM redox active components. OP^{AA}/μg but not OP^{GSH}/μg displayed significant positive associations with the total and metal dependant ascorbate depletion rates across both PM fractions.

Associations between OP parameters and aqueous metal concentrations – DTT oxidation rates displayed significant positive associations with Ba, Mn and Mo when both PM fractions were considered. OP^{GSH}/μg was similarly associated with Cu and Mn, whereas OP^{AA}/μg displayed correlations with Ba, Mn and Mo when all fractions were considered. When the total ascorbate depletion rates were considered only Ba was found to be significantly associated with the observed rates, which was consistent for both the metal dependent and independent rates. Surprisingly, no other positive associations were noted between the panel of aqueous metal examined and the metal dependent ascorbate depletion rate, though significant negative correlations were noted for Cu and Fe.

Variability in PM oxidative potential - Both $PM_{2.5}$ and PM_{10} samples from Marylebone Road displayed considerable temporal variability in their OP, irrespective of which of the

methods was employed to establish this parameter (Figures 1.1-1.4). Considering DDT depletion (Figure 1.1), the greatest rates observed were associated with PM_{10} samples, both when all samples were considered (0.005 ± 0.001 [$PM_{2.5}$] vs. 0.007 ± 0.001 [PM_{10}] nmol/s, $P<0.001$), or only those covering equivalent periods (0.006 ± 0.001 vs. 0.007 ± 0.001 nmol/s, $P<0.05$). A similar pattern was observed for both OP^{AA}/μg (1.0 ± 0.2 [$PM_{2.5}$] vs. 1.2 ± 0.3 [PM_{10}], $P<0.05$ - Figure 1.2) and OP^{GSH}/μg (0.8 ± 0.4 [$PM_{2.5}$] vs. 1.1 ± 0.4 [PM_{10}], $P<0.05$ - Figure 1.3), although here the contrast between the two fractions for OP^{GSH}/μg was no longer significant when the analysis was restricted to equivalent periods: 1.0 ± 0.4 [$PM_{2.5}$] vs. 1.1 ± 0.4 [PM_{10}], $P=0.81$ - Figure 1.3. It was notable that whilst the incubation of the PM samples in the synthetic RTLF resulted in significant losses of ascorbate and glutathione, no impact was seen on urate, consistent with earlier observations. The total ascorbate depletion rate was also found to be greatest in PM_{10} samples when these were considered over equivalent periods (0.80 ± 0.32 [$PM_{2.5}$] vs. 1.92 ± 1.10 [PM_{10}] nmol/s, $P<0.01$), though no statistically significant contrasts were observed when these rates were separated into their metal dependent 0.34 ± 0.49 [$PM_{2.5}$] vs. 1.23 ± 1.22 [PM_{10}] nmol/s, $P=0.06$ – Figure 1.4) and independent components 0.45 ± 0.46 [$PM_{2.5}$] vs. 0.69 ± 0.53 [PM_{10}] nmol/s, $P=0.27$ – Figure 1.4).

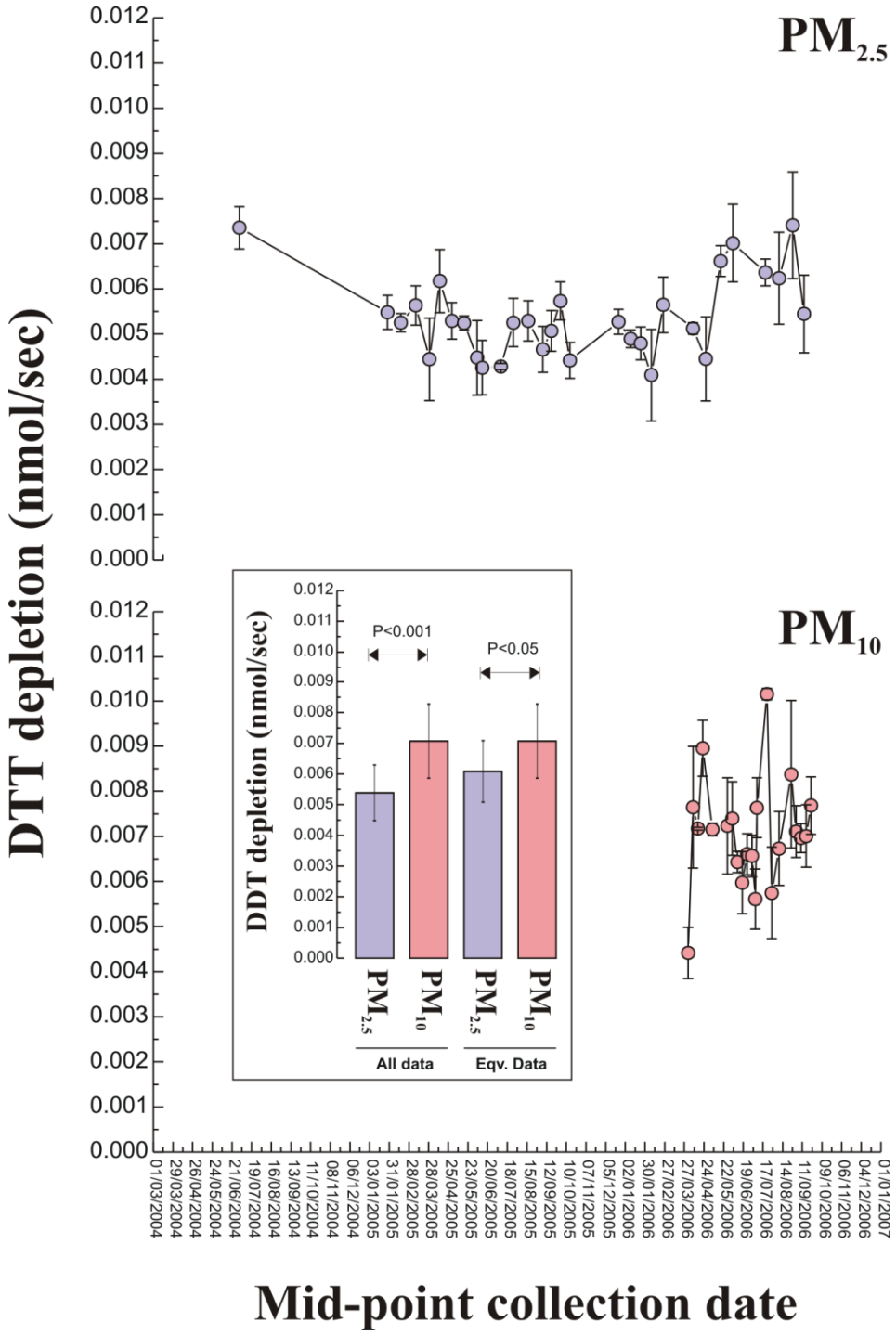

Figure 1.1: DTT oxidation/depletion rates associated with a 60 minute incubation with $PM_{2.5}$ (upper panel) and PM_{10} (lower panel) samples (10μg/mL) obtained from Marylebone Road. All data points represent the mean ± 2SD of triplicate incubations, with the points plotted to the midpoint date of their sampling interval. The inset figure illustrates the contrast in $PM_{2.5}$ and PM_{10} DTT oxidation rates for all of the considered samples, or only those covering the equivalent period: 29 – March 06 to the 22-27 – Sept 06. Comparisons of rates between the two PM size fractions were performed using an unpaired t-rest with the resultant P-value illustrated.

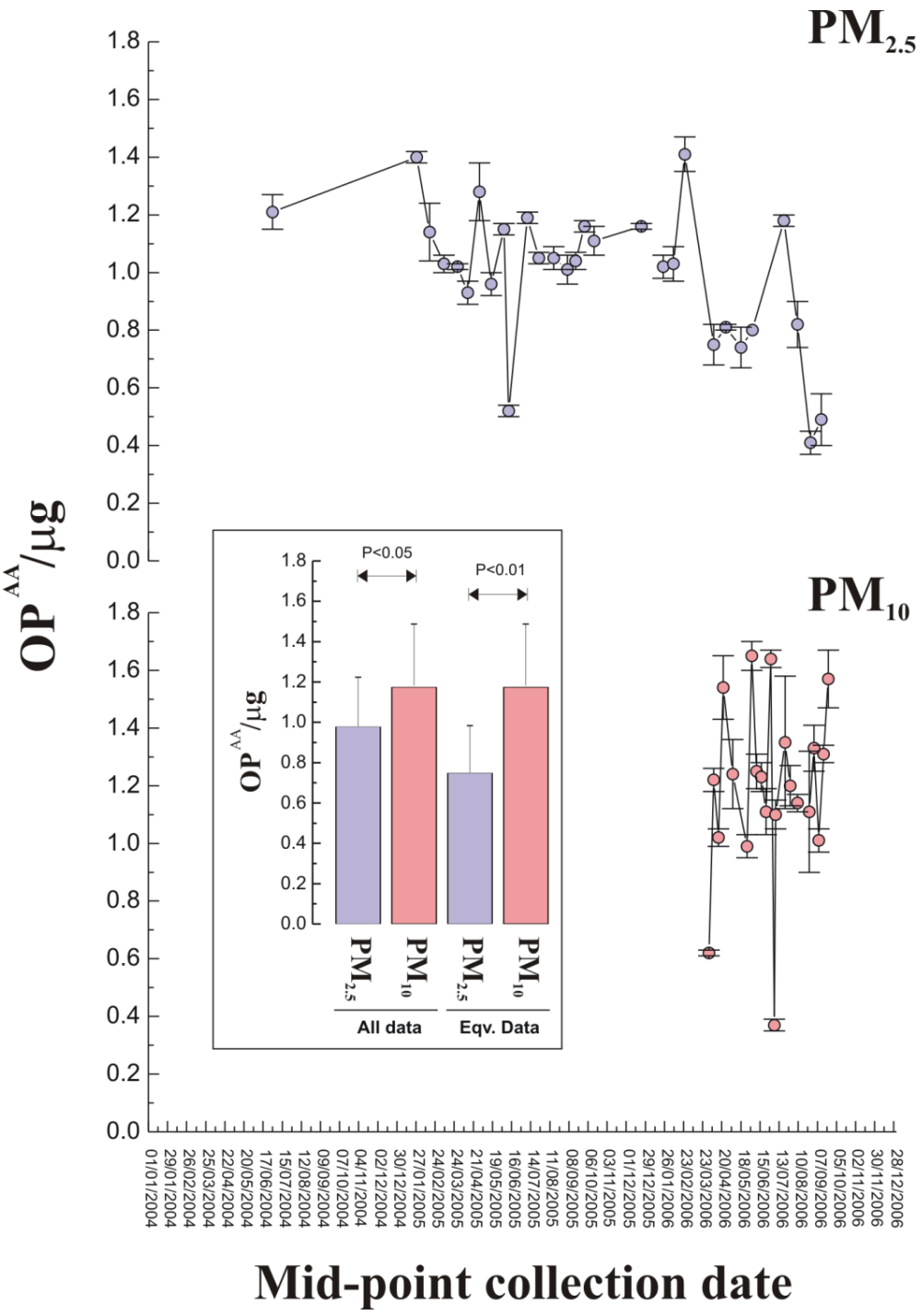

Figure 1.2: Ascorbate dependent oxidative potential, established in the synthetic RTLF model, expressed per µg of PM for $PM_{2.5}$ (upper panel) and PM_{10} (lower panel) samples obtained from Marylebone Road over the indicated periods. Figure layout is as outlined in the legend to figure 1.1

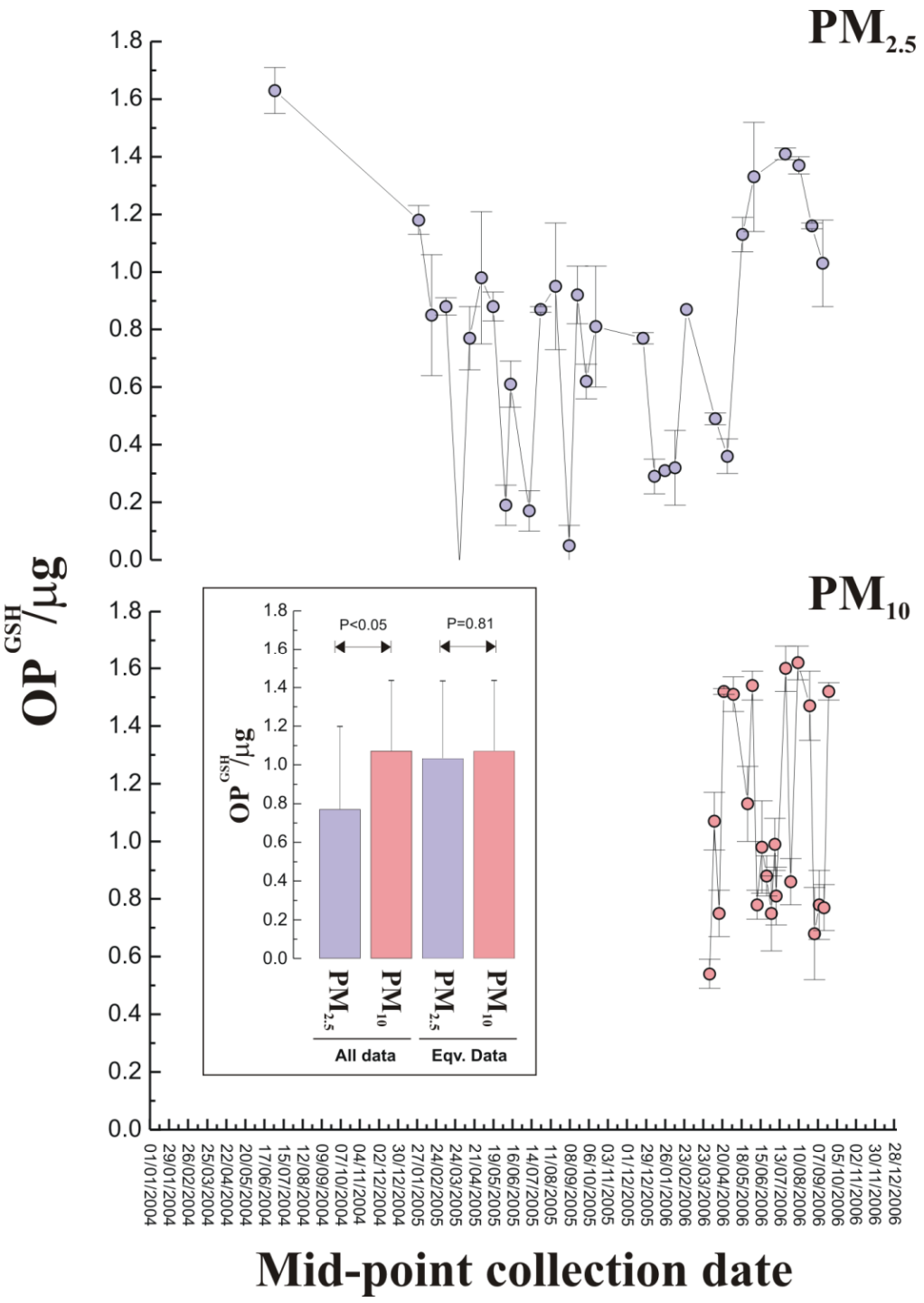

Figure 1.3: Glutathione dependent oxidative potential, established in the synthetic RTLF model expressed per µg of PM for $PM_{2.5}$ (upper panel) and PM_{10} (lower panel) samples obtained from Marylebone Road over the indicated periods. The figure layout is as outlined in the legend to figure 1.1

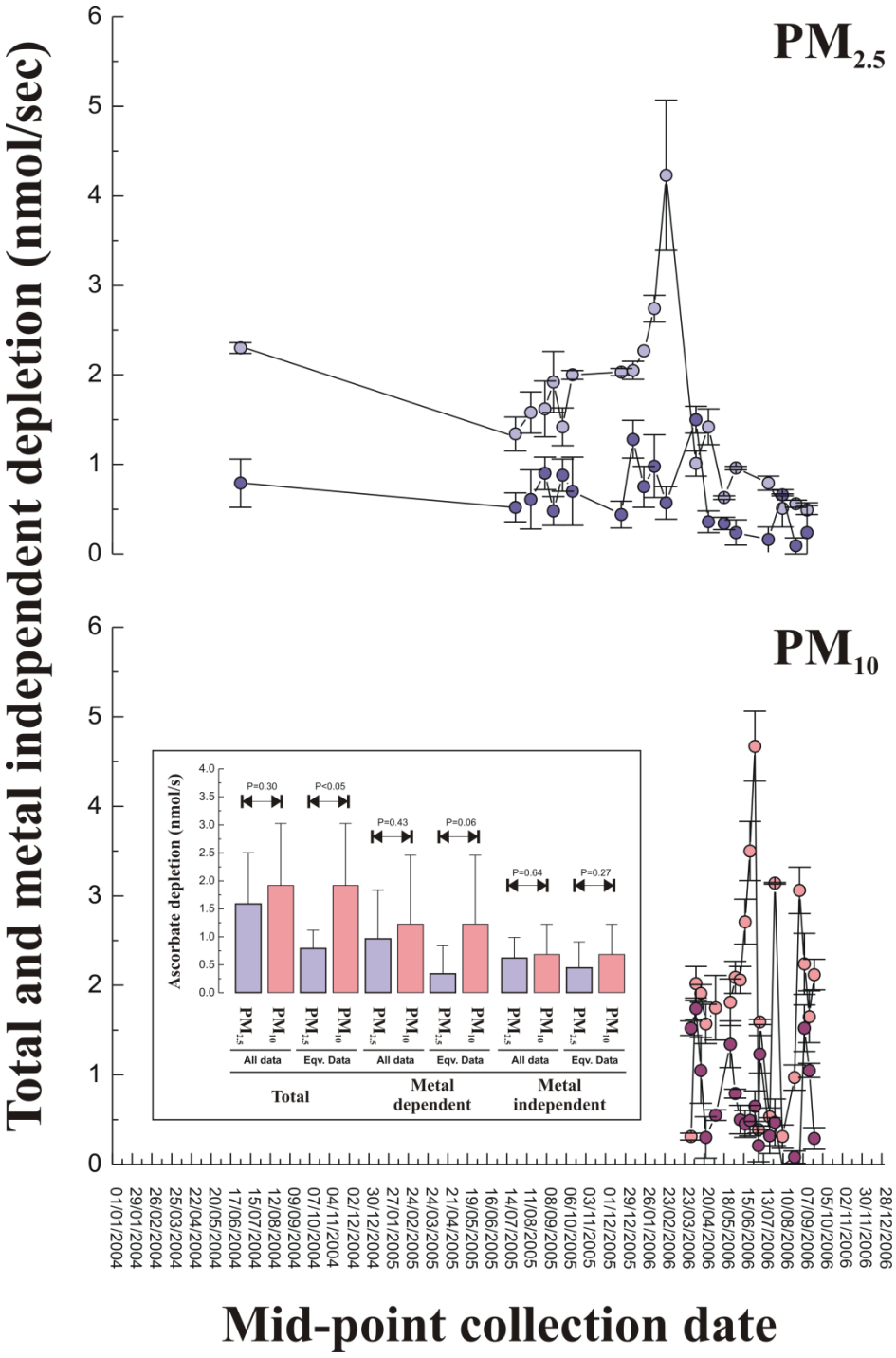

Figure 1.4: Total and metal independent ascorbate oxidation rates, the later determined after incubation with a excess of DTPA, associated with $PM_{2.5}$ (upper panel) and PM_{10} (lower panel) samples obtained from Marylebone Road over the indicated periods. In inset panel illustrates the contrasts between rates for $PM_{2.5}$ and PM_{10}, overall, as well as over equivalent sampling periods are shown. The metal dependent rate was determined by subtracting the residual rate following the DTPA co-incubation from the total measured rate. All other aspects of the figure layout and analysis is as outlined in the legend to figure 1.1

Correlations between different OP methodologies - Overall (based on both $PM_{2.5}$ and PM_{10} samples) DDT depletion was found to correlate with both OP^{AA}/μg and OP^{GSH}/μg (r-0.36, P=0.01 and r=0.74, P<0.001 respectively - Pearson's correlation, Figure 1.5), but not with any of the ascorbate depletion rates (total, metal dependent and metal independent, Figure 6), established in the ascorbate only model (Table 1.1). Notably the association between DTT depletion rate and OP^{GSH}/μg was strongest in the $PM_{2.5}$ fraction (r=0.80, P<0.001) where there it displayed little association with the OP^{AA}/μg (Table 1.1). PM OP^{AA}/μg and OP^{GSH}/μg were not simplistically associated in either fraction, suggesting that these two measures obtained from the synthetic RTLF model (Table 1.1, Figure 1.7), were sensitive to different PM redox active components. OP^{AA}/μg but not OP^{GSH}/μg displayed significant positive associations with the total and metal dependant ascorbate depletion rates across both PM fractions (Table 1.1, Figures 1.8-1.9).

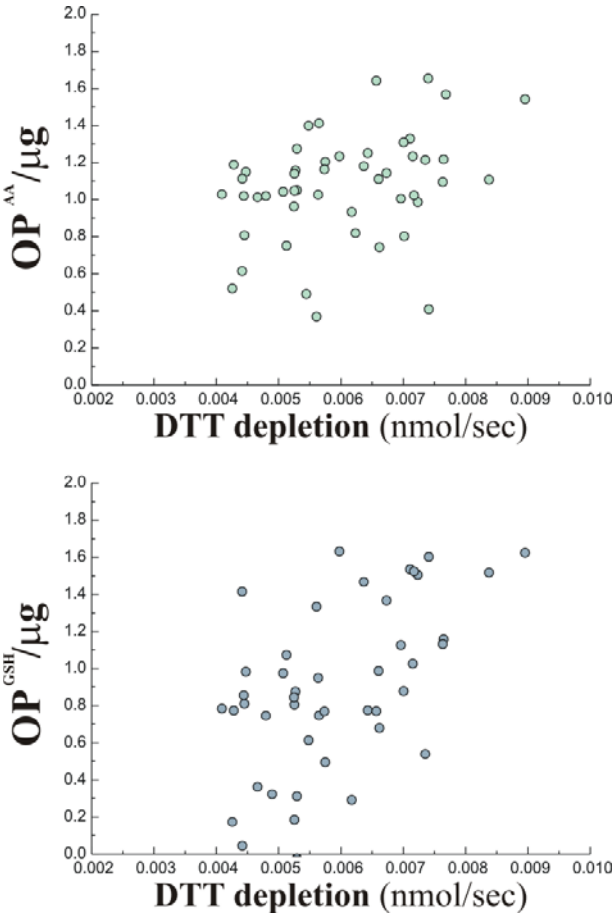

Figure 1.5: The degree of association between DTT depletion rates with ascorbate and glutathione dependent oxidative potential per μg established in the synthetic RTLF model in all PM samples. Details of the correlation analyses illustrated in this figure are given in Table 1.1.

Table 1.1: Associations between the PM oxidative activity metrics derived from each of the tested models. Analyses are presented for both $PM_{2.5}$ and PM_{10} combined and for each of these fractions separately. Significant interactions are highlighted with red text.

		OPaa	OPgsh	DTT	AAdep	AAdep_nonmetal	AAdep_metal
Correlations: All data							
OPaa	Pearson Correlation	1	0.234	0.360	0.610	-0.018	0.592
	Sig. (2-tailed)		0.102	0.010	0.000	0.913	0.000
	N		50	50	40	40	40
OPgsh	Pearson Correlation			0.739	-0.278	-0.433	-0.080
	Sig. (2-tailed)			0.000	0.079	0.005	0.618
	N			51	41	41	41
DTT	Pearson Correlation				-0.091	-0.191	-0.006
	Sig. (2-tailed)				0.570	0.231	0.971
	N				41	41	41
AAdep	Pearson Correlation					0.123	0.905
	Sig. (2-tailed)					0.443	0.000
	N					41	41
AAdep_nonmetal	Pearson Correlation						-0.311
	Sig. (2-tailed)						0.048
	N						41
Correlations: PM2.5							
OPaa	Pearson Correlation	1	-0.043	-0.168	0.744	0.270	0.675
	Sig. (2-tailed)		0.826	0.383	0.000	0.264	0.002
	N		29	29	19	19	19
OPgsh	Pearson Correlation			0.810	-0.325	-0.564	-0.106
	Sig. (2-tailed)			0.000	0.162	0.010	0.658
	N			30	20	20	20
DTT	Pearson Correlation				-0.376	-0.466	-0.200
	Sig. (2-tailed)				0.102	0.038	0.398
	N				20	20	20
AAdep	Pearson Correlation					0.320	0.917
	Sig. (2-tailed)					0.169	0.000
	N					20	20
AAdep_nonmetal	Pearson Correlation						-0.084
	Sig. (2-tailed)						0.726
	N						20
Correlations: PM10							
OPaa	Pearson Correlation	1	0.377	0.519	0.506	-0.227	0.556
	Sig. (2-tailed)		0.092	0.016	0.019	0.322	0.009
	N		21	21	21	21	21
OPgsh	Pearson Correlation			0.629	-0.376	-0.444	-0.145
	Sig. (2-tailed)			0.002	0.093	0.044	0.529
	N			21	21	21	21
DTT	Pearson Correlation				-0.139	-0.195	-0.040
	Sig. (2-tailed)				0.548	0.396	0.864
	N				21	21	21
AAdep	Pearson Correlation					0.002	0.900
	Sig. (2-tailed)					0.992	0.000
	N					21	21
AAdep_nonmetal	Pearson Correlation						-0.435
	Sig. (2-tailed)						0.049
	N						21

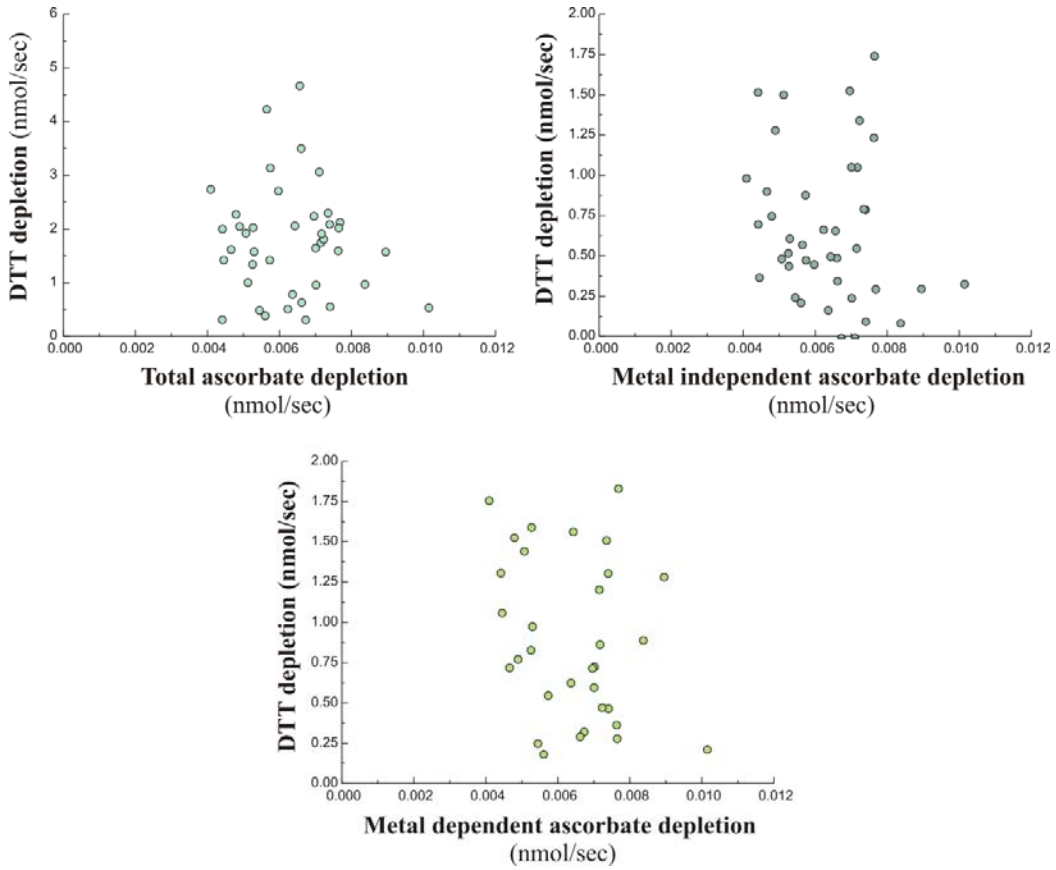

Figure 1.6: The degree of association between DTT depletion rates with total, metal dependent and metal independent ascorbate depletion rates, both expressed as nmol/s. Details of the correlation analyses in this figure are given in Table 1.1.

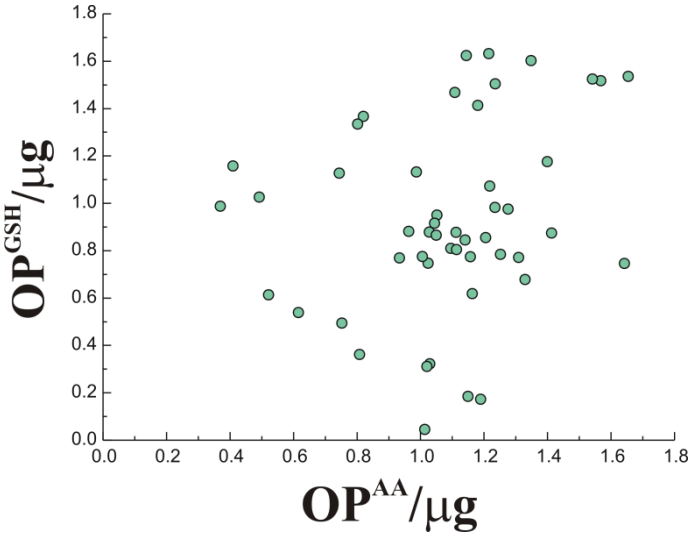

Figure 1.7: The absence of an association between ascorbate and glutathione dependent oxidative potentials established in the synthetic RTLF model across all of the analysed samples. Details of the correlation analyses in this figure are given in Table 1.1

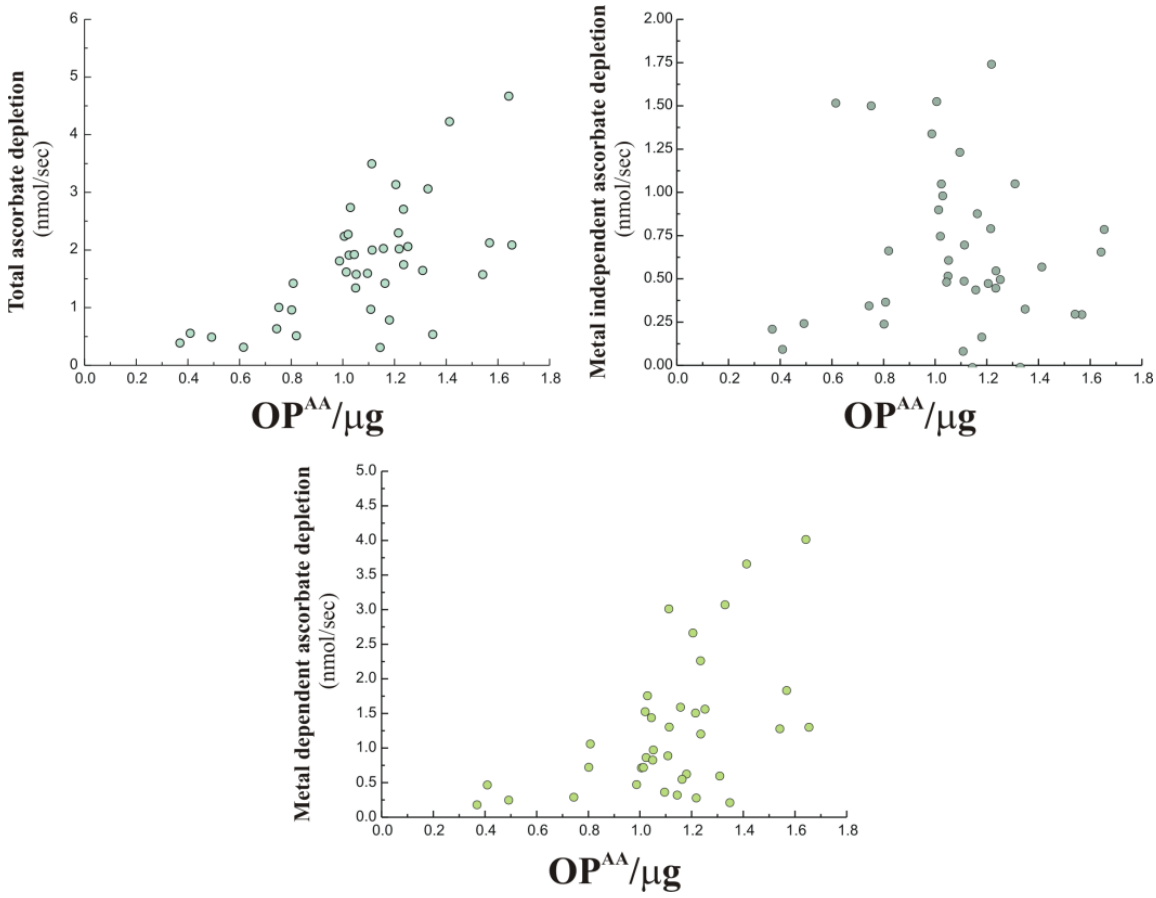

Figure 1.8: The degree of association between OP^{AA}/µg with total, metal dependent and metal independent ascorbate depletion rates established in the single antioxidant model. Details of the correlation analyses in this figure are given in Table 1.1.

Associations between OP parameters and aqueous metal concentrations – DTT oxidation rates displayed significant positive associations with Ba (r=0.28,P<0.05), Cu (r=0.41, P<0.001), Mn (r=0.37, P<0.01) and Mo (r=0.64, P<0.001) when both PM fractions were considered (Table 1.2). OP^{GSH}/µg was similarly associated with Cu (r=0.46, P<0.001) and Mn (r=0.63, P<0.001), whereas OP^{AA}/µg displayed significant correlations with Ba (r=0.42, P<0.01), Mn (r=0.40, P<0.01) and Mo (r=0.30,P<0.05) when all fractions were considered (Table 1.3). When the total ascorbate depletion rates were considered only Ba was found to be significantly associated with the observed rates (r=0.49, P=0.01), which was consistent for both the metal dependent and independent rates (Table1. 4).

Surprisingly, no other positive associations were noted between the panel of aqueous metal examined and the metal dependent ascorbate depletion rate, though significant negative correlations were noted for Cu ($r=-0.57$, $P<0.01$) and Fe ($r=-0.46$, $P<0.05$).

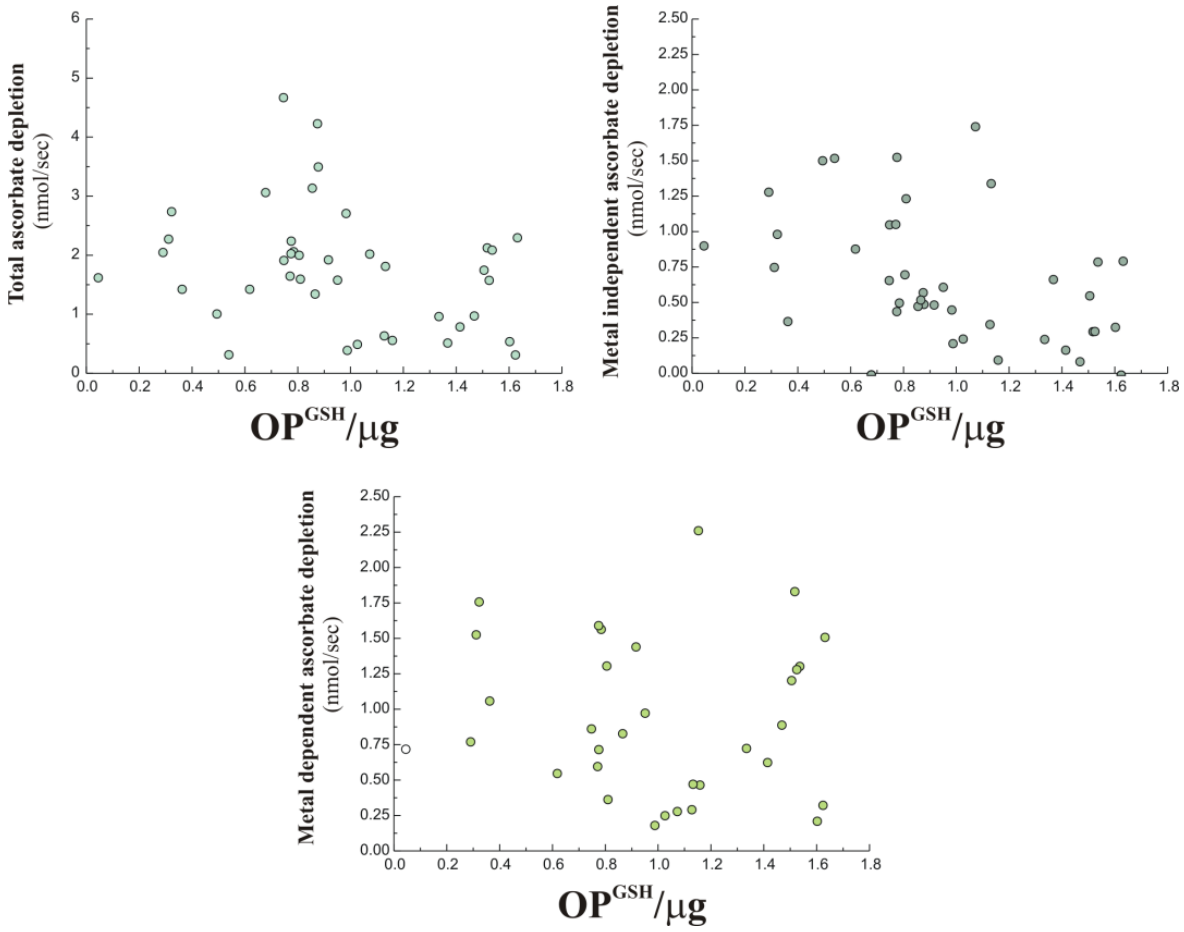

Figure 1.9: The degree of association between OP^{GSH}/µg with total, metal dependent and metal independent ascorbate depletion rates established in the single antioxidant model. Details of the correlation analyses in this figure are given in Table 1.1.

Table 1.2: The degree of association between DTT oxidation rates and the concentration of water soluble metals determined in all PM samples, as well as segregated by fraction. Significant associations determined using the Pearson correlation are highlighted in red text.

OP Parameter	Fraction		PM water soluble metal content												
			Al	As	Ba	Cd	Cu	Fe	Mn	Mo	Ni	Pb	V	Zn
			ng/mg PM											
DTT oxidation	All PM	Pearson Correlation	-0.344	-0.391	0.277	-0.078	0.406	0.122	0.366	0.645	-0.103	-0.381	-0.150	-0.354
		Sig. (2-tailed)	0.014	0.005	0.049	0.587	0.003	0.395	0.008	0.000	0.471	0.006	0.292	0.011
		N	51	51	51	51	51	51	51	51	51	51	51	51
DTT oxidation	PM2.5	Pearson Correlation	-0.230	-0.184	-0.321	0.347	0.455	0.219	0.000	0.404	0.279	0.034	-0.173	0.033
		Sig. (2-tailed)	0.222	0.331	0.084	0.061	0.012	0.245	1.000	0.027	0.135	0.860	0.361	0.864
		N	30	30	30	30	30	30	30	30	30	30	30	30
DTT oxidation	PM10	Pearson Correlation	0.408	0.472	-0.150	0.455	0.182	0.412	0.127	0.548	0.363	0.382	0.530	0.332
		Sig. (2-tailed)	0.067	0.031	0.517	0.038	0.429	0.064	0.584	0.010	0.106	0.088	0.013	0.142
		N	21	21	21	21	21	21	21	21	21	21	21	21

Table 1.3: The degree of association (Pearson correlation) between ascorbate and glutathione dependent oxidative potentials and the concentration of water soluble metals determined in all PM samples, as well as segregated by fraction. Significant associations are highlighted in red text.

OP Parameter	Fraction		PM water soluble metal content											
			Al	As	Ba	Cd	Cu	Fe	Mn	Mo	Ni	Pb	V	Zn
			ng/mg PM											
$OP^{AA}/\mu g$	All PM	Pearson Correlation	-0.086	-0.031	0.416	-0.114	0.159	-0.024	0.404	0.298	-0.067	-0.025	0.113	-0.074
		Sig. (2-tailed)	0.553	0.833	0.003	0.429	0.269	0.871	0.004	0.035	0.643	0.864	0.435	0.611
		N	50	50	50	50	50	50	50	50	50	50	50	50
$OP^{AA}/\mu g$	PM2.5	Pearson Correlation	0.126	0.273	0.400	-0.102	-0.158	-0.177	0.046	-0.179	-0.065	0.426	0.095	0.165
		Sig. (2-tailed)	0.516	0.152	0.032	0.597	0.413	0.358	0.811	0.354	0.737	0.021	0.624	0.392
		N	29	29	29	29	29	29	29	29	29	29	29	29
$OP^{AA}/\mu g$	PM10	Pearson Correlation	0.135	0.341	0.250	0.449	0.396	0.224	0.400	0.532	0.585	0.224	0.538	0.411
		Sig. (2-tailed)	0.560	0.130	0.274	0.041	0.075	0.328	0.072	0.013	0.005	0.329	0.012	0.064
		N	21	21	21	21	21	21	21	21	21	21	21	21
$OP^{GSH}/\mu g$	All PM	Pearson Correlation	-0.196	-0.160	-0.025	0.152	0.459	0.251	0.133	0.627	0.018	-0.058	-0.133	-0.187
		Sig. (2-tailed)	0.169	0.263	0.859	0.287	0.001	0.075	0.353	0.000	0.902	0.684	0.353	0.190
		N	51	51	51	51	51	51	51	51	51	51	51	51
$OP^{GSH}/\mu g$	PM2.5	Pearson Correlation	-0.253	-0.147	-0.422	0.305	0.338	0.173	-0.112	0.406	0.184	0.168	-0.243	-0.055
		Sig. (2-tailed)	0.178	0.440	0.020	0.101	0.068	0.361	0.557	0.026	0.331	0.376	0.195	0.771
		N	30	30	30	30	30	30	30	30	30	30	30	30
$OP^{GSH}/\mu g$	PM10	Pearson Correlation	0.698	0.779	-0.365	0.755	0.542	0.593	0.012	0.819	0.375	0.770	0.502	0.569
		Sig. (2-tailed)	0.000	0.000	0.104	0.000	0.011	0.005	0.958	0.000	0.094	0.000	0.020	0.007
		N	21	21	21	21	21	21	21	21	21	21	21	21

Table 1.4: Correlation matrix for the degree of association between total, metal dependent and independent ascorbate depletion rates with PM aqueous metal concentrations. Table formatting is as outlined in the legend to Table 1.2.

OP Parameter	Fraction		PM water soluble metal content												
			Al	As	Ba	Cd	Cu	Fe	Mn	Mo	Ni	Pb	V	Zn
			ng/mg PM												
Total AA depletion	All PM	Pearson Correlation	-0.294	-0.194	0.489	-0.207	-0.232	-0.364	0.282	-0.065	-0.259	-0.139	-0.145	-0.207
		Sig. (2-tailed)	0.062	0.224	0.001	0.195	0.144	0.019	0.074	0.688	0.103	0.387	0.365	0.193
		N	41	41	41	41	41	41	41	41	41	41	41	41
Non-metal AA depletion	PM2.5	Pearson Correlation	-0.207	0.016	0.509	-0.122	-0.573	-0.457	-0.058	-0.271	-0.465	0.166	-0.265	-0.157
		Sig. (2-tailed)	0.382	0.948	0.022	0.607	0.008	0.043	0.808	0.249	0.039	0.485	0.258	0.510
		N	20	20	20	20	20	20	20	20	20	20	20	20
Metal-dependant AA depletion	PM10	Pearson Correlation	-0.339	-0.265	0.517	-0.196	0.025	-0.268	0.445	-0.058	0.226	-0.375	0.070	-0.136
		Sig. (2-tailed)	0.133	0.246	0.016	0.396	0.916	0.239	0.043	0.802	0.326	0.094	0.763	0.556
		N	21	21	21	21	21	21	21	21	21	21	21	21
Total AA depletion	All PM	Pearson Correlation	-0.334	-0.219	0.092	-0.401	-0.429	-0.644	-0.083	-0.443	-0.373	-0.322	-0.303	-0.218
		Sig. (2-tailed)	0.033	0.169	0.568	0.009	0.005	0.000	0.607	0.004	0.016	0.040	0.054	0.171
		N	41	41	41	41	41	41	41	41	41	41	41	41
Non-metal AA depletion	PM2.5	Pearson Correlation	-0.037	-0.064	0.565	-0.543	-0.574	-0.448	0.190	-0.422	-0.504	-0.322	-0.227	-0.165
		Sig. (2-tailed)	0.877	0.787	0.009	0.013	0.008	0.047	0.422	0.064	0.023	0.167	0.336	0.486
		N	20	20	20	20	20	20	20	20	20	20	20	20
Metal-dependant AA depletion	PM10	Pearson Correlation	-0.750	-0.437	-0.076	-0.469	-0.387	-0.753	-0.316	-0.590	-0.418	-0.634	-0.369	-0.476
		Sig. (2-tailed)	0.000	0.048	0.742	0.032	0.083	0.000	0.163	0.005	0.060	0.002	0.099	0.029
		N	21	21	21	21	21	21	21	21	21	21	21	21
Total AA depletion	All PM	Pearson Correlation	-0.138	-0.092	0.429	-0.026	-0.039	-0.073	0.305	0.127	-0.089	0.006	-0.010	-0.105
		Sig. (2-tailed)	0.390	0.568	0.005	0.873	0.807	0.652	0.053	0.428	0.580	0.971	0.952	0.512
		N	41	41	41	41	41	41	41	41	41	41	41	41
Non-metal AA depletion	PM2.5	Pearson Correlation	-0.201	0.043	0.298	0.099	-0.362	-0.294	-0.142	-0.110	-0.279	0.310	-0.185	-0.097
		Sig. (2-tailed)	0.396	0.858	0.202	0.679	0.117	0.209	0.549	0.645	0.234	0.184	0.434	0.684
		N	20	20	20	20	20	20	20	20	20	20	20	20
Metal-dependant AA depletion	PM10	Pearson Correlation	0.022	-0.047	0.500	0.030	0.191	0.087	0.538	0.205	0.385	-0.061	0.225	0.086
		Sig. (2-tailed)	0.924	0.838	0.021	0.898	0.408	0.707	0.012	0.372	0.084	0.793	0.327	0.710
		N	21	21	21	21	21	21	21	21	21	21	21	21

Exploring the active components in the DTT and AA depletions assays - Both 9,10-PQ (0.2-20 μM) and $CuSO_4$ (0.1-10 μM) elicited dose dependent losses of DTT (Figure 1.10) over a 1h incubation, with the former displaying the greatest depletion rates, resulting in complete loss of DTT at concentrations in excess of 1 μM. Similar dose dependant losses of AA were also observed with 9,10-PQ and $CuSO_4$ (Figure 1.11), though in this assay the rate of AA oxidation was in excess of that observed for DTT at equivalent molar concentrations. Co-incubation with the chelator DTPA completely abolished the Cu-induced oxidative loss of both AA and DTT (Figure 1.10 and 1.11), but had no measurable impact on the quinone dependent losses observed in either model system. The impact of metal and non-metal redox catalysts on both AA and DTT oxidation rates was examined further using a panel of model (carbon black and ROFA) and environmental PM samples ($PM_{2.5}$, PM_{10} and $PM_{2.5\text{-}10}$,). All particle types, with the exception of the negative control carbon black displayed dose dependent increases in oxidation rates (2 – 15 μg/mL), with the rate of DTT oxidation being in general in excess of that observed for AA (Figure 1.12). Addition of DTPA to each PM sample at the highest dose (15 μg/mL) elicited significant reductions in the observed oxidation rates in both assays (Table 1.5), indicating clear metal dependant contributions to the losses observed. Notably, however significant residual rates were also observed following the DTPA treatment indicative of non metal contributions (Table 1.5). A secondary consideration, regarding the practical application of these assays to the quantitative assessment of PM oxidative activity was their repeatability. Considering the data from all of the PM samples, and across all of the considered doses (Figure 1.12) the coefficients of variation based on each set of triplicate determination was 32.8 and 15.6% for the DTT and AA depletion assays respectively. The observed CVs were highest at the lowest PM doses and were reduced when only the highest dose was considered: 23.5% (DTT) and 3.9% (AA).

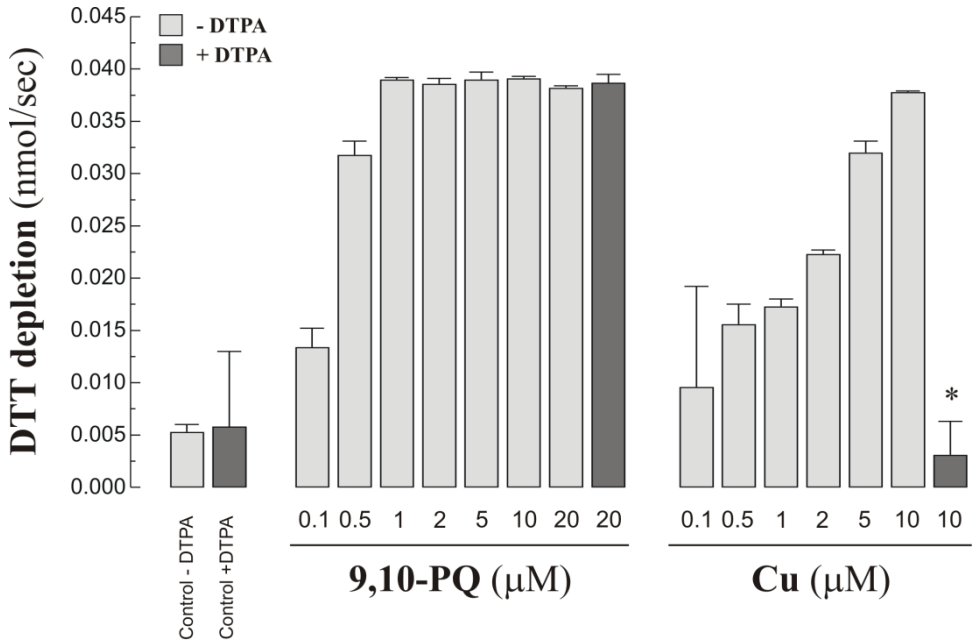

Figure 1.10: Dose dependant Cu ($CuSO_4$) and 9,10-phenathroquinone (9,10-PQ) dependent DTT oxidation rates, with and without the addition of DTPA (at the highest dose considered), relative to the particle free control. All data are represented as the mean ± 1SD of triplicate incubations with the comparison of rates plus and minus DTPA performed using an unpaired t-rest (*P<0.05). All of the DTT was oxidised after the 1h following incubation with 9,10-PQ at concentrations ≥ 1μM reflected by the levelling off of the observed oxidation rates.

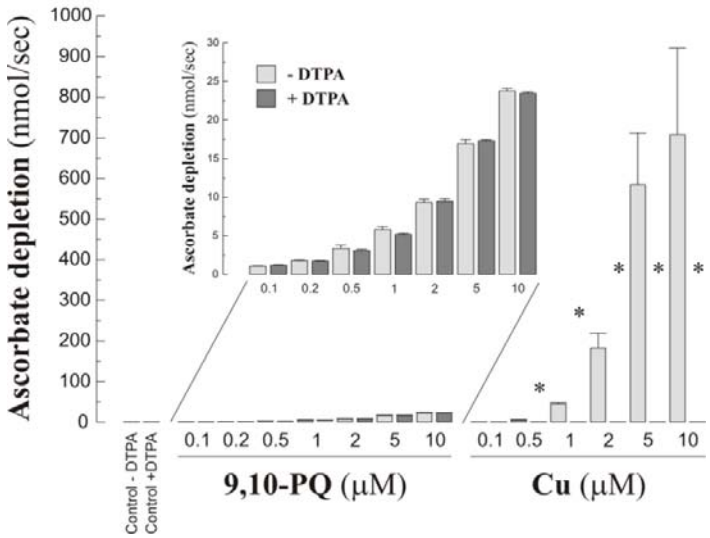

Figure 1.11: Ascorbate depletion rates with increasing doses of Cu ($CuSO_4$) and 9,10-phenathroquinone (9,10-PQ) with and without co-incubation with DTPA relative to a particle free control. All data are represented as the mean ± 1SD of triplicate incubations with the comparison of rates plus and minus DTPA performed using an unpaired t-rest (*P<0.05).

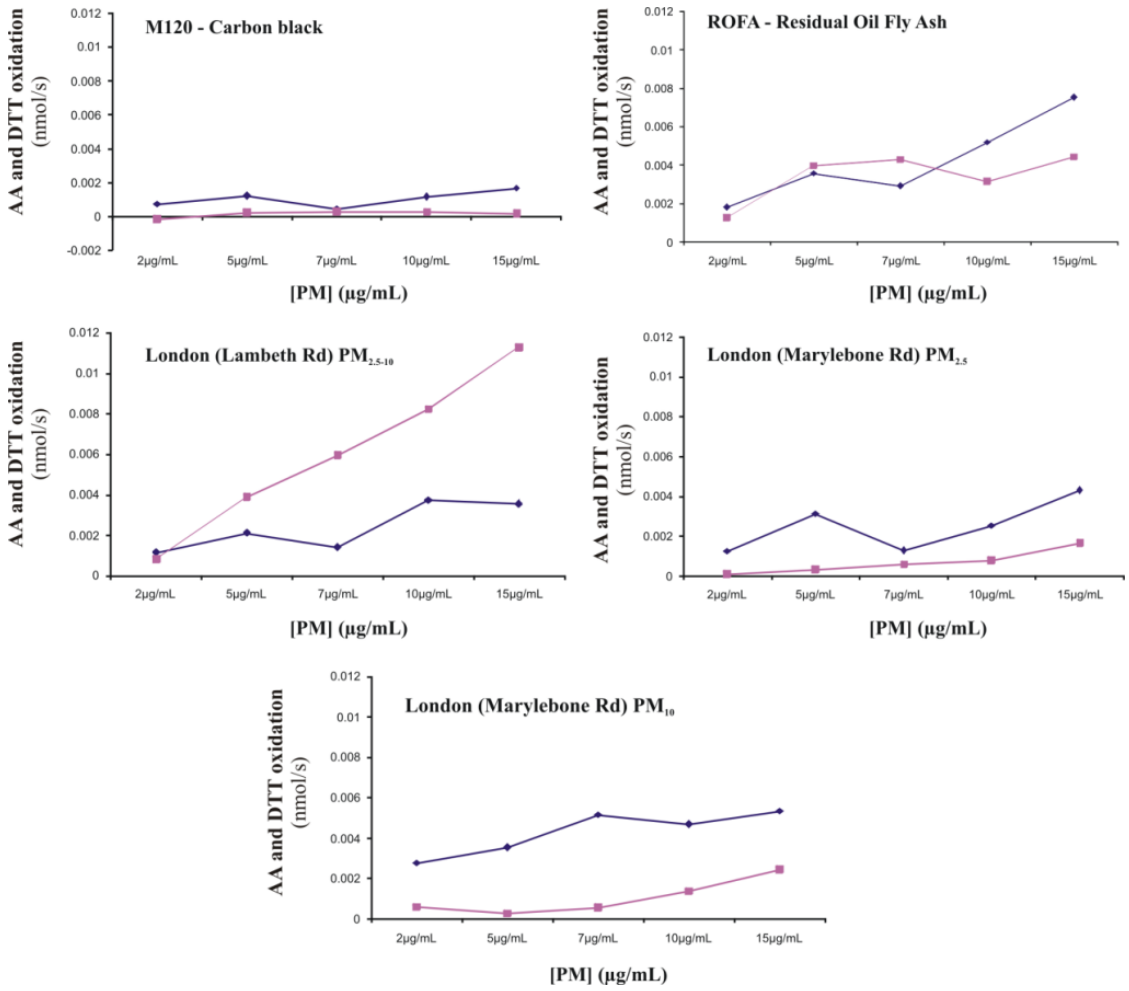

Figure 1.12: Rates of DTT (maroon squares) and AA (blue diamonds) oxidation over a range of concentration with a panel of model and environmental PM samples. All points represent the mean rate of triplicate incubations, following subtraction of the background auto-oxidation rate established in the particle free control.

Table 1.5: DTT and AA depletion rates (minus background auto-oxidation rates) for representative PM samples at 15 μg/mL, with and without co-incubation with the metal chelator DTPA (200 μM). All data represent the mean ± 1SD of triplicate determinations, with the % reduction in the rate following the addition of DTT indicated. Comparison of rates with and without DTPA was performed using an unpaired t-test with '*' indicting a P value of <0.05.

Particle Type	DTT oxidation (pmol/s)			AA oxidation (pmol/s)		
	-DTPA	+DTPA	%	-DTPA	+DTPA	%
M120 - Carbon black	1.66 ± 0.23	1.20 ± 0.13*	-27.9	-	-	-
Residual Oil Fly Ash	7.50 ± 0.50	1.79 ± 1.63*	-76.1	4.45 ± 0.05	0.99 ± 0.19*	-77.7
London $PM_{2.5-10}$	3.55 ± 2.57	1.29 ± 1.22*	-63.6	11.28 ± 0.15	0.33 ± 0.17*	-97.1
Marylebone Rd $PM_{2.5}$	4.32 ± 0.40	0.89 ± 0.42*	-79.5	1.66 ± 0.12	0.71 ± 0.42*	-57.2
Marylebone Rd PM_{10}	5.35 ± 0.45	1.70 ± 0.31*	-68.1	2.46 ± 0.15	0.60 ± 0.17*	-75.7

Discussion

In response to the increasing scientific consensus that the capacity of inhaled PM to cause oxidative stress is a primary pathway leading to the observed respiratory and cardiovascular responses seen in exposed populations (*Li et al, 2002; 2003*) numerous groups have developed assays that attempt to quantify the oxidative properties of ambient PM (*Oberdörster G, 2005; Ayres et al, 2008*). Various assays have been developed that provide some measure of PM oxidative potential, based on the capacity of particles, or particle extracts to oxidise a range of substrates (DNA (*Gilmour et al, 1995; Shi et al, 2006*), antioxidants (*Zeilinski et al, 1999; Mudway et al, 2004*) and fluorescent probes (Cohn et al, 2008)), or generate radicals (*Shi et al, 2003*), mostly in acellular systems (*Ayres et al, 2008*). Whilst all of these assays undoubtedly measure aspects of PM oxidative potential, little is known about how these various endpoints relate to one another, whether they display differential sensitivity to different pro-oxidants and redox catalysts, whether they're additive or complementary, or how prognostic they are of in vivo toxicity and ultimately the observed heath effects in exposed populations. Also, as these methods gain more widespread usage in large scale epidemiological studies, significant questions remain on the uncertainty inherent within these measurements and their applicability to high throughput analysis. It's clear however that if the oxidative potential metric is to be a value in formulating policy a better understanding of what is actually being measured is required with the ultimate aim of establishing robust gold standard methodologies that can be consistently applied and interpreted.

The current study examined the capacity of ambient $PM_{2.5}$ and PM_{10} obtained from a high traffic site in London (Marylebone Road) to drive oxidation reactions in vitro, as a proxy of their in vivo toxicity. PM oxidative potential was assessed in PM extracts derived from TEOM filters using a suite of commonly employed literature methods based on the oxidation of physiological antioxidants, ascorbate and glutathione (*Mudway et al, 2004; Zielinski et al, 1999*) and the dithiol DTT (*Cho et al ,2005*). In addition to this primary aim, the relationship between these measures of PM oxidative potential was examined and related to PM composition to address their comparability and establish whether they displayed differential sensitivity to PM pro-oxidant components: aqueous metals and quinones. We observed considerable temporal variation in the oxidative potential of both

$PM_{2.5}$ and PM_{10} samples from Marylebone Road, irrespective of which method was employed to establish this parameter, with evidence that the PM_{10} fraction had equivalent, or greater activity than parallel $PM_{2.5}$ collections. The two output measures of oxidative potential derived from the synthetic RTLF, OP^{AA}/μg and OP^{GSH}/μg were not simplistically associated, raising the possibility that a truer measure of total PM oxidative potential may be a sum of these two outputs (OP^{total}/μg). Consistent with this view the ascorbate depletion rate observed in the simple ascorbate-only model was found to be quantitatively associated with OP^{AA}/μg, but not OP^{GSH}/μg, whilst the opposite was true for DTT oxidation. This discrimination between the endpoints was reflected by differences in the pattern of associations observed with PM metals; with DTT oxidation and OP^{GSH}/μg being significantly associated with Cu, whilst OP^{AA}/μg and the ascorbate depletion rates displayed significant associations with barium.

The metals examined in the aqueous extracts were chosen to reflect known traffic sources related to exhaust and non-exhaust (tyre, brake and carriage wear) emissions (*Weckwerth et al, 2001; Harrison et al, 2003; deMiguel et al, 1997; Onianwa et al, 2001; Lashober et al, 2004; Manoli, 2002*). Whilst the contribution of non-exhaust PM to the airshed at roadside locations has been widely acknowledged, relatively few studies have investigated their contribution to the toxicity of ambient PM. Of these non-exhaust sources tyre wear is believed to be the largest (*Lukewille et al, 2001*), with published emission rates of 100μg/vehicle Km (*Boulter, 2006*), which are enhanced HGVs (*Legret and Pagotto, 1999*). Consistent with this Zn, which has been employed as a tyre wear tracer (*Fauser, 1999*) was found at the highest concentration in the PM samples examined. It's concentration was not however predictive of PM oxidative potential in any of the assays employed. In contrast Ba and Cu, both markers of brake wear (*Boulter, 2006, Sternbeck et al, 2002*) were shown to be associated with the OP, though the strength of the associations differed between the various assays and the PM fractions examined. Overall however it appeared as though non-exhaust sources of PM, specifically those attributable to brake wear were contributing significantly to the PM oxidative potential at this roadside location.

The association between the measured OP parameters and PM aqueous metal concentrations appeared to indicate that redox active metals and particularly Cu were associated with the oxidative consumption of DTT. Whilst the consumption of both GSH

and AA have been shown to be catalysed by redox active metals (*Buettner, 1990*), it has been previously argued that DTT oxidation was predominately reflective of PM quinone content and was insensitive to the action of metal catalysts (*Cho et al, 2005*). The consumption of DTT has been proposed to be based on the ability of quinones to catalyse the transfer of electrons from it to oxygen to generate superoxide, with the DTT molecule becoming oxidised to its disulphide form (*Kumagai et al, 2002*). Subsequently the superoxide produced and hydrogen peroxide formed via dismutation can further drive the oxidation of free thiols (*Paolicchi et al, 2002*). It has been reported that Fe and Cu are unlikely to contribute meaningfully to DTT oxidation as hydroxyl radicals would be generated via Fenton chemistry which are not reactive toward DTT (*Cho et al, 2002*). This claim appears flawed as hydroxyl radicals display a considerable reaction rate toward thiol groups (*Sjoberg et al, 198*2). In addition, urate a highly effective hydroxyl radical scavenger (*Kaur and Halliwell, 1990*) was not consumed in the synthetic RTLF models, suggesting that hydroxyl radicals were not formed to any great extent. The associations between the extent of DTT oxidation seen with PM samples and their aqueous metal content was also supported by evidence of its oxidation in the presence of Cu and the capacity of the metal chelators DTPA to significantly reduce the rate of DTT oxidation in a panel of model and ambient PM samples. This observation implies that the extent to which quinones contribute to the oxidative potential of ambient PM, where this has been muted to be significant *(Cho et al, 2005*) needs to be revisited. Our data do not however exclude the involvement of organic radicals/redox catalysts, as significant non-metal dependent OP signals were apparent in the AA depletion assay, as well as in the DTT assay when experiments were run in the presence of DTPA.

These data suggest that the information derived from the synthetic RTLF model captures that obtained separately in the DTT and ascorbate-only depletion assays. As this method has been well validated (Zielinski et al, 1999; *Mudway et al, 2004; Ayres et al, 2008*) and been shown to be highly repeatable this will remain our preferred method for assessing PM oxidative activity. In addition, ascorbate and glutathione depletion rates measured in the synthetic RTLF model are available for both NO_2 (*Kelly and Tetley, 1997*) and ozone (*Mudway and Kelly, 1998*), which raises the possibility of generating an expression for the total oxidative potential of the ambient airshed.

Conclusion

All three methods examined provided contrasts in OP between samples extracted from $PM_{2.5}$ and PM_{10} TEOM filters, with evidence that the OP was greatest in the $PM_{2.5-10}$ size range. It was notable that there was not a simplistic association between OP^{AA} and $OP^{GSH}/\mu g$ with the ambient PM concentration, nor between the two individual OP metrics. DTT oxidation was found to equate broadly with $OP^{GSH}/\mu g$ established in the synthetic RTLF model, whilst the ascorbate depletion rate was more reflective of the $OP^{AA}/\mu g$ metric. Co-incubations with DTPA indicated that upwards of 60% of the observed activity could be attributed to redox active metals, with aqueous Cu, Mn and Mo concentrations appearing the most strongly associated with the OP metrics measured at Marylebone Road. The associations between PM metals and the DTT oxidation rate contradicted the reported specificity of this assay for quinones /environmentally persistent free radicals. To confirm this we performed additional experiments that demonstrated that DDT is highly sensitive to both quinone and Cu driven oxidation and that PM-induced DTT losses could be inhibited using DTPA. In light of these data there is a need to revisit those studies that have employed the DTT assay and attributed the measured oxidative activity observed solely to non-metal sources. Overall these studies support the use of the synthetic RTLF model to obtain measures of PM oxidative potential, based on a single incubation, rather than the application of numerous separate assays with the associated increase in variability.

Policy relevance

Whilst there is a consensus that ambient PM oxidative potential represents a new and potentially important 'health relevant' metric there is no definitive gold standard for its determination. At one level if all the methods produced similarly weighted endpoints this would not be a problem, but this information is simply not known. It is also unclear whether different methods are more-or-less sensitive to certain PM components or size fractions making the drawing of policy relevant conclusions from previously published studies difficult. The work presented in Part I of this report represents the first systematic attempt to address these issues and has highlighted both where the established methods agree and disagree, as well as highlighting errors in previous perceptions of the specificity of certain assays for pro-oxidant species. These data will permit a more coherent review of the PM oxidative potential literature, as well as less biased interpretation of the contribution of PM components to the biological activity of ambient particulates.

PART II - Quantifying the London Specific Component of PM_{10} Oxidative Activity

Abstract

Exposure to traffic related pollutants, particularly particulate matter has been associated with impaired lung growth and increased rates of allergic and respiratory symptoms in both children and adults. Whilst PM concentrations and numbers are enhanced at the roadside, the composition and hence the potential toxicity of particles at high traffic sites are also likely to contribute to the enhanced health effects reported in the literature. To establish the contribution that roadside PM emissions make to the oxidative potential of the London urban airshed we performed a classic Lenschow analysis using PM_{10} TEOM filters collected from three sites over a full calendar year, Jan 2008 – Jan 2009, representing rural (*Harwell*), urban background (*North Kensington*) and roadside (*Marylebone Road*) site classifications. PM extracted from these samples were then analysed to assess their intrinsic oxidative potential and quantify their aqueous and total metal content. The local roadside contributions to these measurements were then calculated based on the subtraction of the rural and urban background activities and concentrations. A clear increment was observed in the annual mean rural and urban (background and roadside) OP^{AA}/μg values: 0.64±0.28 vs. 1.11±0.25 and 1.24±0.21 respectively. Overall the rural and urban background contributions to the ascorbate-dependent oxidative potential at the roadside site were 51.3 and 37.9%, implying that only 10.8% of the signal was attributable to local sources. No statistical difference was apparent in this measure between the urban background and roadside sites until the data were expressed per volume of air (OP^{AA}/m^3): 20.40±7.57 vs. 45.05±14.38, reflecting the mass increment between the two site types. In contrast, significant differences were observed for OP^{GSH}/μg between each of the sites: 0.15±0.13 (rural), 0.42±0.17 (urban background) and 0.65±0.18 (roadside), with 34.5% of the measure attributable to local roadside sources. This proportion of the measured signal increased to 68.5% once the data were expressed per m^3. This data suggested that the OP^{GSH} metric was more strongly associated with PM components with limited dispersion from the roadside, whilst OP^{AA} was sensitive to components more widely dispersed through the urban airshed. Consistent with this view OP^{GSH}/μg was strongly associated with a panel of metals (Cu, Sb, Fe, Mn and Mo) reflecting non-exhaust vehicle contributions to the roadside airshed, with a clear brake wear signature based on the Cu:Sb ratio. These associations were not apparent at either the

background or rural sites consistent with a lack of dispersion. In contrast OP^{AA}/μg was associated with PM_{10} Ni, V and Cr content, at both the roadside and urban background sites indicative of a more dispersed source. These data therefore demonstrate a clear increment in the OP of roadside PM_{10} in London ranging from 50-70% when expressed per m^3. In addition they clearly show that the ascorbate and glutathione OP metrics display differential sensitivity to PM components, reflective of different PM sources, with OP^{GSH}/μg sensitive to non-exhaust abrasion derived PM and OP^{AA}/μg PM derived from oil combustion.

Key words: Oxidative potential, PM_{10}, Lenschow, Road side, urban background, rural, source appointment, metals, vehicular abrasion, oil combustion

Figures

Figure 2.10: Total and aqueous PM_{10} Fe concentrations at Marylebone Road, North Kensington and Harwell, Jan 2008 – 2009.

Figure 2.11: Relationship between measures of oxidative potential expressed per μg of filter extracted PM_{10} with total Fe concentrations at Marylebone Road between Jan 2008 and Jan 2009.

Figure 2.12: Total and aqueous PM_{10} Mo concentrations at Marylebone Road, North Kensington and Harwell, Jan 2008 – 2009.

Figure 2.13: Relationship between measures of oxidative potential expressed per μg of filter extracted PM_{10} with total Mo concentrations at Marylebone Road between Jan 2008 and Jan 2009.

Figure 2.14: Total and aqueous PM_{10} Mn concentrations at Marylebone Road, North Kensington and Harwell, Jan 2008 – 2009.

Figure 2.15: Relationship between measures of oxidative potential expressed per μg of filter extracted PM_{10} with total Mn concentrations at Marylebone Road between Jan 2008 and Jan 2009.

Figure 2.16: Total and aqueous PM_{10} Sr concentrations at Marylebone Road, North Kensington and Harwell, Jan 2008 – 2009.

Figure 2.17: Total and aqueous PM_{10} Ba concentrations at Marylebone Road, North Kensington and Harwell, Jan 2008 – 2009.

Figure 2.18: Relationship between measures of oxidative potential expressed per μg of filter extracted PM_{10} with total Ba concentrations at Marylebone Road between Jan 2008 and Jan 2009.

Figure 2.19: Total and aqueous PM_{10} Zn concentrations at Marylebone Road, North Kensington and Harwell, Jan 2008 – 2009.

Figure 2.20: Relationship between measures of oxidative potential expressed per μg of filter extracted PM_{10} with total Zn concentrations at Marylebone Road between Jan 2008 and Jan 2009.

Figure 2.21: Total and aqueous PM_{10} Ni concentrations at Marylebone Road, North Kensington and Harwell, Jan 2008 – 2009.

Figure 2.22: Total and aqueous PM_{10} Cr concentrations at Marylebone Road, North Kensington and Harwell, Jan 2008 – 2009.

Figure 2.23: Relationship between measures of oxidative potential expressed per μg of filter extracted PM_{10} with total Cr concentrations at Marylebone Road between Jan 2008 and Jan 2009.

Figure 2.24: Total and aqueous PM_{10} V concentrations at Marylebone Road, North Kensington and Harwell, Jan 2008 – 2009.

Figure 2.25: Relationship between measures of oxidative potential expressed per μg of filter extracted PM_{10} with total V concentrations at Marylebone Road between Jan 2008 and Jan 2009.

Figure 2.26: Total and aqueous PM_{10} Cu concentrations at Marylebone Road, North Kensington and Harwell, Jan 2008 – 2009.

Figure 2.27: Relationship between measures of oxidative potential expressed per μg of filter extracted PM_{10} with total Cu concentrations at Marylebone Road between Jan 2008 and Jan 2009.

Figure 2.28: Total and aqueous PM_{10} Sb concentrations at Marylebone Road, North Kensington and Harwell, Jan 2008 – 2009.

Figure 2.29: Relationship between measures of oxidative potential expressed per μg of filter extracted PM_{10} with total Sb concentrations at Marylebone Road between Jan 2008 and Jan 2009.

Figure 2.30: Total and aqueous PM_{10} Al concentrations at Marylebone Road, North Kensington and Harwell, Jan 2008 – 2009.

Figure 2.31: Relationship between measures of oxidative potential expressed per μg of filter extracted PM_{10} with total Al concentrations at Marylebone Road between Jan 2008 and Jan 2009.

Figure 2.32: Total and aqueous PM_{10} Pb concentrations at Marylebone Road, North Kensington and Harwell, Jan 2008 – 2009.

Figure 2.33: Relationship between measures of oxidative potential expressed per μg of filter extracted PM_{10} with total Pb concentrations at Marylebone Road between Jan 2008 and Jan 2009.

Tables

Table 2.12: Associations between PM_{10} Al concentrations, both total and aqueous with measures of oxidative potential (OP^{AA}, OP^{GSH} and OP^{TOT} per μg and m^3).

Table 2.13: Associations between PM_{10} Pb concentrations, both total and aqueous with measures of oxidative potential (OP^{AA}, OP^{GSH} and OP^{TOT} per μg and m^3).

Table 2.14: Correlation matrix illustrating the association (Spearman Rank Order correlation) between roadside PM10 oxidative potential (OP^{AA} and OP^{GSH} per μg and m^3) with roadside PM_{10} metal content at Marylebone Road, Jan 2008 – Jan 2009.

Table 2.15: Correlation matrix illustrating the association between the true urban background PM_{10} oxidative potential (OP^{AA} and OP^{GSH}) and metal content at the North Kensington, Jan 2008 – Jan 2009.

Table 2.16: Correlation matrix illustrating the association (Spearman Rank Order correlation) between PM_{10} oxidative potential (OP^{AA} and OP^{GSH}) and metal content at the rural background site at Harwell, Oxfordshire, Jan 2008 – Jan 2009.

Aims

In the first section of this report we indentified a preferred method for assessing the oxidative activity of ambient PM_{10} based on the incubation of PM samples extracted from TEOM filters in a synthetic RTLF. Here we report the use of this model to refine our understanding of the actual contribution local traffic sources make to the oxidative potential of the particulate airshed in the urban environment, both the roadside micro-environment and the urban background. To achieve this, we employed the Lenschow approach, examining PM_{10} oxidative activity at three sentinel sites reflecting the rural, urban background and roadside environment over a full calendar year, Jan 2008 –Jan 2009. To further interrogate the likely source determinants of the measured ascorbate and glutathione dependent OP's, total and aqueous metal concentrations were also measured. In addition, the relationship between the OP metrics and wind direction was explored at the roadside site to further characterise the likely sources contributing to these measures. We hypothesised that PM OP at roadside sites would be enhanced relative to the urban background and that this would reflect the enrichment of the PM with traffic derived pro-oxidant components.

Background

In the UK emissions from road traffic represent a significant proportion of the PM airshed within urban areas, with primary traffic related PM further elevated at the roadside (*Charron et al., 2007*). The significance of the increased PM numbers and concentrations at roadside locations is highlighted by a growing body of literature demonstrating enhanced negative health impacts in individuals with high exposures in these environments, either through residence (*Morgenstern et al, 2008*), school attendance (*Janssen et al, 2003*), or occupation (*Ingle et al, 2005*). Children attending schools, or living in close to busy roads have been shown to have impaired lung function/growth and increased rates of allergic and respiratory symptoms (*Janssen et al, 2003; Nicolai et al, 2003; Gauderman et al, 2004 and 2005; van Vliet et al, 1997; Dales et al, 2008; Oftedal et al, 2008; Migliore et al 2009*). This linkage is supported by the observed inverse relationship between children's lung function with traffic density (*Wjst et al, 1993*) and between the magnitudes of symptoms with the distance of roads from residential or school sites (*Kim et al, 2008; Morgenstern et al, 2008*). Similar negative impacts on lung function and allergic airway disease have also been observed in adults resident in areas characterised by high traffic (*Sekine et al, 2004; Cesaroni et al, 2008*).

In the majority of these studies, in addition to traffic density, the greatest health impacts have been reported to be associated with roads carrying a high proportion of diesel powered heavy and light goods vehicles (*Janssen et al, 2003; Brunekreef et al, 1997*). Consistent with these observational studies, diesel exhaust emissions have been shown to elicit pulmonary inflammation (*Salvi et al, 1999*), impaired lung function (*Stenfors et al, 2004*) and alterations in vascular tone (*Mills et al, 2007*) in controlled human exposure studies, as well as real world exposure scenarios (*McCreaner et al, 2007*). In these studies the symptomatic responses observed have been attributed in part to the oxidative properties of the exhaust PM (*Mudway et al, 2004*), via the induction of intra-cellular redox sensitive signal pathways (*Pourazar et al, 2005*). Whilst it's clear that diesel exhaust PM is bioactive in vivo, it should also be noted that the airshed at roadside environments comprises not only of primary tail pipe emissions, largely elemental and organic carbon, but also has significant contributions from brake wear, tyre wear, road surface abrasion and

resuspension in the wake of passing traffic (*Thorpe and Harrison, 2008*). These later non-exhaust sources, often characterised by elevated concentrations of transition metals (reviewed in *Zechmeister et al, 2005*), have been estimated to account for approximately half of the PM concentration observed at the roadside (*Querol et al., 2004; Lenschow et al, 2001; Harrison et al, 2001*), and often predominate in countries with significant road sanding and studded tyre use during the Winter months (*Omstedt et al., 2005; Forsberg et al., 2005*). The potential contribution of these components to the observed health effects is largely ignored at regulatory level, which focuses on the reduction of tail pipe emissions through improvements in engine technology.

The potential significance of these non-exhaust PM sources arises from the fact that many of the metal components associated with brake and mechanical wear processes (Fe, Cu, Ni, Mo, Mn etc, (*Schauer et al, 2006; Garg et al, 2000; Boulter, 2006; Zechmeister et al, 2005*) are redox catalysts capable of generating reactive oxygen species in vivo (*Valko et al, 2005*). As the capacity of inhaled PM to elicit inflammation and injury at the air-lung interface has been attributed to their capacity to induce oxidative stress (Kelly, 2003; *Xia et al, 2006; Ayres et al, 2008*), metals from these sources are likely to contribute significantly to the toxicity of PM in the urban airshed. Despite this, these metals and their traffic sources are currently unregulated. In a recent study we demonstrated that the oxidative potential of PM_{10} in London was enhanced in samples collected from roadside environments relative to urban background locations (*Kelly et al, 2009*), reflecting an enrichment in these samples of Cu and Ba, markers of brake wear (*Schauer et al, 2006; Garg et al, 2000; Boulter, 2006*). Moreover, the PM_{10} oxidative potential appeared to increase over the 6 years of the study at Marylebone Road, paralleling an increase in aqueous Cu concentrations (*Kelly et al, 2009*). These data viewed in the context of the increase in primary PM_{10}, also observed at roadside sites in London (*Fuller and Green, 2006*) and throughout Europe (*Harrison et al, 2008*) suggest that non-tailpipe sources of PM have partially offset the gains predicted to have occurred through improved engine technology. Furthermore, they suggest a relative increase in the metal content of roadside PM, which would be predicted to increase the toxicity of roadside PM on a per unit mass basis.

In light of these concerns in the present study we sought to clarify the contribution of roadside derived PM to the oxidative potential and composition of London's airshed. To

isolate the actual roadside contribution we adopted the experimental approach of Lenschow (*Lenschow et al, 2001*), performing parallel sampling campaigns at roadside, urban background and rural sentinel sites. We focused on assessment of PM_{10} ascorbate and glutathione dependent oxidative potentials (OP^{AA} and OP^{GSH}), expressed per unit mass of extracted PM (μg), or per unit volume of sampled air (m^3), as well as total and water soluble metal concentrations. The metals examined were selected to provide information on a range of non-tail pipe traffic sources: road dust resuspension (Fe, Al, Ca) (*Viana M et al., 2008*), tyre (Zn) (*Legret and Pagotto, 1999*) and brake abrasion (Cu, Ba, Sb) (*Sternbeck et al 2002; Boulter, 2006; Garg et al, 2000*), as well as oil/fuel combustion processes, either as trace elements or fuel additives (Mn, Pb, Cr, Ni and V) (*Viana M et al., 2008*). Embedded within this design was the potential to examine the PM compositional determinants of the OP metrics, to further clarify and validate the observations made in Part I of this report

Methods

Study area and sampling description - Sampling was performed between Jan 2008 and Jan 2009 at three locations in the South of England, reflecting rural, urban background and roadside site classifications. The rural site (away from major population centres, roads, industrial areas or other pollution sources) was situated in Harwell, Oxfordshire (Building 573.2, Harwell Laboratory, Didcot, Oxfordshire, OX11 0RA). Both the urban (away from major sources and broadly representative of town/city-wide background concentrations) background and roadside site (with sample inlets between 1m and 5m of the kerbside) were located within London, North Kensington and Marylebone Road respectively, with full site details available via the London Air Quality Network website (http://www.londonair.org.uk).

Details of the filter archive - A full set of TEOM PM_{10} filters were obtained from each of the sites examined in this study covering the full calendar year Jan 2008 – Jan 2009. Filters once collected from the monitoring stations were placed in 50mL Falcon tubes and transferred to King's College London (by post from Harwell) prior to storage in a temperature controlled room (4^oC). All subsequent extractions were performed in these tubes to minimise losses of material from the filters during transport.

Chemicals and Chelex-resin treated water preparation - All chemicals were obtained from Sigma Chemical Company Ltd (Poole, UK) and were of high pressure liquid chromatography (HPLC) grade unless otherwise stated, Water for PM chemical composition and oxidative potential analysis was deionised and ultra-filtered using an Elga-stat filtration system, In addition, prior to use all water was further treated with Chelex-100 resin to reduce background metal contamination. Removal of contaminating metals from the water-methanol mixture was achieved by the addition of 3g of Chelex-100 resin per 100 mL, with over-night stirring at 4^oC. The resin was then removed by centrifugation (3,000 rpm for 15 minutes, 4^oC) and the purified 5% methanol solution carefully decanted. Prior to use the pH of the water-methanol solution was adjusted to neutrality using Chelex resin treated 1M HCl or 1M NaOH.

Extraction and re-suspension of TEOM filter PM -TEOM filters were extracted using the methodology outlined in Part I of this report. Samples were prepared and archived (-80^{o}C) at either 150 or 55.56 μg/mL for determination of metals by ICP-MS and oxidative potential in the synthetic RTLF model respectively. Once PM samples had been re-suspended, the pH of the resultant suspension was checked and where necessary the pH was adjusted to 7 as outlined above, prior to their use in the incubation protocols.

Measuring PM oxidative activities in the synthetic RTLF model - All incubations in the synthetic RTLF were performed as outlined in the previous section of this report at a standardised final concentration in the incubation vessels of 50 μg/mL. All incubations were performed at 37^{o}C and at pH 7. To guarantee inter-assay standardisation, known particle and particle free controls (positive: residual oil fly ash; negative: carbon black) were run in parallel with the filter extracted PM samples in each batch. Compositional details of the control particles used in these incubations have been published previously (*Miller et al, 1998; Zielinski et al, 1999*).

ICP-MS analysis of PM extracts - Both aqueous and total metals were determined by ICP-MS. For the determination of aqueous metal concentrations 1-2 mL of the particle suspensions (150 μg/mL) prepared in Chelex100-resin treated ultra-pure water (containing 5% HPLC-grade methanol) were centrifuged at 13,000 rpm for 1 h (4^{o}C) to remove particles. To ensure the removal of all particulate material prior to analysis the resultant supernatant was passed through Anotop-0.02μm Whatman filters. A volume of the filtrate (0.9 mL) was then added to an equal volume of Chelex-100 resin treated water prior to analysis by ICP-MS. Samples were then transferred to the Mass Spectroscopy Unit at King's College London for the quantification of Al (*isotope* 27*; natural abundance* 100%), Ba (135; 6.592%), Cu (63; 69.15%), Fe (56; 91.72%), Mn (55; 100%), Mo (95; 15.92%), Ni (60; 26.223%), Pb (208; 52.4%), Cr (52; 83.789%), Sr (88; 82.58%), V (50; 0.25%), Sb (121; 57.36%) and Zn (56; 91.72%) by ICP-MS using a ELAN DRC ICP-MS (MSF008). The selected isotopes were chosen to avoid known potential isotopic interferences. The potential ArO+ interference for the major isotope of iron (^{56}Fe) was removed using the dynamic reaction cell through its reaction with ammonia. Elemental concentrations were determined with reference to a 7-point standard curve based on an ICP multi element standard solution VI CertiPUR® (Merck, Lot. No. OC529648). Antimony which is not present in this multi-elemental standard was analysed against its own standard curve

(Antimony ICP standard , MERCK). All concentrations were corrected for the background elemental concentrations determined in the Chelex-100 resin treated water blank ran in parallel to each batch of samples. Each batch of samples were also ran in parallel to purified water blanks, as well as aqueous extracts derived from ROFA and a stock environmental $PM_{2.5-10}$ sample (both derived from a 150 μg/mL stock suspension) collected from London. The London sample was ran to provide Fe and Cu measurements, as these metals were in low abundance in the aqueous extract obtained from the ROFA sample. These controls, plus one of the dilutions of the certified multi-elemental standard were interspersed at set intervals throughout the experimental run to provide information on the potential drift in instrument sensitivity throughout the run. For total metal determinations 100 μL of the 150 μg/mL PM stock suspensions were digested in 0.9 mL of dilute Aqua Regia (1:3 HNO_3(60%):HCl (30%)) in sealed Teflon vessels in a hot water bath at 90°C for 90 minutes. At the end of this acid digestion the resultant solution was further diluted with 6 ml of HPLC grade water to achieve final concentrations of 1.69% HNO_3, 2.53% HCl and 2.14 μg/mL PM. Thereafter the acid extracts were analyzed as outlined above for the aqueous extracts, with digestion blanks (prepared using 100 μl of the purified water, 5% methanol solution used for the PM re-suspensions) and NIST 1648a samples digested using the same procedure, analyzed at regular intervals throughout the experimental run to estimate the extraction efficiency of the method and potential instrument drift. All digestion vessels and pipette tips that came into contact with the PM suspensions in either protocol were acid washed in 2% HNO_3 prior to use.

Data analysis and statistics - SPSS for windows (version 16) was used for all statistical analyses. For the purposes of accepting data as normally distributed we required values of skewness and kurtosis to be less than 1. Using these criteria and with reference to normality plots all measures of oxidative potential and PM metal concentrations were found to be highly skewed, either when expressed per unit mass of extracted PM_{10} or per m^3. Consequentially all the data are reported as median values with inter-quartile ranges and the Spearman rank order correlation was employed to examine the relationship between PM OP, co-pollutant concentrations and aqueous/total metals. Comparison of median PM OPs or metal concentrations was performed using Kruskal-Wallis H-test, prior to post-hoc testing using the Mann Whitney U test.

To derive roadside (*rs*) increments of the measured parameters, or measures of the 'true' urban background a simple subtractive approach was adopted. Generally monthly sampling periods at the rural and urban background sites, coincided with the 4 weekly filter collections at the roadside site, such that a single background value could be subtracted from 4 separate roadside measurements to derive the *rs* increment. Where dates failed to coincide, the degree of overlap between the weekly filters and the consecutive monthly filters was used which of the background periods was subtracted from the 7-day value.

To attempt to discriminate the main pollution sources in this study, factor analysis was performed employing a varimax rotated component matrix using the elemental data from all filters across each site, as well as on a site-by-site basis. Such factor analysis uncovers latent structures within a set of variables, based on the strength of their internal correlations, which can then be attributed sources; though the actual source attribution is subjective and often varies markedly between studies for similar groupings of components (reviewed in *Viana et al., 2008*). Whilst this approach has been widely employed (*Viana et al., 2008*) it should be noted that considerable debate exists about the required sample size requirements for a robust PCA analysis (*Osborne and Costello, 2004*), with the general contention that sample sizes of between 50 – 100 are not ideal. Additionally, the components identified by these analyses most likely reflect mixed, rather than discrete sources and thus the sources can only be generalised and must be regarded with caution. Thus whilst these results are described on a site by site basis in this report, the results should be interpreted with caution, especially for the urban background and rural sites due to the limited number of data points available.

Results

A full set of TEOM PM_{10} filters were obtained from each of the three sites examined covering the full calendar year Jan 2008 – Jan 2009. This included 16 filters from Harwell (02/01/08 – 14/01/09), including one filter, which was excluded, covering an approximate 4 hour collection (27/02/08, 8:30 am – 27/02/08, 11:45 am – collected mass of PM_{10} 10.58 μg). The mean (SD) collection interval for each filter was 25.2±9.9 days, with intervals ranging from 7-35 days and the collected mass of PM_{10} ranging from 306.8 – 2332.4 μg. Fifteen filters were obtained from the North Kensington urban background site over the identical period, with the mean collection interval being 21.1±6.2 days, ranging from 7-28 days, with filters containing 482.5 – 2414.37 μg PM_{10}. Fifty-six filters were collected from the roadside Marylebone Road site, covering collection intervals of between 7-14 days (mean interval 6.8±2.0 days), with individual filter PM_{10} masses varying from 231.1 – 2633.5 μg. PM extracted from these filters were re-suspended at 55.56 and 150 μg/ml in a purified water, methanol (5% v/v) solution for the subsequent determination of PM oxidative potential and total/ aqueous metal concentrations respectively.

The time series of PM_{10} ascorbate and glutathione dependent OPs (per unit mass and m^3) from the roadside, urban background and rural sites are illustrated in *Figure 2.1*, with the statistical comparison of the annual values shown in *Figure 2.2*. These data demonstrate clear increments between OP^{AA} and OP^{GSH} expressed per m^3 of PM_{10} between the roadside site (MY1) and the urban background (KC1), and between the rural (HA1) and urban background (KC1) locations, with OP at the later two sites tracking each other closely over the period examined (*Figure 2.1*). The increments between the roadside and urban background site ascorbate and glutathione dependent OPs were less clear cut when the data were examined on a per unit mass of PM_{10} basis. Whilst annual OP^{GSH}/μg differed significantly between each of the site types (*Figure 2.2*), it was clear from the temporal profile in *Figure 2.1*, that the roadside to urban background increment was most marked during the summer to early autumn period (mid June – late October), with considerable overlap in activities over the winter period. For OP^{AA}/μg no significant roadside annual increment was observed over the activities measured at KC1, *Figure 2.1*, though there was again evidence of a June – August increment at MY1.

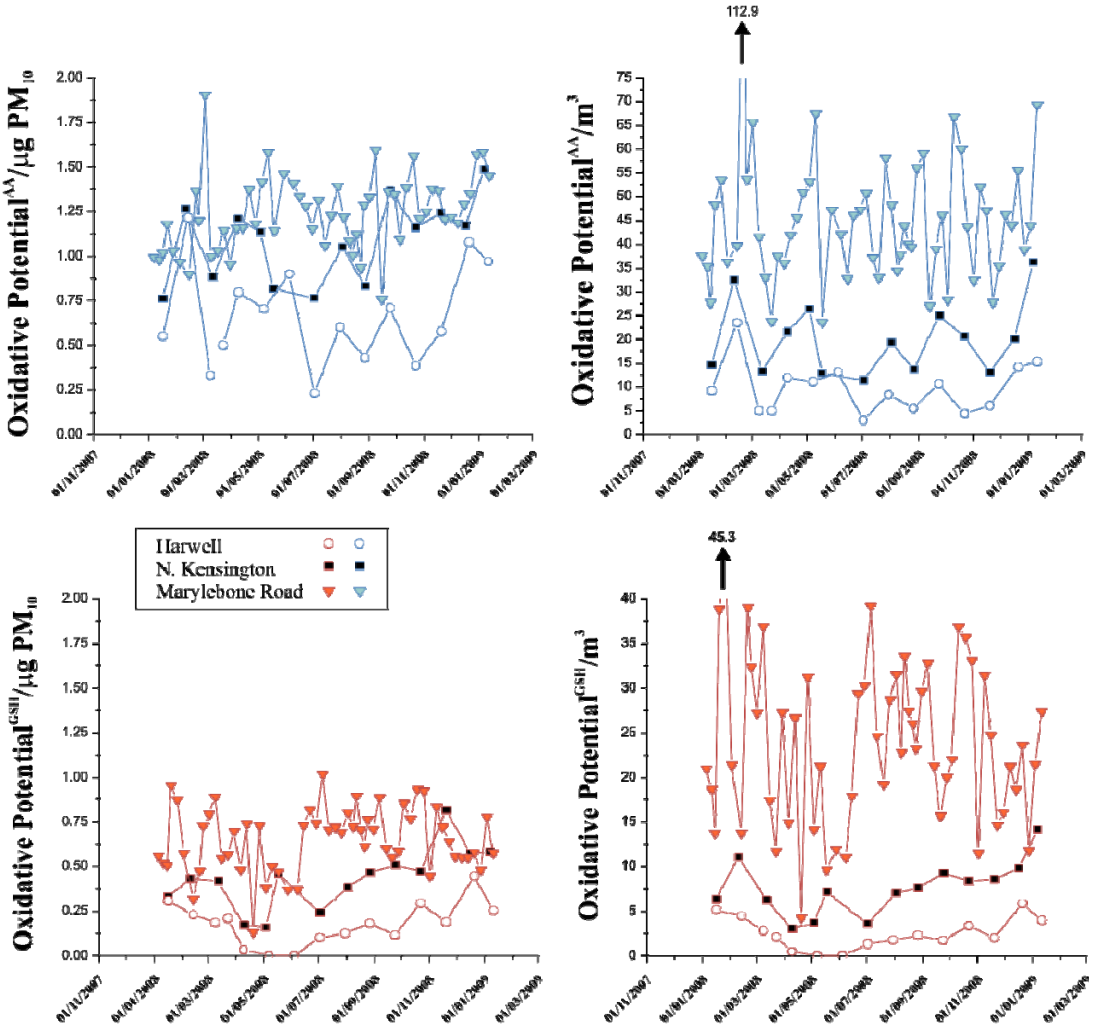

Figure 2.1: Temporal trends in PM_{10} oxidative potential (OP) at Marylebone Road (MY1 - inner London roadside site), North Kensington (KC1 - London urban background) and Harwell (HA1 - rural site, Oxfordshire) from Jan 2008 – Jan 2009. Ascorbate and glutathione dependent OPs are illustrated expressed per unit mass (left hand panel) of PM_{10} or per m^3 (left hand panel). All data points represent the mean of triplicate incubations. In all cases the SD was less than 5% of the mean value. Each data point is plotted to the mid date covered by the sampling interval over which the filter was collected.

Based on these data the overall rural and urban background contributions to the OP^{AA}/µg at the roadside site were 51.3 and 37.9%, implying that only 10.8% of the signal was attributable to locally produced sources. This roadside contribution to the ascorbate dependent OP increased to 54.7% when the data was expressed per m^3, reflecting the PM_{10} concentration increment at this site relative to the North Kensington urban background. In contrast, for OP^{GSH}/µg at MY1 34.8% of the signal was attributable to local roadside

sources (23.4% and 41.8% rural and urban background contributions respectively). This proportion of the measured signal increased to 68.5% once the data were expressed per m^3. This data suggested that the OP^{GSH} metric was more strongly associated with PM components with limited dispersion from the roadside, whilst OP^{AA} was sensitive to components more widely dispersed throughout the urban airshed.

As was noted previously in Part I of this report there was no statistically significant relationship between OP^{AA} and OP^{GSH}/μg with the average PM_{10} concentrations observed across each of the sampling intervals for any of the site classifications, F*igure 2.3*. Furthermore, ascorbate and glutathione dependent OPs expressed per unit mass were not simplistically related at any of the three sites, *Figure 2.4*. Based on the assumption that OP^{GSH} and OP^{AA} therefore reflect the contribution of different PM-associated components to the overall oxidative activity of the PM airshed we derived a total expression, OP^{TOT}, expressed both per μg and m^3 of PM_{10}, which demonstrated significant increments between the rural (lowest OP), urban background and roadside (highest OP) sites, *Figure 2.2*. Using this overall measure of OP, local roadside PM emissions contributed 19% to the observed activity on a per unit mass basis, increasing to 59.5% when expressed per m^3.

To isolate the roadside specific (*rs*) contribution to PM_{10} oxidative potential at Marylebone Road, we subtracted the values observed at the nearby urban background site at North Kensington. As the background site OP values were derived from filters covering 4-5weeks, whilst the PM_{10} samples from MY1 were derived from 7 day collections, each of the roadside filters had a single background OP value substrated corresponding each overlapping background period, *Figure 2.5*. Figure 2.5 illustrates the impact of this approach on the strength of the relationship between OP^{AA} and OP^{GSH}/μg, which as outlined above was not significant (r=-0.009 – Spearman's Rank Order Correlation). Removal of the background ascorbate and glutathione dependent OP values resulted in an improved relationship between these two metrics at MY1: *rs*OP^{AA}/μg versus *rs*OP^{GSH}/μg, r=0.310, P<0.05. The temporal relationship between these two *rs*OP metrics appeared good throughout the majority of the year, but began to deviate between Nov 2008 – Jan 2009.

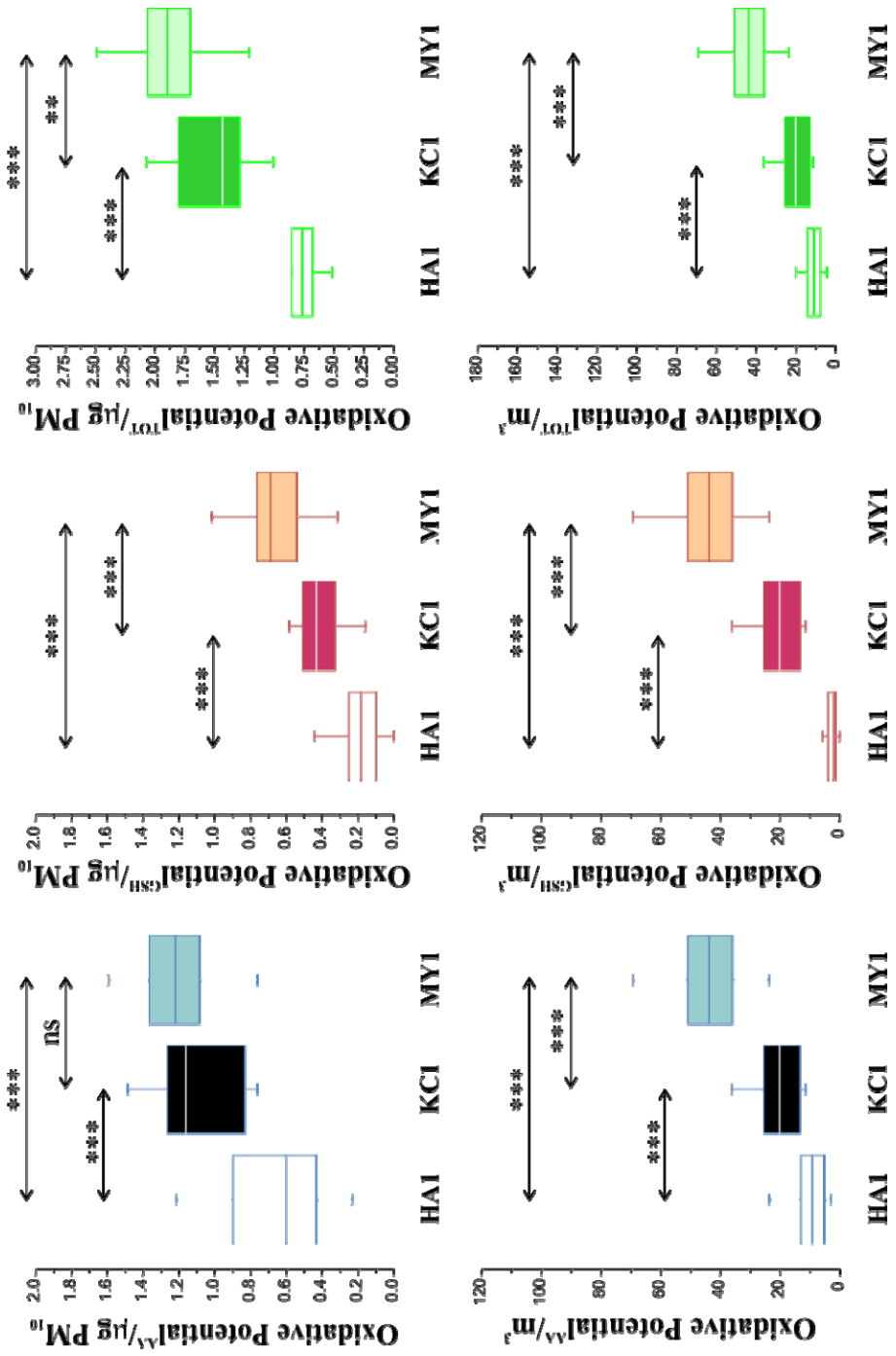

Figure 2.2: Annual contrasts in PM_{10} OP (per µg and per m^3) between the inner London roadside (MY1, n=56) and background site (KC1, n=15) with the samples obtained from the rural location (HA1, n=15). Contrasts are illustrated for OP^{AA} and OP^{GSH}, as well as aggregated into a total measurement (OP^{TOT}). Data are presented as box plots with the median represented as a solid line, the 25 and 75th percentiles as the upper and lower boundaries of the box and the 95th percent confidence intervals by the whiskers. Data were initially analysed using the Kruskal-Wallis H-test, prior to post-hoc testing using the Mann Whitney U test. Results of these analyses are highlights above: P<0.05 *; P<0.01 **; P<0.001 ***.

To further explore the relationship between OP^{AA}/μg and OP^{GSH}/μg, with traffic derived pollutants at Marylebone Road we examined their association with NOx concentrations, both with and without the removal of the urban background signal. Significant associations were observed between OP^{GSH}/μg with NOx (r-0.405, P<0.01), but not with OP^{AA}/μg (r=-0.171), *Figure 2.6*. Removal of the background values significantly strengthen the association between *rs*OP^{GSH}/μg with *rs*NOx (r-0.556, P<0.001) and revealed a weak association with *rs*OP^{AA}/μg (r=0.296, P<0.05) suggesting that the glutathione OP measurement was the most sensitive to PM components derived from the roadside environment, whist the ascorbate dependent metric was influenced by components association with the urban and rural background.

The influence of wind direction on the road side specific and total OP metrics was also examined at Marylebone Road using fifteen minute averaged wind direction measurements from Heathrow, equivalent to each 7 day PM_{10} collection period (*Figure 2.7)* and wind roses generated for total and roadside-specific OP and NOx (*Figure 2.8*). This data is treated her e in purely descriptive terms due to the limitations of employing 7-day wind direction averages, especially at a site, where canyon effects have been reported (*Scaperdas and Colvile, 1999*). When the OP^{AA} and OP^{GSH}/μg metrics were employed in this analysis there was no clear relationship with wind direction in contrast to NOx where elevated concentrations where associated with SW – E wind directions, broadly in line with the NSW – ENE orientation of Marylebone Road, *Figure 2.8*. Removal of the background OPs and NOx concentrations resulted in the *rs*OP^{AA} and *rs*OP^{GSH}/μg wind roses moving more in line with that for NOx, with the greatest activities occurring when the wind direction was from the SW-E.

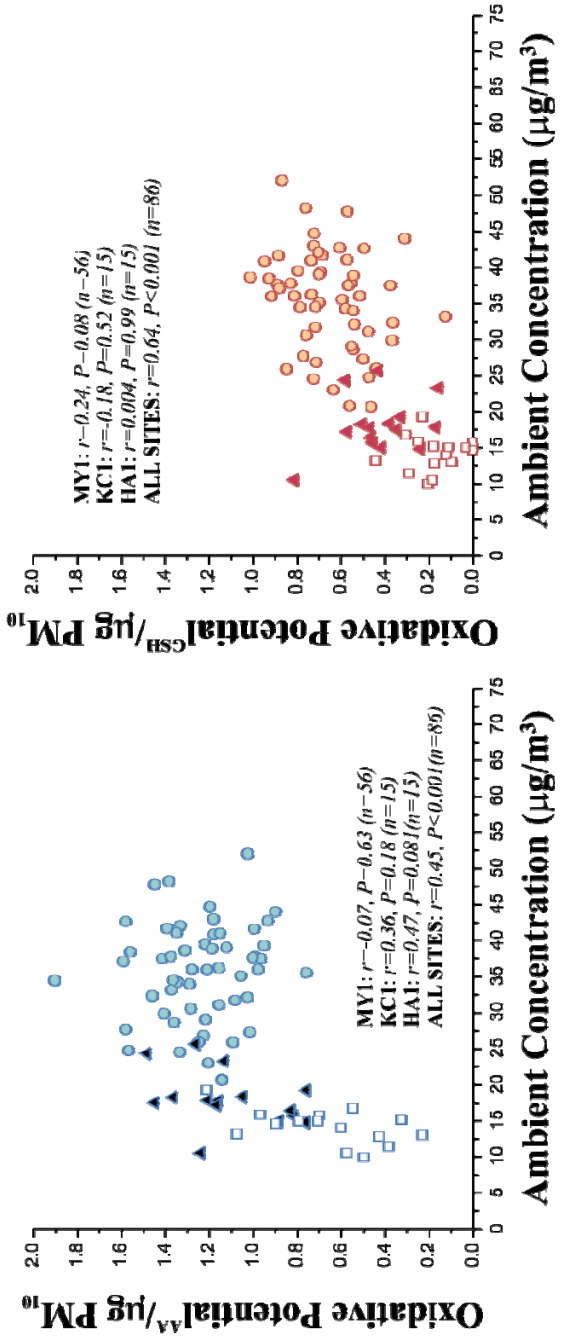

Figure 2.3: Associations (Spearman's Rank Order correlation) between OP^{AA}/µg and OP^{GSH}/µg with the ambient PM_{10} concentrations across each of the sites. Results of the correlation analysis are given in each of the panel across all sites, or separately for MY1 (circles), KC1 (triangles) and HA1 (squares).

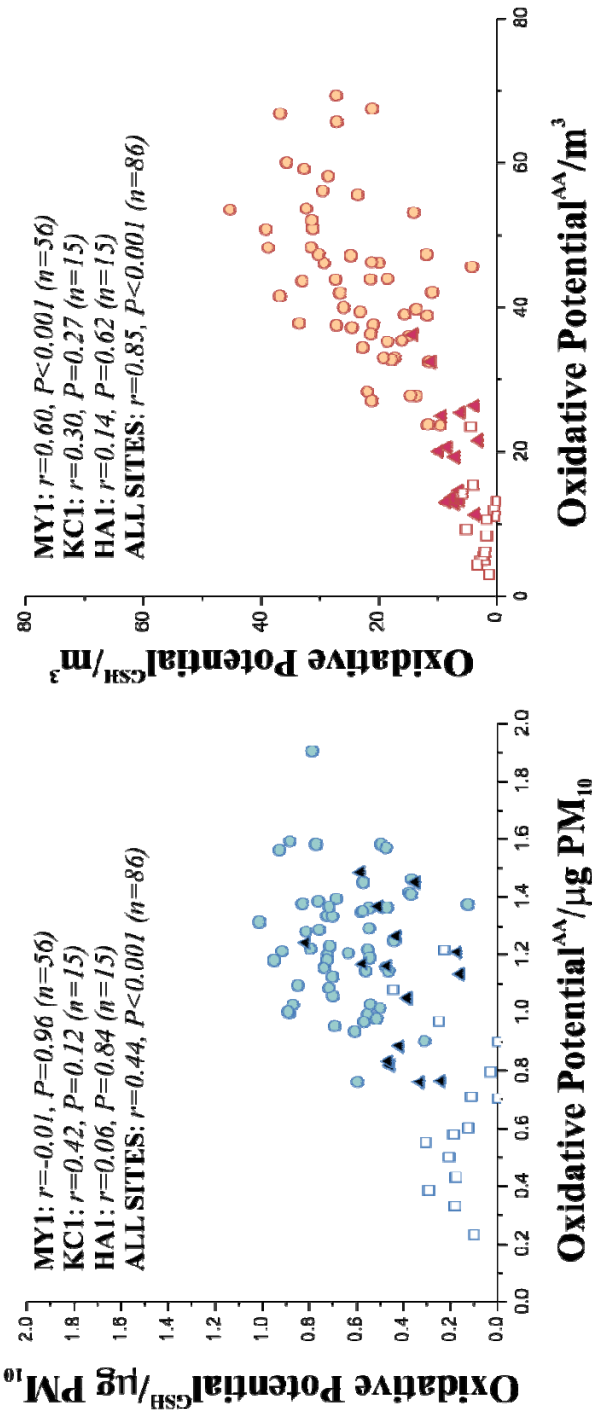

Figure 2.4: Associations (Spearman's Rank Order correlation) between OP^{AA} and OP^{GSH} expressed both per μg and per m^3 of PM_{10}. Results of the correlation analysis are given in each of the panels, across all sites, or separately for MY1 (circles), KC1 (triangles) and HA1 (squares).

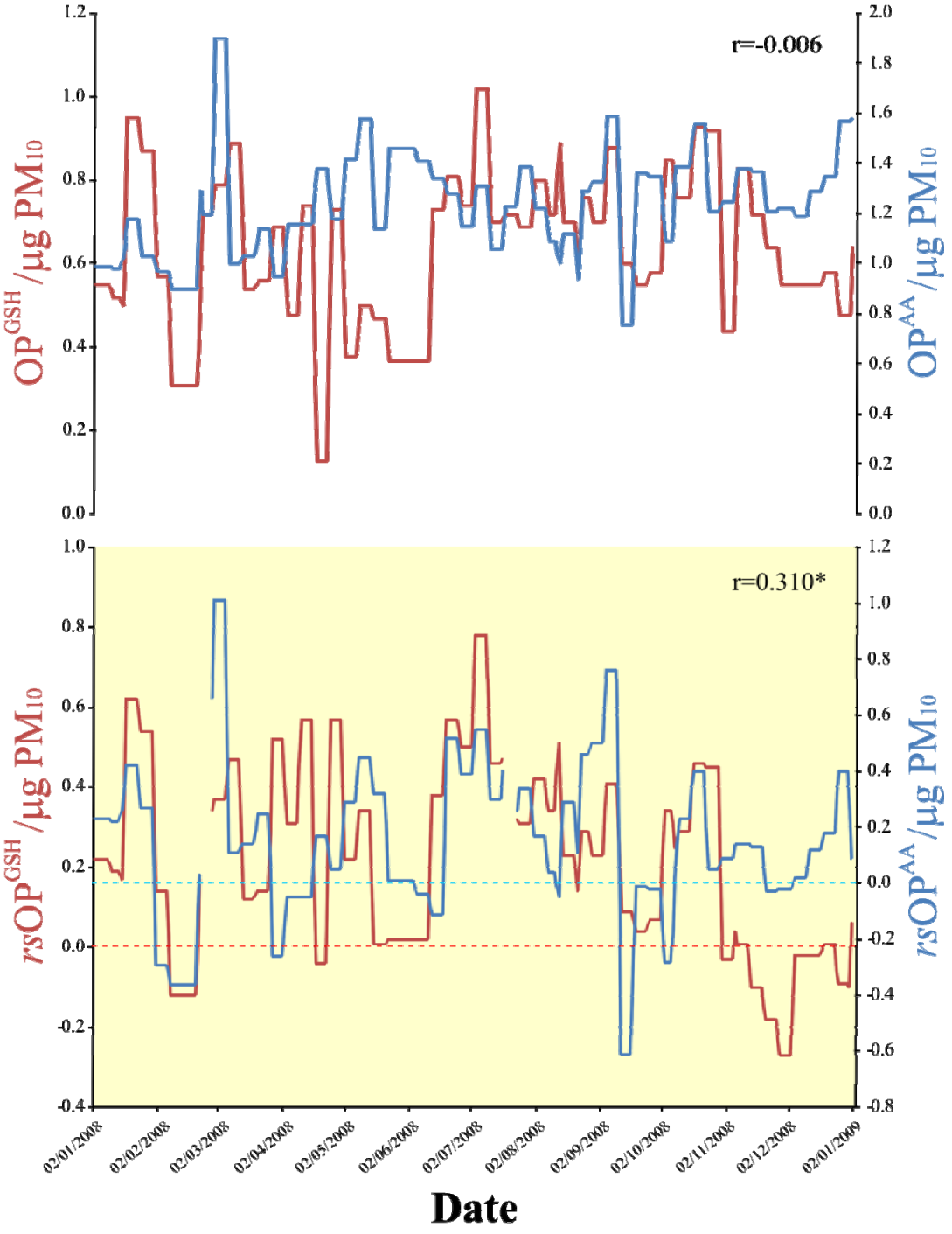

Figure 2.5: Temporal relationship between ascorbate and glutathione dependant PM_{10} oxidative potentials measured at Marylebone Road over a full calendar year, with (upper panel) and without (lower panel) the urban background OP being subtracted to derive a road side (*rs*) specific signature. The results of a correlation analysis (Spearman's Rank Order) using the full or restricted OP parameters are inset. $P<0.05$ *.

Total and aqueous metal concentrations were also determined in samples from each of the sites. The temporal profiles for total (acid digested) PM_{10} Fe, Mo, Mn, Sr, Ba, Zn, Ni, Cr, V, Cu, Sb, Al and Pb measured at Marylebone Road Jan 2008 – Jan 2009 are illustrated in *figure 2.9*, with the elements grouped through A to F based on similarities in their profiles and a high degree of association in univarient correlation analysis. The relationship between PM_{10} total metals at each of the sites was further investigated using a principle component analysis, with Varimax rotation and Kaiser normalisation, as outlined in the methods section.

For Marylebone road this analysis identified 3 components with Eigen values greater than 1.Component 1 had significant loadings (partial correlations r >0.5) for Mn (r=0.92), Sb (0.94), Cu (0.88), Mo (0.92), Pb (0.86), Zn (0.52), Sr (0.62), Fe (0.89) and Al (0.52), providing a compositional signature consistent with generic vehicular abrasion processes (*Schauer et al, 2006; Garg et al, 2000; Boulter, 2006; Zechmeister et al, 2005; Viana et al., 2008*). The second component was dominated by elements consistent with oil combustion: V (0.93), Cr (0.96) and Ni (0.90) (*Viana et al., 2008; Pakkanen et al, 2003; Allen et al, 2001*); whilst component 3 was associated with Ba (0.95), Zn (0.72), Sr (0.72) and Al (0.70). This later component provides an ambiguous source signature containing elements associated in the literature with both brake (Ba) and tire (Zn) wear, however the lack of association with Cu and Sb, may suggest the former is the more likely.

A similar analysis restricted to the samples collected at the North Kensington background site similarly extracted three components with Eigen values greater than 1: Component 1, Mn (0.51), Sb (0.98), Cu (0.86), Mo (0.96), Pb (0.81), Sr (0.69) and Fe (0.90); component 2, V (0.89), Cr (0.95) and Ni (0.92); and component 3, Ba (0.60), Mn (0.57), Zn (0.75) and Al (0.77). These component signatures were broadly consistent with those reported at the roadside site. Three components were also isolated at the rural site (Eigen values > 2), with component one again being consistent with mechanical wear: Mn (0.93); Sb (0.95), Cu (0.94), Mo (0.98) and Fe (0.99). The second component at the rural site was more characteristic of the third factor from the within London sites: Ba (0.96). Zn (0.97) and Sr (0.84), whilst the third component contained the elements interpreted here as indicative of long range oil combustion processes: V (0.62), Cr (0.95), Ni (0.88) and Al (0.67).

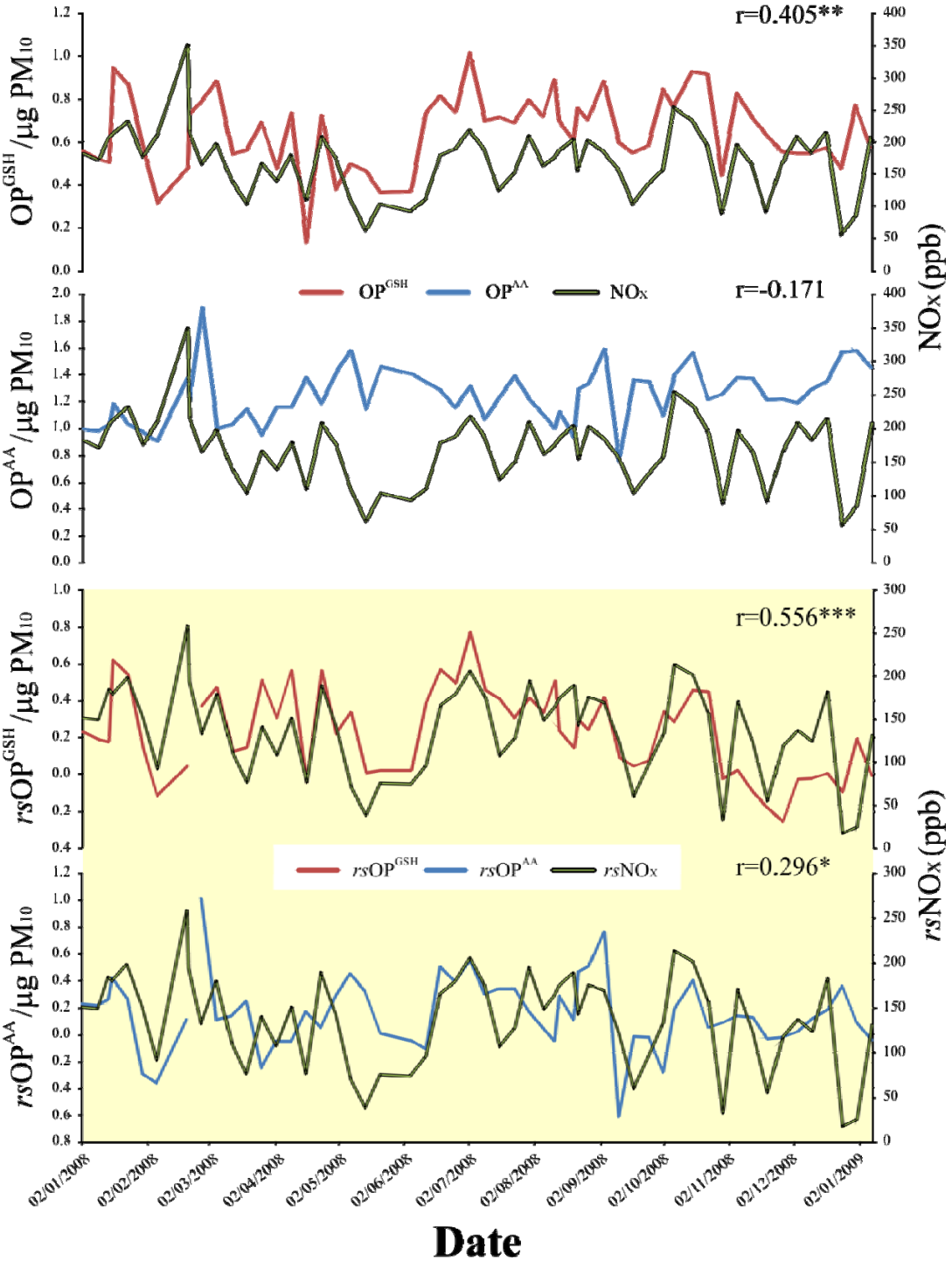

Figure 2.6: Relationship between measures of PM_{10} oxidative potential expressed per µg of filter extracted PM_{10} with the ambient NO*x* concentrations (ppb) measured at Marylebone Road between Jan 2008 and Jan 2009. Data are expressed with (lower panel) and without (upper panel) the subtraction of the background oxidative potentials and NO*x* concentration (derived from KC1) to derive the roadside increment. The results of a correlation analysis (Spearman's Rank Order) using the full or restricted OP parameters are inset. P<0.05 *; P<0.01**; P<0.001***.

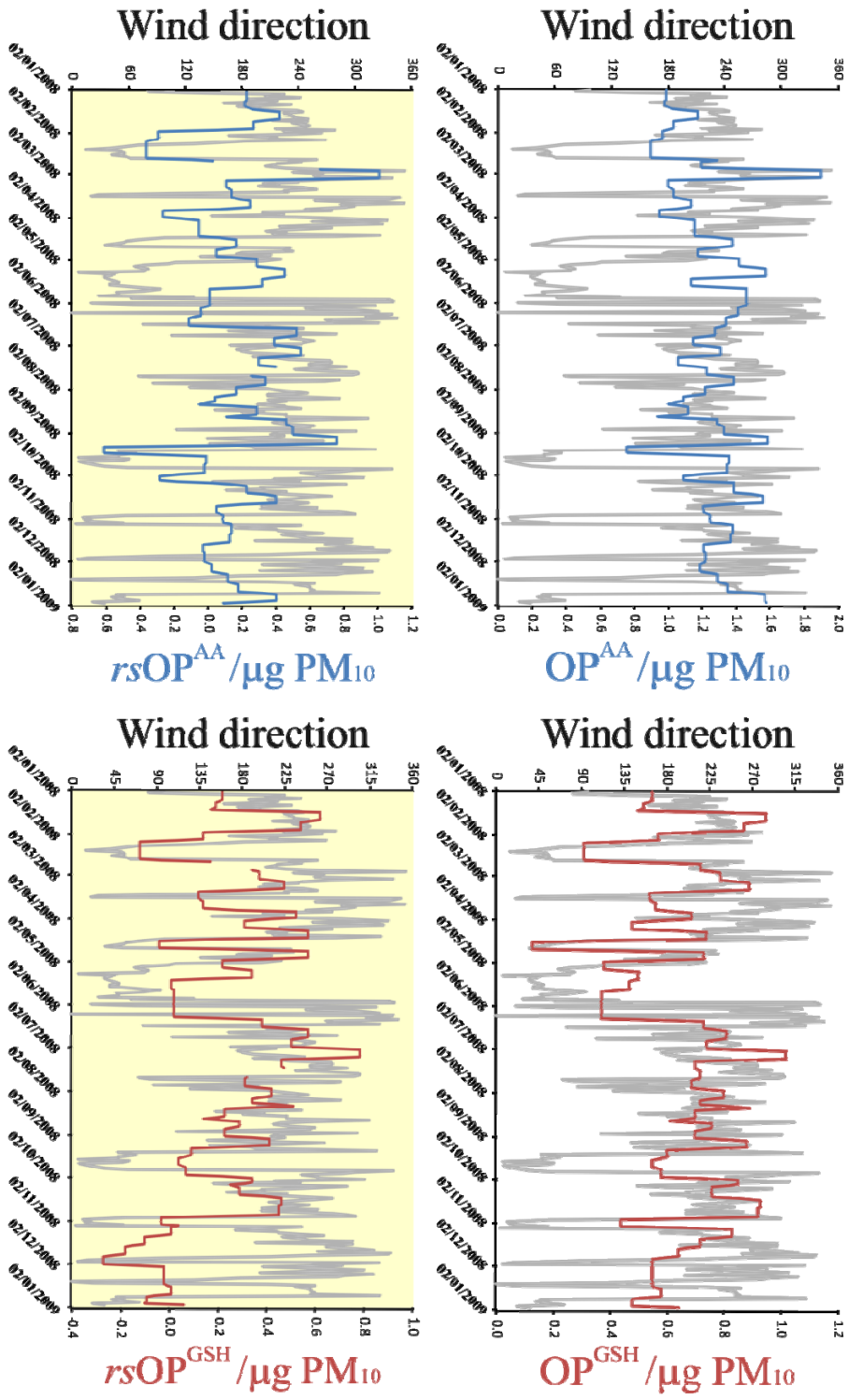

Figure 2.7: Relationship between measures of PM_{10} oxidative potential expressed per µg and per m^3 with wind direction at Marylebone Road, Jan 2008 – Jan 2009. OP data are presented with and without substation of the background OPs established at KC1, with the former representing the roadside signal.

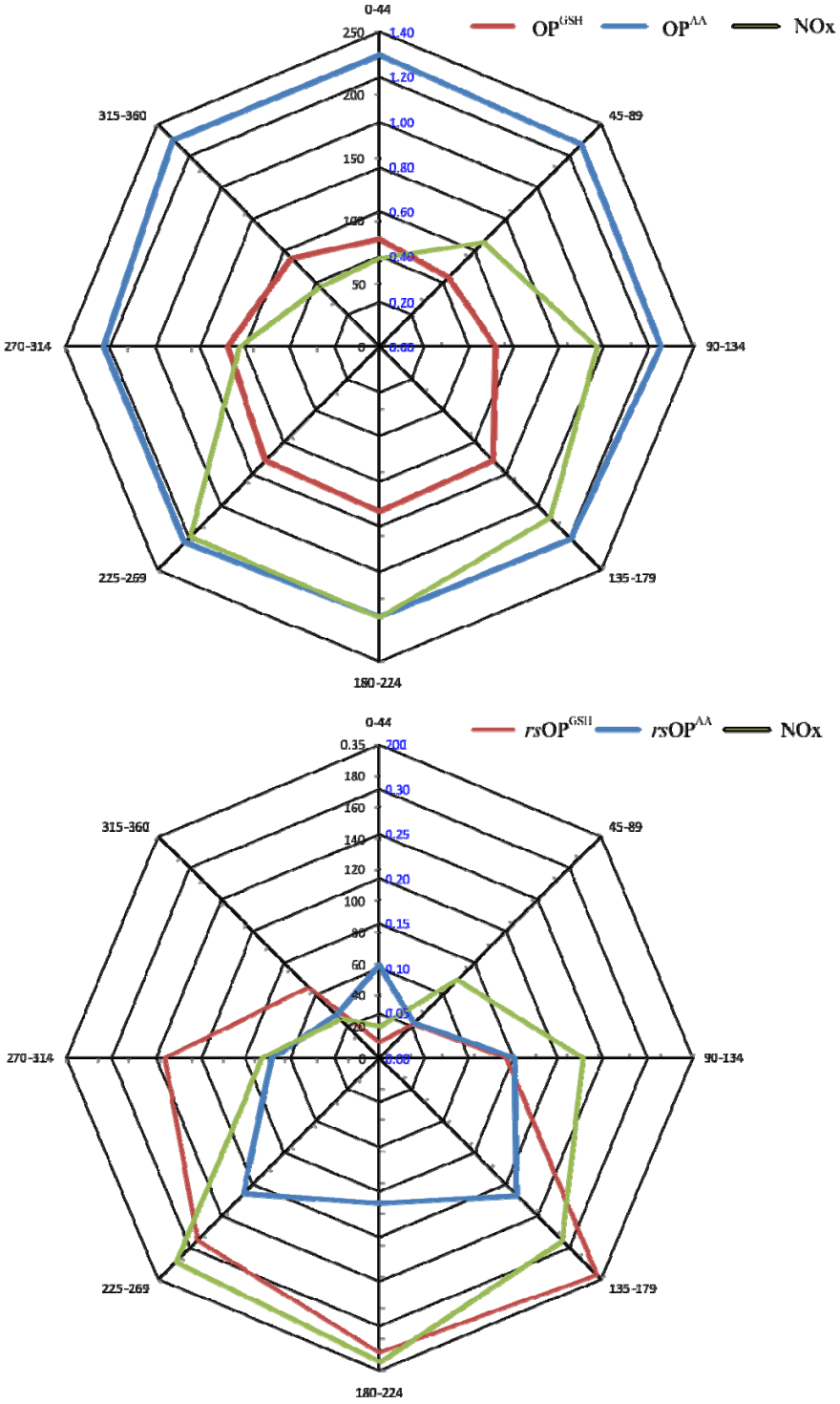

Figure 2.8: Wind roses of ascorbate and glutathione dependent OP (per μg), as well as NO*x* centred on MY1, with (lower rose) and without (upper rose) subtraction of the background (KC1) activities and concentrations to derive a roadside specific signal.

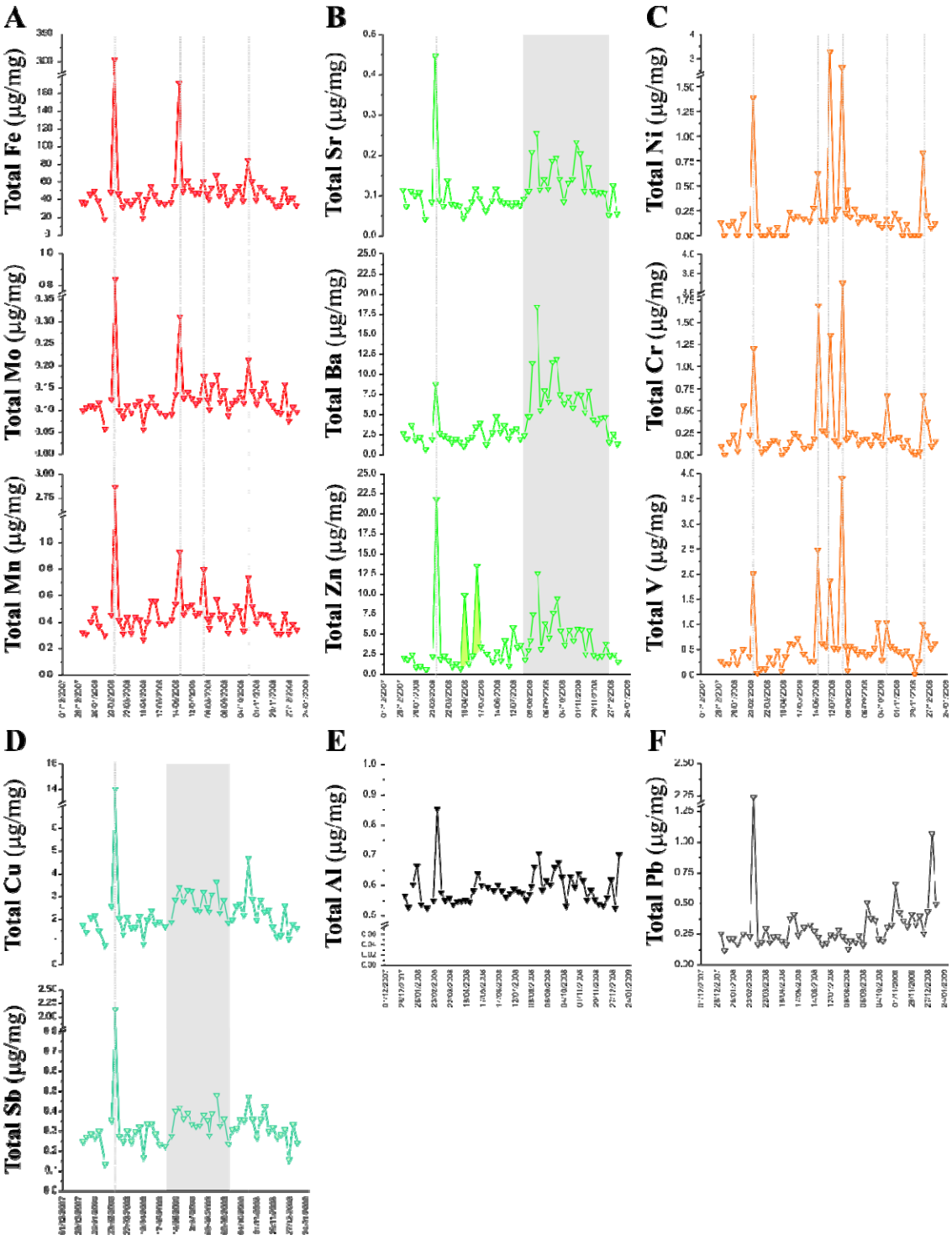

Figure 2.9: Temporal trends in PM_{10} total metal concentrations at Marylebone Road, Jan 2008 – Jan 2009. The metals have been grouped (A-F) based on similarities in the temporal profile; highlighted either by the shaded areas or the indicated peaks All data points represent the mean of triplicate readings, with the SD being less than 5% of the mean value in all cases. Each data point is plotted to the mid date covered by the sampling interval over which the filter was collected.

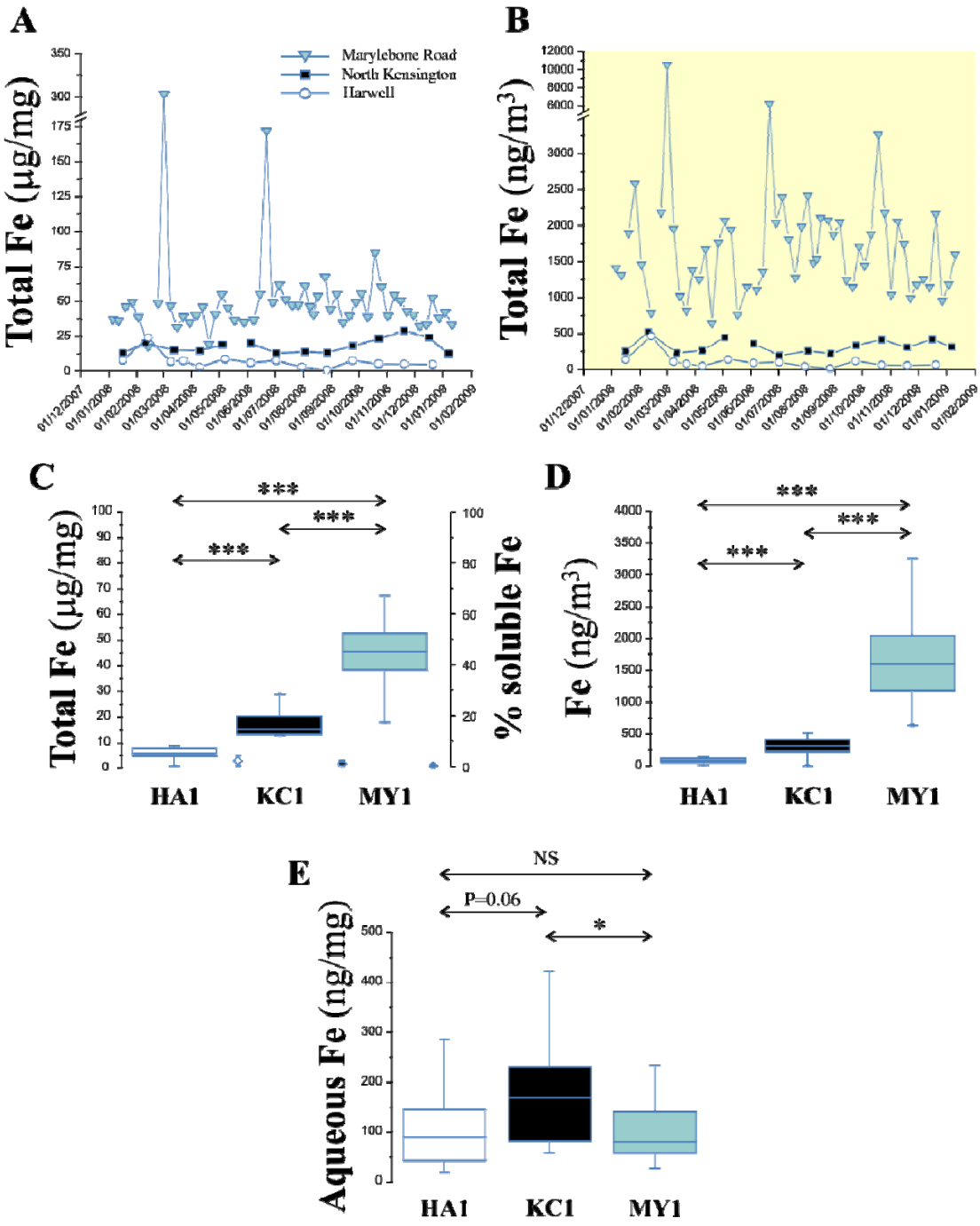

Figure 2.10: Total and aqueous PM_{10} Fe concentrations at Marylebone Road, North Kensington and Harwell, Jan 2008 – 2009. Panels **A** and **B** illustrate the temporal profile of PM_{10} Fe concentrations expressed per µg or m^3 at each of the selected sites, with the data formatted as outlined in the legend to *Figure 2.9*. Panel **C** illustrates the statistical comparison of the Fe concentrations (µg/mg) at each site, with the figure formatting and details of the analyses as outlined in the legend to *Figure 2.2*. Panel **C** also illustrates the contribution aqueous Fe makes to total PM Fe, with the data summarised as a mean % ± SD. Panel **D** illustrates the statistical comparison of PM total Fe, expressed as ng/m^3, with panel **E** showing the site contrasts in aqueous Fe. P<0.05*; P<0.01**; P<0.001***.

Table 2.1: Associations (Spearman's Rank Order) between PM_{10} Fe concentrations, both total and aqueous with measures of oxidative potential (OP^{AA}, OP^{GSH} and OP^{TOT} per µg and m^3).

Parameters		All sites	MY1	KC1	HA1
OP^{AA}/µg	Total Fe (µg/mg)	0.543*** (n=81)	0.274* (n=53)	0.370 (n=14)	0.090 (n=14)
OP^{AA}/µg	Aqueous Fe (ng/mg)	0.483*** (n=86)	0.705** (n=56)	0.436 (n=15)	0.704** (n=15)
OP^{AA}/m^3	Total Fe (ng/m^3)	0.890*** (n=81)	0.661*** (n=53)	0.749** (n=14)	0.279 (n=14)
OP^{GSH}/µg	Total Fe (µg/mg)	0.831*** (n=81)	0.700*** (n=53)	0.327 (n=14)	0.024 (n=14)
OP^{GSH}/µg	Aqueous Fe (ng/mg)	-0.316** (n=86)	-0.362** (n=56)	-0.264 (n=15)	-0.386 (n=15)
OP^{GSH}/m^3	Total Fe (ng/m^3)	0.929*** (n=81)	0.813*** (n=53)	0.420 (n=14)	0.064 (n=14)
OP^{TOT}/µg	Total Fe (µg/mg)	0.820*** (n=81)	0.682*** (n=53)	0.427 (n=14)	0.093 (n=14)
OP^{TOT}/µg	Aqueous Fe (ng/mg)	0.091 (n=86)	0.242 (n=56)	0.206 (n=15)	0.379 (n=15)
OP^{TOT}/m^3	Total Fe (ng/m^3)	0.942*** (n=81)	0.824*** (n=53)	0.807*** (n=14)	0.330 (n=14)
Total Fe (µg/mg)	Aqueous Fe (ng/mg)	-0.091 (n=81)	-0.087 (n=53)	-0.095 (n=14)	0.099 (n=14)

In *Figure 2.9* the PM_{10} Fe, Mn and Mo concentrations observed at MY1 have been placed in grouping 'A', based both on similar peak concentrations in late June and Mid October and strong internal correlations between the three metals: Fe versus Mn, r=0.92, P<0.001; Fe versus Mo, r=0.90, P<0.001; Mn versus Mo, r=0.83, P<0.001 (n=53). The Fe data is explored in greater detail in *Figure 2.10*, where the temporal profile at all sites in total Fe concentrations expressed per µg (panel A) and m^3 (panel B) of PM_{10} is illustrated.

These data demonstrate clear increments in PM_{10} Fe content between the rural (lowest), background and roadside (highest) sites, with some evidence of that the rural and background sites track one another. Whilst these increments are apparent on a per unit mass basis, *Figure 2.10, panel C*, they are magnified once the data are expressed per m^3, *panel D*, with considerable temporal variability apparent in the weekly samples from Marylebone Road.

Aqueous Fe content was also established in these samples, but differed markedly from the total Fe data with significantly lower concentrations measured in the PM samples from MY1 compared with KC1. This reflected an enrichment of insoluble Fe in the roadside sample with the soluble fraction falling from 2.2±2.0 at HA1, to 1.1±0.7 at KC1 and 0.3±0.3% at MY1, *Figure 2.10, panel C*. As would be expected for Fe no relationship was apparent between the aqueous and total Fe concentrations at any of the sites examined, *Table 2.1*.

Whilst it has been argued that PM aqueous metal content may be a better determinant of their biological activity than concentrations determined by acid digestion the relationship between Fe and the OP metrics was not clear cut with variable relationships apparent at each site, *Table 2.1*. At the roadside and rural sites significant associations were noted between aqueous Fe and OP^{AA}/μg, but not at the KC1, *Table 2.1*. In contrast only a weak association was noted between total Fe and OP^{AA}/μg at MY1 ($r=0.274$, $P<0.05$). No positive associations between aqueous Fe and OP^{GSH}/μg were observed, with an actual negative association apparent at the roadside site ($r=-0.316$, $P<0.01$) and in contrast to the ascorbate dependent metric the strongest association being with total Fe ($r=0.700$, $P<0.001$). When tot OP^{TOT}/μg metric was derived, only the total Fe measurement remained predictive ($r=0.682$, $P<0.001$), though here the relationship was restricted to the roadside site only. The relationships with PM_{10} total Fe content were strengthened when the data were expressed per m^3, though the significant associations were largely restricted to the roadside and urban background sites, (*Table 2.1, gray shaded rows*).

To examine whether the relationship between PM_{10} Fe content at the roadside site and the determined ascorbate and glutathione oxidative potentials would be improved by isolating the roadside specific components in these measures, the background activities and concentrations were removed and the associations re-examined, *Figure 2.11*. Removal of the KC1background had little effect on the association between Fe and OP^{GSH}/μg ($r=0.730$, $P<0.001$ versus 0.700, $P<0.0014$), but significant strengthen the association between Fe and OP^{AA}/μg ($r=0.564$, $P<0.001$ versus 0.274, $P<0.05$), *Figure 2.11*.

The increments between the three site types for Mo were identical to those observed for Fe, *Figure 2.12*, with the highest concentrations seen in PM_{10} samples from MY1. In contrast to PM Fe, enhanced concentrations of aqueous Mo were also noted at MY1 and KC1 compared to the rural site, though no contrast was apparent between PM from the roadside and urban background locations, *Figure 2.12, panels E and F*.

As with the PM_{10} Fe data the largest increments in roadside Mo, expressed per unit mass, appeared to occur between June and October, with evidence of an upward drift in urban background concentrations from October to December to roadside levels. The most notable difference between PM associated Fe and Mo was its degree of solubility, with

97.0±30.0% of the total Mo appearing in the aqueous extract in the samples from the rural location, falling to 41.8±12.7 and 22.0±8.1% at the urban background and roadside site respectively. The high proportion of soluble Mo and the increasing enrichment of the urban background and roadside PM with insoluble forms of this metal were reflected by the relationships between the two Mo pools at each of the site classifications, *Table 2.2, row shaded light blue*, with the highest correlations observed at Harwell ($r=0.81$, $P<0.001$, $n=14$) and the lowest at Marylebone Road ($r=0.30$, $P<0.05$, $n=53$). Unsurprisingly, given the high degree of association between PM_{10} Fe and Mo concentrations, similar relationships between Mo and the OP metrics were observed (*Table 2.2*), with aqueous Mo appearing more predictive of OP^{AA}/μg than the total measurement across all sites, whilst the total Mo concentrations was the more predictive of OP^{GSH}/μg. When the ascorbate and glutathione dependent OPs were combined to derive OP^{TOT}/μg total Mo was more predictive at Marylebone Road, whilst the strength of the association between aqueous and total Mo was equivalent at North Kensington. No statistically significant associations were noted at the rural Harwell site. As was previously noted with the Fe data, expressing the metal and OP metric per m^3, strengthen the underlying associations reported previously. Whilst the total PM_{10} Mo concentration at the roadside site demonstrated only a relatively weak correlation with OP^{AA}/μg, removal of the background concentrations and OP activity significantly strengthened the association ($r=0.675$, $P<0.001$ versus $r=0.279$, $P<0.05$), *Figure 2.13*. In contrast the strength of the association with OP^{GSH}/μg remained similar with and without the removal of the background values to derive the roadside specific signal, *Figure 2.13*.

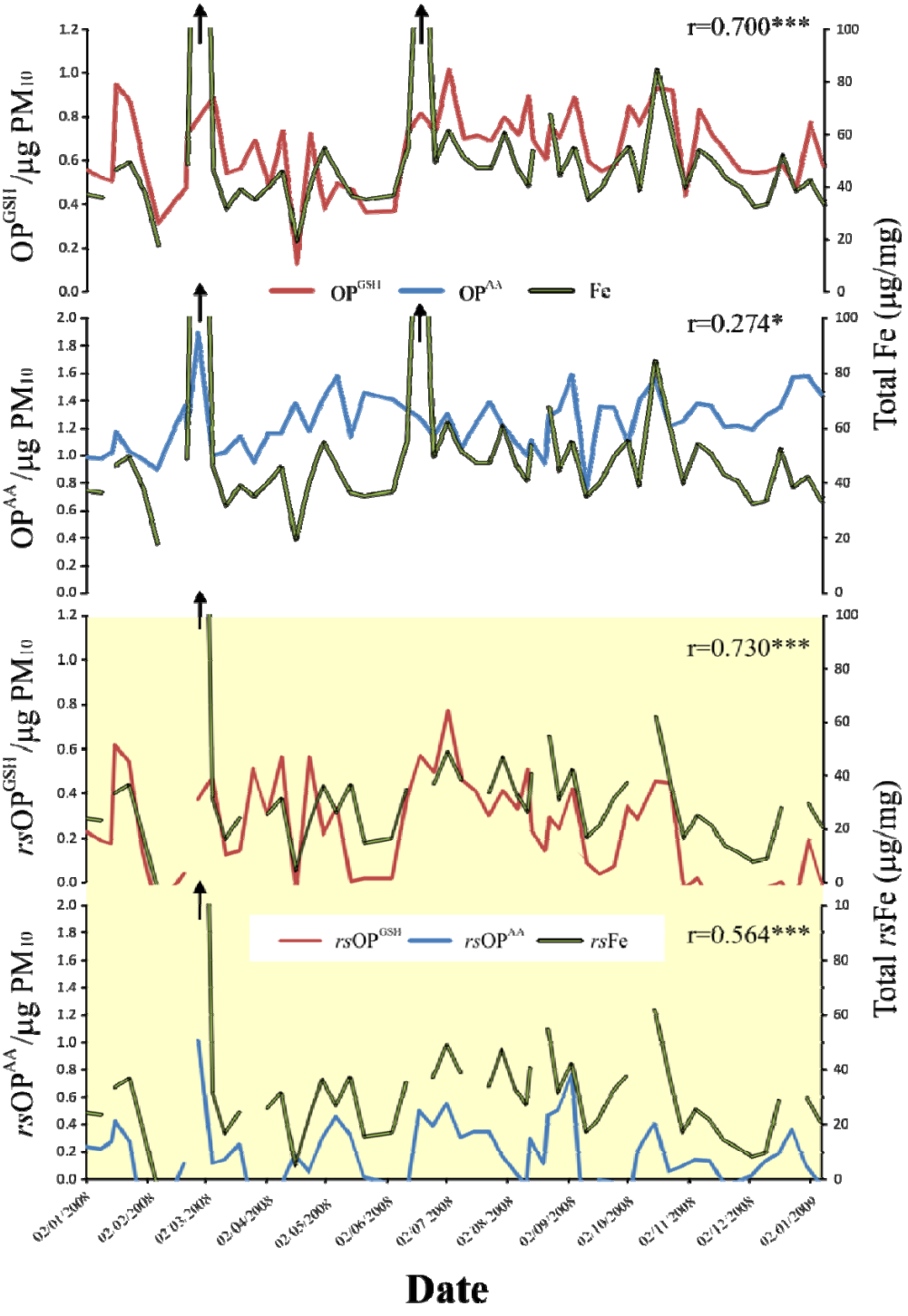

Figure 2.11: Relationship between measures of oxidative potential expressed per µg of filter extracted PM_{10} with total Fe concentrations at Marylebone Road between Jan 2008 and Jan 2009. Data are expressed with (lower panel) and without (upper panel) the subtraction of the background oxidative potentials and Fe concentration (derived from KC1) to derive the roadside increment. The results of a correlation analysis (Spearman's Rank Order) using the full or restricted OP parameters are inset. P<0.05 *; P<0.01**; P<0.001***.

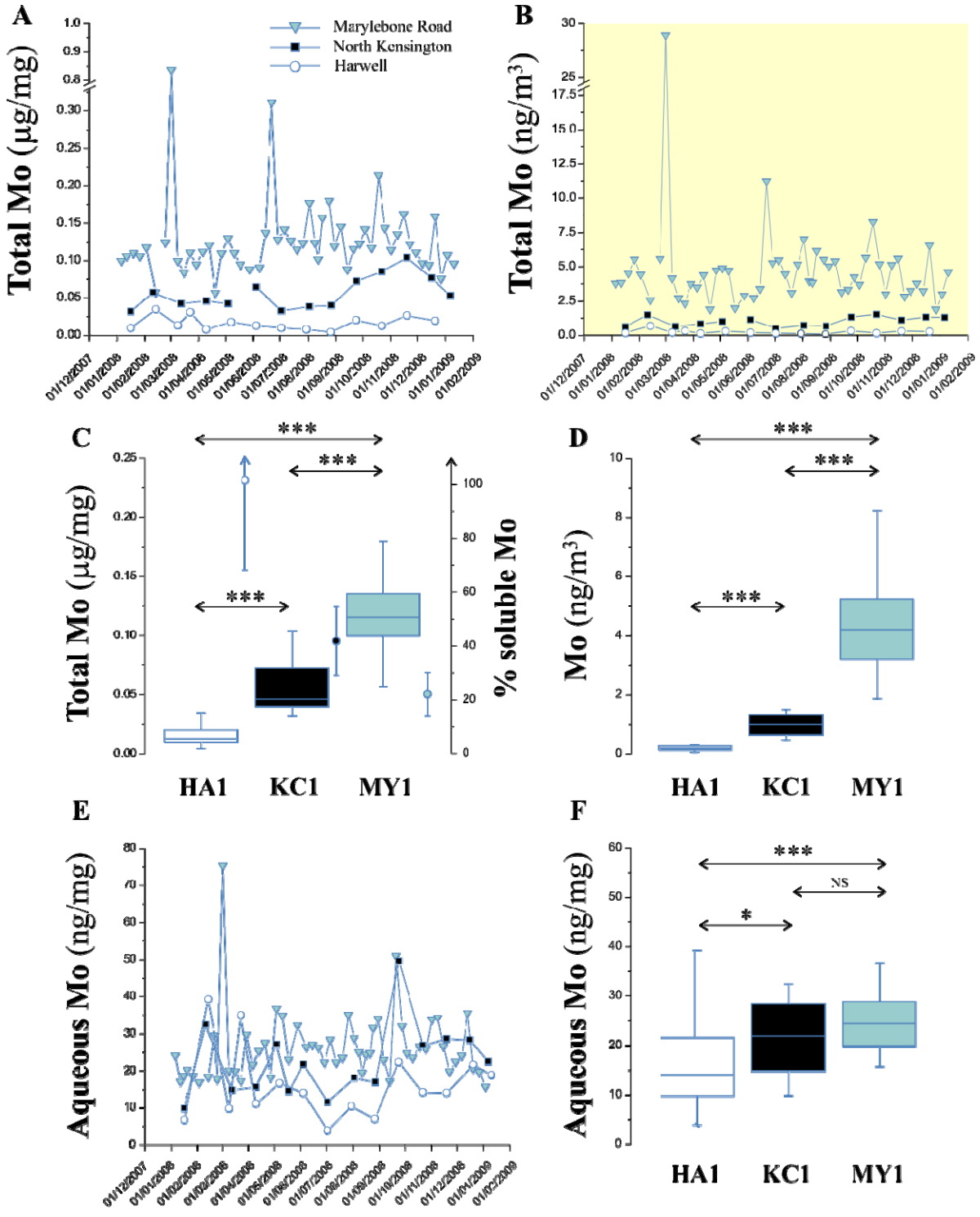

Figure 2.12: Total and aqueous PM_{10} Mo concentrations at Marylebone Road, North Kensington and Harwell, Jan 2008 – 2009. Figure formatting and details of the data analyses are as outlined in the legend to *Figure 2.10*.

Table 2.2: Associations between PM_{10} Mo concentrations, both total and aqueous with measures of oxidative potential (OP^{AA}, OP^{GSH} and OP^{TOT} per μg and m^3).

Parameters		All sites	MY1	KC1	HA1
OP^{AA}/μg	Total Mo (μg/mg)	0.585*** *(n=81)*	0.279* *(n=53)*	0.703**(n=14)	0.424 *(n=14)*
OP^{AA}/μg	Aqueous Mo (ng/mg)	0.664*** *(n=86)*	0.543*** *(n=56)*	0.742** *(n=15)*	0.614* *(n=15)*
OP^{AA}/m^3	Total Mo (ng/m^3)	0.899*** *(n=81)*	0.663*** *(n=53)*	0.651* *(n=14)*	0.324 *(n=14)*
OP^{GSH}/μg	Total Mo (μg/mg)	0.819*** *(n=81)*	0.592*** *(n=53)*	0.685**(n=14)	0.258 *(n=14)*
OP^{GSH}/μg	Aqueous Mo (ng/mg)	0.340** *(n=86)*	-0.056 *(n=56)*	0.525* *(n=15)*	0.254 *(n=15)*
OP^{GSH}/m^3	Total Mo (ng/m^3)	0.926*** *(n=81)*	0.787*** *(n=53)*	0.664* *(n=14)*	0.130 *(n=14)*
OP^{TOT}/μg	Total Mo (μg/mg)	0.814*** *(n=81)*	0.611*** *(n=53)*	0.806** *(n=14)*	0.375 *(n=14)*
OP^{TOT}/μg	Aqueous Mo (ng/mg)	0.544*** *(n=86)*	0.331* *(n=56)*	0.761** *(n=15)*	0.490 *(n=15)*
OP^{TOT}/m^3	Total Mo (ng/m^3)	0.945*** *(n=81)*	0.832*** *(n=53)*	0.810*** *(n=14)*	0.282 *(n=14)*
Total Mo (μg/mg)	Aqueous Mo (ng/mg)	0.494*** *(n=81)*	0.301* *(n=53)*	0.785** *(n=14)*	0.808*** *(n=14)*

The final element in the first group of strongly inter-related metals was Mn. As with Fe and Mo statistically significant increments in total PM_{10} Mn were observed between each of the site types, with the magnitude of the increments increasing when the data were expressed per m^3, *Figure 2.14, panels A – D*. Considerable weekly variation was apparent in Mn concentrations at MY1 with evidence again the increment between the roadside and background site was largest during the summer months. The solubility of Mn was intermediate between Fe and Mo, with the % of the total pool present within the aqueous extract being 14.3±5.7, 9.1±1.5 and 4.4±1.5% at the rural, background and roadside sites respectively. In contrast to the total Mn increments between sites, no contrast was apparent between aqueous Mn in the rural and urban background samples, with the PM samples from MY1 demonstrating a trend (P=0.05) toward reduced aqueous Mn concentrations compared with North Kensington, *Figure 2.14, panel E*. It was also notable that as the proportion of soluble Mn fell from the rural to roadside sites, so the underlying association between the aqueous and total pools apparent in samples from HA1 and KC1 was lost (*Table 2.3, blue shaded row).*

As was the case for both Mo and Fe, aqueous Mn appeared more strongly associated with OP^{AA}/μg at the roadside and urban background sites, than the total pool, with the reverse being the case for OP^{GSH}/μg, though in this later case a significant positive association was only noted at MY1, table 2.3. These associations were strengthen when the data were expressed per m^3, reflecting the common denominator.

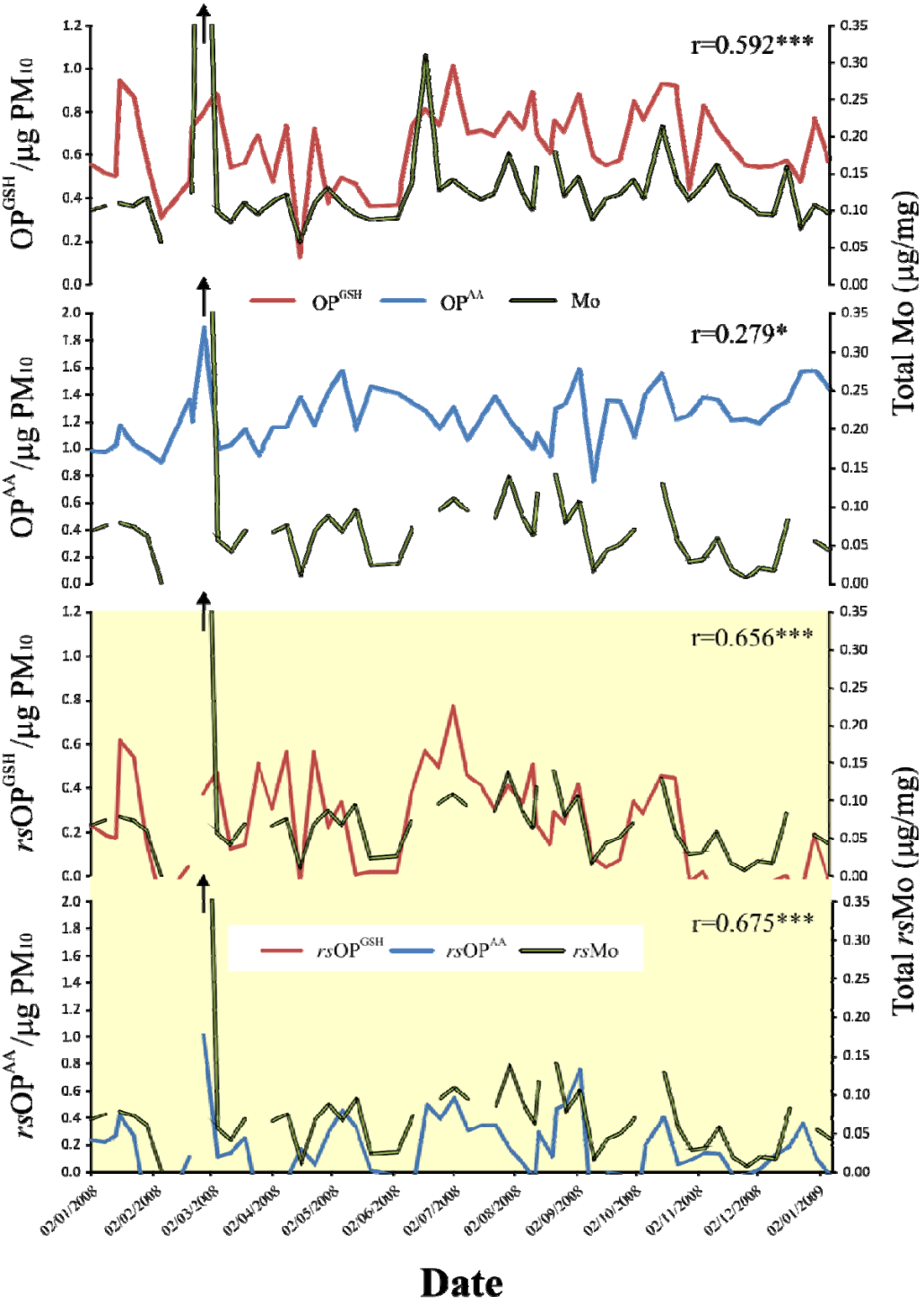

Figure 2.13: Relationship between measures of oxidative potential expressed per µg of filter extracted PM_{10} with total Mo concentrations at Marylebone Road between Jan 2008 and Jan 2009. Data are expressed with (lower panel) and without (upper panel) the subtraction of the background oxidative potentials and Mo concentration (derived from KC1) to derive the roadside increment. The results of a correlation analysis (Spearman's Rank Order) using the full or restricted OP parameters are inset. P<0.05 *; P<0.01**; P<0.001***.

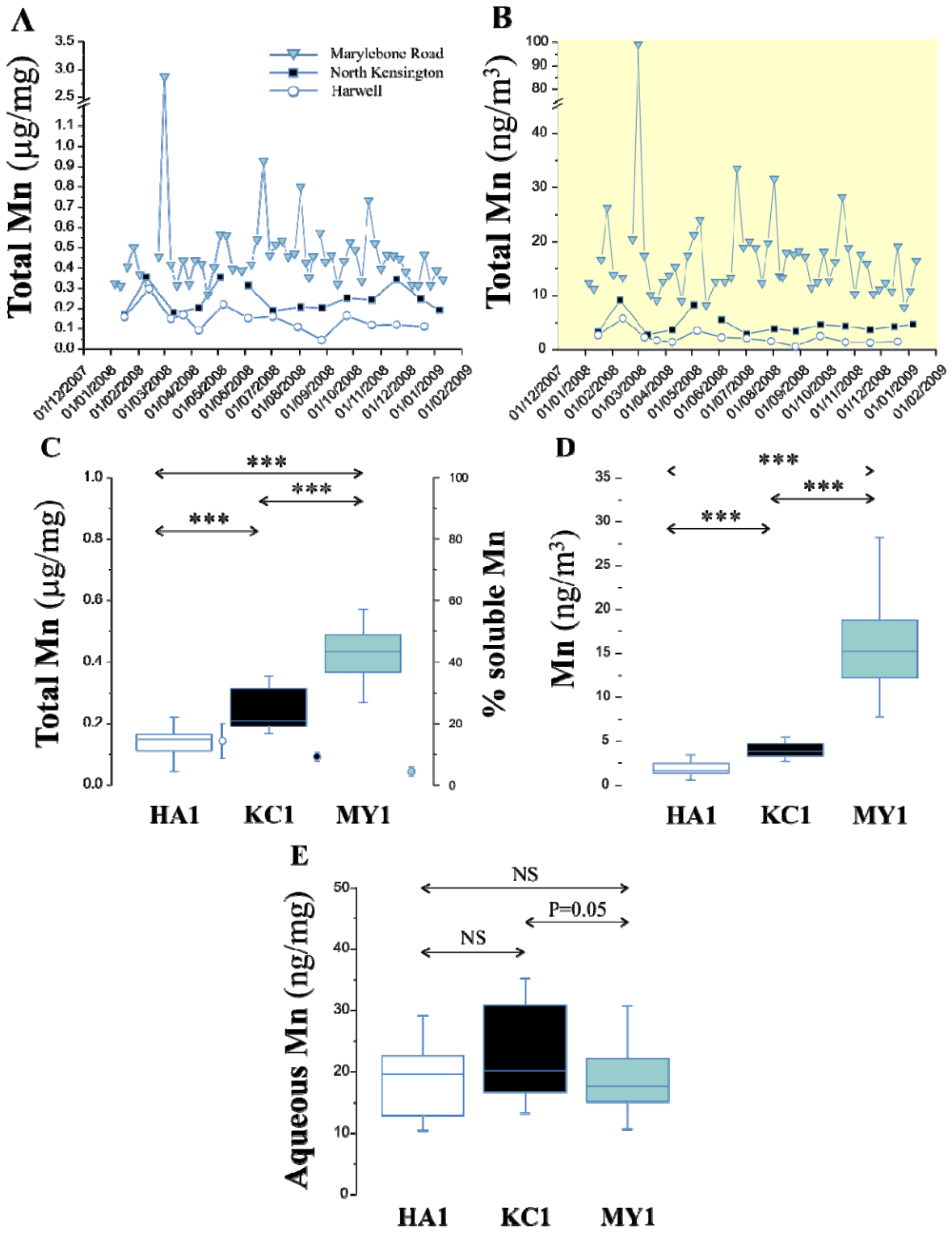

Figure 2.14: Total and aqueous PM_{10} Mn concentrations at Marylebone Road, North Kensington and Harwell, Jan 2008 – 2009. Figure formatting and details of the data analyses are as outlined in the legend to *Figure 2.10*.

Table 2.3: Associations between PM_{10} Mn concentrations, both total and aqueous with measures of oxidative potential (OP^{AA}, OP^{GSH} and OP^{TOT} per µg and m^3).

Parameters		All sites	MY1	KC1	HA1
OP^{AA}/µg	Total Mn (µg/mg)	0.596*** *(n=81)*	0.327* *(n=53)*	0.522 *(n=14)*	0.066 *(n=14)*
OP^{AA}/µg	Aqueous Mn (ng/mg)	0.436*** *(n=86)*	0.558*** *(n=56)*	0.612* *(n=15)*	0.339 *(n=15)*
OP^{AA}/m^3	Total Mn (ng/m^3)	0.904*** *(n=81)*	0.704*** *(n=53)*	0.908*** *(n=14)*	0.371 *(n=14)*
OP^{GSH}/µg	Total Mn (µg/mg)	0746*** *(n=81)*	0.497*** *(n=53)*	0.157 *(n=14)*	-0.007 *(n=14)*
OP^{GSH}/µg	Aqueous Mn (ng/mg)	-0.230* *(n=86)*	-0.385** *(n=56)*	0.088 *(n=15)*	-0.254 *(n=15)*
OP^{GSH}/m^3	Total Mn (ng/m^3)	0.893*** *(n=81)*	0.699*** *(n=53)*	0.380 *(n=14)*	-0.051 *(n=14)*
OP^{TOT}/µg	Total Mn (µg/mg)	0.782*** *(n=81)*	0.588*** *(n=53)*	0.432 *(n=14)*	0.022 *(n=14)*
OP^{TOT}/µg	Aqueous Mn (ng/mg)	0.124 *(n=86)*	0.152 *(n=56)*	0.470 *(n=15)*	0.159 *(n=15)*
OP^{TOT}/m^3	Total Mn (ng/m^3)	0.936*** *(n=81)*	0.799*** *(n=53)*	0.938*** *(n=14)*	0.400 *(n=14)*
Total Mn (µg/mg)	Aqueous Mn (ng/mg)	0.123 *(n=81)*	0.260 *(n=53)*	0.838*** *(n=14)*	0.616**(n=14)*

When the total OP metric was employed only total Mn was found to be significantly associated with this metric, with the association restricted to the roadside site only, *table 2.3*. As was previously noted for both Fe and Mo isolating the roadside specific Mn concentrations and OPs, resulted in a marked strengthening of the association between OP^{AA}/µg and Mn (r=0.59, P<0.001 versus r=0.33, P<0.05), but in contrast to the other metals in this group also appeared to strengthen the relationship with OP^{GSH}/µg (r=0.50, P<0.001 versus r=0.60, P<0.05), *Figure 2.15*.

The second group of elements (Sr, Ba and Zn), group B, *figure 2.9*, were characterised by a marked elevation in concentrations between the end of July to mid December, with peaks mid August, late September and for Sr only, during the first week of November, based on the total metal data from Marylebone Road. Strong internal correlations were also apparent between these three metals at this site: Sr versus Ba, r=0.84, P<0.001; Sr versus Zn, r=0.56, P<0.001; Ba versus Zn, r=0.73, P<0.001 (n=53). Of these elements Sr was selected as a marker of firework activity to account for short term emissions likely to occur in the Capital during the Diwali, Guy Fawkes Night and the New Year's celebrations. The observation that Sr is present throughout the year at all three sites and is highly associated with both a marker of tyre (Zn) and brake (Ba) wear was unexpected.

In this study we examined Sr88, the most abundant isotope, which although potentially susceptible to interferences from Yb^{2+}, Hf^{2+} and Lu^{2+}, was unlikely as doubly

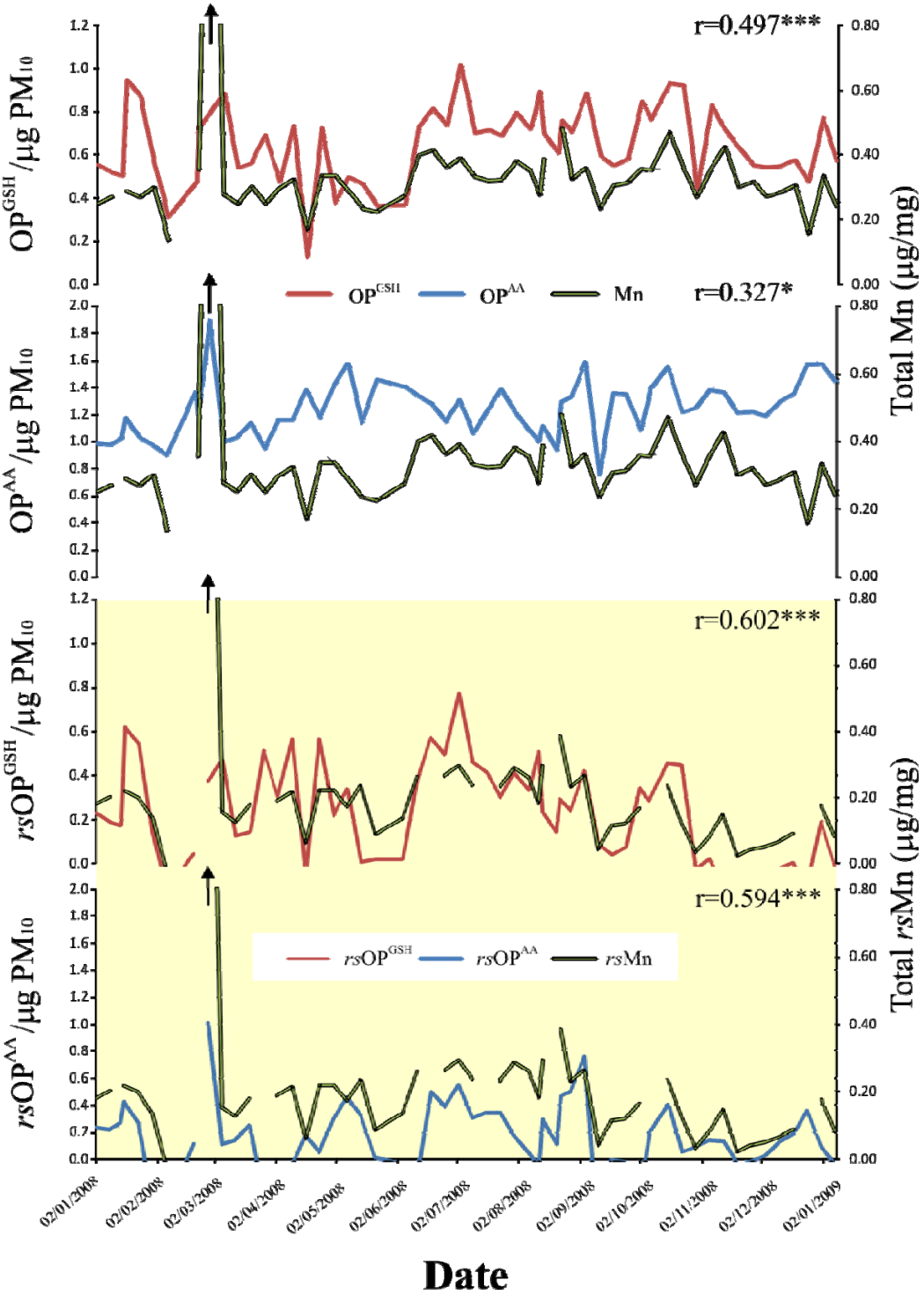

Figure 2.15: Relationship between measures of oxidative potential expressed per µg of filter extracted PM_{10} with total Mn concentrations at Marylebone Road between Jan 2008 and Jan 2009. Data are expressed with (lower panel) and without (upper panel) the subtraction of the background oxidative potentials and Mn concentration (derived from KC1) to derive the roadside increment. The results of a correlation analysis (Spearman's Rank Order) using the full or restricted OP parameters are inset. P<0.05 *; P<0.01**; P<0.001***.

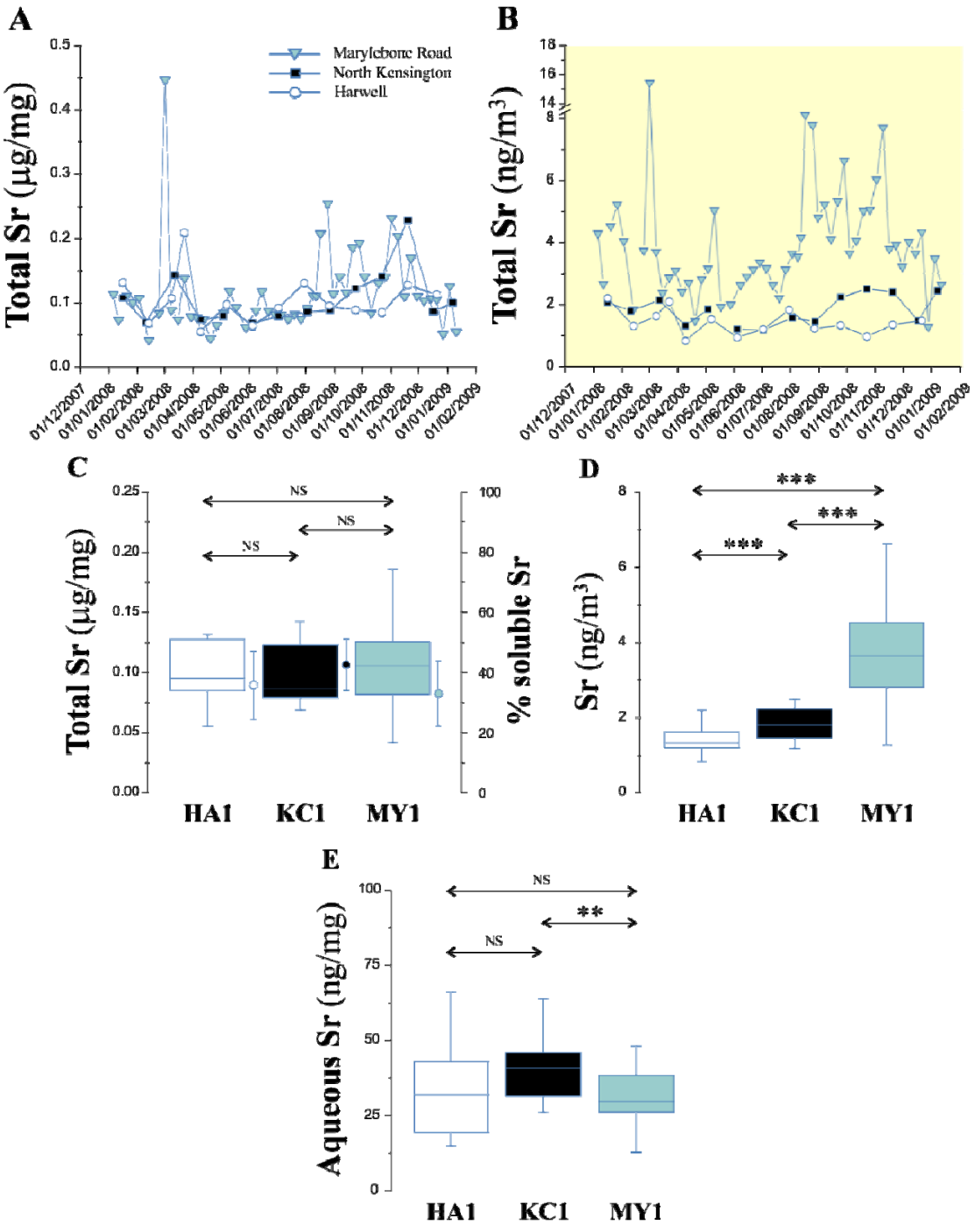

Figure 2.16: Total and aqueous PM_{10} Sr concentrations at Marylebone Road, North Kensington and Harwell, Jan 2008 – 2009. Figure formatting and details of the data analyses are as outlined in the legend to *Figure 2.10*.

Table 2.4: Associations between PM_{10} Sr concentrations, both total and aqueous with measures of oxidative potential (OP^{AA}, OP^{GSH} and OP^{TOT} per μg and m^3).

Parameters		All sites	MY1	KC1	HA1
OP^{AA}/μg	Total Sr (μg/mg)	0.038 *(n=81)*	0.133 *(n=53)*	-0.112 *(n=14)*	-0.337 *(n=14)*
OP^{AA}/μg	Aqueous Sr (ng/mg)	-0.182 *(n=86)*	-0.032 *(n=56)*	-0.345 *(n=15)*	-0.593* *(n=14)*
OP^{AA}/m^3	Total Sr (ng/m^3)	0.720*** *(n=81)*	0.318* *(n=53)*	0.174 *(n=14)*	-0.116 *(n=14)*
OP^{GSH}/μg	Total Sr (μg/mg)	0.109 *(n=81)*	0.318* *(n=53)*	0.604* *(n=14)*	0.445 *(n=14)*
OP^{GSH}/μg	Aqueous Sr (ng/mg)	-0.163 *(n=86)*	0.173 *(n=56)*	0.189 *(n=15)*	0.271 *(n=15)*
OP^{GSH}/m^3	Total Sr (ng/m^3)	0.690*** *(n=81)*	0.451** *(n=53)*	0.560* *(n=14)*	0.389 *(n=14)*
OP^{TOT}/μg	Total Sr (μg/mg)	0.214 *(n=81)*	0.305* *(n=53)*	0.219 *(n=14)*	-0.123 *(n=14)*
OP^{TOT}/μg	Aqueous Sr (ng/mg)	-0.073 *(n=86)*	0.124 *(n=56)*	-0.138 *(n=15)*	-0.351 *(n=15)*
OP^{TOT}/m^3	Total Sr (ng/m^3)	0.781*** *(n=81)*	0.440** *(n=53)*	0.266 *(n=14)*	0.015 *(n=14)*
Total Sr (μg/mg)	Aqueous Sr (ng/mg)	0.433*** *(n=81)*	0.387** *(n=53)*	0.696** *(n=14)*	0.458 *(n=14)*

charged ions were tuned down relative to Ba^{2+}/Ba which has a very low second ionisation potential. As for polyatomics, $Ca(44)_2$, GeC, SeC, GeN & GeO are also possible interferences but again highly unlikely as oxides are tuned down to 3% of the CeO/Ce ratio. We therefore contend that the Sr measurement is an accurate reflection of the concentrations of this element in ambient PM_{10}.

Unlike the group A metals no increment in the annual concentrations of total Sr were apparent between the rural urban, background or roadside sites when the data were expressed per μg of PM_{10}, *Figure 2.17, panels A and C*, though a significant increase in Sr concentration was observed at MY1 relative to HA1 and KC1 when the data were expressed per m^3, *figure 2.17, panels B and D*. Aqueous Sr concentrations represented 35.8±11.3, 43.8±8.6 and 32.9±10.8% of the total pool at HA1, KC1 and MY1 respectively, with the proportion at MY1 significantly reduced ($P<0.01$) with respect to the urban background site, *Figure 2.17, panel B*. Consistent with this the annual concentration of aqueous Sr at Marylebone Road was significantly reduced compared with North Kensington, through equivalent to the concentrations measured at Harwell. No positive associations were noted between total or aqueous Sr expressed per μg of PM_{10} with OP^{AA}/μg, whilst total Sr was positively associated with OP^{GSH}/μg at MY1 and KC1, *Table 2.4*. When the OP^{TOT} metric was derived this was only found to be associated with total Sr at the roadside site.

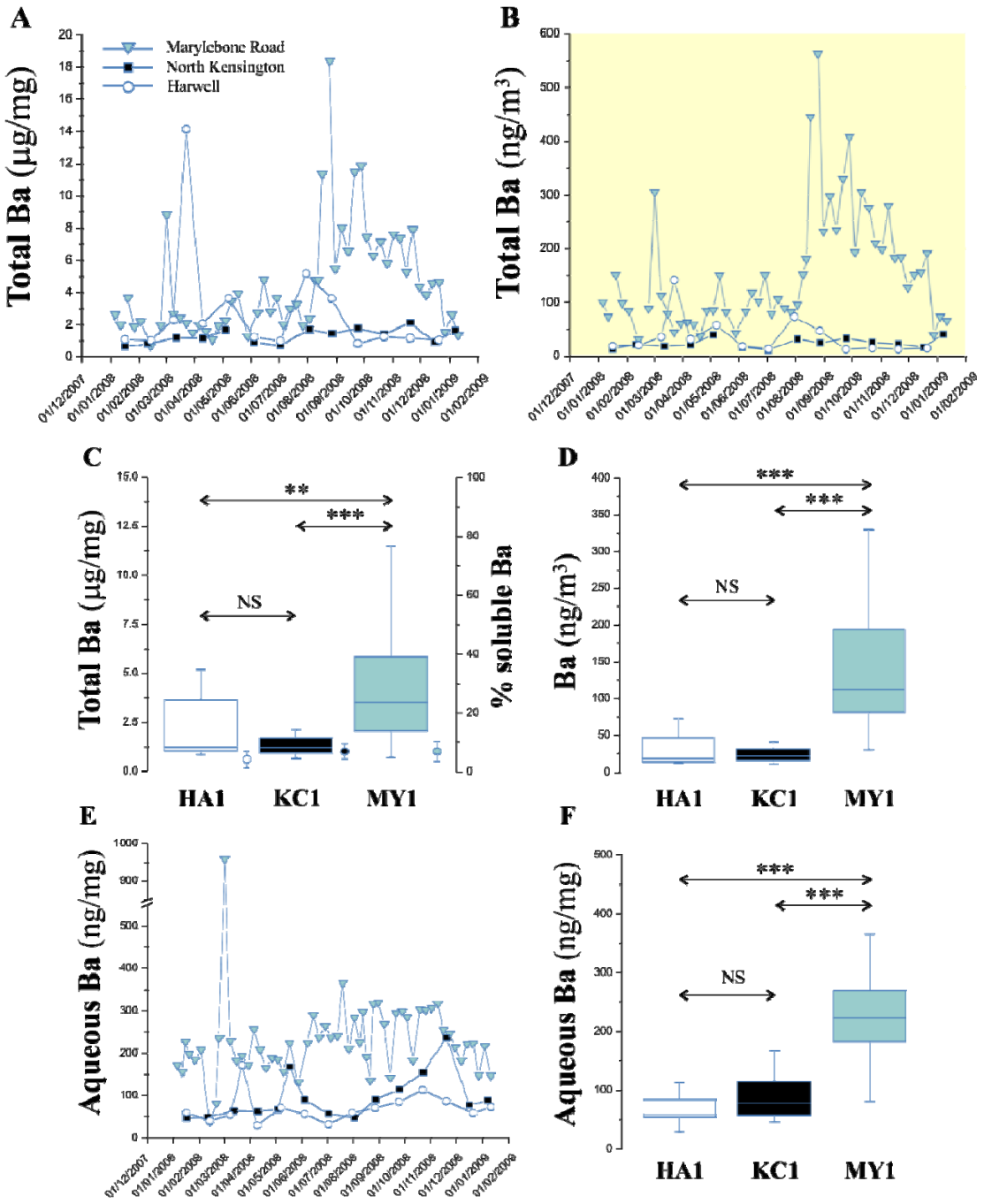

Figure 2.17: Total and aqueous PM_{10} Ba concentrations at Marylebone Road, North Kensington and Harwell, Jan 2008 – 2009. Panels **A** and **B** illustrate the temporal profile of PM_{10} Ba concentrations expressed per µg or m^3 at each of the selected sites, with the data formatted as outlined in the legend to *figure 2.9*. Panel **C** illustrates the statistical comparison of the Ba concentrations (µg/mg) at each site, with the figure formatting and details of the analyses as outlined in the legend to *figure 2.2*. Panel **C** also illustrates the contribution aqueous Ba makes to total PM Ba, with the data summarised as a mean % ± SD. Panel **D** illustrates the statistical comparison of PM total Ba, expressed as ng/m^3. Panel **E** illustrates the temporal profile for aqueous Ba at each of the sites with panel **F** showing the site contrasts in aqueous Ba. $P<0.05$*; $P<0.01$**; $P<0.001$***.

Table 2.5: Associations between PM_{10} Ba concentrations, both total and aqueous with measures of oxidative potential (OP^{AA}, OP^{GSH} and OP^{TOT} per µg and m^3).

Parameters		All sites	MY1	KC1	HA1
OP^{AA}/µg	Total Ba (µg/mg)	0.265* *(n=81)*	0.172 *(n=53)*	0.304 *(n=14)*	-0.260 *(n=14)*
OP^{AA}/µg	Aqueous Ba (ng/mg)	0.490*** *(n=86)*	0.204 *(n=56)*	0.313 *(n=15)*	-0.175 *(n=15)*
OP^{AA}/m^3	Total Ba (ng/m^3)	0.656*** *(n=81)*	0.171 *(n=53)*	0.513 *(n=14)*	-0.051 *(n=14)*
OP^{GSH}/µg	Total Ba (µg/mg)	0.511*** *(n=81)*	0.313* *(n=53)*	0.442 *(n=14)*	-0.154 *(n=14)*
OP^{GSH}/µg	Aqueous Ba (ng/mg)	0.768*** *(n=86)*	0.506*** *(n=56)*	0.631* *(n=15)*	0.318 *(n=15)*
OP^{GSH}/m^3	Total Ba (ng/m^3)	0.720*** *(n=81)*	0.341* *(n=53)*	0.398 *(n=14)*	-0.064 *(n=14)*
OP^{TOT}/µg	Total Ba (µg/mg)	0.466*** *(n=81)*	0.333*** *(n=53)*	0.460 *(n=14)*	-0.389 *(n=14)*
OP^{TOT}/µg	Aqueous Ba (ng/mg)	0730*** *(n=86)*	0.487*** *(n=56)*	0.428 *(n=15)*	-0.107 *(n=15)*
OP^{TOT}/m^3	Total Ba (ng/m^3)	0.696*** *(n=81)*	0.270 *(n=53)*	0.570* *(n=14)*	-0.145 *(n=14)*
Total Ba (µg/mg)	Aqueous Ba (ng/mg)	0.732*** *(n=81)*	0.643*** *(n=53)*	0.554* *(n=14)*	0.290 *(n=14)*

A clear roadside increment in annual PM_{10} Ba concentrations was observed at Marylebone Road compared with the urban background and rural sites, both when the data were expressed per unit mass, *Figure 2.17, panels A and C*, and m^3, *Figure 2.17, panels B and D*. Notably there was no rural to urban background increment in Ba concentration (both total and aqueous), with little temporal relationship between the concentrations measured at these two sites.

Whilst only a small proportion of the total PM_{10} Ba concentration was present in an aqueous form: 4.2±2.9, 7.0±2.5 and 7.1±3.3% at HA1, KC1 and MY1 respectively, significantly higher concentrations of aqueous Ba were observed at the roadside site, relative to the rural and urban background locations, F*igure 2.17, panels E and F*, with significant associations between total and aqueous Ba concentrations at MY1 and KC1, *Table 2.5, blue shaded row*. Whilst significant associations were not observed between total or aqueous Ba concentrations with OP^{AA}/µg or OP^{AA}/m^3, OP^{GSH}/µg was associated with both total and aqueous Ba, although these correlations were restricted to MY1 and KC1 OP^{TOT} was significantly associated with both total and aqueous Ba, with the later association the strongest, though again these associations were only observed at the roadside site, Table *2.5*. Whilst a weak association was apparent between OP^{GSH}/µg and total Ba at Marylebone Road ($r=0.31$, $P<0.05$), in contrast to the metals previously discussed subtraction of the urban background concentrations and OPs failed to improve the strength of the relationship.

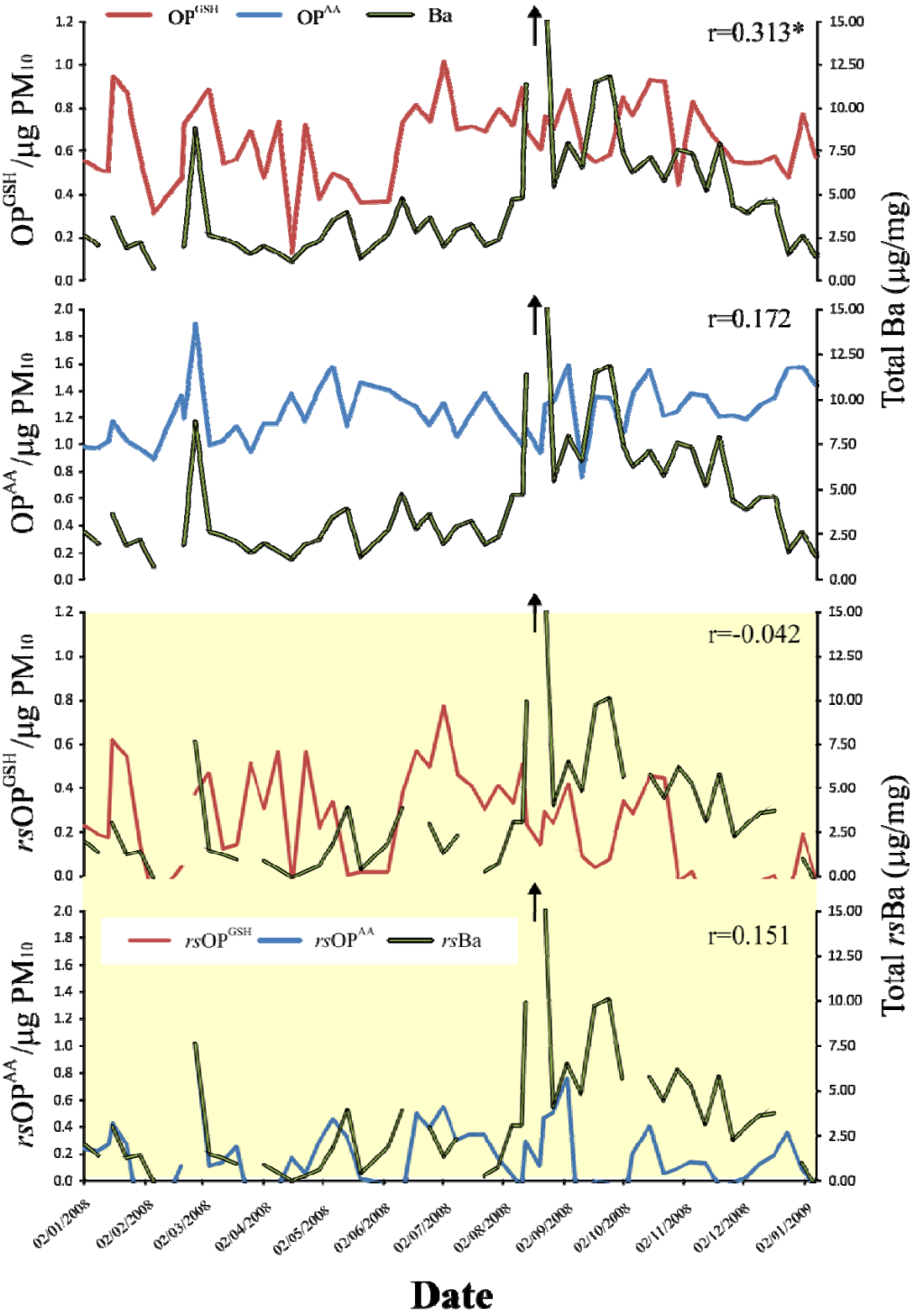

Figure 2.18: Relationship between measures of oxidative potential expressed per µg of filter extracted PM_{10} with total Ba concentrations at Marylebone Road between Jan 2008 and Jan 2009. Data are expressed with (lower panel) and without (upper panel) the subtraction of the background oxidative potentials and Ba concentration (derived from KC1) to derive the roadside increment. The results of a correlation analysis (Spearman's Rank Order) using the full or restricted OP parameters are inset. P<0.05 *.

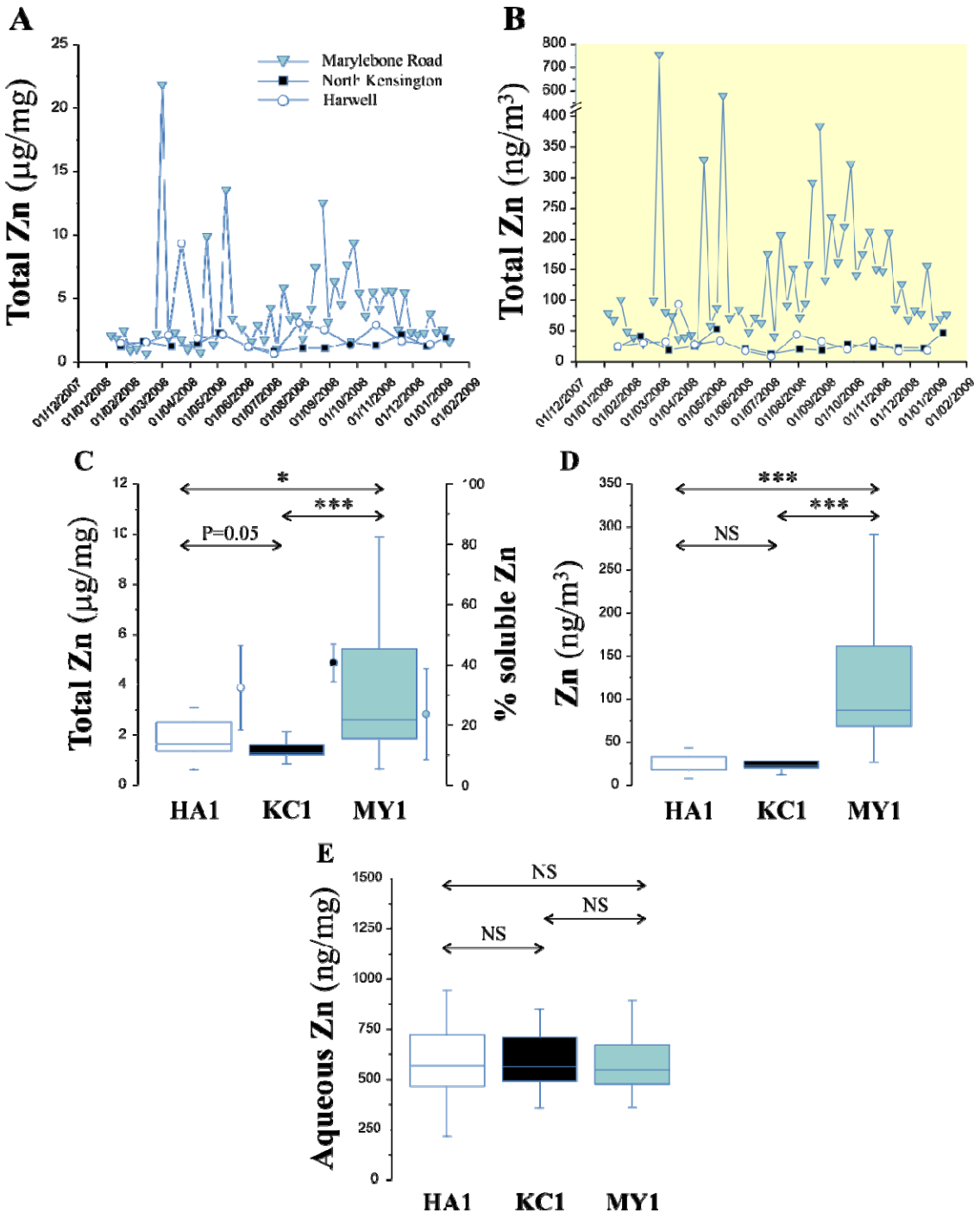

Figure 2.19: Total and aqueous PM_{10} Zn concentrations at Marylebone Road, North Kensington and Harwell, Jan 2008 – 2009. Figure formatting and details of the data analyses are as outlined in the legend to *Figure 2.10*.

Table 2.6: Associations between PM_{10} Zn concentrations, both total and aqueous with measures of oxidative potential (OP^{AA}, OP^{GSH} and OP^{TOT} per µg and m^3).

Parameters		All sites	MY1	KC1	HA1
OP^{AA}/µg	Total Zn (µg/mg)	0.375** *(n=81)*	0.376** *(n=53)*	0.588* *(n=14)*	-0.297*(n=14)*
OP^{AA}/µg	Aqueous Zn (ng/mg)	0.253* *(n=86)*	0.271* *(n=56)*	0.574* *(n=15)*	0.432 *(n=15)*
OP^{AA}/m^3	Total Zn (ng/m^3)	0.704*** *(n=81)*	0.315* *(n=53)*	0.793** *(n=14)*	-0.191 *(n=14)*
OP^{GSH}/µg	Total Zn (µg/mg)	0.311** *(n=81)*	0.089 *(n=53)*	0.295 *(n=14)*	0.169 *(n=14)*
OP^{GSH}/µg	Aqueous Zn (ng/mg)	-0.044 *(n=86)*	-0.208 *(n=56)*	0.504 *(n=15)*	0.529* *(n=15)*
OP^{GSH}/m^3	Total Zn (ng/m^3)	0.651*** *(n=81)*	0.191 *(n=53)*	0.319 *(n=14)*	0.108 *(n=14)*
OP^{TOT}/µg	Total Zn (µg/mg)	0.405*** *(n=81)*	0.292* *(n=53)*	0.481 *(n=14)*	-0.350 *(n=14)*
OP^{TOT}/µg	Aqueous Zn (ng/mg)	0.110 *(n=86)*	0.052 *(n=56)*	0.554* *(n=15)*	0.567* *(n=15)*
OP^{TOT}/m^3	Total Zn (ng/m^3)	0.688*** *(n=81)*	0.257 *(n=53)*	0.705** *(n=14)*	-0.224 *(n=14)*
Total Zn (µg/mg)	Aqueous Zn (ng/mg)	0.262* *(n=81)*	0.277* *(n=81)*	0.911*** *(n=14)*	-0.051 *(n=14)*

Increased Zn concentrations were associated with samples from Marylebone Road compared with the rural and urban background sites, both per µg and m^3 of PM_{10}, *Figure 2.9, panels A –D,* though the increment was mostly apparent from August 2008 to January 2009. In contrast, aqueous Zn concentrations were equivalent between the three sites, *Figure 2.19, panel E*, with the aqueous pool constituting 32.4±14.0, 40.6±6.2 and 23.7±15.0% of the total PM_{10} Zn content. Total Zn, expressed either per µg or m^3 was not associated with OP^{GSH}/µg or m^3 at any of the sites. In contrast both aqueous and total Zn was significantly associated with ascorbate dependent oxidative potential at the roadside and urban background sites, but not at Harwell, *Table 2.6*. Whilst PM_{10} Zn content was correlated with OP^{AA}/µg at MY1 ($r=0.38$, $P<0.05$), removal of the urban background concentrations did not strengthen the underlying relationship ($r=0.37$, $P<0.05$), *Figure 2.20*.

The third group of elements (C in *Figure 2.9*) consisted of Ni, Cr and V, defined by similar temporal profiles at Marylebone Road, with three peaks in the measured concentrations in July – August and a later peak at the end of 2008, and strong internal correlations: Ni versus Cr, $r=0.74$, $P<0.001$; Ni versus V, $r=0.65$, $P<0.001$; Cr versus V, $r=0.74$, $P<0.001$ ($n=53$). These three metals have previously been attributed to oil combustion (*Pakkanen et al, 2003*) and because of their enrichment in the accumulation mode have been proposed to be the result of long range transported combustion sources (*Allen et al, 2001*), including shipping (*Isaksen et al, 2001; Corbett and Fishbeck, 1997*).

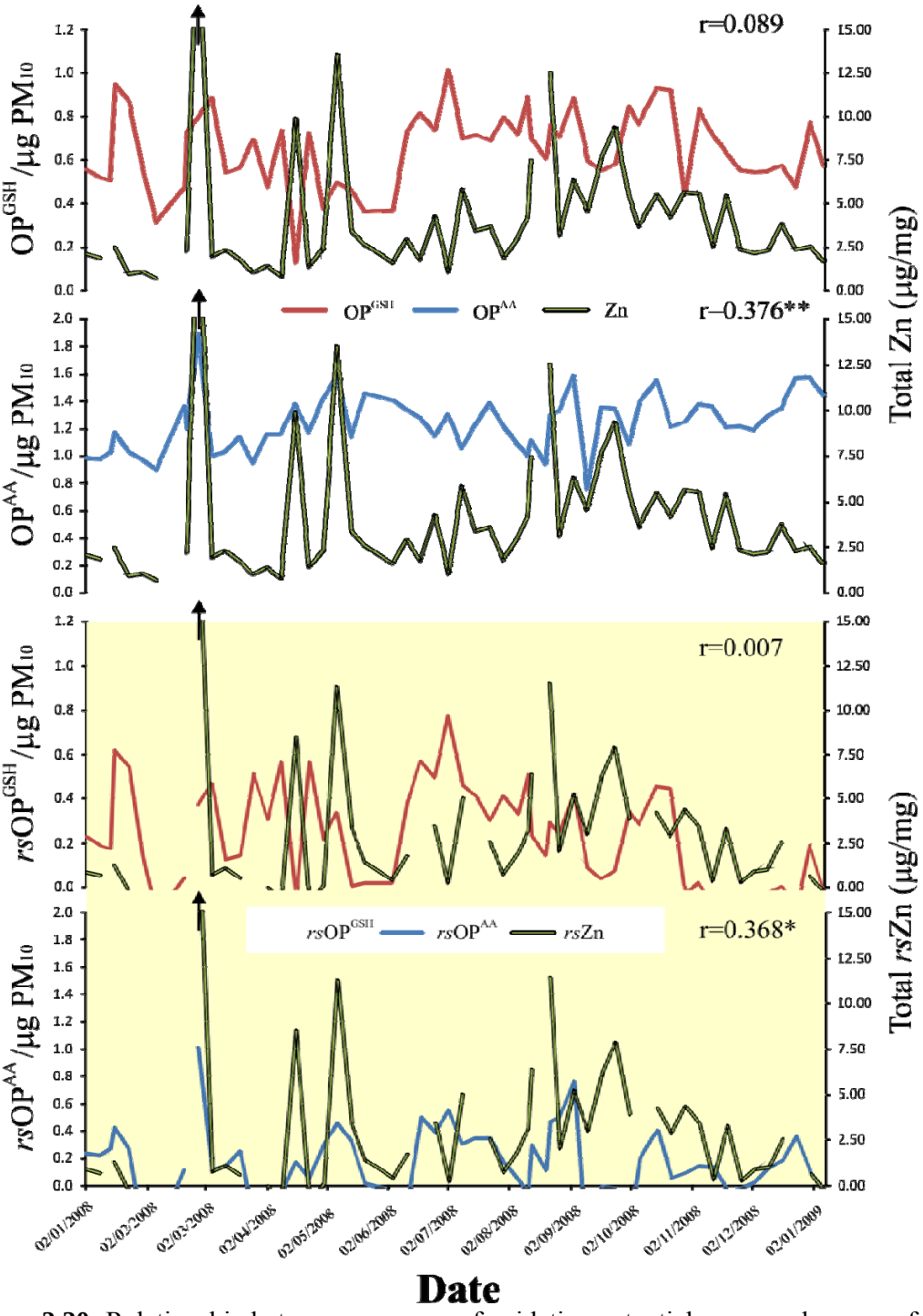

Figure 2.20: Relationship between measures of oxidative potential expressed per µg of filter extracted PM_{10} with total Zn concentrations at Marylebone Road between Jan 2008 and Jan 2009. Data are expressed with (lower panel) and without (upper panel) the subtraction of the background oxidative potentials and Zn concentration (derived from KC1) to derive the roadside increment. The results of a correlation analysis (Spearman's Rank Order) using the full or restricted OP parameters are inset. P<0.05 *; P<0.01**; P<0.001***.

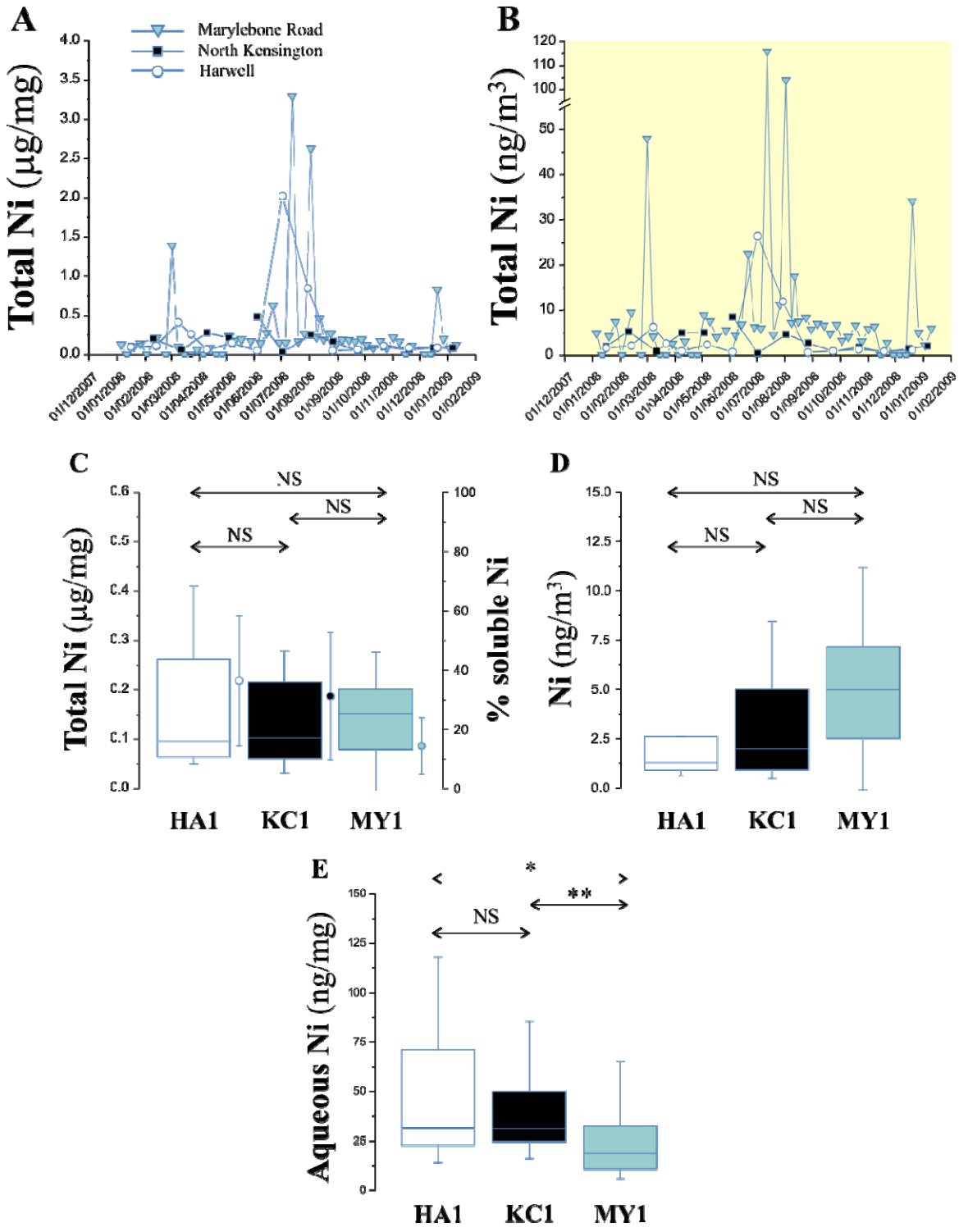

Figure 2.21: Total and aqueous PM_{10} Ni concentrations at Marylebone Road, North Kensington and Harwell, Jan 2008 – 2009. Figure formatting and details of the data analyses are as outlined in the legend to *Figure 2.10*.

Table 2.7: Associations between PM_{10} Ni concentrations, both total and aqueous with measures of oxidative potential (OP^{AA}, OP^{GSH} and OP^{TOT} per μg and m^3).

Parameters		All sites	MY1	KC1	HA1
OP^{AA}/μg	Total Ni (μg/mg)	0.133 *(n=81)*	0.234 *(n=53)*	0.136 *(n=14)*	-0.456 *(n=14)*
OP^{AA}/μg	Aqueous Ni (ng/mg)	0.146 *(n=86)*	0.395** *(n=56)*	0.667** *(n=15)*	0.429 *(n=15)*
OP^{AA}/m^3	Total Ni (ng/m^3)	0.336*** *(n=81)*	0.310* *(n=53)*	0.666** *(n=14)*	-0.367 *(n=14)*
OP^{GSH}/μg	Total Ni (μg/mg)	0.041 *(n=81)*	0.137 *(n=53)*	-0.471 *(n=14)*	0.123 *(n=14)*
OP^{GSH}/μg	Aqueous Ni (ng/mg)	-0.410*** *(n=86)*	-0.268* *(n=56)*	-0.079 *(n=15)*	0.168 *(n=15)*
OP^{GSH}/m^3	Total Ni (ng/m^3)	0.316** *(n=81)*	0.256 *(n=53)*	-0.134 *(n=14)*	0.073 *(n=14)*
OP^{TOT}/μg	Total Ni (μg/mg)	0.111 *(n=81)*	0.274* *(n=53)*	-0.074 *(n=14)*	-0.452 *(n=14)*
OP^{TOT}/μg	Aqueous Ni (ng/mg)	-0.146 *(n=86)*	0.096 *(n=56)*	0.402 *(n=15)*	0.291 *(n=15)*
OP^{TOT}/m^3	Total Ni (ng/m^3)	0.350** *(n=81)*	0.338* *(n=53)*	0.477 *(n=14)*	-0.312 *(n=14)*
Total Ni (μg/mg)	Aqueous Ni (ng/mg)	0.339** *(n=81)*	0.449** *(n=53)*	0.194 *(n=14)*	0.170 *(n=81)*

No contrast was apparent in total Ni concentrations between the three site types (*Figure 2.21, panels A-E*), though the proportion of aqueous Ni fell from the rural to the roadside sites: 36.4±21.8 (HA1), 29.6±21.5 (KC1) and 14.3±9.4% (MY1), consistent with an enrichment of insoluble forms of Ni at the roadside. Aqueous and total Ni was only found to be associated at the roadside site, *Table 2.7, row highlighted in blue*. Consistent with this, the concentration of Ni was significantly reduced in samples from Marylebone Road, compared with the rural and background sites, *Figure 2.21, panel E*. On a per mass basis only aqueous Ni was associated with OP^{AA}/μg at MY1 and KC1 (*Table 2.7*), with negative associations apparent at these sites with OP^{GSH}/μg.

In contrast to Ni, PM_{10} total Cr displayed a clear roadside increment in concentration compared with the rural and urban background sites, both when the concentrations were expressed per unit mass (*Figure 2.22, panels A and C*) or m^3 of PM_{10} (*Figure 2.22, panels B and D*). In contrast both total and aqueous Cr was equivalent at the rural and urban background sites suggesting a very local roadside source, with the proportion of soluble Cr lowest in samples from Marylebone Road: 7.7±6.3 (HA1), 9.9±10.6 (KC1) and 2.3±2.4% (MY1). This enrichment of the roadside sample with insoluble forms of Cr was reflected in the reduced concentration of aqueous Cr observed at Marylebone Road compared to Harwell and North Kensington (*Figure 2.22, panel E*). As with Ni as significant association between PM_{10} aqueous and total Cr was only observed at the roadside site, *Table 2.8*. At both MY1 and KC1, aqueous, but not total Cr was

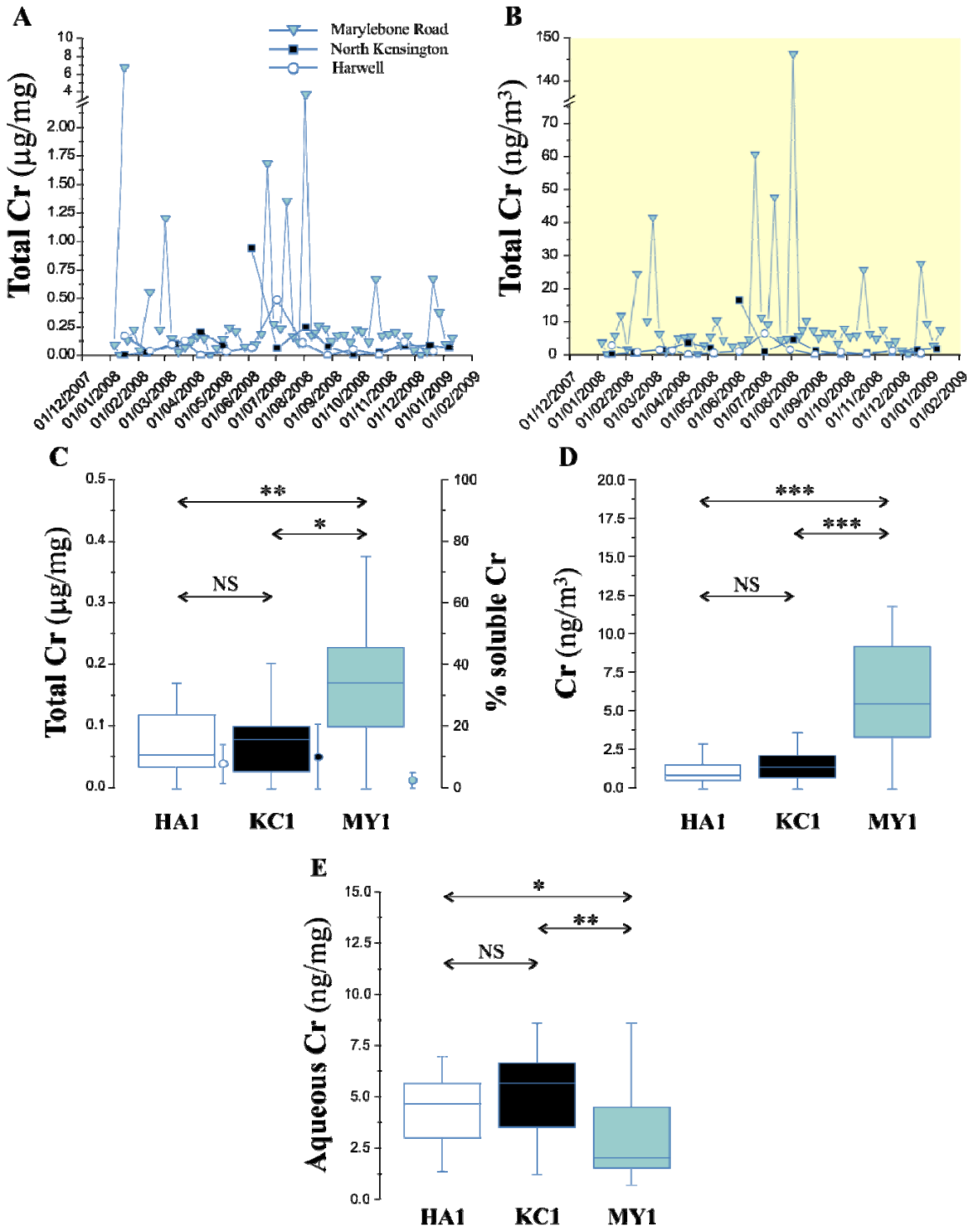

Figure 2.22: Total and aqueous PM_{10} Cr concentrations at Marylebone Road, North Kensington and Harwell, Jan 2008 – 2009. Figure formatting and details of the data analyses are as outlined in the legend to *Figure 2.10*.

Table 2.8: Associations between PM_{10} Cr concentrations, both total and aqueous with measures of oxidative potential (OP^{AA}, OP^{GSH} and OP^{TOT} per µg and m^3).

Parameters		All sites	MY1	KC1	HA1
OP^{AA}/µg	Total Cr (µg/mg)	0.253* *(n=81)*	0.073 *(n=53)*	0.052 *(n=14)*	-0.361 *(n=14)*
OP^{AA}/µg	Aqueous Cr (ng/mg)	0.268* *(n=86)*	0.520*** *(n=56)*	0.649** *(n=15)*	0.537* *(n=15)*
OP^{AA}/m^3	Total Cr (ng/m^3)	0.620*** *(n=81)*	0.415** *(n=53)*	0.226 *(n=14)*	-0.376 *(n=14)*
OP^{GSH}/µg	Total Cr (µg/mg)	0.440*** *(n=81)*	0.372** *(n=53)*	-0.277 *(n=14)*	0.132 *(n=14)*
OP^{GSH}/µg	Aqueous Cr (ng/mg)	-0.414*** *(n=86)*	-0.357** *(n=56)*	0.086 *(n=15)*	0.224 *(n=15)*
OP^{GSH}/m^3	Total Cr (ng/m^3)	0.673*** *(n=81)*	0.531*** *(n=53)*	-0.385 *(n=14)*	-0.011 *(n=14)*
OP^{TOT}/µg	Total Cr (µg/mg)	0.434*** *(n=81)*	0.368** *(n=53)*	0.011 *(n=14)*	-0.115 *(n=14)*
OP^{TOT}/µg	Aqueous Cr (ng/mg)	0.090 *(n=86)*	0.111 *(n=56)*	0.568* *(n=15)*	0.418 *(n=15)*
OP^{TOT}/m^3	Total Cr (ng/m^3)	0.669*** *(n=81)*	0.526*** *(n=53)*	0.130 *(n=14)*	-0.277 *(n=14)*
Total Cr (µg/mg)	Aqueous Cr (ng/mg)	-0.076 *(n=81)*	0.140 *(n=53)*	0.381 *(n=14)*	-0.280 *(n=14)*

significantly associated with OP^{AA}/µg, with no positive correlations observed with OP^{GSH}/µg. In contrast, total Cr was significantly associated with the glutathione dependant oxidative potential, though this association was restricted to the roadside site only. This association was weakened by removing the background Cr and OP^{GSH}/µg using the data from North Kensington, r=0.37, (P<0.01) versus r=0.21, *Figure 2.23*. In contrast OP^{AA}/µg was only associated with PM_{10} total Cr following the removal of the background concentrations and activities (r=0.07 versus r=0.33(P<0.01)), *Figure 2.23*.

The pattern of PM_{10} V concentrations across the three site types was identical to that observed for Cr, with clear increments in concentration between the roadside site with the rural and urban background locations, but no contrast in the concentrations in these later two site types, *Figure 2.24*. Similarly, aqueous V was decreased at MY1, compared with the concentrations reported at HA1 and KC1 reflecting the decreased solubility observed across these site classifications: 17.8±17.4 (HA1), 8.3±6.3 (KC1) and 3.5±4.9% (MY1). No simplistic association between PM aqueous and total V was apparent at any of the sites examined, *Table 2.9*. Whilst no positive associations were noted between OP^{GSH}/µg with total or aqueous V at any of the sites considered, both V measures were significantly associated with OP^{AA}/µg at MY1, *Table 2.9*. The strength of the association with total V at MY1 was only marginally improved by the subtraction of the background metal concentration and OP^{AA}/µg activity, r=0.33, P<0.05 versus r=0.40, P<0.01, *Figure 2.25*.

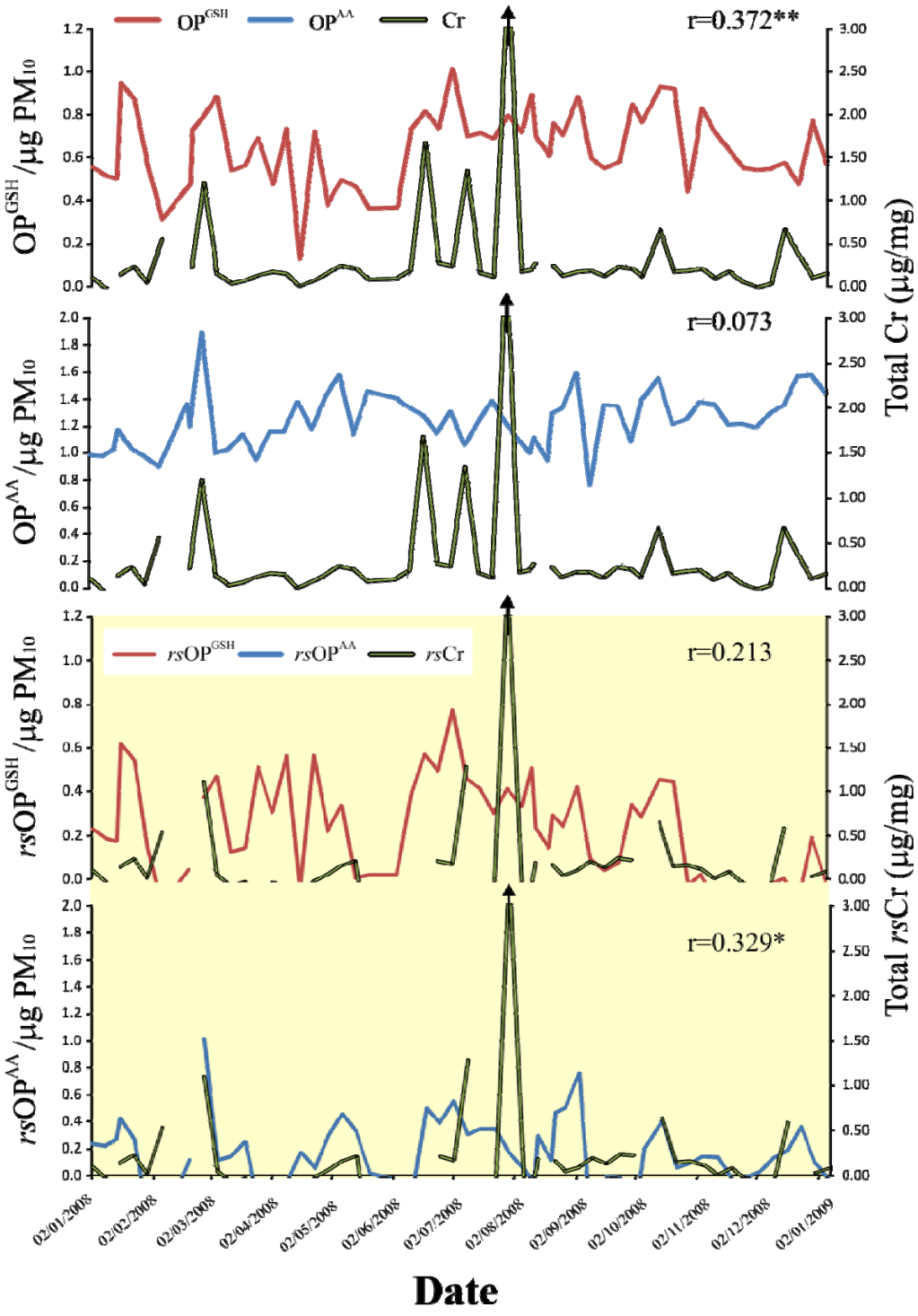

Figure 2.23: Relationship between measures of oxidative potential expressed per µg of filter extracted PM_{10} with total Cr concentrations at Marylebone Road between Jan 2008 and Jan 2009. Data are expressed with (lower panel) and without (upper panel) the subtraction of the background oxidative potentials and Cr concentration (derived from KC1) to derive the roadside increment. The results of a correlation analysis (Spearman's Rank Order) using the full or restricted OP parameters are inset. P<0.05 *; P<0.01**; P<0.001***.

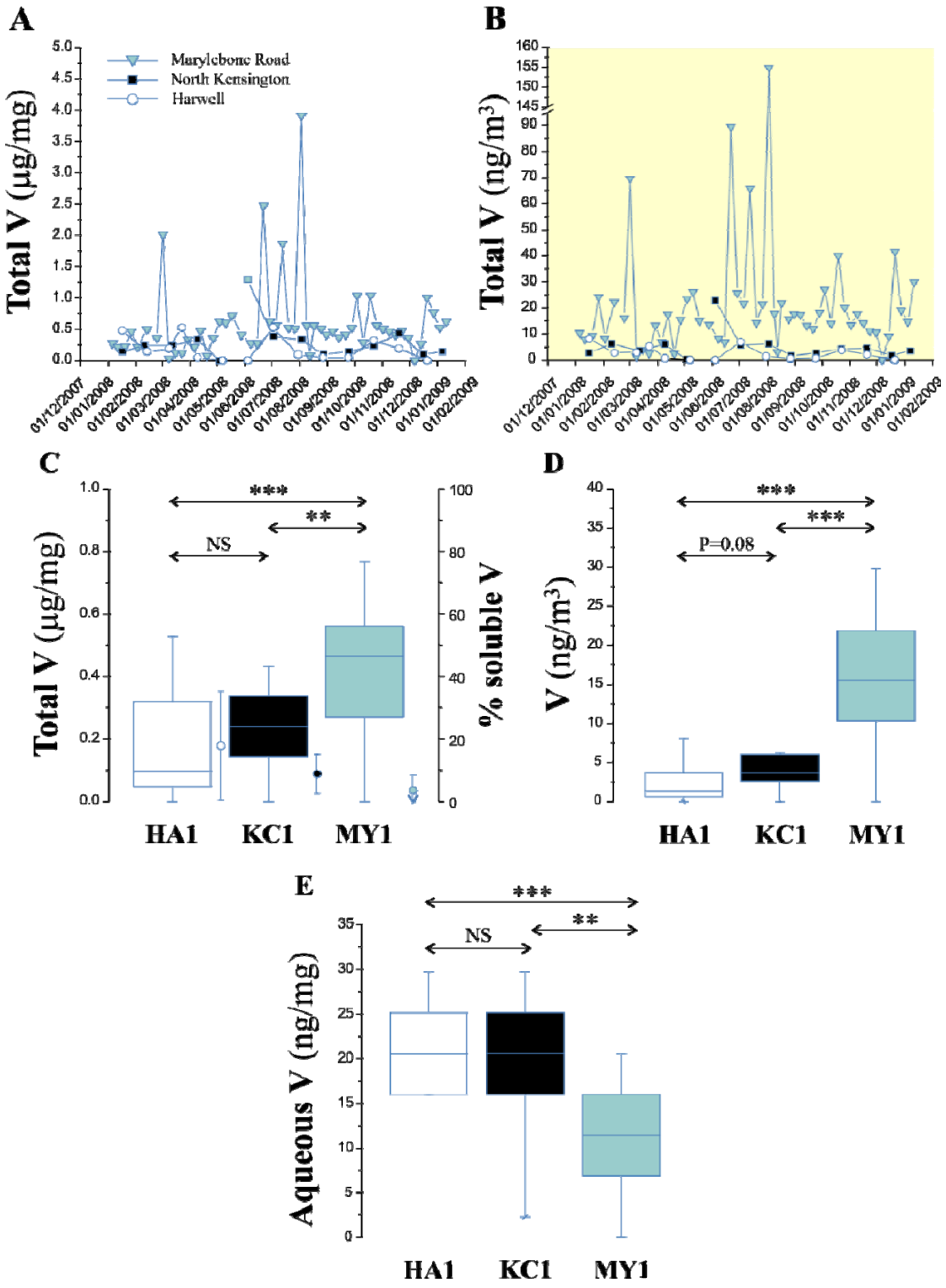

Figure 2.24: Total and aqueous PM_{10} V concentrations at Marylebone Road, North Kensington and Harwell, Jan 2008 – 2009. Figure formatting and details of the data analyses are as outlined in the legend to *Figure 2.10*.

Table 2.9: Associations between PM_{10} V concentrations, both total and aqueous with measures of oxidative potential (OP^{AA}, OP^{GSH} and OP^{TOT} per µg and m^3).

Parameters		All sites	MY1	KC1	HA1
OP^{AA}/µg	Total V (µg/mg)	0.425*** *(n=81)*	0.331* *(n=53)*	0.162 *(n=14)*	-0.673** *(n=14)*
OP^{AA}/µg	Aqueous V (ng/mg)	0.025 *(n=86)*	0.401** *(n=56)*	0.479 *(n=15)*	0.374 *(n=15)*
OP^{AA}/m^3	Total V (ng/m^3)	0.702*** *(n=81)*	0.493*** *(n=53)*	0.011 *(n=14)*	-0.614* *(n=14)*
OP^{GSH}/µg	Total V (µg/mg)	0.432*** *(n=81)*	0.203 *(n=53)*	-0.098 *(n=14)*	0.394 *(n=14)*
OP^{GSH}/µg	Aqueous V (ng/mg)	-0.495*** *(n=86)*	-0.301* *(n=56)*	0.209 *(n=15)*	-0.339 *(n=15)*
OP^{GSH}/m^3	Total V (ng/m^3)	0.676*** *(n=81)*	0.366** *(n=53)*	-0.191 *(n=14)*	0.363 *(n=14)*
OP^{TOT}/µg	Total V (µg/mg)	0.524*** *(n=81)*	0.427** *(n=53)*	0.157 *(n=14)*	-0.333 *(n=14)*
OP^{TOT}/µg	Aqueous V (ng/mg)	-0.254* *(n=86)*	0.084 *(n=56)*	0.486 *(n=15)*	0.210 *(n=15)*
OP^{TOT}/m^3	Total V (ng/m^3)	0.713*** *(n=81)*	0.493*** *(n=53)*	0.020 *(n=14)*	-0.383 *(n=14)*
Total V (µg/mg)	Aqueous V (ng/mg)	-0.107 *(n=81)*	0.259 *(n=53)*	0.386 *(n=14)*	-0.514 *(n=14)*

PM_{10} Cu and Sb were grouped together (group D) and not with Zn, Ba and Sr (group B), as was suggested by the principal factor analysis, due to differences in their temporal profile at Marylebone Road, *figure 2.9*. Whilst the later three elements demonstrated peak concentrations between the 1st week in August to the end of December, Cu and Sb demonstrated elevated concentrations earlier in the year from mid-May through to the first week of September. Together this grouping of elements can be viewed as indicative of vehicle-related erosion processes, Cu, Sb and Ba reflecting brake wear (*Garg et al. 2000; Weckwerth 2001; Sternbeck et al. 2002*), whilst Zn is commonly employed as a marker of tyre wear (*Sternbeck et al. 2002*). Separating these elements therefore provides a clearer marker of tyre (Zn) and brake wear (Cu and Sb), through the basis for the relationship between Zn, Ba and Sr remains unclear. Additionally, Sternbeck *et al* (2002), who examined PM-metal emissions from tunnel sites in Gothenburg, Sweden, calculated that a ratio of Cu:Sb of 4.3±2.1 was predictive of Cu released from brake pads. In the present study the ratios of these elements at each of the site types were: 5.0±3.5 (HA1), 4.3±1.1 (KC1), and 7.3±2.5 (MY1) for total metals and 3.4±1.5 (HA1), 5.6±1.4 (KC1), and 7.1±1.2 (MY1) for the aqueous fraction consistent with the brake signature.

Total Cu concentrations showed clear rural to urban background and background to roadside increments in concentration both on a per unit mass (*Figure 2.26, panels A and C*) and m^3 basis (*Figure 2.26, panels B and D*), with the roadside increment sustained throughout the year bar late December. Notably, there was little apparent temporal

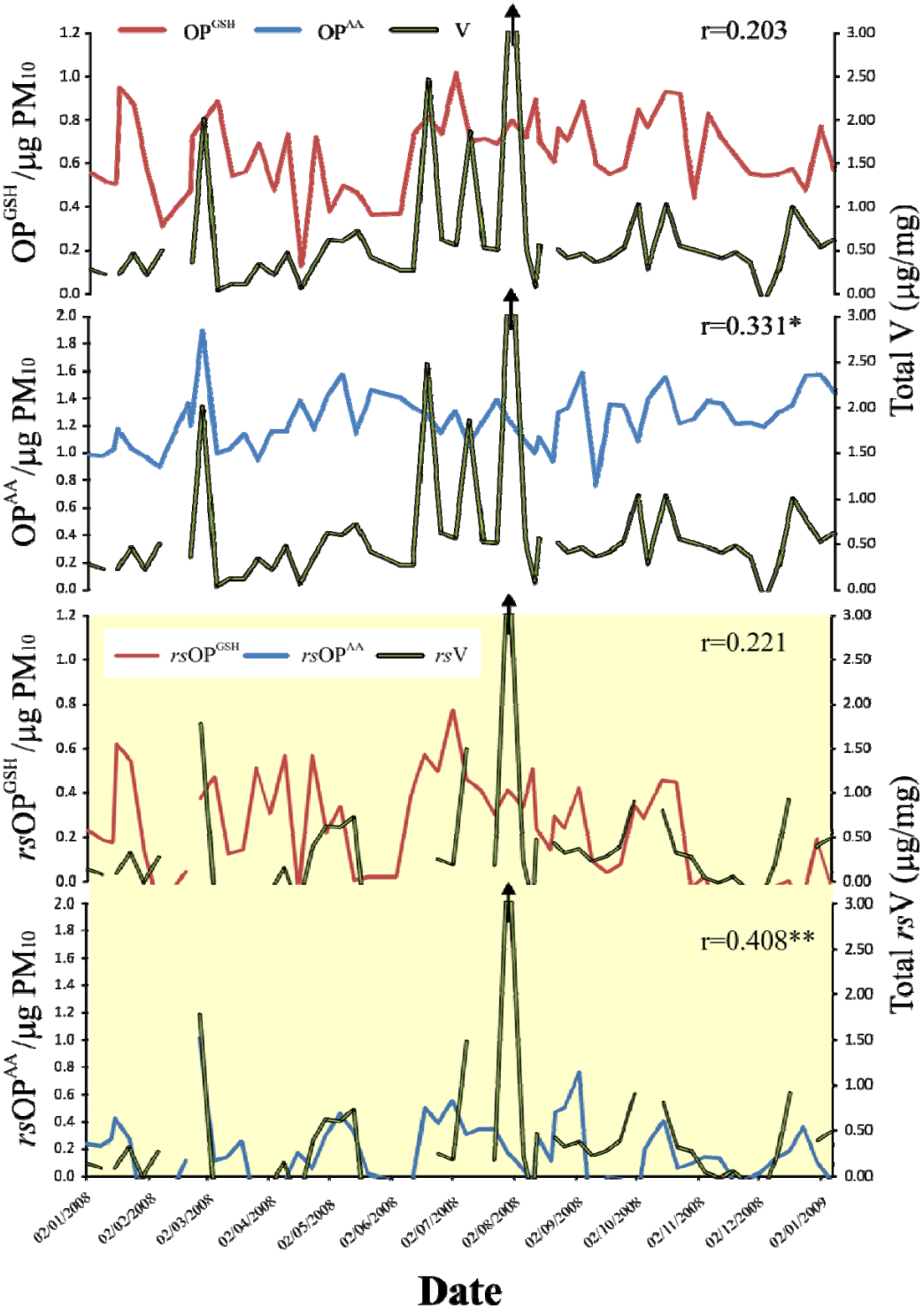

Figure 2.25: Relationship between measures of oxidative potential expressed per µg of filter extracted PM_{10} with total V concentrations at Marylebone Road between Jan 2008 and Jan 2009. Data are expressed with (lower panel) and without (upper panel) the subtraction of the background oxidative potentials and V concentration (derived from KC1) to derive the roadside increment. The results of a correlation analysis (Spearman's Rank Order) using the full or restricted OP parameters are inset. P<0.05 *; P<0.01**; P<0.001***.

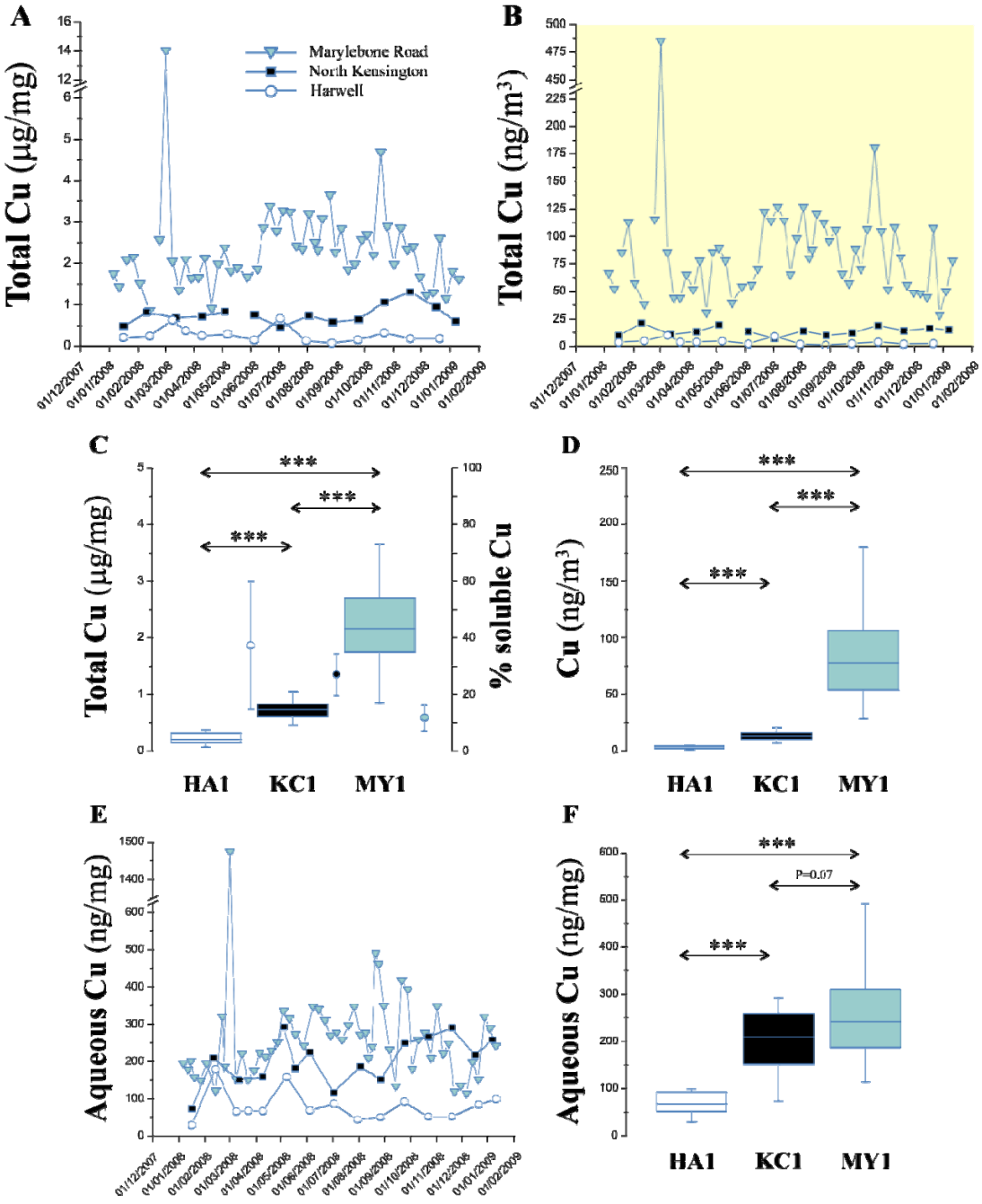

Figure 2.26: Total and aqueous PM_{10} Cu concentrations at Marylebone Road, North Kensington and Harwell, Jan 2008 – 2009. Panels **A** and **B** illustrate the temporal profile of PM_{10} Cu concentrations expressed per µg or m^3 at each of the selected sites, with the data formatted as outlined in the legend to *figure 2.9*. Panel **C** illustrates the statistical comparison of the Cu concentrations (µg/mg) at each site, with the figure formatting and details of the analyses as outlined in the legend to *figure 2.2*. Panel **C** also illustrates the contribution aqueous Fe makes to total PM Cu, with the data summarised as a mean % ± SD. Panel **D** illustrates the statistical comparison of PM total Cu, expressed as ng/m^3. Panel **E** illustrates the temporal profile for aqueous Cu at each of the sites with panel **F** showing the site contrasts in aqueous Cu. P<0.05*; P<0.01**; P<0.001***.

Table 2.10: Associations between PM_{10} Cu concentrations, both total and aqueous with measures of oxidative potential (OP^{AA}, OP^{GSH} and OP^{TOT} per µg and m^3).

Parameters		All sites	MY1	KC1	HA1
OP^{AA}/µg	Total Cu (µg/mg)	0.527*** *(n=81)*	0.202 *(n=53)*	0.392 *(n=14)*	-0.464 *(n=14)*
OP^{AA}/µg	Aqueous Cu (ng/mg)	0.734*** *(n=86)*	0.539*** *(n=56)*	0.674** *(n=15)*	0.518* *(n=15)*
OP^{AA}/m^3	Total Cu (ng/m^3)	0.865*** *(n=81)*	0.589*** *(n=53)*	0.640* *(n=14)*	-0.103 *(n=14)*
OP^{GSH}/µg	Total Cu (µg/mg)	0.830*** *(n=81)*	0.693*** *(n=53)*	0.297 *(n=14)*	0.084 *(n=14)*
OP^{GSH}/µg	Aqueous Cu (ng/mg)	0.465*** *(n=86)*	-0.023 *(n=56)*	0.414 *(n=15)*	-0.182 *(n=15)*
OP^{GSH}/m^3	Total Cu (ng/m^3)	0.924*** *(n=81)*	0.792*** *(n=53)*	0.468 *(n=14)*	0.029 *(n=14)*
OP^{TOT}/µg	Total Cu (µg/mg)	0.786*** *(n=81)*	0.608*** *(n=53)*	0.440 *(n=14)*	-0.410 *(n=14)*
OP^{TOT}/µg	Aqueous Cu (ng/mg)	0.679*** *(n=86)*	0.375** *(n=56)*	0.667** *(n=15)*	0.245 *(n=15)*
OP^{TOT}/m^3	Total Cu (ng/m^3)	0.919*** *(n=81)*	0.757*** *(n=53)*	0.705** *(n=14)*	-0.084 *(n=14)*
Total Cu (µg/mg)	Aqueous Cu (ng/mg)	0.633*** *(n=81)*	0.363** *(n=53)*	0.714** *(n=14)*	0.293 *(n=16)*

correlation between the concentrations measured at the rural and urban background site. Aqueous Cu concentrations were also enriched in the roadside and urban background PM_{10} samples relative to the rural samples (*Figure 2.26, panels E and F*), with some evidence of trend (P=0.07) toward an increase in water soluble Cu at MY1, with the increment being clearest during the Sumer months. In line with many of the metals examined the proportion of soluble Cu fell from the rural to roadside site: 37.3±22.6 (HA1), 25.8±7.4 (KC1) and 11.8±4.8% (MY1), with significant associations between the total and aqueous Cu pools observed at the roadside and urban background sites, *Table 2.10*.

No association was observed between total Cu and OP^{AA}/µg at any of the sites, with more consistent relationships apparent with the aqueous pool, *Table 2.10*. In contrast aqueous Cu was not related to OP^{GSH}/µg, with significant associations only noted with total Cu at MY1. Subtraction of the urban background Cu concentration and oxidative potential did not strengthen this relationship: r=0.69, P<0.001 versus r=0.63, P<0.001, *Figure 2.27*. In contrast subtracting the background significantly improved the relationship between OP^{AA}/µg with total PM_{10} Cu: r=0.202 versus r=0.50, P<0.001.

The pattern of relationships between the site classifications with total Sb was similar to that reported for Cu, with clear increases in Sb content at the roadside site relative to the urban background and between the rural and background sites, *Figure 2.28, panels A - E*. In contrast to Cu, where there was little temporal relationship between the

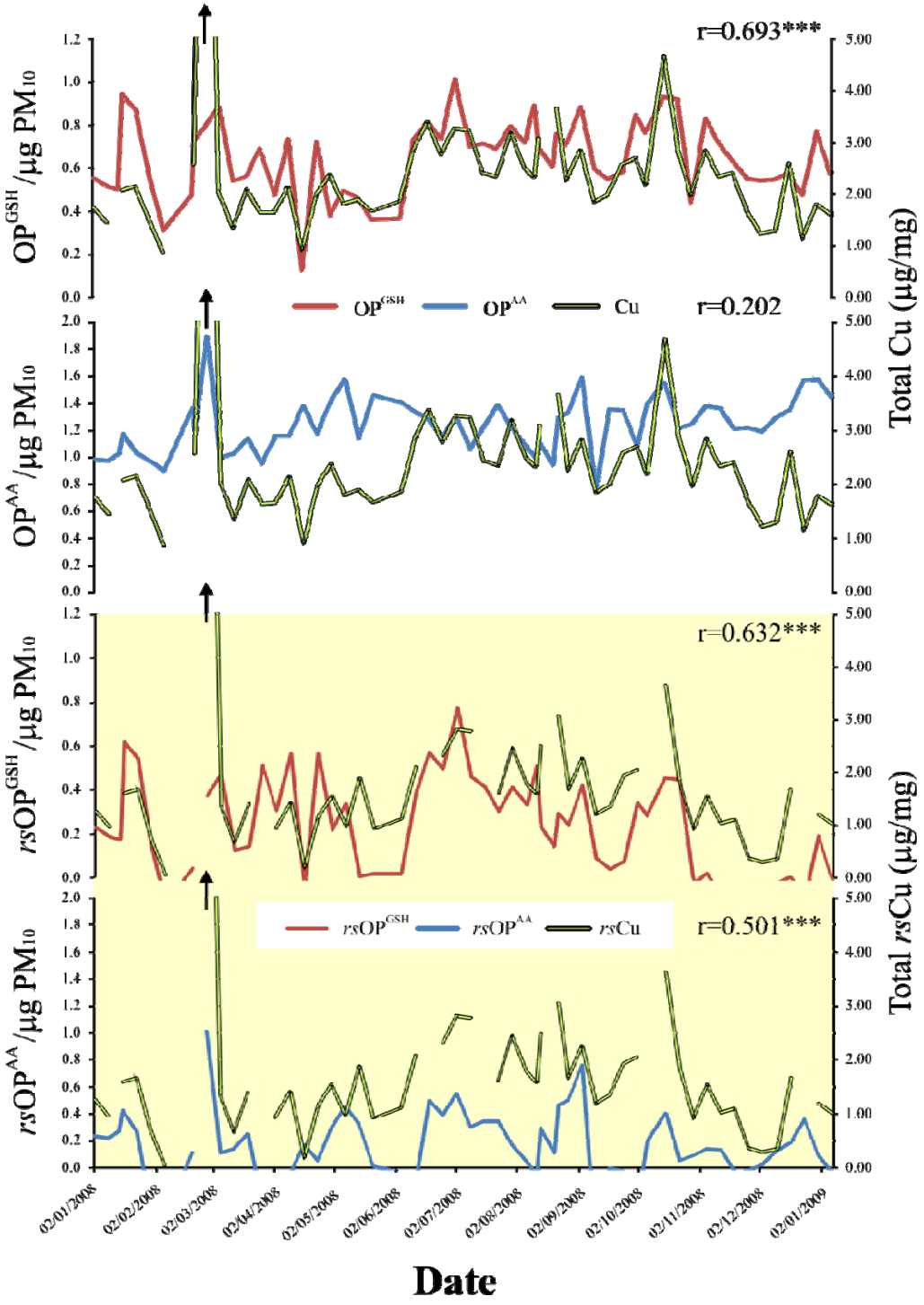

Figure 2.27: Relationship between measures of oxidative potential expressed per µg of filter extracted PM_{10} with total Cu concentrations at Marylebone Road between Jan 2008 and Jan 2009. Data are expressed with (lower panel) and without (upper panel) the subtraction of the background oxidative potentials and Cu concentration (derived from KC1) to derive the roadside increment. The results of a correlation analysis (Spearman's Rank Order) using the full or restricted OP parameters are inset. P<0.05 *; P<0.01**; P<0.001***.

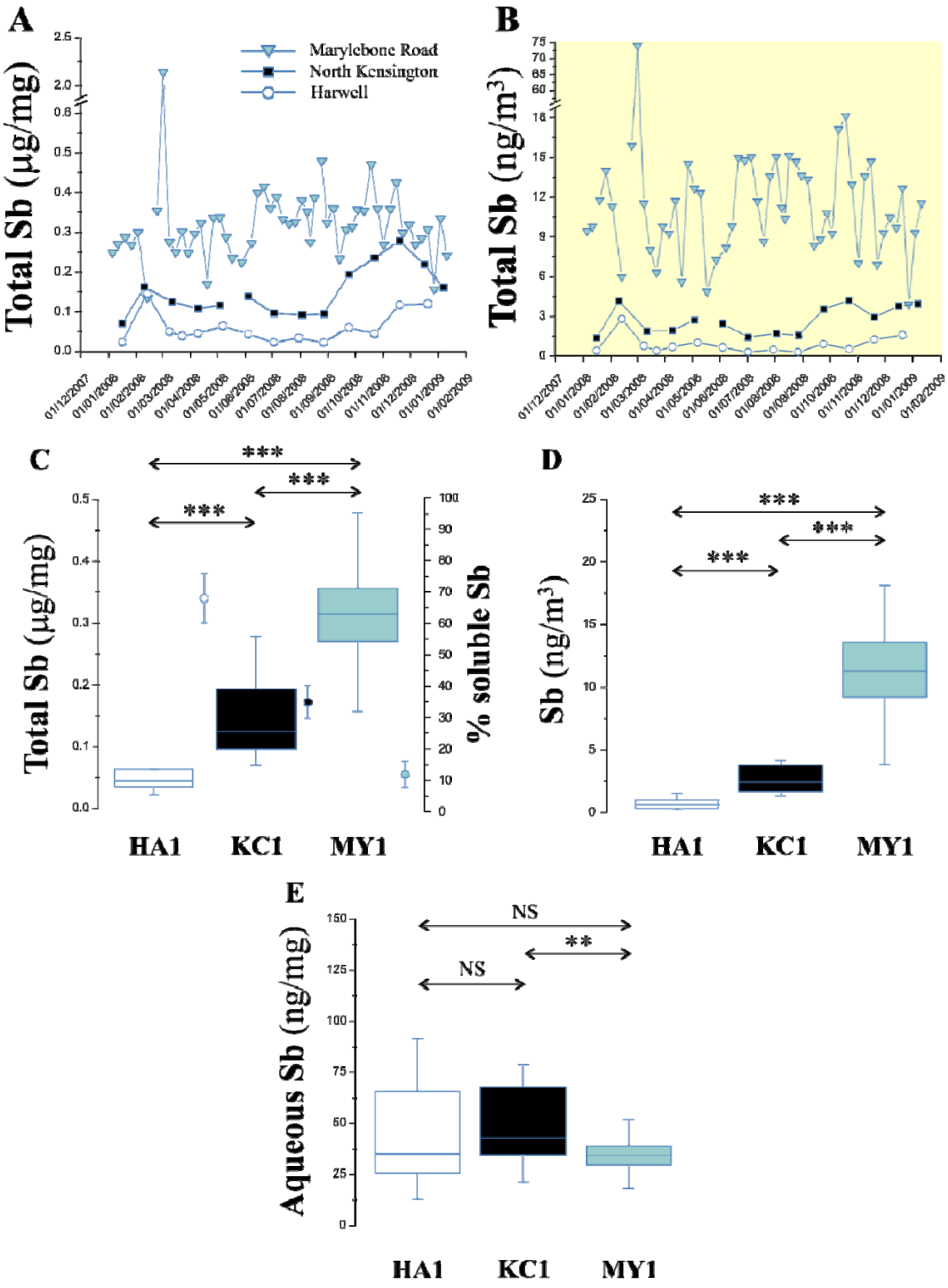

Figure 2.28: Total and aqueous PM_{10} Sb concentrations at Marylebone Road, North Kensington and Harwell, Jan 2008 – 2009. Figure formatting and details of the data analyses are as outlined in the legend to *Figure 2.10*.

Table 2.11: Associations between PM_{10} Sb concentrations, both total and aqueous with measures of oxidative potential (OP^{AA}, OP^{GSH} and OP^{TOT} per µg and m^3).

Parameters		All sites	MY1	KC1	HA1
OP^{AA}/µg	Total Sb (µg/mg)	0.595*** *(n=81)*	0.291* *(n=53)*	0.664* *(n=14)*	0.634* *(n=14)*
OP^{AA}/µg	Aqueous Sb (ng/mg)	0.539*** *(n=86)*	0.772*** *(n=56)*	0.835*** *(n=15)*	0.718** *(n=15)*
OP^{AA}/m^3	Total Sb (ng/m^3)	0.906*** *(n=81)*	0.712*** *(n=53)*	0.622* *(n=14)*	0.670** *(n=14)*
OP^{GSH}/µg	Total Sb (µg/mg)	0.843*** *(n=81)*	0.662*** *(n=53)*	0.699** *(n=14)*	0.138 *(n=14)*
OP^{GSH}/µg	Aqueous Sb (ng/mg)	-0.102** *(n=86)*	-0.161 *(n=56)*	0.632* *(n=15)*	0.146 *(n=15)*
OP^{GSH}/m^3	Total Sb (ng/m^3)	0.933*** *(n=81)*	0.814*** *(n=53)*	0.671** *(n=14)*	0.125 *(n=14)*
OP^{TOT}/µg	Total Sb (µg/mg)	0.835*** *(n=81)*	0.660*** *(n=53)*	0.753** *(n=14)*	0.462 *(n=14)*
OP^{TOT}/µg	Aqueous Sb (ng/mg)	0.249* *(n=86)*	0.425** *(n=56)*	0.890*** *(n=15)*	0.556* *(n=15)*
OP^{TOT}/m^3	Total Sb (ng/m^3)	0.953*** *(n=81)*	0.854*** *(n=53)*	0.763** *(n=14)*	0.627* *(n=14)*
Total Sb (µg/mg)	Aqueous Sb (ng/mg)	0.063 *(n=81)*	0.208 *(n=53)*	0.937*** *(n=14)*	0.966*** *(n=14)*

concentrations measured at the rural and urban background sites, Sb concentrations tracked closely throughout the year, peaking during the winter. Also in contrast to Cu there was no enrichment of soluble Cu in roadside PM_{10}, but rather a significant decrease relative to the background site, reflecting the sharp reduction in the aqueous pool: 68.8±7.8 (HA1), 34.2±5.2 (KC1) and 11.9±4.3% (MY1), *Figure 2.28, panel C*. Both total and aqueous Sb was significantly correlated with OP^{AA}/µg at all sites, though the strength of the relationship was stronger with the soluble pool, *Table 2.11*. The relationship between Sb and OP^{GSH}/µg was more site specific, with total Sr being significantly associated with the glutathione metric at MY1, both pools being equally predictive at KC1, and no association apparent at HA1, *Table 2.11*. As with Cu removing background total Sb and OPs had little effect on the strength of the association between OP^{GSH}/µg and Sb: r=0.66, P<0.001 versus r=0.73, P<0.001, *Figure 3.29*. In contrast removing background concentrations and activities significantly improved the strength of association between OP^{AA}/µg with total Sb, r=0.29, P<0.05 versus r=0.60, P<0.001, *Figure 2.29*

The temporal profile of Al at MY1 was not easily related to any of the other elements examined, though a significant roadside increment was apparent irrespective of whether the data were expressed per unit mass (*Figure 2.30, panels A and C*) or m^3 (*Figure 2.30, panels B and D*). Like the majority of the elements considered the proportion of the total pool present as aqueous Al was reduced at the roadside site relative to the rural and urban background locations, Figure 2.30, panel C, reflected by a decreased concentration

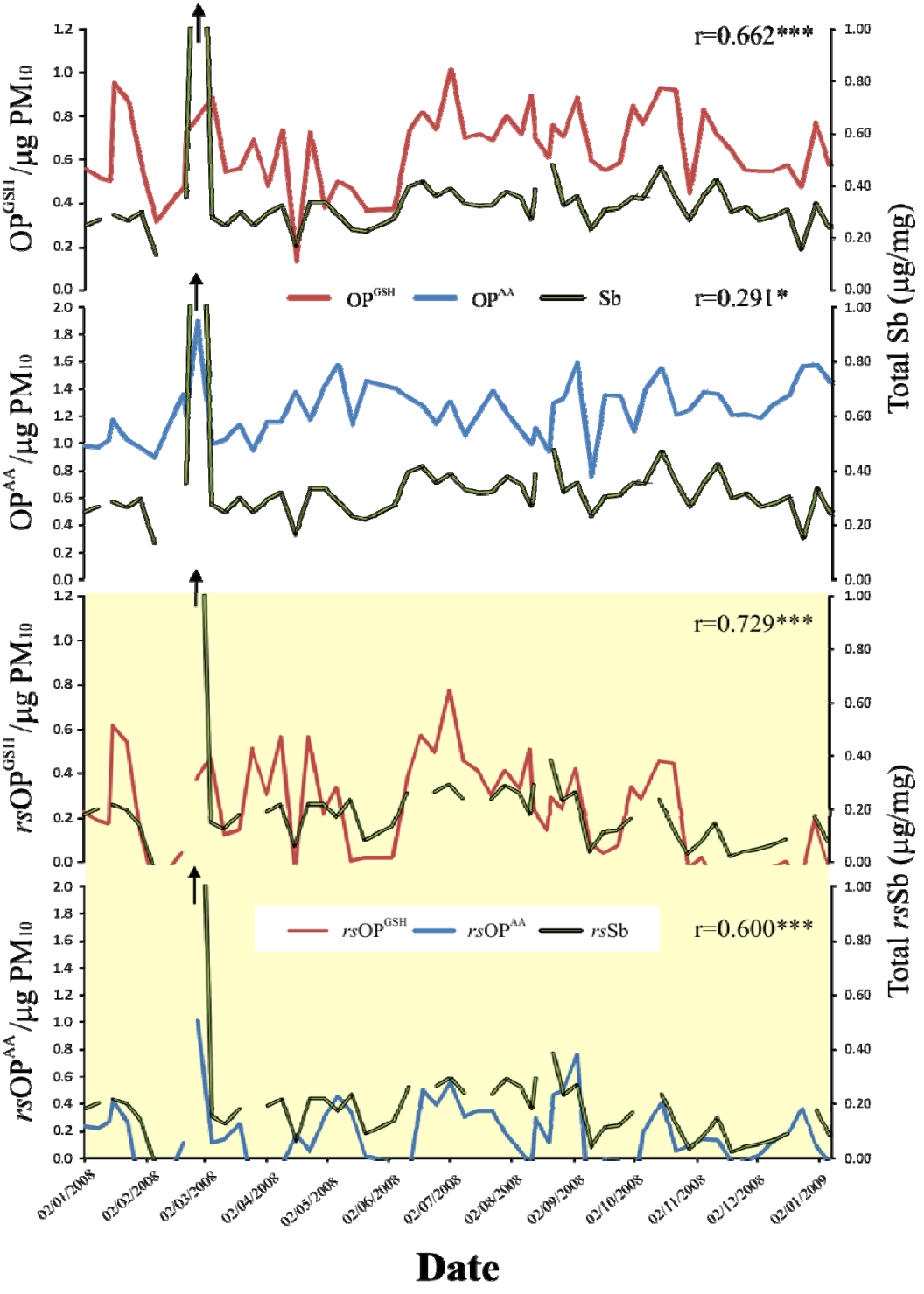

Figure 2.29: Relationship between measures of oxidative potential expressed per µg of filter extracted PM_{10} with total Sb concentrations at Marylebone Road between Jan 2008 and Jan 2009. Data are expressed with (lower panel) and without (upper panel) the subtraction of the background oxidative potentials and Sb concentration (derived from KC1) to derive the roadside increment. The results of a correlation analysis (Spearman's Rank Order) using the full or restricted OP parameters are inset. P<0.05 *; P<0.01**; P<0.001***.

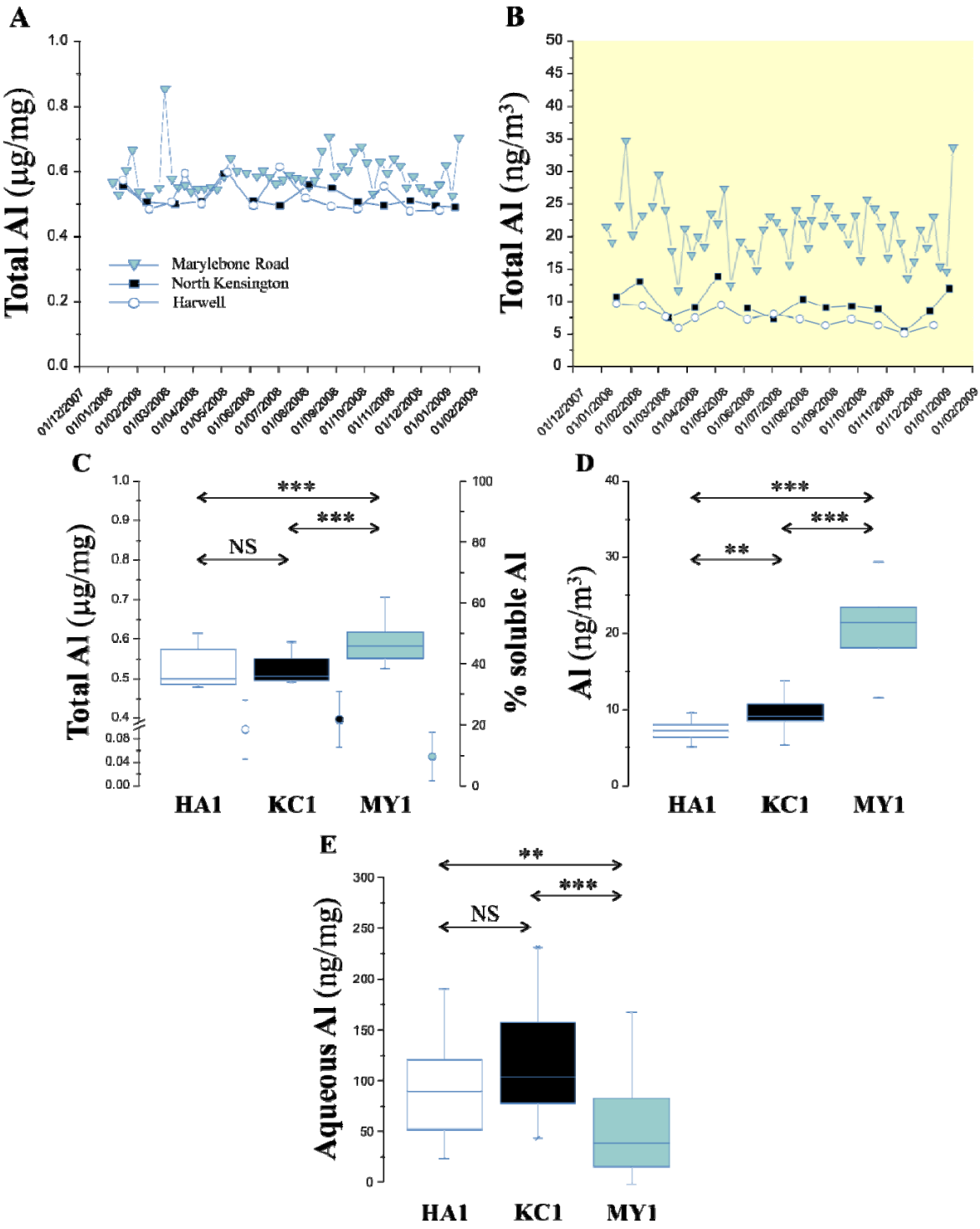

Figure 2.30: Total and aqueous PM_{10} Al concentrations at Marylebone Road, North Kensington and Harwell, Jan 2008 – 2009. Figure formatting and details of the data analyses are as outlined in the legend to *Figure 2.10*.

Table 2.12: Associations between PM_{10} Al concentrations, both total and aqueous with measures of oxidative potential (OP^{AA}, OP^{GSH} and OP^{TOT} per μg and m^3).

Parameters		All sites	MY1	KC1	HA1
OP^{AA}/μg	Total Al (μg/mg)	0.300** *(n=81)*	0.291* *(n=53)*	-0.239 *(n=14)*	-0.584* *(n=14)*
OP^{AA}/μg	Aqueous Al (ng/mg)	0.082 *(n=86)*	0.362** *(n=56)*	0.460 *(n=15)*	0.602* *(n=15)*
OP^{AA}/m^3	Total Al (ng/m^3)	0.921*** *(n=81)*	0.785*** *(n=53)*	0.745** *(n=14)*	0.231 *(n=14)*
OP^{GSH}/μg	Total Al (μg/mg)	0.423*** *(n=81)*	0.218 *(n=53)*	-0.439 *(n=14)*	-0.250 *(n=14)*
OP^{GSH}/μg	Aqueous Al (ng/mg)	-0.427*** *(n=86)*	-0.260 *(n=56)*	0.107 *(n=15)*	-0.214 *(n=15)*
OP^{GSH}/m^3	Total Al (ng/m^3)	0.882*** *(n=81)*	0.709*** *(n=53)*	0.160 *(n=14)*	-0.064 *(n=14)*
OP^{TOT}/μg	Total Al (μg/mg)	0.445*** *(n=81)*	0.367** *(n=53)*	-0.314 *(n=14)*	-0.561* *(n=14)*
OP^{TOT}/μg	Aqueous Al (ng/mg)	-0.221* *(n=86)*	0.081 *(n=56)*	0.385 *(n=15)*	0.303 *(n=15)*
OP^{TOT}/m^3	Total Al (ng/m^3)	0.943*** *(n=81)*	0.856*** *(n=53)*	0.578* *(n=14)*	0.343 *(n=14)*
Total Al (μg/mg)	Aqueous Al (ng/mg)	-0.059 *(n=81)*	0.451*** *(n=53)*	0.355 *(n=14)*	0.104 *(n=14)*

of soluble Al at MY1 relative to HA1 and KC1 (*panel E*). Whilst PM_{10} Al concentrations were not associated with OP^{GSH}/μg at any of the sites, a weak positive association between total and aqueous Al was noted with OP^{AA}/μg at MY1, *Table 2.12*. Removal of the background OPs and total Al concentrations from the measurements made at MY1 failed to improve these associations and in the case of OP^{AA}/μg actually weaken the original association, r=0.29, P<0.05 versus r=0.01, *Figure 2.31*.

Pb concentrations in PM_{10} from each of the site classifications are shown in *Figure 2.32*, and demonstrate the absence of a clear increase in roadside concentrations when either total or aqueous Pb are considered on a per unit mass basis (*panels A, C and E*). Pb concentrations, both total and aqueous, were decreased at Marylebone Road relative to the concentrations found in the samples from North Kensington. Notably the temporal profile of PM_{10} Pb at the rural and urban background locations tracked each other closely, with clear evidence of increased concentrations from Mid September 2008 – Jan 2009 (*panel A*). A similar temporal trend was also apparent at MY1 with the concentrations closely tracking and being equivalent to those reported at the rural site. Consistent with the decreased concentration of aqueous Pb at MY1 the percentage of the total Pb pool present in its water soluble form fell from the rural to roadside site: 27.5±11.7 (HA1), 17.9±8.3 (KC1) and 6.4±4.7% (MY1), *Figure 3.32, panel C*, with evidence that the total and aqueous pools were statistically associated only at HA1 and MY1 (*Table 2.13, row highlighted in blue*).

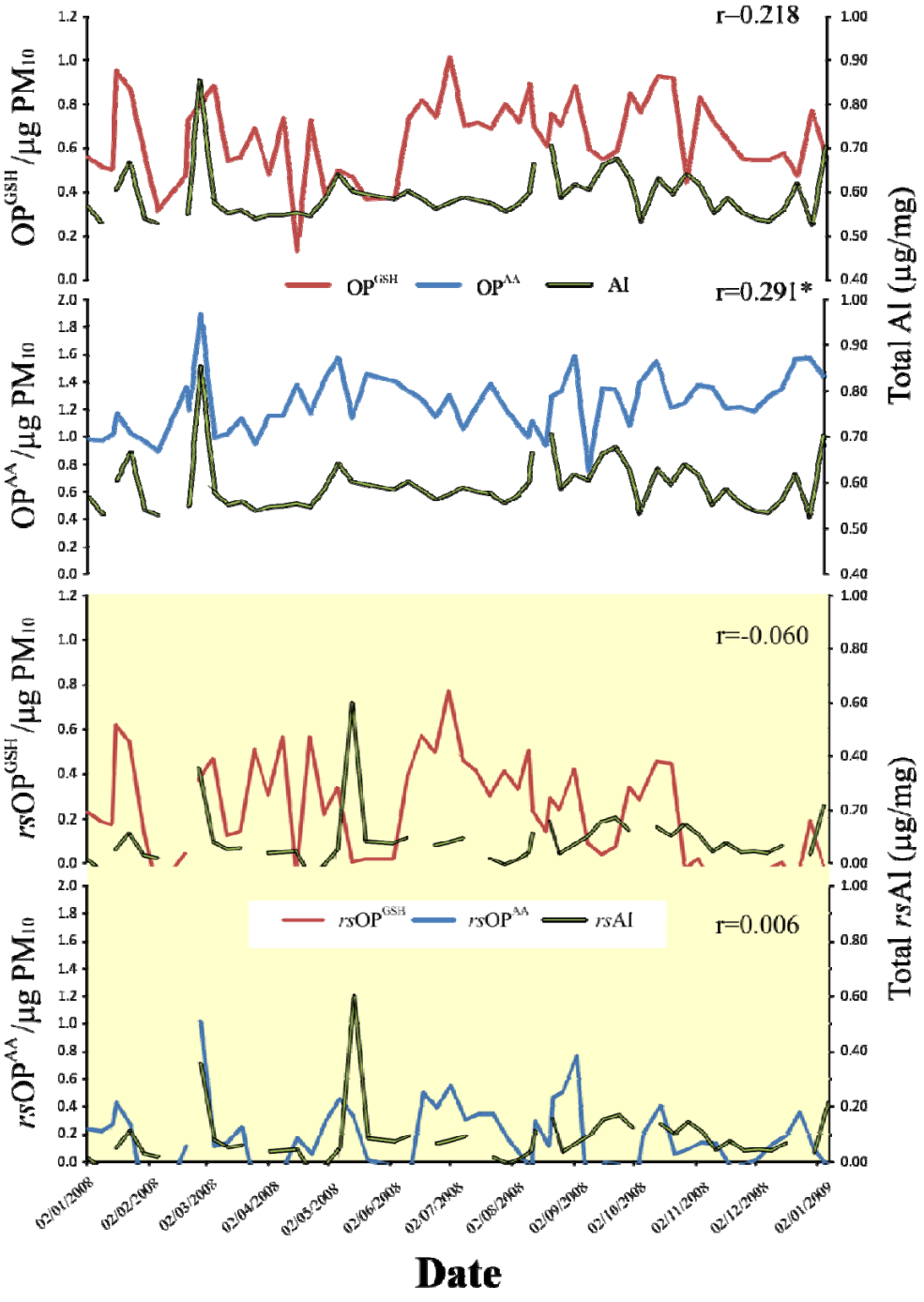

Figure 2.31: Relationship between measures of oxidative potential expressed per µg of filter extracted PM_{10} with total Al concentrations at Marylebone Road between Jan 2008 and Jan 2009. Data are expressed with (lower panel) and without (upper panel) the subtraction of the background oxidative potentials and Al concentration (derived from KC1) to derive the roadside increment. The results of a correlation analysis (Spearman's Rank Order) using the full or restricted OP parameters are inset. P<0.05 *; P<0.01**; P<0.001***.

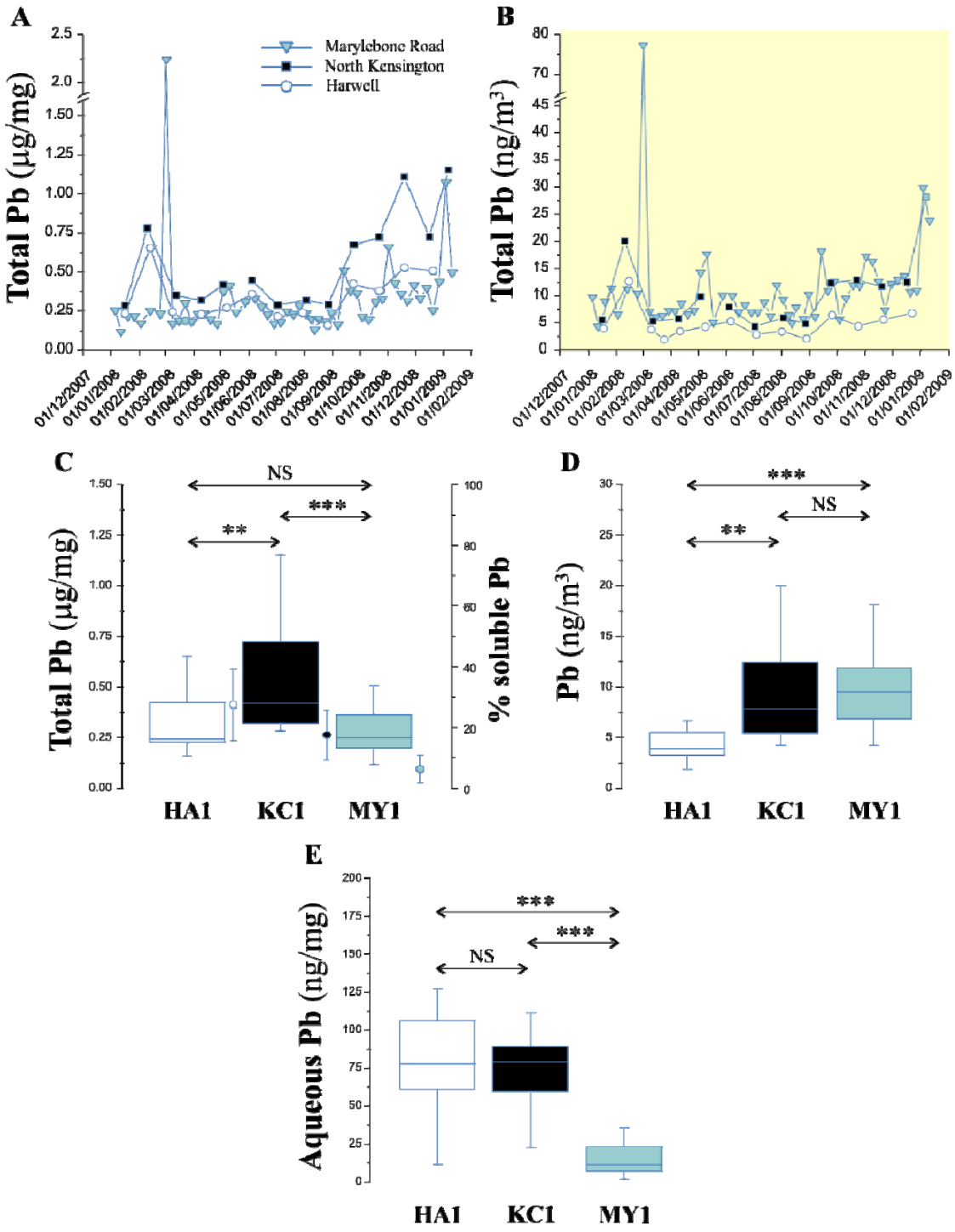

Figure 2.32: Total and aqueous PM_{10} Pb concentrations at Marylebone Road, North Kensington and Harwell, Jan 2008 – 2009. Figure formatting and details of the data analyses are as outlined in the legend to *Figure 2.10*.

Table 2.13: Associations between PM_{10} Pb concentrations, both total and aqueous with measures of oxidative potential (OP^{AA}, OP^{GSH} and OP^{TOT} per µg and m^3).

Parameters		All sites	MY1	KC1	HA1
OP^{AA}/µg	Total Pb (µg/mg)	0.331** *(n=81)*	0.503*** *(n=53)*	0.802** *(n=14)*	0.590* *(n=14)*
OP^{AA}/µg	Aqueous Pb (ng/mg)	-0.215* *(n=86)*	0.263* *(n=56)*	0.436 *(n=15)*	0.561* *(n=15)*
OP^{AA}/m^3	Total Pb (ng/m^3)	0.601*** *(n=81)*	0.465*** *(n=53)*	0.705** *(n=14)*	0.653* *(n=14)*
OP^{GSH}/µg	Total Pb (µg/mg)	-0.228* *(n=81)*	-0.320* *(n=53)*	0.712** *(n=14)*	0.236 *(n=14)*
OP^{GSH}/µg	Aqueous Pb (ng/mg)	-0.628** *(n=86)*	-0.430** *(n=56)*	0.314 *(n=15)*	-0.029 *(n=15)*
OP^{GSH}/m^3	Total Pb (ng/m^3)	0.422*** *(n=81)*	0.006 *(n=53)*	0.736** *(n=14)*	0.231 *(n=14)*
OP^{TOT}/µg	Total Pb (µg/mg)	0.037 *(n=81)*	0.152 *(n=53)*	0.851*** *(n=14)*	0.524 *(n=14)*
OP^{TOT}/µg	Aqueous Pb (ng/mg)	*-0.477 (n=86)*	-0.080 *(n=56)*	0.409 *(n=15)*	0.426 *(n=15)*
OP^{TOT}/m^3	Total Pb (ng/m^3)	0.543*** *(n=81)*	0.315* *(n=53)*	0.851*** *(n=14)*	0.671** *(n=14)*
Total Pb (µg/mg)	Aqueous Pb (ng/mg)	0.647*** *(n=81)*	0.686*** *(n=53)*	0.331 *(n=14)*	0.683** *(n=14)*

Throughout the discussion of the metal components of PM_{10} and their relationship to the ascorbate and glutathione dependent oxidative potentials the general pattern that has emerged is that *rs*OP^{GSH}/µg is significantly and positively correlated with a panel of metals (Fe, Mn, Mo, Cu and Sb), but that associations only emerge for OP^{AA}/µg once the urban background contribution is removed. Conversely *rs*OP^{GSH}/µg is significantly associated with PM_{10} V, Cr and Ni, whilst the ascorbate sensitive metric is not related to these elements. The relationships between the OP metric and PM components at the roadside following the subtraction of the urban background are summarised in *table 2.14*, both per µg and per m^3. In addition, the correlation matrix illustrates the association between the *rs* PM components, specifically between groups of highly associated elements, reflecting non-exhaust abrasion processes (Cu, Fe, Sb, Mn and Mo), long range oil combustion (V, Cr and Ni) and an additional grouping including Zn, Ba and Sr, with no defined single source.

A similar correlation matrix is presented in *table 2.15* for the 'true' urban background (minus the rural contribution) to illustrate the associations between PM_{10} oxidative potentials and components. What is notable in this data set is the absence of any association between OP^{GSH}/µg with the panel of metals observed at the roadside, whilst the significant relationships between OP^{AA}/µg with elements indicative of oil combustion remain. This suggests limited dispersion of Cu, Fe, Sb, Mn and Mo from the roadside environment and hence these elements are likely to be largely enriched within the

Table 2.14: Correlation matrix illustrating the association (Spearman Rank Order correlation) between roadside PM_{10} oxidative potential (OP^{AA} and OP^{GSH} per µg and m^3) with roadside PM_{10} metal content at Marylebone Road, Jan 2008 – Jan 2009. The upper right hand portion of the matrix illustrates the association between roadside increments (with the urban background subtracted) in metals and OP for the data expressed per unit mass of PM_{10}, whilst the lower left hand portion shows the associations for the data expressed per m^3. All significant associations are highlighted in red text, with the portion of the matrix addressing OP versus metal association's shaded grey. The associations between metal components, per unit mass and per m^3 are illustrated in the non-grey shaded area with significant associations with a Spearman rho of >0.70 shaded light blue, >0.50 light green and <0.50 lilac.

		OPAA	OPGSH	Al	Ba	Mn	V	Sb	Cr	Cu	Mo	Ni	Pb	Zn	Sr	Fe
OPAA	*Correlation Coefficient*		.310*	.006	.151	.594**	.408**	.600**	.329*	.501**	.675**	.263	.569**	.368*	.183	.564**
	Sig. (2-tailed)		.021	.964	.311	.000	.004	.000	.024	.000	.000	.074	.000	.011	.217	.000
	N		55	55	47	47	47	47	47	47	47	47	47	47	47	47
OPGSH	*Correlation Coefficient*	.672**		-.060	-.042	.602**	.221	.729**	.213	.632**	.656**	.186	.382**	.007	.145	.730**
	Sig. (2-tailed)	.000		.665	.778	.000	.136	.000	.151	.000	.000	.209	.008	.964	.330	.000
	N	56		55	47	47	47	47	47	47	47	47	47	47	47	47
Al	*Correlation Coefficient*	.817**	.690**		.591**	.440**	.302*	.005	.473**	.432**	.097	.536**	-.031	.551**	.292*	.328*
	Sig. (2-tailed)	.000	.000		.000	.002	.039	.971	.001	.002	.518	.000	.838	.000	.046	.025
	N	52	52		47	47	47	47	47	47	47	47	47	47	47	47
Ba	*Correlation Coefficient*	.318*	.280*	.452**		.294*	.263	.093	.392**	.464**	.179	.452**	-.134	.710**	.536**	.314*
	Sig. (2-tailed)	.022	.044	.001		.045	.075	.534	.006	.001	.228	.001	.369	.000	.000	.032
	N	52	52	52		47	47	47	47	47	47	47	47	47	47	47
Mn	*Correlation Coefficient*	.790**	.784**	.776**	.391**		.556**	.738**	.554**	.870**	.812**	.560**	.502**	.377**	.377**	.912**
	Sig. (2-tailed)	.000	.000	.000	.004		.000	.000	.000	.000	.000	.000	.000	.009	.009	.000
	N	52	52	52	52		47	47	47	47	47	47	47	47	47	47
V	*Correlation Coefficient*	.486**	.374**	.445**	.212	.645**		.370*	.787**	.558**	.561**	.597**	.254	.333*	.367*	.592**
	Sig. (2-tailed)	.000	.006	.001	.132	.000		.010	.000	.000	.000	.000	.085	.022	.011	.000
	N	52	52	52	52	52		47	47	47	47	47	47	47	47	47
Sb	*Correlation Coefficient*	.781**	.839**	.709**	.355**	.895**	.534**		.216	.780**	.930**	.210	.559**	.152	.387**	.845**
	Sig. (2-tailed)	.000	.000	.000	.010	.000	.000		.145	.000	.000	.157	.000	.308	.007	.000
	N	52	52	52	52	52	52		47	47	47	47	47	47	47	47
Cr	*Correlation Coefficient*	.422**	.444**	.562**	.370**	.637**	.818**	.496**		.558**	.421**	.768**	.105	.353*	.224	.533**
	Sig. (2-tailed)	.002	.001	.000	.007	.000	.000	.000		.000	.003	.000	.483	.015	.130	.000
	N	52	52	52	52	52	52	52		47	47	47	47	47	47	47
Cu	*Correlation Coefficient*	.695**	.796**	.731**	.482**	.922**	.629**	.911**	.673**		.833**	.635**	.309*	.439**	.418**	.939**
	Sig. (2-tailed)	.000	.000	.000	.000	.000	.000	.000	.000		.000	.000	.034	.002	.003	.000
	N	52	52	52	52	52	52	52	52		47	47	47	47	47	47
Mo	*Correlation Coefficient*	.786**	.798**	.737**	.396**	.920**	.623**	.967**	.592**	.925**		.386**	.513**	.228	.399**	.894**
	Sig. (2-tailed)	.000	.000	.000	.004	.000	.000	.000	.000	.000		.007	.000	.124	.005	.000
	N	52	52	52	52	52	52	52	52	52		47	47	47	47	47
Ni	*Correlation Coefficient*	.377**	.351*	.516**	.401**	.609**	.659**	.427**	.747**	.656**	.495**		.149	.489**	.260	.518**
	Sig. (2-tailed)	.006	.011	.000	.003	.000	.000	.002	.000	.000	.000		.318	.000	.078	.000
	N	52	52	52	52	52	52	52	52	52	52		47	47	47	47
Pb	*Correlation Coefficient*	.402**	.264	.333*	.082	.445**	.215	.352*	.185	.329*	.309*	.405**		.171	.399**	.413**
	Sig. (2-tailed)	.003	.058	.016	.565	.001	.126	.010	.190	.017	.026	.003		.251	.006	.004
	N	52	52	52	52	52	52	52	52	52	52	52		47	47	47
Zn	*Correlation Coefficient*	.407**	.152	.437**	.747**	.382**	.232	.257	.340*	.414**	.299*	.477**	.194		.477**	.334*
	Sig. (2-tailed)	.003	.283	.001	.000	.005	.098	.065	.014	.002	.031	.000	.169		.001	.022
	N	52	52	52	52	52	52	52	52	52	52	52	52		47	47
Sr	*Correlation Coefficient*	.397**	.393**	.512**	.788**	.516**	.279*	.476**	.439**	.552**	.519**	.462**	.314*	.578**		.394**
	Sig. (2-tailed)	.004	.004	.000	.000	.000	.045	.000	.001	.000	.000	.001	.023	.000		.006
	N	52	52	52	52	52	52	52	52	52	52	52	52	52		47
Fe	*Correlation Coefficient*	.748**	.829**	.753**	.421**	.948**	.634**	.939**	.646**	.958**	.961**	.570**	.367**	.332*	.565**	
	Sig. (2-tailed)	.000	.000	.000	.002	.000	.000	.000	.000	.000	.000	.000	.007	.016	.000	
	N	52	52	52	52	52	52	52	52	52	52	52	52	52	52	

coarse PM mode. Finally, an equivalent correlation matrix is presented for the rural site (*table 2.16*). At this regional background level the relationship between OP^{AA}/µg with V, Cr and Ni is no longer apparent. Instead significant correlations between OP^{AA}/µg and Sb, Mn and Sr are observed, suggesting no clear source contribution. These data also suggest that either the 'long-range' oil combustion source impacting on the London airshed is predominately derived from the East of the city (Harwell being situated to the West), or that the Cr, Ni and V signature is derived from sources (other than vehicular traffic) within the cities metropolitan area.

Table 2.15: Correlation matrix illustrating the association between the true urban background PM_{10} oxidative potential (OP^{AA} and OP^{GSH}) and metal content at the North Kensington, Jan 2008 – Jan 2009. The upper right hand portion of the matrix illustrates the association between the true urban background (following subtraction of the rural component) metal content and OP for the data expressed per unit mass of PM_{10}, whilst the lower left hand portion shows the associations for the data expressed per m^3. All significant associations are highlighted in red text, with the portion of the matrix addressing OP versus metal association's shaded grey. The associations between metal components, per unit mass and per m^3 are illustrated in the non-grey shaded area with significant associations with a Spearman rho of >0.70 shaded light blue, >0.50 light green and <0.50 lilac.

		OPAA	OPGSH	Al	Ba	Mn	V	Sb	Cr	Cu	Mo	Ni	Pb	Zn	Sr	Fe
OPAA	*Correlation Coefficient*		.057	-.584*	-.260	.066	-.673**	.634*	-.361	-.464	.424	-.456	.590*	-.297	-.337	.090
	Sig. (2-tailed)		.840	.028	.370	.821	.008	.015	.205	.094	.130	.101	.026	.303	.239	.759
	N		15	14	14	14	14	14	14	14	14	14	14	14	14	14
OPGSH	*Correlation Coefficient*	.139		-.250	-.154	-.007	.394	.138	.132	.084	.258	.123	.236	.169	.445	.024
	Sig. (2-tailed)	.621		.389	.599	.982	.164	.638	.653	.776	.372	.674	.417	.563	.111	.935
	N	15		14	14	14	14	14	14	14	14	14	14	14	14	14
Al	*Correlation Coefficient*	.231	-.064		.338	.353	.416	-.611*	.365	.576*	-.263	.619*	-.611*	.223	.169	.303
	Sig. (2-tailed)	.427	.829		.238	.215	.139	.020	.199	.031	.365	.018	.020	.443	.562	.292
	N	14	14		14	14	14	14	14	14	14	14	14	14	14	14
Ba	*Correlation Coefficient*	-.051	-.064	.147		-.242	-.038	-.288	-.163	-.004	-.199	.193	-.509	.867**	.366	-.403
	Sig. (2-tailed)	.864	.829	.615		.405	.898	.317	.578	.988	.494	.508	.063	.000	.198	.153
	N	14	14	14		14	14	14	14	14	14	14	14	14	14	14
Mn	*Correlation Coefficient*	.371	-.051	.767**	.108		.256	.221	.391	.463	.564*	.396	.173	-.186	.040	.959**
	Sig. (2-tailed)	.191	.864	.001	.714		.376	.448	.166	.095	.036	.162	.554	.524	.892	.000
	N	14	14	14	14		14	14	14	14	14	14	14	14	14	14
V	*Correlation Coefficient*	-.614*	.363	.183	-.062	.097		-.410	.645*	.542*	.026	.519	-.318	.142	.350	.201
	Sig. (2-tailed)	.020	.202	.532	.834	.742		.146	.013	.045	.929	.057	.268	.629	.220	.490
	N	14	14	14	14	14		14	14	14	14	14	14	14	14	14
Sb	*Correlation Coefficient*	.670**	.125	.081	-.323	.305	-.420		-.302	.018	.754**	-.154	.816**	-.138	-.148	.234
	Sig. (2-tailed)	.009	.670	.782	.260	.288	.135		.294	.952	.002	.599	.000	.638	.614	.422
	N	14	14	14	14	14	14		14	14	14	14	14	14	14	14
Cr	*Correlation Coefficient*	-.376	-.011	.279	-.033	.367	.609*	-.288		.226	.190	.498	-.159	-.240	.586*	.310
	Sig. (2-tailed)	.185	.970	.334	.911	.197	.021	.318		.438	.516	.070	.588	.409	.027	.280
	N	14	14	14	14	14	14	14		14	14	14	14	14	14	14
Cu	*Correlation Coefficient*	-.103	.029	.587*	.099	.521	.365	.174	.152		.166	.640*	-.179	.062	-.023	.453
	Sig. (2-tailed)	.725	.923	.027	.737	.056	.199	.553	.605		.570	.014	.541	.834	.937	.104
	N	14	14	14	14	14	14	14	14		14	14	14	14	14	14
Mo	*Correlation Coefficient*	.324	.130	-.013	-.167	.542*	-.017	.650*	.062	.289		.119	.573*	-.026	.248	.462
	Sig. (2-tailed)	.259	.658	.964	.567	.045	.955	.012	.834	.317		.686	.032	.929	.392	.096
	N	14	14	14	14	14	14	14	14	14		14	14	14	14	14
Ni	*Correlation Coefficient*	-.367	.073	.486	.336	.433	.497	-.143	.631*	.600*	.075		-.173	.276	.382	.298
	Sig. (2-tailed)	.197	.805	.078	.240	.122	.070	.626	.016	.023	.799		.553	.340	.177	.301
	N	14	14	14	14	14	14	14	14	14	14		14	14	14	14
Pb	*Correlation Coefficient*	.653*	.231	.055	-.600*	.305	-.317	.855**	-.244	-.033	.570*	-.319		-.308	-.208	.225
	Sig. (2-tailed)	.011	.427	.852	.023	.288	.270	.000	.401	.911	.033	.267		.283	.476	.440
	N	14	14	14	14	14	14	14	14	14	14	14		14	14	14
Zn	*Correlation Coefficient*	-.191	.108	.002	.855**	.015	.011	-.222	-.174	.037	-.044	.323	-.424		.396	-.327
	Sig. (2-tailed)	.513	.714	.994	.000	.958	.970	.446	.553	.899	.881	.260	.131		.160	.253
	N	14	14	14	14	14	14	14	14	14	14	14	14		14	14
Sr	*Correlation Coefficient*	-.116	.389	.134	.385	.323	.262	-.015	.547*	-.002	.289	.495	-.156	.389		-.071
	Sig. (2-tailed)	.692	.169	.648	.175	.260	.366	.958	.043	.994	.317	.072	.594	.169		.810
	N	14	14	14	14	14	14	14	14	14	14	14	14	14		14
Fe	*Correlation Coefficient*	.279	.064	.679**	-.103	.938**	.169	.376	.301	.604*	.656*	.354	.415	-.121	.253	
	Sig. (2-tailed)	.334	.829	.008	.725	.000	.563	.185	.296	.022	.011	.215	.140	.681	.383	
	N	14	14	14	14	14	14	14	14	14	14	14	14	14	14	

Table 2.16: Correlation matrix illustrating the association (Spearman Rank Order correlation) between PM_{10} oxidative potential (OP^{AA} and OP^{GSH}) and metal content at the rural background site at Harwell, Oxfordshire, Jan 2008 – Jan 2009. The upper right hand portion of the matrix illustrates the association metals and OP for the data expressed per unit mass of PM_{10}, whilst the lower left hand portion shows the associations for the data expressed per m^3. All significant associations are highlighted in red text, with the portion of the matrix addressing OP versus metal association's shaded grey. The associations between metal components, per unit mass and per m^3 are illustrated in the non-grey shaded area with significant associations with a Spearman rho of >0.70 shaded light blue, >0.50 light green and <0.50 lilac.

		OPAA	OPGSH	Al	Ba	Mn	V	Sb	Cr	Cu	Mo	Ni	Pb	Zn	Sr	Fe
OPAA	*Correlation Coefficient*		.363	-.037	.386	.285	.162	.627*	-.023	.158	.549*	-.311	.317	.192	.675**	.427
	Sig. (2-tailed)		.167	.901	.173	.323	.580	.016	.937	.590	.042	.279	.270	.512	.008	.128
	N		16	14	14	14	14	14	14	14	14	14	14	14	14	14
OPGSH	*Correlation Coefficient*	.312		.576*	.057	.438	.406	.380	.192	.318	.361	-.031	.339	.101	.365	.346
	Sig. (2-tailed)	.240		.031	.846	.117	.150	.181	.511	.269	.205	.917	.236	.730	.200	.226
	N	16		14	14	14	14	14	14	14	14	14	14	14	14	14
Al	*Correlation Coefficient*	.473	.433		.059	.577*	.621*	-.047	.425	.511	.408	.295	.169	.091	.119	.391
	Sig. (2-tailed)	.088	.122		.842	.031	.018	.874	.130	.062	.147	.305	.563	.758	.686	.167
	N	14	14		14	14	14	14	14	14	14	14	14	14	14	14
Ba	*Correlation Coefficient*	.138	.336	-.077		.259	.172	.519	-.360	.403	.640*	.018	.476	.649*	.638*	.330
	Sig. (2-tailed)	.637	.240	.794		.372	.557	.057	.206	.153	.014	.952	.085	.012	.014	.249
	N	14	14	14		14	14	14	14	14	14	14	14	14	14	14
Mn	*Correlation Coefficient*	.451	.530	.789**	.182		.662**	.356	.589*	.757**	.723**	.469	.427	.249	.298	.841**
	Sig. (2-tailed)	.106	.051	.001	.533		.010	.212	.027	.002	.003	.091	.128	.390	.301	.000
	N	14	14	14	14		14	14	14	14	14	14	14	14	14	14
V	*Correlation Coefficient*	.288	.508	.358	.165	.495		.066	.683**	.584*	.522	.382	.092	.239	.210	.566*
	Sig. (2-tailed)	.318	.064	.208	.573	.072		.823	.007	.028	.056	.178	.754	.411	.472	.035
	N	14	14	14	14	14		14	14	14	14	14	14	14	14	14
Sb	*Correlation Coefficient*	.490	.591*	.415	.574*	.604*	.248		-.110	.406	.727**	-.244	.684**	.038	.408	.689**
	Sig. (2-tailed)	.075	.026	.140	.032	.022	.392		.709	.150	.003	.401	.007	.898	.148	.006
	N	14	14	14	14	14	14		14	14	14	14	14	14	14	14
Cr	*Correlation Coefficient*	.336	.191	.490	-.371	.503	.609*	.213		.416	.288	.558*	-.086	-.370	-.071	.495
	Sig. (2-tailed)	.240	.513	.075	.191	.067	.021	.464		.139	.318	.038	.770	.193	.810	.072
	N	14	14	14	14	14	14	14		14	14	14	14	14	14	14
Cu	*Correlation Coefficient*	.415	.499	.745**	.407	.842**	.481	.666**	.292		.690**	.249	.572*	.088	.158	.748**
	Sig. (2-tailed)	.140	.069	.002	.149	.000	.081	.009	.311		.006	.391	.032	.765	.590	.002
	N	14	14	14	14	14	14	14	14		14	14	14	14	14	14
Mo	*Correlation Coefficient*	.372	.524	.436	.774**	.620*	.473	.829**	.216	.768**		.173	.543*	.174	.602*	.899**
	Sig. (2-tailed)	.190	.055	.119	.001	.018	.088	.000	.459	.001		.554	.045	.552	.023	.000
	N	14	14	14	14	14	14	14	14	14		14	14	14	14	14
Ni	*Correlation Coefficient*	.282	.262	.484	.165	.686**	.464	.356	.532*	.473	.485		-.029	.051	.095	.202
	Sig. (2-tailed)	.329	.366	.079	.573	.007	.094	.211	.050	.088	.079		.923	.864	.747	.488
	N	14	14	14	14	14	14	14	14	14	14		14	14	14	14
Pb	*Correlation Coefficient*	.297	.642*	.530	.543*	.642*	.196	.805**	.002	.832**	.736**	.307		.132	.372	.529
	Sig. (2-tailed)	.302	.013	.051	.045	.013	.502	.001	.994	.000	.003	.285		.652	.190	.052
	N	14	14	14	14	14	14	14	14	14	14	14		14	14	14
Zn	*Correlation Coefficient*	.218	.240	.156	.578*	.407	.248	.319	-.327	.411	.436	.312	.334		.359	-.002
	Sig. (2-tailed)	.455	.409	.594	.030	.149	.392	.267	.253	.144	.119	.277	.243		.207	.994
	N	14	14	14	14	14	14	14	14	14	14	14	14		14	14
Sr	*Correlation Coefficient*	.371	.389	-.011	.552*	.222	.165	.495	-.055	.354	.515	.275	.572*	.292		.322
	Sig. (2-tailed)	.191	.169	.970	.041	.446	.573	.072	.852	.215	.060	.341	.033	.311		.262
	N	14	14	14	14	14	14	14	14	14	14	14	14	14		14
Fe	*Correlation Coefficient*	.345	.240	.323	.354	.495	.327	.785**	.481	.547*	.752**	.312	.480	.130	.327	
	Sig. (2-tailed)	.227	.409	.260	.215	.072	.253	.001	.081	.043	.002	.277	.083	.659	.253	
	N	14	14	14	14	14	14	14	14	14	14	14	14	14	14	

Discussion

In Part II of this report we adopted the following approaches to investigate the sources and compositional determinants of roadside PM_{10} oxidative potential: (a) examination the relationship of OP with wind direction to identify major source contributions; (b) investigation of the correlation with NOx as a gaseous traffic tracer; and (c) subtraction of the rural and urban background OP from that measured at the roadside to isolate the actual roadside contribution. The Lenschow approach has been widely used for source apportionment studies (*Lenschow et al., 2001*) but has been employed here for the first time to isolate the contribution of traffic derived PM to the oxidative nature of the urban particulate air shed in London. Each of these approaches have employed measures of ascorbate and glutathione dependent OP, expressed per unit mass of collected PM, or per m^3, derived from the synthetic RTLF model described in the first part of this report. In addition, as OP is primarily driven by metals present in/on PM total (acid digested) and aqueous (water soluble) elemental components were measured at each of the site classifications: roadside (Marylebone Road), urban background (North Kensington) and rural (Harwell). These metals, indicative of local roadside emissions with limited dispersion (brake and tyre wear, re-suspension road dust) and more dispersed sources (long range oil combustion sources) were then employed to establish the determinants of PM oxidative potential (*Viana M et al., 2008; Thorpe and Harrison, 2008*). The major findings arising from this work were as follows:

(1) A clear roadside increment in $OP^{GSH}/\mu g$ was observed at Marylebone Road, corresponding to approximately one third of the measured activity. This roadside contribution increased to two-thirds when the data were expressed per unit volume of air (m^3). This observation is consistent with this measure of PM_{10} OP being sensitive to local emissions at the roadside. This view was strengthened by the underlying association between NOx concentrations and $OP^{GSH}/\mu g$ at the roadside site, as well as with the proximity of the signal to the major road sources based on wind direction analysis.

(2) There was no statistical difference between $OP^{AA}/\mu g$ measured in parallel at the roadside and urban background locations, suggesting that the sources

influencing this measure were more widely dispersed within the urban environment. Consistent with this view OP^{AA}/μg was not significantly associated with NOx at Marylebone Road. A roadside increment in this parameter (35% of the total) was noted when the data were expressed per m^3, reflecting the increased PM_{10} concentration at the roadside. The wind rose for OP^{AA}/μg at Marylebone Road did not show any clear relationship with the major road sources until the urban background contribution was removed.

(3) OP^{AA} and OP^{GSH} were not simply related to one another suggesting that these two measures are influenced by different panels of metals, reflecting differing sources, one local with limited dispersion from the roadside and the other, more widely dispersed. Based on this observation we contend that the combined sum of these two measures is indicative of the total oxidative potential of the ambient PM air shed.

(4) Based on a principal component analysis of the total metal measurements, allied to a descriptive examination of the temporal profile in the metals measured at each of the sentinel sites, three to four source profiles were apparent reflecting brake wear (Sb, Cu), generic mechanical wear (Fe, Mn and Mo), other abrasion processes, including tyre wear (Zn, Ba and Sr) and oil combustion (Ni, V and Cr).

(5) Roadside increments in the concentration of the following metals were apparent at Marylebone Road, expressed per μg of PM_{10}: Fe, Mo, Mn, Ba, Zn, Cr, Cu, Sb and Al. Of these metals, those associated with engine and brake wear (Fe, Mo, Mn, Cu and Sb) demonstrated decreased aqueous solubility across the rural, urban background to roadside site classifications. Only Ba, which has traditionally been employed as a tyre wear marker (*Viana M et al., 2008; Thorpe and Harrison, 2008*) displayed enhanced solubility at the roadside and in the present investigation, was not simplistically related to the measured Cu and Sb concentrations.

(6) OP^{GSH}/μg at Marylebone Road was significantly associated with the Fe, Mo, Mn, Cu, Cr and Sb content of roadside PM_{10}, suggesting that this OP measure was sensitive to components derived from mechanical abrasion. For these

metals removal of the urban background concentrations did not improve the correlations observed. In contrast, associations with each of these metals with OP^{AA}/μg were only apparent after the subtraction of the background concentrations.

(7) The following metal components did not show enrichment in roadside PM_{10} and are therefore treated as being indicative of more dispersed or mixed sources: Sr, Ni and Pb. Both Ni and Pb have been employed as markers of oil combustion, especially in association with Ni and V, however the source contributing Sr remains unknown.

(8) Of the metals examined only Mn, Zn, V and Al were significantly associated with OP^{GSH}/μg at Marylebone Road

The present study has demonstrated a clear increment in roadside PM_{10} oxidative potential that appears to be driven in part by metals associated with either abrasion (engine (Fe, Mn, Mo) and brake wear (Cu, Sb)) or oil combustion processes (Ni, V, Cr, local and long-range). The two OP metrics employed appear to discriminate between these two broad source classifications, with the glutathione dependent measurement appearing the more strongly influenced by local sources. It is now accepted that roadside PM does not simply reflect tailpipe emissions, but also includes contributions from fugitive sources, including the re-suspension of road dust and primary PM emissions from brake, clutch and tyre wear (Winiwarter et al., 2009). The relative contribution of these sources to roadside PM concentrations is contentious, but a number of reports have estimated non-exhaust sources to account for approximately half of the PM concentration observed at the roadside (*Querol et al., 2004; Lenschow et al, 2001*). This is extremely important as emissions from these sources are largely ignored at the regulatory level, which focuses on the reduction of tail pipe emissions through improvements in engine technology.

Importantly many of the metals associated with these processes are also established redox catalysts capable of generating reactive oxygen species in vivo (*Valko et al, 2005*). Given the established toxicity of many of these metals there is no reason why they should be viewed as being any less toxic than PM_{10} PAHs, or other characteristics of the ambient aerosol. These data therefore highlight a need for a better understanding of

interaction of PM associated metals at the air lung interface and on health within the exposed population generally.

One might also have expected an enrichment of Zn at the roadside location reflecting tyre wear, but this was not observed, despite a literature supporting its use as tracer for this source (*Adachi and Tainosho, 2004; Councell et al, 2004*). While Zn has been shown to be the only metal present in significant quantities in ground tyre samples (*Schauer et al. 2006*), it now appears unlikely that the concentrations released under real-world conditions are sufficient to account for the measured atmospheric levels. Thus one must conclude that other unidentified sources contribute significantly to ambient PM_{10} Zn content and that its utility as a tracer of tyre wear is limited (*Schauer et al. 2006; Thorpe and Harrison, 2008.* Within the current study in addition to its lack of enrichment at Marylebone Road, Zn was also associated with a factor containing both Ba and Sr, for which there is no single unambiguous source.

A further compositional signature related to PM_{10} is itsV, Ni and Cr content. The United Kingdom National Atmospheric Emissions Inventory reports that Ni and V are primarily emitted from industrial fuel oil combustion and shipping sources which do not have persistent local sources within the Greater London urban area. Interpretation of this data is however limited by our focus on PM_{10}, but a study performed in Birmingham suggested that these metals were enriched in the accumulation mode and therefore reflected long range transported combustion sources (*Allen et al, 2001*). All of these metals have established redox activity *(Valko et al, 2005*) and are therefore likely to impact on the oxidative potential of PM. This appears to fit well with the two patterns of response observed for the two OP metrics considered in this study. The glutathione-dependent metric appearing sensitive to local source contributions, but relatively insensitive to the regional components, whilst the ascorbate dependent metric is the more sensitive to redox active components which are widely dispersed such as vanadium.

.

Conclusions

In this study we have demonstrated that the oxidative potential of ambient PM_{10} collected at a busy London roadside site is enhanced relative to the urban and rural background. The precise increment depends on the metric employed, but if one assumes that the ascorbate and glutathione OP metrics are additive, based on their differing sensitivities to redox active PM components, then on a unit mass basis the roadside contribution is approximately 20%, increasing to 60% when the metric is expressed per m^3. This increment, in a metric designed to predict biological toxicity, is coherent with the increasing body of literature demonstrating enhanced health effects in populations with high exposures to busy roads. This study has also identified two key sources that appear to contribute to the oxidative activity of the particulate airshed; one characterised by limited dispersion and with a compositional signature consistent with brake and mechanical wear, and the other more dispersed source, possibly reflecting widely dispersed products of oil combustion. While components associated with each source: Cu, Fe, Mo and Mn for non-exhaust vehicular wear and Ni, V and Cr, for oil combustion are known redox catalyst and hence likely to be mechanistically related to the oxidative properties of PM_{10}, it must always be borne in mind that they may simply be acting as surrogate markers of other pro-oxidant components of the airshed which have not been measured in the current study. These results are important as they highlight the contribution of sources that are currently unregulated to the potential toxicity of urban PM. The roadside increments observed are not insignificant and the components identified as determinants of this oxidative activity have established toxicity in man.

Policy Significance

It is an established and inconvenient fact that despite improved engine technologies and modelled projections of falling urban PM_{10}, the actual measured concentrations of this pollutant have remained fairly static over the last 5 years. Indeed recent data from London suggested that primary traffic related emissions of PM_{10} have actually increased over this period. As a significant proportion of roadside PM is derived from fugitive sources, brake and tyre wear, re-suspension of road dust, all of which are unregulated, there is merit in understanding how these sources contribute to urban PM_{10}, both to the measured concentration, but also its biological toxicity. This study has produced robust evidence for an increment in the potential toxicity of roadside PM_{10}, using a simple acellular screen, designed to mimic PM interactions at the air-lung interface in the human lung. The demonstration that brake wear in particular contributes to the oxidative potential of PM_{10} at roadside locations emphasises the need to examine the regulation of this source, both its components and emissions as a function of driving activity and vehicle weight. One issue that requires further investigation is the source of the urban oil combustion signature (Cr, Ni and V). Given its widespread dispersion, consistent with its presence in the accumulation mode, we cannot exclude the possibility that it reflects a long range impact of shipping emissions from ports located to the East of London.

Part III – Daily assessment of PM_{10} oxidative potential at a London urban background Site

Abstract

To date assessment of PM oxidative potential has been limited to PM samples extracted from filters collected over extended periods, ranging from 7 – 28 days at roadside and urban background sites respectively. Whilst PM samples reflecting long term averages are useful for examining the spatial variation in these measures, they cannot be integrated into classical time series analysis examining short-term health effects in the exposed population. There is therefore merit in examining whether the current methodology can be scaled to provide a daily time series. To assess the feasibility of this approach two separate Partisol-based sampling campaigns were performed at the urban background monitoring station at North Kensington during early spring (*05/03/08 -31/03/08*) and winter (*1/11/08 – 28/11/08*) 2008. Over the two sampling periods the masses obtained on daily filters ranged from 150.0 – 511.3 μg which permit assessment of ascorbate and glutathione dependent oxidative potential and quantification of PM_{10} metal content with relatively minor modification to the pre-existing methodologies. The results from the two campaigns demonstrated considerable temporal variability in both OP^{AA} and OP^{GSH} measurements, expressed both per μg of extracted PM, or per m^3 at this background location. These measures were not correlated and neither was associated with the ambient PM_{10} mass concentration. OP^{AA}/μg was found to be strongly correlated with a panel of redox active metals: Cu, Fe, Cr, Mn, Ni and V in the samples obtained during the winter collection. In contrast, OP^{GSH}/μg was only associated with Fe during the spring campaign. The OP parameters were also examined in relation to co-pollutant concentrations (NO_2, NO_x, O_3, PM_{10} and CO) and particle numbers at this site over the study period. During the spring campaign no associations were noted between the OP parameters expressed per m^3 with co-pollutant concentrations. In contrast, associations were noted between both OP^{AA} and OP^{GSH}/m^3 parameters with NOx, CO and PM_{10} during the winter period where concentrations in all these parameters were significantly increased above the spring time values. These data therefore demonstrate that OP measurements can be obtained on daily basis and provide a basis for future integration of this metric into time series studies.

Key words: Particulate matter, PM_{10}, Partisol, urban background, oxidative potential, ascorbate, glutathione, metals, time series.

Figures

Figure 3.1: The daily time series of ascorbate (left hand panels) and glutathione (right hand panels) dependent OPs (expressed both per μg and m^3) measured at North Kensington between 05/03/08 and 31/03/08.

Figure 3.2: Associations between daily ascorbate and glutathione dependent oxidative potentials (per μg) with the ambient PM_{10} concentrations during the first Partisol sampling campaign.

Figure 3.3: Total PM_{10} oxidative potentials (OP^{TOT}) based on the addition of the OP^{AA} (lilac bars) and OP^{GSH} (orange bars) metrics, expressed per μg (left hand panel) and per m^3.

Figure 3.4: Time series of daily PM_{10} (μg/m^3) and PM_{10} aqueous metal concentrations (ng/mg) associated with the first Partisol sampling campaign during March 2008.

Figure 3.5: Associations between daily PM_{10} aqueous Fe and Cu concentrations with OP^{AA}/μg and OP^{GSH}/μg.

Figure 3.6: Particle number and co-pollutant concentrations measured as the North Kensington monitoring station during the first Partisol sampling campaign, March 2008.

Figure 3.7: Daily PM_{10} ascorbate and glutathione-dependent oxidative activity (per μg and per m^3) during the winter Partisol sampling campaign at the North Kensington urban background site.

Figure 3.8: Relationship between ascorbate and glutathione dependent OP per unit mass with ambient daily PM_{10} mass concentration, based on data obtained during with Winter Partisol sampling campaign.

Figure 3.9: Total PM_{10} OP based on the sum of the ascorbate and glutathione dependent signals per unit mass (μg) and per m^3, based on data obtained during with Winter Partisol sampling campaign.

Figure 3.10: Time series of daily PM_{10} (μg/m^3) and PM_{10} aqueous metal concentrations (ng/mg) associated with the second Partisol sampling campaign during November 2008.

Figure 3.11: Time series of daily PM_{10} (μg/m^3) and PM_{10} aqueous metal concentrations (ng/mg) associated with the second Partisol sampling campaign during November 2008.

Figure 3.12: Particle number and co-pollutant concentrations measured as the North Kensington monitoring station during the first Partisol Winter sampling campaign, November 2008.

Tables

Table 3.1: Correlation matrix illustrating the degree of association (*Spearman Rank Order correlation*) between daily PM_{10} oxidative potentials (OP^{AA}, OP^{GSH} and OP^{TOT} per μg) and aqueous metal concentrations in samples collected during the first Partisol sampling campaign, March 2008.

Table 3.2: Correlation matrix illustrating the degree of association (*Spearman Rank Order correlation*) between roadside PM_{10} oxidative potentials (OP^{AA}, OP^{GSH} and OP^{TOT} per μg and m^3) with co-pollutant concentrations measured at North Kensington between 05/03/08 and 31/03/08.

Table 3.3: Correlation matrix illustrating the associations (*Spearman Rank Order correlation*) between daily PM_{10} oxidative potentials (OP^{AA}, OP^{GSH} and OP^{TOT} per μg) with roadside PM_{10} aqueous metal content at the North Kensington urban background site between 01/11/08 – 28/11/08.

Table 3.4: Correlation matrix illustrating the associations (*Spearman Rank Order correlation*) between daily PM_{10} oxidative potentials (OP^{AA}, OP^{GSH} and OP^{TOT} per μg and m^3) with PM_{10} total metal content at the North Kensington urban background site during the November 2008 sampling campaign.

Table 3.5: Correlation matrix illustrating the degree of association (*Spearman Rank Order correlation*) between roadside PM_{10} oxidative potentials (OP^{AA}, OP^{GSH} and OP^{TOT} per μg and m^3) with co-pollutant concentrations measured at North Kensington during the Winter sampling campaign, Nov 2008.

Aims

The principle aim of this study was to investigate the feasibility of determining PM_{10} oxidative potential on a daily basis, including parallel metal analyses (aqueous and total), in samples collected using a Partisol sampler located at the North Kensington urban background site. Allied to this, as secondary objectives we sought to further clarify the sources and compositional determinants of OP^{AA} and OP^{GSH}, as well as to establish the relationship between these metrics with co-pollutants concentrations and particle number measured at this background location.

Background

The majority of evidence linking particulate air pollution with poor cardiovascular and respiratory health are derived either from long tern exposure cohort studies (*Chen et al, 2008*) or short term time series analysis (*Dockery, 2009*). Whilst the data presented thus far in this report, examining location dependent contrasts in PM oxidative potential, could be used to identify locations of contrast for cohort studies, the long averaging periods encompassed by PM extracted from filters prevents their application in classical time series analyses. To integrate this novel PM metric into these powerful population based analyses requires comprehensive time series of daily OP measurements. The feasibility of adopting this approach is however limited by the quantity of PM that can be collected over a 24 hour period, allied to the difficulty in operating high volume samplers over extended periods in the field. In Part III of this report we have performed two pilot studies to examine the feasibility of employing daily PM_{10} samples collected from a Partisol sampler located at the North Kensington urban background site. An urban background site was employed to reflect a generalised population exposure, with the campaigns performed over the spring and winter to provide seasonal contrast.

Methods

An R&P Partisol 2025 sampler was employed to collect particulate matter onto 47-mm Teflon coated filters at a volumetric flow rate of 1 $m^3 h^{-1}$ for 24 h between midnight and midnight each day over a 4-week period. The instrument incorporated two filter magazines for filter storage pre and post-exposure, which allowed unattended operation for the duration of the sampling campaign. The filters were pre-weighed and re-weighed at a central laboratory after conditioning at 20°C and 50% relative humidity as specified for the European reference method for PM_{10} (*CEN, 1998*).

The details of the filter extractions, resuspension (at 150 and 55.56 μg/mL), incubations in the synthetic RTLF (at a final concentration of 50 μg/mL) and the quantification of ascorbate and glutathione were as outlined in the previous two sections of this report, with two minor amendments. First, the total volumes employed during the incubation were reduced by halve where insufficient volume of stock PM suspension was available. In addition, while aqueous metal concentrations were determined in filtrates obtained from the 150 μg/mL PM suspensions, acid extractions were only possible using the 55.56 μg/mL stocks obtained during the winter sampling campaign.

Results

Daily Partisol PM_{10} filters were collected across 27 days (5-31 March 2008) for the first sampling campaign at North Kensington, with the collected masses ranging from 160.8 – 511.3 μg. The ascorbate and glutathione dependent OPs associated with the sampled PM over the collection period are illustrated in *Figure 3.1*, expressed per μg of PM_{10} (lower panels) and per m^3 of sampled air (upper panel). Overall there was no statistical association between the two OP metrics (*Table 3.1*), with neither displaying a simplistic relationship with the measured ambient PM_{10} concentration, *Figure 3.2*. OP^{AA}/μg was in fact inversely associated with the measured mass concentration: r=-0.51, P=0.007.

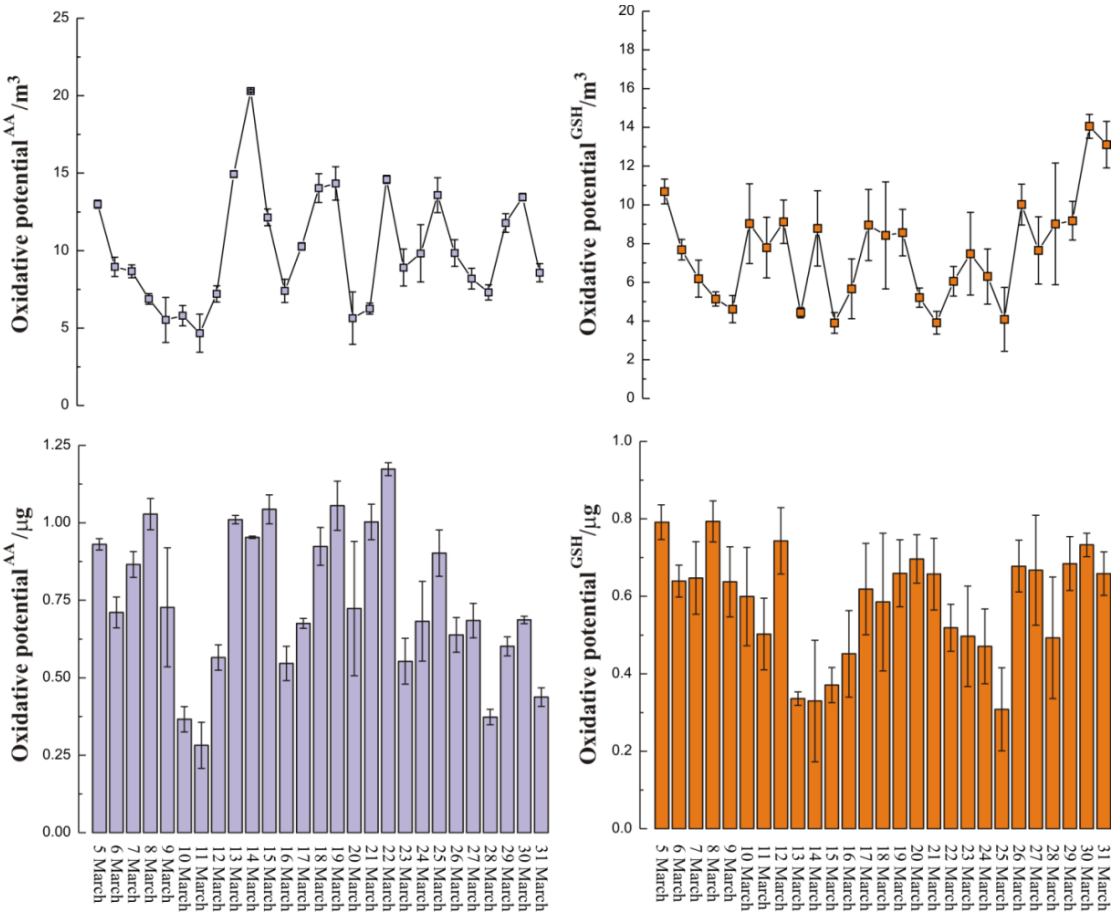

Figure 3.1: The daily time series of ascorbate (left hand panels) and glutathione (right hand panels) dependent OPs (expressed both per μg and m^3) measured at North Kensington between 05/03/08 and 31/03/08. Data are expressed as the mean values derived from triplicate incubations ± 2SD.

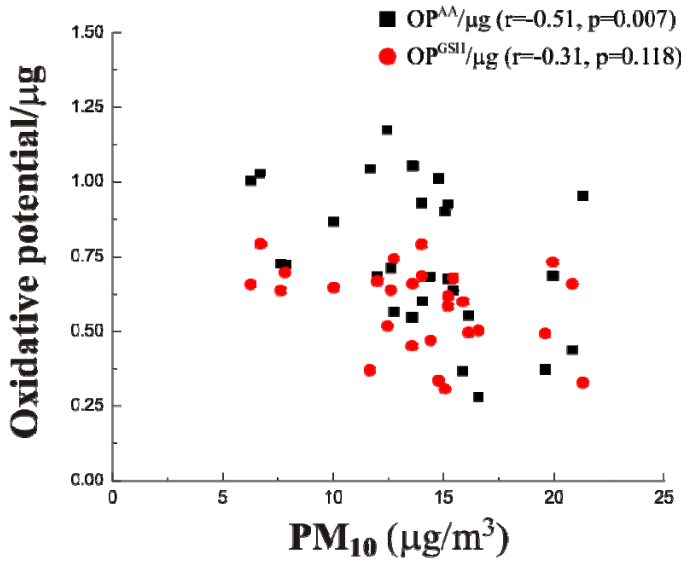

Figure 3.2: Associations between daily ascorbate and glutathione dependent oxidative potentials (per µg) with the ambient PM_{10} concentrations during the first Partisol sampling campaign. Results of the Spearman Rank Order correlation between these endpoints are illustrated.

On the basis of the lack of a statistical association between the two OP metrics, consistent with the observations made in this report, we derived a measure for the total OP by summing the ascorbate and glutathione dependent measures (*Figure 3.3*). The individual and composite OPs were subsequently related to the concentration of aqueous metals (Cu, Zn, Fe, Mn, Cr, Mo, Ni, Ba and V), illustrated in *Figure 3.4*. Of the metals examined Mn, V, Cr, Cu, Mo, Zn and Fe were all positively correlated with OP^{AA}/µg, *Table 3.1*, with a particularly strong association with Cu (r=0.83).

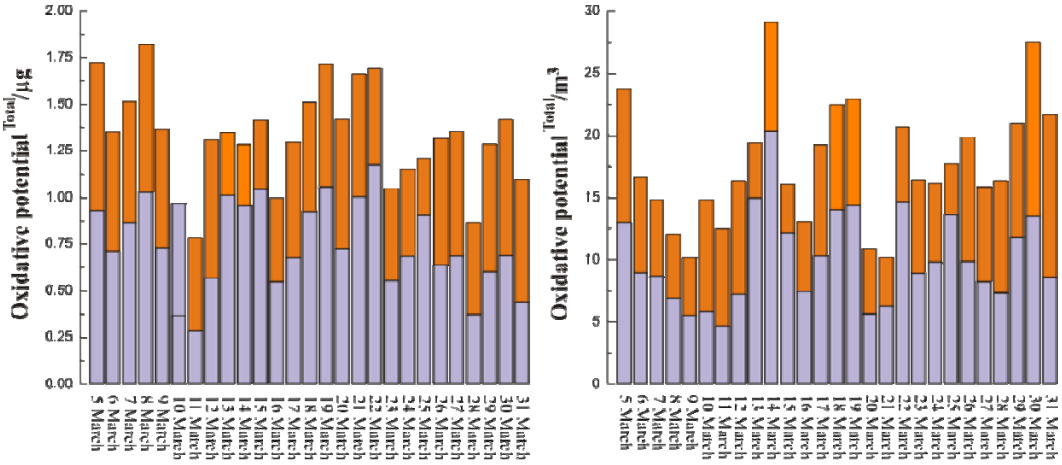

Figure 3.3: Total PM_{10} oxidative potentials (OP^{TOT}) based on the addition of the OP^{AA} (lilac bars) and OP^{GSH} (orange bars) metrics, expressed per µg (left hand panel) and per m^3. Individual mean OPs for each day are stacked with the total height reflecting OP^{TOT}.

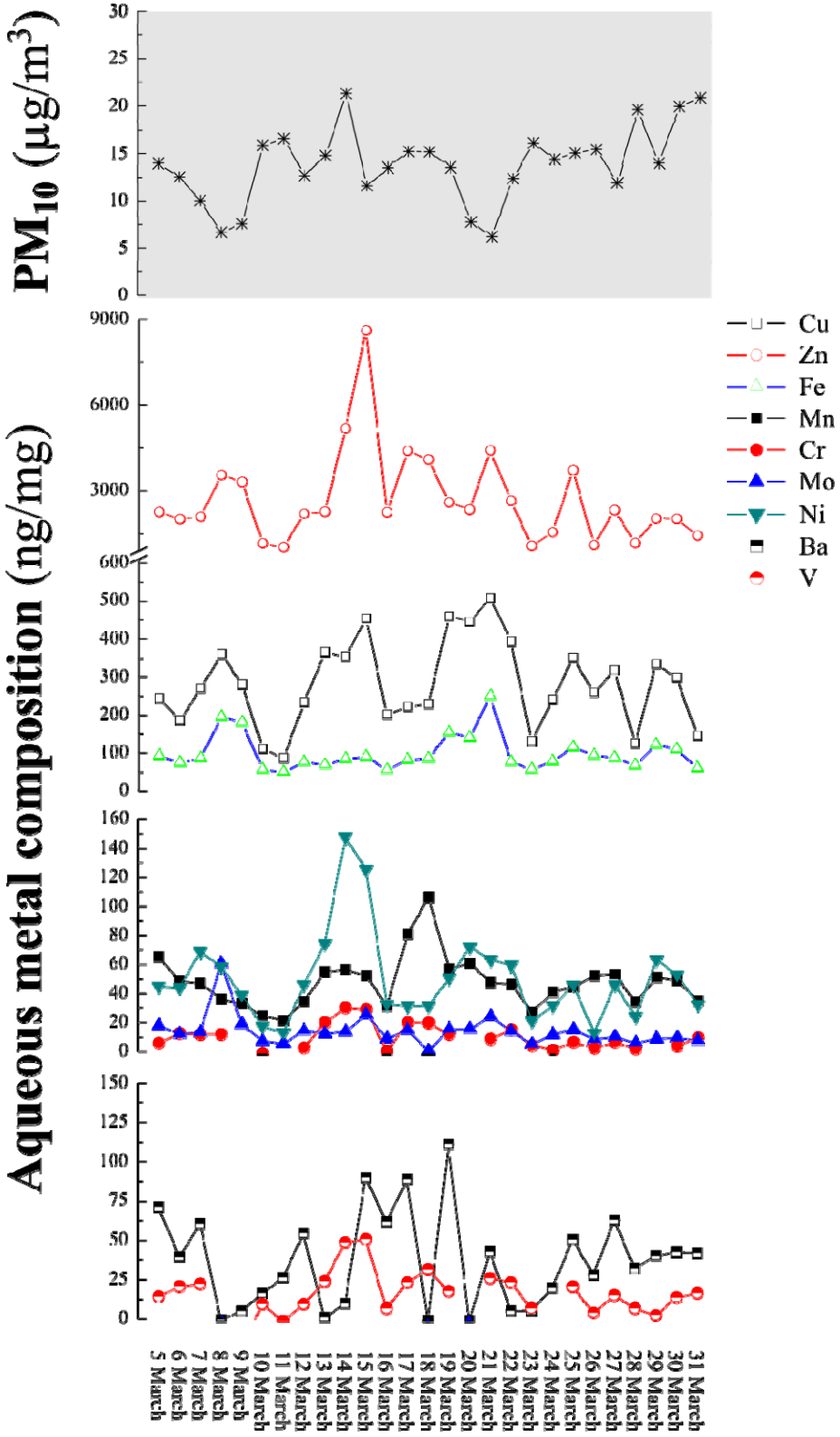

Figure 3.4: Time series of daily PM_{10} ($\mu g/m^3$) and PM_{10} aqueous metal concentrations (ng/mg) associated with the first Partisol sampling campaign during March 2008.

Table 3.1: Correlation matrix illustrating the degree of association (Spearman Rank Order correlation) between daily PM10 oxidative potentials (OP^{AA}, OP^{GSH} and OP^{TOT} per µg) and aqueous metal concentrations in samples collected during the first Partisol sampling campaign, March 2008. All significant associations are highlighted in red text, with the portion of the matrix addressing OP versus metal association's shaded grey. The associations between individual aqueous metal components, expressed per unit mass are illustrated in the non-grey shaded area with significant associations with a Spearman rho of >0.70 shaded light blue, >0.50 light green and <0.50 lilac.

		OP^{AA}	OP^{GSH}	OP^{TOT}	Ba	Mn	V	Cr	Cu	Mo	Ni	Zn	Fe
OP^{AA}	*Correlation Coefficient*		-.013	.814**	-.020	.558**	.507**	.618**	.834**	.705**	.704**	.756**	.594**
	Sig. (2-tailed)		.949	.000	.921	.002	.007	.001	.000	.000	.000	.000	.001
	N		27	27	27	27	27	27	27	27	27	27	27
OP^{GSH}	*Correlation Coefficient*			.511**	.113	.187	-.361	-.238	.112	.220	.064	-.128	.467*
	Sig. (2-tailed)			.006	.574	.350	.064	.232	.578	.270	.753	.526	.014
	N			27	27	27	27	27	27	27	27	27	27
OP^{TOT}	*Correlation Coefficient*				.048	.560**	.251	.380	.686**	.650**	.553**	.546**	.705**
	Sig. (2-tailed)				.814	.002	.206	.051	.000	.000	.003	.003	.000
	N				27	27	27	27	27	27	27	27	27
Ba	*Correlation Coefficient*					.162	.308	.156	.042	.216	.052	.107	.070
	Sig. (2-tailed)					.418	.118	.436	.837	.279	.796	.594	.730
	N					27	27	27	27	27	27	27	27
Mn	*Correlation Coefficient*						.476*	.510**	.505**	.311	.426*	.540**	.453*
	Sig. (2-tailed)						.012	.007	.007	.114	.027	.004	.018
	N						27	27	27	27	27	27	27
V	*Correlation Coefficient*							.856**	.285	.141	.393*	.537**	-.049
	Sig. (2-tailed)							.000	.150	.482	.043	.004	.810
	N							27	27	27	27	27	27
Cr	*Correlation Coefficient*								.320	.252	.405*	.557**	.006
	Sig. (2-tailed)								.103	.204	.036	.003	.975
	N								27	27	27	27	27
Cu	*Correlation Coefficient*									.726**	.824**	.692**	.746**
	Sig. (2-tailed)									.000	.000	.000	.000
	N									27	27	27	27
Mo	*Correlation Coefficient*										.622**	.706**	.683**
	Sig. (2-tailed)										.001	.000	.000
	N										27	27	27
Ni	*Correlation Coefficient*											.609**	.475*
	Sig. (2-tailed)											.001	.012
	N											27	27
Zn	*Correlation Coefficient*												.552**
	Sig. (2-tailed)												.003
	N												27
Fe	*Correlation Coefficient*												
	Sig. (2-tailed)												
	N												

P<0.05 *; P<0.01**

In contrast the daily OP^{GSH}/µg measurements were only weakly associated with PM_{10} Fe concentrations. OP^{TOT}/µg displayed a weaker association with Cu than the ascorbate dependent metric, but a stronger association with Fe, *Figure 3.5*. Co-pollutant concentrations and particle numbers expressed as 24 hour averages (*Figure* 3.6) were also correlated against the various OP metrics, both on a per mass and per volume basis, *table 3.2*. Of these pollutants full time series were available with the exception of particle number due to an equipment failure between the 18th – 31st of March.

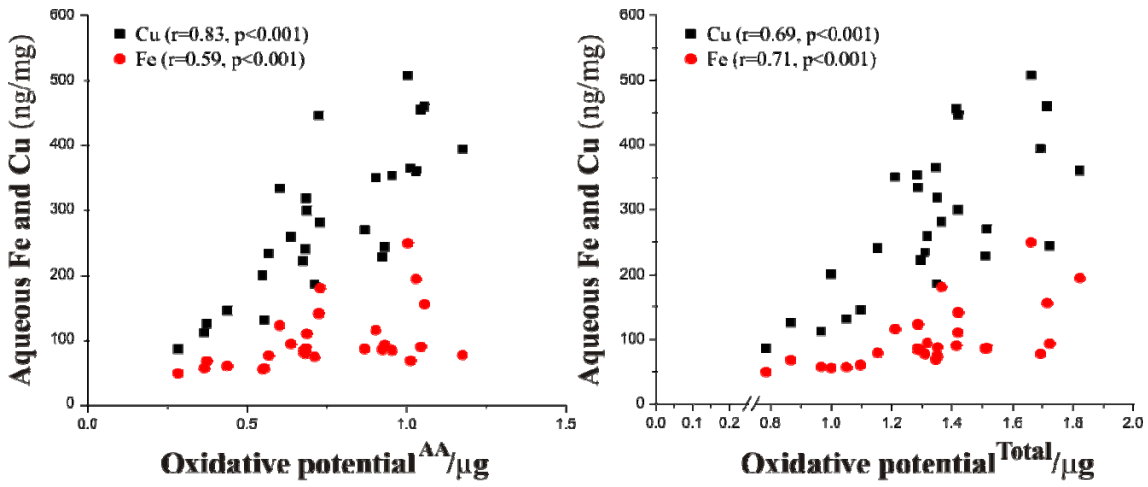

Figure 3.5: Associations between daily PM_{10} aqueous Fe and Cu concentrations with OP^{AA}/µg and OP^{GSH}/µg. Results of the Spearman Rank Order correlation for each of the comparisons are illustrated.

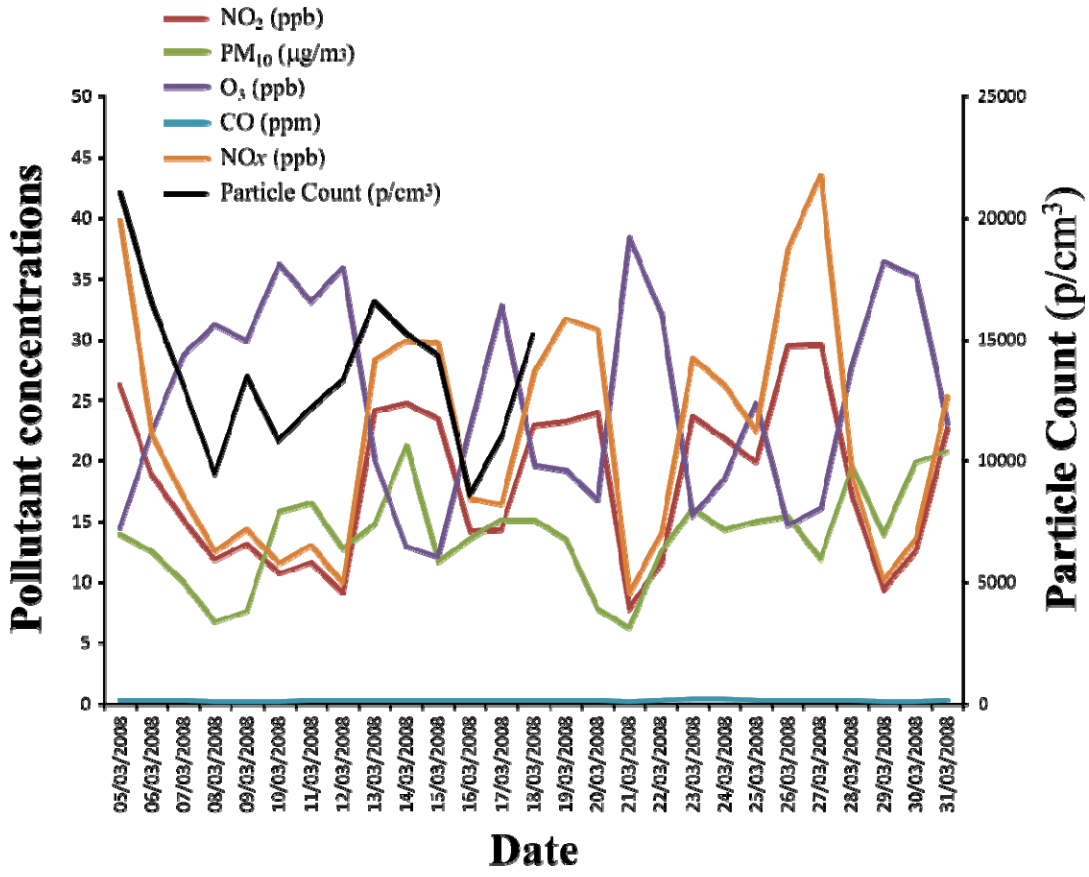

Figure 3.6: Particle number and co-pollutant concentrations measured as the North Kensington monitoring station during the first Partisol sampling campaign, March 2008.

Table 3.2: Correlation matrix illustrating the degree of association (*Spearman Rank Order correlation*) between roadside PM_{10} oxidative potentials (OP^{AA}, OP^{GSH} and OP^{TOT} per µg and m^3) with co-pollutant concentrations measured at North Kensington between 05/03/08 and 31/03/08. The upper right hand portion of the matrix illustrates the associations between OP^{AA}, OP^{GSH} and OP^{TOT} expressed per µg with the co-pollutant concentrations measured over the equivalent periods, whilst the lower left hand portion of the matrix illustrates the correlations when the OP parameters are expressed per m^3. Formatting of the matrix is as outlined in the legend to *Table 3.1*.

		OP^{AA}	OP^{GSH}	OP^{TOT}	Particles	NO_2	SO_2	O_3	CO	NOx
OP^{AA}	*Correlation Coefficient*		.114	.231	.670**	.400*	.375	-.374	.413*	.408*
	Sig. (2-tailed)		.571	.247	.009	.039	.054	.054	.032	.035
	N		27	27	14	27	27	27	27	27
OP^{GSH}	*Correlation Coefficient*	-.013		.882**	.051	.021	.304	.096	.001	.016
	Sig. (2-tailed)	.949		.000	.864	.918	.123	.632	.996	.937
	N	27		27	14	27	27	27	27	27
OP^{TOT}	*Correlation Coefficient*	.814**	.511**		.169	.181	.268	-.073	.148	.149
	Sig. (2-tailed)	.000	.006		.563	.365	.176	.716	.462	.458
	N	27	27		14	27	27	27	27	27
Particles	*Correlation Coefficient*	.481	-.130	.323		.758**	.584*	-.675**	.550*	.741**
	Sig. (2-tailed)	.081	.659	.260		.002	.028	.008	.042	.002
	N	14	14	14		14	14	14	14	14
NO_2	*Correlation Coefficient*	.201	-.142	.078	.758**		.285	-.930**	.543**	.979**
	Sig. (2-tailed)	.315	.481	.698	.002		.149	.000	.003	.000
	N	27	27	27	14		27	27	27	27
SO_2	*Correlation Coefficient*	.104	.122	.123	.584*	.285		-.119	-.011	.234
	Sig. (2-tailed)	.607	.544	.539	.028	.149		.555	.956	.240
	N	27	27	27	14	27		27	27	27
O_3	*Correlation Coefficient*	-.260	.231	-.089	-.675**	-.930**	-.119		-.602**	-.940**
	Sig. (2-tailed)	.190	.246	.661	.008	.000	.555		.001	.000
	N	27	27	27	14	27	27		27	27
CO	*Correlation Coefficient*	.044	-.340	-.099	.550*	.543**	-.011	-.602**		.582**
	Sig. (2-tailed)	.829	.083	.623	.042	.003	.956	.001		.001
	N	27	27	27	14	27	27	27		27
NOx	*Correlation Coefficient*	.239	-.122	.133	.741**	.979**	.234	-.940**	.582**	
	Sig. (2-tailed)	.229	.544	.508	.002	.000	.240	.000	.001	
	N	27	27	27	14	27	27	27	27	

P<0.05 *; P<0.01**; particles = particle number (p/cm^3)

OP^{AA}/µg was positively associated with particle number, NOx, NO_2 and CO, *table 3.2*, indicative of a traffic source influencing the OP at this background In contrast no associations with the co-pollutants and OP^{GSH}/µg of OP^{TOT}/µg. No significant correlations were observed with any of the OP metrics once the measures were expressed per m^3.

The winter time series of OP measurements is illustrated in *Figure 3.7*, with a data gap between the 22-23rd of Nov due to an equipment failure. Across the remaining 26 days the individual filters contained between 149.5 and 499.8 µg of PM_{10}. Again, as in the

spring data set considerable temporal variability was noted across the sampling period, with generally higher activities observed in the winter PM_{10} sample sets. A peak in the OP^{AA}/m^3 metric was also observed during the first week of sampling, reflecting a peak in ambient PM_{10} concentrations at this time. A similar peak was not observed in the glutathione dependent OPs, again emphasising that these two measures are not equivalent. As with the spring campaign little association was noted between either of the OP metrics and the ambient PM_{10} concentration, beyond weak positive correlation with $OP^{AA}/\mu g$ (r=0.43, P=0.03), *Figure 3.8*. OP^{TOT} measurements were also derived by summing the individual OP metrics and are illustrated in Figure 3.9.

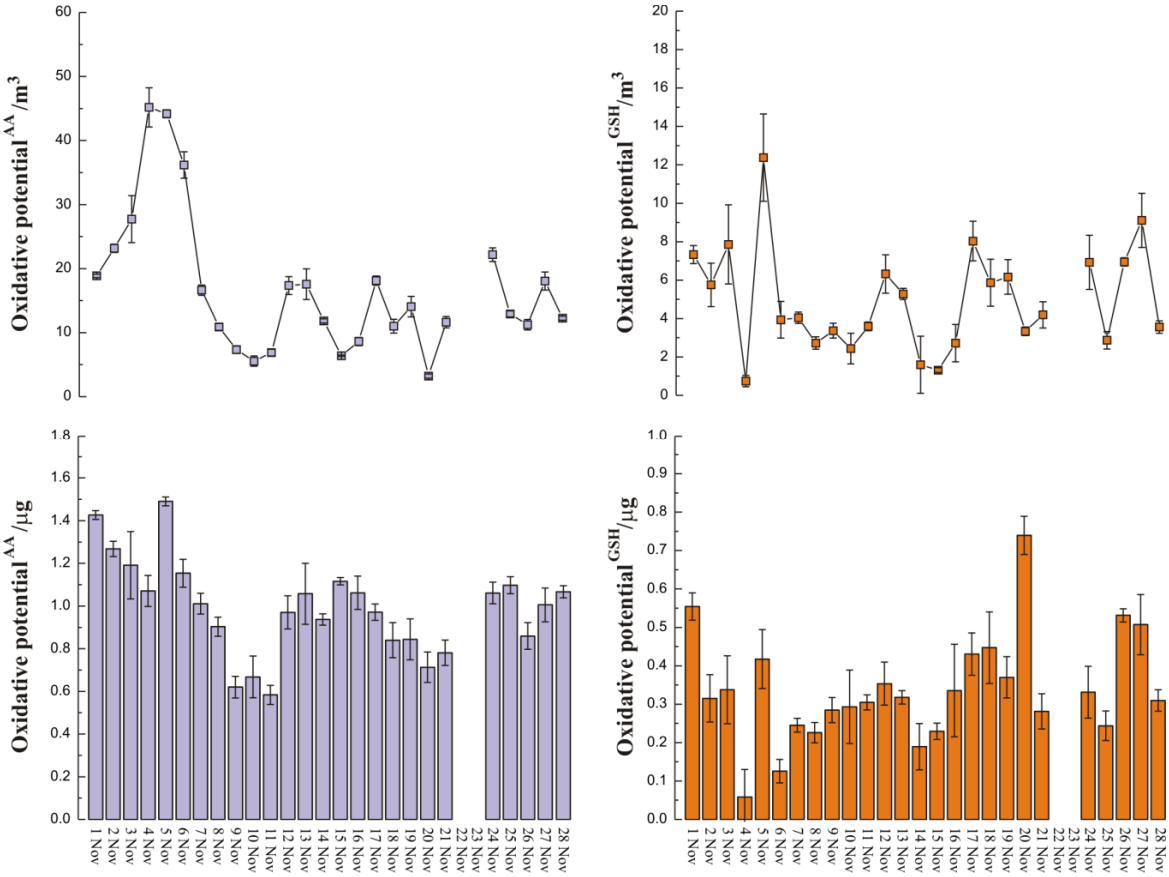

Figure 3.7: Daily PM_{10} ascorbate and glutathione-dependent oxidative activity (per µg and per m^3) during the winter Partisol sampling campaign at the North Kensington urban background site. Data represent the mean and SD of triplicate PM incubations in the synthetic RTLF.

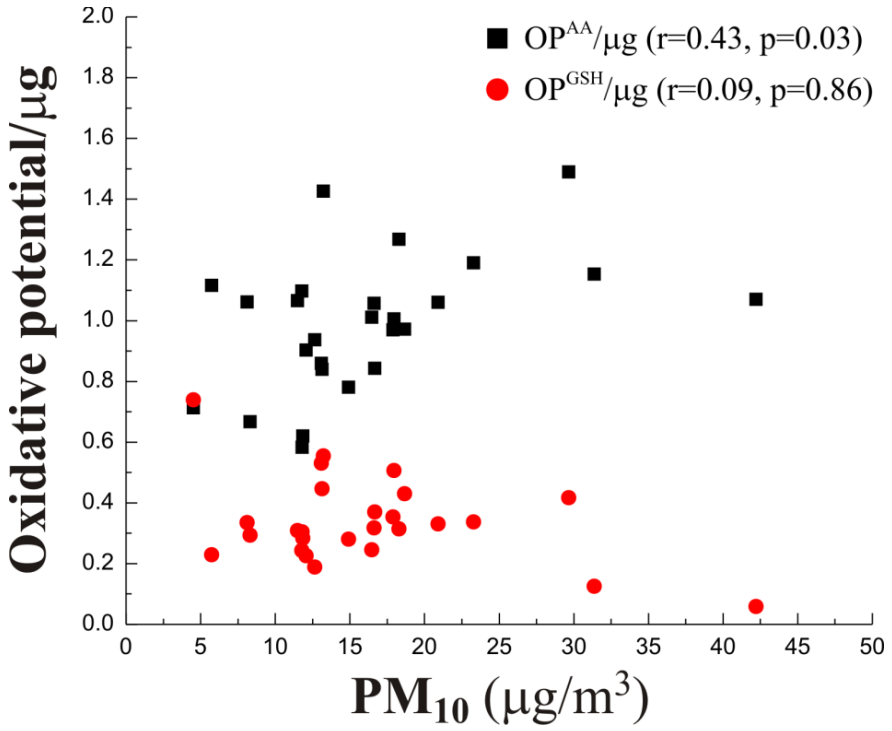

Figure 3.8: Relationship between ascorbate and glutathione dependent OP per unit mass with ambient daily PM_{10} mass concentration, based on data obtained during with Winter Partisol sampling campaign.

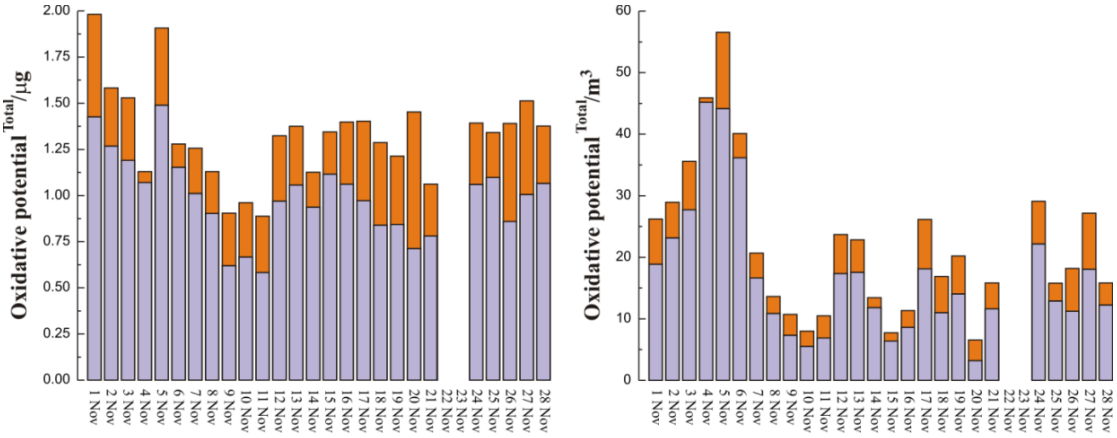

Figure 3.9: Total PM_{10} OP based on the sum of the ascorbate and glutathione dependent signals per unit mass (µg) and per m^3, based on data obtained during with Winter Partisol sampling campaign.

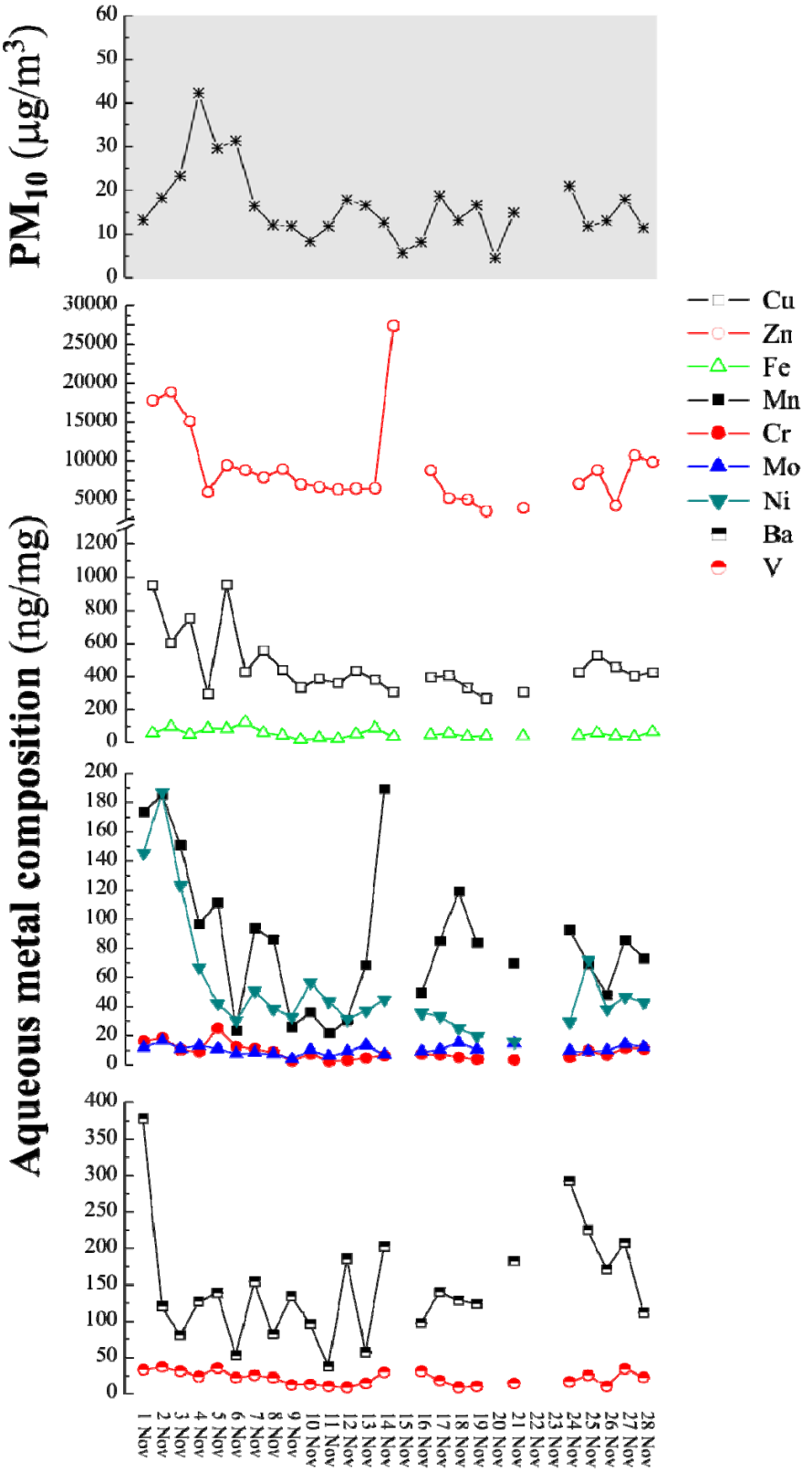

Figure 3.10: Time series of daily PM_{10} (µg/m^3) and PM_{10} aqueous metal concentrations (ng/mg) associated with the second Partisol sampling campaign during November 2008.

Table 3.3: Correlation matrix illustrating the associations (*Spearman Rank Order correlation*) between daily PM_{10} oxidative potentials (OP^{AA}, OP^{GSH} and OP^{TOT} per µg) with roadside PM_{10} aqueous metal content at the North Kensington urban background site between 01/11/08 – 28/11/08. Formatting of the matrix is as outlined in the legend to *Table 2.1*.

		OP^{AA}	OP^{GSH}	OP^{TOT}	Ba	Mn	V	Cr	Cu	Mo	Ni	Zn	Fe
OP^{AA}	*Correlation Coefficient*		-.122	.565**	.089	.460*	.770**	.812**	.652**	.297	.471*	.618**	.815**
	Sig. (2-tailed)		.546	.002	.680	.024	.000	.000	.001	.159	.020	.001	.000
	N		27	27	24	24	24	24	24	24	24	24	24
OP^{GSH}	*Correlation Coefficient*			.682**	.285	.147	-.037	.045	.254	.423*	-.111	-.107	-.119
	Sig. (2-tailed)			.000	.176	.493	.865	.835	.231	.039	.606	.617	.579
	N			27	24	24	24	24	24	24	24	24	24
OP^{TOT}	*Correlation Coefficient*				.258	.444*	.592**	.630**	.672**	.472*	.281	.441*	.493*
	Sig. (2-tailed)				.223	.030	.002	.001	.000	.020	.184	.031	.014
	N				24	24	24	24	24	24	24	24	24
Ba	*Correlation Coefficient*					.320	.149	.042	.151	.096	.015	.076	-.137
	Sig. (2-tailed)					.127	.489	.846	.480	.657	.945	.725	.522
	N					24	24	24	24	24	24	24	24
Mn	*Correlation Coefficient*						.593**	.471*	.243	.434*	.403	.474*	.229
	Sig. (2-tailed)						.002	.020	.252	.034	.051	.019	.282
	N						24	24	24	24	24	24	24
V	*Correlation Coefficient*							.832**	.513*	.203	.658**	.815**	.443*
	Sig. (2-tailed)							.000	.010	.340	.000	.000	.030
	N							24	24	24	24	24	24
Cr	*Correlation Coefficient*								.668**	.287	.603**	.692**	.616**
	Sig. (2-tailed)								.000	.174	.002	.000	.001
	N								24	24	24	24	24
Cu	*Correlation Coefficient*									-.008	.473*	.555**	.489*
	Sig. (2-tailed)									.971	.020	.005	.015
	N									24	24	24	24
Mo	*Correlation Coefficient*										.098	-.051	.297
	Sig. (2-tailed)										.648	.813	.158
	N										24	24	24
Ni	*Correlation Coefficient*											.633**	.253
	Sig. (2-tailed)											.001	.233
	N											24	24
Zn	*Correlation Coefficient*												.274
	Sig. (2-tailed)												.195
	N												24
Fe	*Correlation Coefficient*												
	Sig. (2-tailed)												
	N												

P<0.05 *; P<0.01**

Similar to the situation with the OP metrics measured during the winter sampling campaign, significant associations were noted between OP^{AA}/µg with a range of aqueous redox active (MN, V, Cr, Cu, Ni and Fe) and redox inactive metals (Zn), reflective of mechanical abrasion processes, *Table 3.3*. These associations were absent for the OP^{GSH}/µg metric, but persisted in the summed OP expression. In addition, due to the generally greater masses of PM collected during the winter campaign it was also possible to obtained measures of total acid extracted metals, illustrated in *Figure 3.11*. Based on their temporal profiles, similar to the approach adopted in Part II of this report, the metals were grouped into 4 classes: A (Zn, Cu, Mn and Ba), B (Ni and Cr), C (V and Fe) and D (Mo). These groupings differed markedly from those associated with the roadside site

described in Part II, with only the Ni, Cr, grouping being consistent with the oil combustion signature previously reported. Group A appeared to reflect mechanical wear, but in contrast to our earlier observations did not include Fe or Mo. Sb was not detected in these samples, suggesting a sensitivity issue with the PM concentration employed in these digestions (50 µg/mL). Consequently the total metal measurements should be interpreted with some caution, though generally they were in line with the concentrations noted from the TEOM filter extracted PM obtained from this site and reported in part II of this report, with only Zn showing an approximate 5-fold increase in concentration.

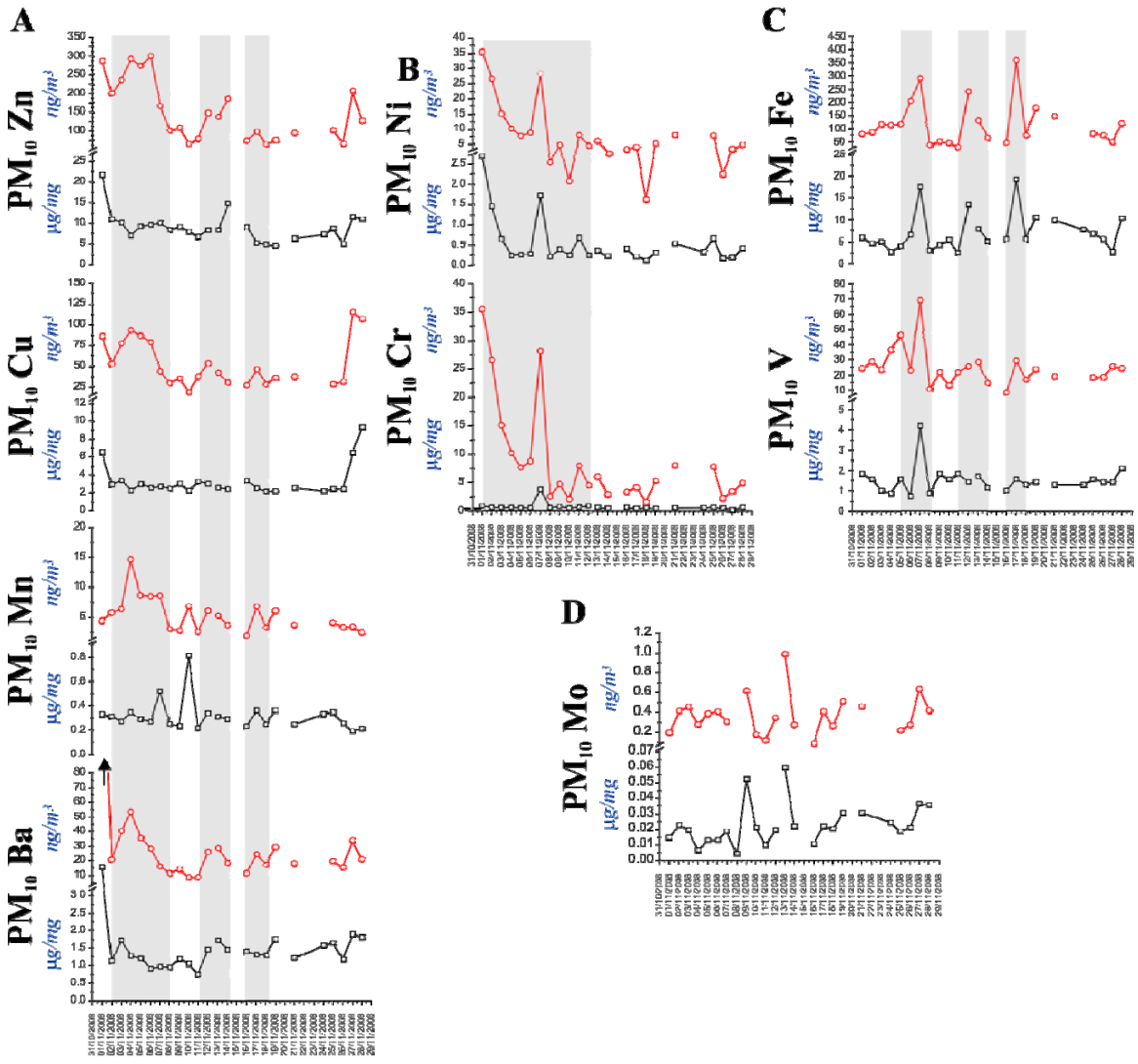

Figure 3.11: Time series of daily PM_{10} (µg/m^3) and PM_{10} aqueous metal concentrations (ng/mg) associated with the second Partisol sampling campaign during November 2008.

Table 3.4: Correlation matrix illustrating the associations (*Spearman Rank Order correlation*) between daily PM_{10} oxidative potentials (OP^{AA}, OP^{GSH} and OP^{TOT} per µg and m^3) with PM_{10} total metal content at the North Kensington urban background site, November 2008. The upper right hand portion of the matrix illustrates the associations between metal content and OP for the data expressed per unit mass of PM_{10}, whilst the lower left hand portion shows the associations for the data expressed per m^3. All significant associations are highlighted in red text, with the portion of the matrix addressing OP versus metal associations shaded grey. The associations between metal components, per unit mass and per m^3 are illustrated in the non-grey shaded area with significant associations with a Spearman rho of >0.70 shaded light blue, >0.50 light green and <0.50 lilac.

		OP^{AA}	OP^{GSH}	OP^{TOT}	Ba	Mn	V	Cr	Cu	Mo	Ni	Zn	Fe
OP^{AA}	*Correlation Coefficient*		-.065	.654**	.318	.162	-.062	.190	.317	-.249	.337	.572**	.014
	Sig. (2-tailed)		.754	.000	.130	.449	.772	.374	.132	.240	.107	.003	.949
	N		26	26	24	24	24	24	24	24	24	24	24
OP^{GSH}	*Correlation Coefficient*	.527**		.650**	.454*	-.099	.207	-.189	.218	.213	-.169	-.124	.148
	Sig. (2-tailed)	.006		.000	.026	.645	.331	.376	.307	.317	.430	.562	.490
	N	26		26	24	24	24	24	24	24	24	24	24
OP^{TOT}	*Correlation Coefficient*	.971**	.630**		.488*	.007	.063	-.028	.378	.030	.106	.371	.109
	Sig. (2-tailed)	.000	.001		.016	.973	.769	.896	.069	.891	.622	.074	.613
	N	26	26		24	24	24	24	24	24	24	24	24
Ba	*Correlation Coefficient*	.912**	.561**	.880**		.016	.074	-.031	.226	.424*	.067	.240	.293
	Sig. (2-tailed)	.000	.004	.000		.942	.731	.886	.289	.039	.754	.259	.165
	N	25	25	25		24	24	24	24	24	24	24	24
Mn	*Correlation Coefficient*	.745**	.319	.737**	.630**		.117	-.036	-.480*	-.082	.095	-.189	.430*
	Sig. (2-tailed)	.000	.121	.000	.001		.587	.869	.018	.704	.659	.376	.036
	N	25	25	25	25		24	24	24	24	24	24	24
V	*Correlation Coefficient*	.803**	.553**	.796**	.718**	.683**		.434*	.393	.332	.481*	.172	.233
	Sig. (2-tailed)	.000	.004	.000	.000	.000		.034	.058	.113	.017	.422	.273
	N	25	25	25	25	25		24	24	24	24	24	24
Cr	*Correlation Coefficient*	.742**	.332	.723**	.609**	.725**	.759**		.492*	-.198	.694**	.271	.120
	Sig. (2-tailed)	.000	.105	.000	.001	.000	.000		.015	.355	.000	.200	.575
	N	25	25	25	25	25	25		24	24	24	24	24
Cu	*Correlation Coefficient*	.826**	.532**	.817**	.814**	.504*	.835**	.648**		.015	.498*	.635**	-.111
	Sig. (2-tailed)	.000	.006	.000	.000	.010	.000	.000		.944	.013	.001	.606
	N	25	25	25	25	25	25	25		24	24	24	24
Mo	*Correlation Coefficient*	.522**	.526**	.531**	.591**	.364	.624**	.412*	.592**		-.028	.005	.344
	Sig. (2-tailed)	.007	.007	.006	.002	.074	.001	.041	.002		.897	.981	.099
	N	25	25	25	25	25	25	25	25		24	24	24
Ni	*Correlation Coefficient*	.692**	.275	.624**	.602**	.561**	.663**	.821**	.657**	.395		.374	.164
	Sig. (2-tailed)	.000	.183	.001	.001	.004	.000	.000	.000	.051		.071	.445
	N	25	25	25	25	25	25	25	25	25		24	24
Zn	*Correlation Coefficient*	.860**	.284	.793**	.786**	.601**	.683**	.717**	.829**	.445*	.726**		-.199
	Sig. (2-tailed)	.000	.170	.000	.000	.002	.000	.000	.000	.026	.000		.351
	N	25	25	25	25	25	25	25	25	25	25		24
Fe	*Correlation Coefficient*	.686**	.481*	.663**	.618**	.686**	.725**	.733**	.566**	.632**	.559**	.464*	
	Sig. (2-tailed)	.000	.015	.000	.001	.000	.000	.000	.003	.001	.004	.020	
	N	25	25	25	25	25	25	25	25	25	25	25	

P<0.05 *; P<0.01**

In contrast to the aqueous metal concentrations, we observed relatively few significant associations between total metals (µg/mg) with the OP metrics expressed on a per unit mass basis, *Table 3.4*, with on Zn and Ba being significantly associated with OP^{AA} and OP^{GSH}/µg respectively. Once these data were expressed on a per m^3 basis then a much more comprehensive series of interactions were noted, with OP^{AA}/m^3 showing positive associations with all of the measured metals, and OP^{GSH}/m^3, a slightly restricted set, excluding Mn, Cr, Ni and Zn.

The OP metric measured at North Kensington during the winter campaign were also related to the co-pollutant concentration and particle number measured at this site, *figure 3.12*. These associations are illustrated in table 3.5, based on a comparison of the OP metrics per μg (upper right portion of the matrix) and per m^3 (lower left hand corner).

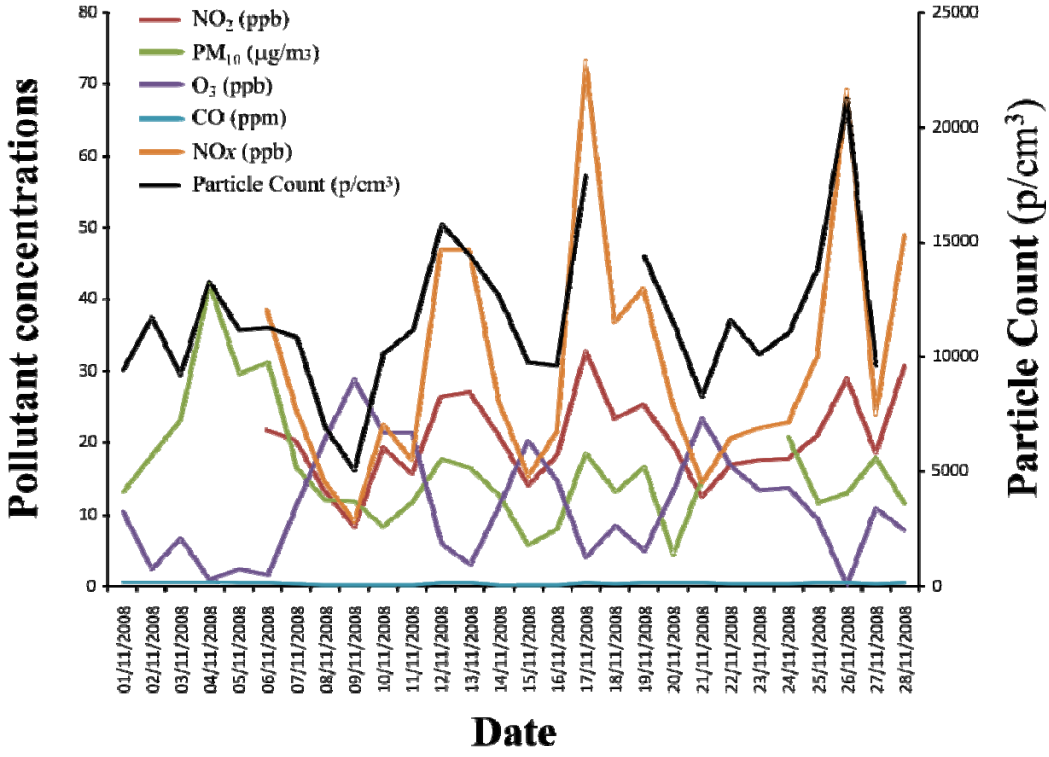

Figure 3.12: Particle number and co-pollutant concentrations measured as the North Kensington monitoring station during the first Partisol Winter sampling campaign, November 2008.

The ascorbate dependent OP metric was only associated with CO when the data were examined on a per mass basis, but a more comprehensive series of associations were noted when the data were compared per m^3; with classical traffic tracers: NO_2, NOx, and CO. OPGSH/mg was not associated with any of the co-pollutants, but as with the ascorbate dependant metric demonstrated significant associations with NO_2, NOx, and CO when expressed per m^3.

Table 3.5: Correlation matrix illustrating the degree of association (*Spearman Rank Order correlation*) between roadside PM_{10} oxidative potentials (OP^{AA}, OP^{GSH} and OP^{TOT} per µg and m^3) with co-pollutant concentrations measured at North Kensington during the Winter sampling campaign, Nov 2008. The upper right hand portion of the matrix illustrates the associations between OP^{AA}, OP^{GSH} and OP^{TOT} expressed per µg with the co-pollutant concentrations measured over the equivalent periods, whilst the lower left hand portion of the matrix illustrates the correlations when the OP parameters are expressed per m^3. Formatting of the matrix is as outlined in the legend to *Table 3.1*.

		OP^{AA}	OP^{GSH}	OP^{TOT}	Particle	NO_2	SO_2	O_3	CO	NOx
OP^{AA}	*Correlation Coefficient*		-.065	.654**	-.010	.257	-.034	-.508**	.483*	.291
	Sig. (2-tailed)		.754	.000	.962	.260	.868	.008	.012	.201
	N		26	26	25	21	26	26	26	21
OP^{GSH}	*Correlation Coefficient*	.527**		.650**	.180	.383	.291	-.212	.325	.413
	Sig. (2-tailed)	.006		.000	.390	.086	.150	.299	.105	.063
	N	26		26	25	21	26	26	26	21
OP^{TOT}	*Correlation Coefficient*	.971**	.630**		.078	.382	.121	-.436*	.540**	.447*
	Sig. (2-tailed)	.000	.001		.711	.088	.558	.026	.004	.042
	N	26	26		25	21	26	26	26	21
Particle	*Correlation Coefficient*	.208	.144	.187		.920**	.512**	-.704**	.276	.932**
	Sig. (2-tailed)	.319	.493	.371		.000	.009	.000	.182	.000
	N	25	25	25		20	25	25	25	20
NO_2	*Correlation Coefficient*	.469*	.431	.458*	.920**		.393	-.903**	.570**	.988**
	Sig. (2-tailed)	.032	.051	.037	.000		.078	.000	.007	.000
	N	21	21	21	20		21	21	21	21
SO_2	*Correlation Coefficient*	.112	.076	.107	.512**	.393		-.371	.381	.373
	Sig. (2-tailed)	.585	.714	.602	.009	.078		.062	.055	.096
	N	26	26	26	25	21		26	26	21
O_3	*Correlation Coefficient*	-.698**	-.411*	-.703**	-.704**	-.903**	-.371		-.649**	-.939**
	Sig. (2-tailed)	.000	.037	.000	.000	.000	.062		.000	.000
	N	26	26	26	25	21	26		26	21
CO	*Correlation Coefficient*	.606**	.427*	.597**	.276	.570**	.381	-.649**		.626**
	Sig. (2-tailed)	.001	.030	.001	.182	.007	.055	.000		.002
	N	26	26	26	25	21	26	26		21
NOx	*Correlation Coefficient*	.529*	.498*	.519*	.932**	.988**	.373	-.939**	.626**	
	Sig. (2-tailed)	.014	.022	.016	.000	.000	.096	.000	.002	
	N	21	21	21	20	21	21	21	21	

P<0.05 *; P<0.01**

Discussion

The present pilot study demonstrated the feasibility of obtaining a daily time series of PM_{10} OP measurements at an urban background monitoring station in London. This paves the way for the construction of more detailed time series of these metrics that can be employed in population based studies. Metal measurements were also obtained, aqueous and total, and those detected were broadly consistent with the concentrations obtained from the TEOM filters collected at the North Kensington site. Several of the metals determined in Part II of this report were however not quantifiable, highlighting some limitations of using daily samples for these analyses.

Whilst these two campaigns were ostensibly pilot studies, several interesting observations have arisen. First, these data clearly highlight a high degree of temporal variability in these measures, expressed on a per unit mass basis. This observation implies that the composition of PM at this background site, especially of redox active components varies markedly with time, with some evidence of a mixed vehicle abrasion/resuspension (Zn, Cu, Mn and Ba) signature (*Viana M et al., 2008; Thorpe and Harrison, 2008*). Thus one would conclude that on certain days this urban background site is influenced by traffic sources. This possibility could be explored by examining the relationship between these measures and wind direction in relation to local sources, which has not been conducted at this time. The presence of these abrasion markers at a background site also suggests a more extensive dispersion away from the roadside than was implied by the results in Part II, where markers characteristic of vehicular abrasion processes were associated with the glutathione dependent OP metric. Here the same markers appeared more strongly associated with $OP^{AA}/\mu g$, especially when the aqueous fraction was examined. The reason for this discrepancy requires a more detailed understanding of the composition and speciation of size fractionated PM at these various sites. In addition to the abrasion signature, we also observed a high correlation between aqueous Ni and V at this site, which we have formerly attributed to oil combustion, with significant correlations to the $OP^{AA}/\mu g$ metric. This observation is consistent with the findings of part II and one might therefore speculate that some of the apparent associations between abrasion metals and OP at this urban background may reflect underlying associations between these metals.

Conclusion

The present study has demonstrated the feasibility of producing daily measurements of PM_{10} OP, as well as metal concentrations in Partisol PM_{10} extracts. This capacity therefore provides a basis for producing more detailed time series of these metrics for integration into short term health effect studies. There are however significant caveats and limitations: First, while its traditional to employ urban background site data for this type of analysis, our findings suggest that these sites may be influenced by contributions from the roadside, depending on meteorology, and thus not all background sites are likely to be equivalent. The extent of variation in this measure across the London background therefore needs to be better understood if we are to derive measures that are truly reflective of the overall population exposure. Second, there is also an apparent mismatch between the pattern of predictive metals for the ascorbate and glutathione OP metrics between the TEOM PM_{10} extracts, covering long sampling periods, and the daily samples. To fully understand this discrepancy more information will be required examining daily variations in the composition and OP of size fractionate PM from roadside and background sites. Third, whilst daily OP can be obtained, logistically the effort and cost of this exercise will be considerable. The current methods for measuring OP are by no means high-though put and any such method development will need to be validated against the current gold standard methodologies.

Policy Significance

Previous studies by our group have utilised $PM_{2.5}$ and PM_{10} samples extracted from TEOM filters to assess particulate oxidative activity. The data thus generated have reflected period averages covering between 7-14 days at roadside sites and up to 4 weeks at urban background locations. Whilst these samples have proven useful in establishing location dependent contrasts in PM oxidative potential, the temporal resolution is insufficient for utilisation of this metric in conventional time series analyses to assess its relevance to cardio-respiratory health in the urban population. This limitation is particularly marked at background sites which have traditionally been employed in time series analyses to reflect the generalised population exposures to ambient pollutants. The work outlined in this section of the report examined the feasibility of performing OP measurements on daily PM_{10} samples collected using a Partisol located at the North Kensington urban background site, during two separate four week sampling campaigns in March and November 2008. The demonstration that both OP^{AA} and OP^{GSH} metrics, as well as total and aqueous metal concentrations can be obtained from daily filters containing as little as 100 - 150 μg PM_{10} represents a considerable milestone in the potential application of this metric to future health studies.

References

Adachi K, Tainosho Y. 2004. Characterization of heavy metal particles embedded in tire dust. Environ Int 30: 1009–1017.

Allen AG, Nemitz E, Shi JP, Harrison RM, Greenwood JC. 2001. Size distributions of trace metals in atmospheric aerosols in the United Kingdom. Atmospheric Environment 35 (27): 4581-4591

Aust AE, Ball JC, Hu AA, Lighty JS, Smith KR, Straccia AM, Veranth JM, Young WC. 2002. Particle characteristics responsible for effects on human lung epithelial cells. Res Rep Health Eff Inst 110:1-65.

Ayres JG, Borm P, Cassee FR, Castranova V, Donaldson K, Ghio A, Harrison RM, Hider R, Kelly F, Kooter IM, Marano F, Maynard RL, Mudway I, Nel A, Sioutas C, Smith S, Baeza-Squiban A, Cho A, Duggan S, Froines J. 2008. Evaluating the toxicity of airborne particulate matter and nanoparticles by measuring oxidative stress potential--a workshop report and consensus statement. Inhal Toxicol 20(1):75-99.

Baker MA, Cerniglia GJ, Zaman A. 1990. Microtiter plate assay for the measurement of glutathione and glutathione disulfide in large numbers of biological samples. Anal Biochem 190(2): 360-5.

Bell ML, Samet JM, Dominici F. 2004. Time-Series Studies of Particulate Matter. Annu Rev Public Health 25:247-280.

Bonvallot V, Baeza-Squiban A, Baulig A, Brulant S, Boland S, Muzeau F, Barouki R, Marano F. 2001. Organic compounds from diesel exhaust particles elicit a proinflammatory response in human airway epithelial cells and induce cytochrome p450 1A1 expression. Am J Respir Cell Mol Biol 25(4): 515-21.

Bonvallot V, Baulig A, Boland S, Marano F, Baeza A. 2002. Diesel exhaust particles induce an inflammatory response in airway epithelial cells: involvement of reactive oxygen species. Biofactors 16(1-2):15-7.

Boulter PG. 2006. A review of emission factors and models for road vehicle non-exhaust particulate matter. A report produced for the Department foe the Environment, Scottish Executive, Welsh Assembly Government, and the Department of Environment Northern Ireland.

Borm PJ, Kelly F, Künzli N, Schins RP, Donaldson K. 2007. Oxidant generation by particulate matter: from biologically effective dose to a promising, novel metric. Occup Environ Med 64(2):73-4

Brunekreef B, Janssen NA, de Hartog J, Harssema H, Knape M, van Vliet P. 1997. Air pollution from truck traffic and lung function in children living near motorways. Epidemiology 8(3):298-303.

Brunekreef B, Holgate ST. 2002. Air pollution and health. Lancet 360:1233-42.

Buettner GR. 1990. Ascorbate oxidation: UV absorbance of ascorbate and ESR spectroscopy of the ascorbyl radical as assays for iron. Free Radic Res Commun 10(1-2):5-9.

Cesaroni G, Badaloni C, Porta D, Forastiere F, Perucci CA. 2008. Comparison between various indices of exposure to traffic-related air pollution and their impact on respiratory health in adults. Occup Environ Med 65(10):683-90.

CEN, 1998 CEN (European Committee for Standardisation), 1998. Air quality—determination of the PM10 fraction of suspended particulate matter—reference method and field test procedure to demonstrate reference equivalence of measurement methods, Brussels

Charron A, Harrison RM, Quincey P. 2007. What are the sources and conditions responsible for exceedences of the 24 h PM10 limit value (50 μg m−3) at a heavily trafficked London site? Atmospheric Environment 41(9):1960-1975.

Cho AK, Sioutas C, Miguel AH, Kumagai Y, Schmitz DA, Singh M, Eiguren-Fernandez A, Froines JR. 2005. Redox activity of airborne particulate matter at different sites in the Los Angeles Basin. Environ Res 99(1):40-7.

Cohn CA, Simon SR, Schoonen MA. 2008.Comparison of fluorescence-based techniques for the quantification of particle-induced hydroxyl radicals. Part Fibre Toxicol 28;5:2.

Corbett JJ, Fishbeck P. 1997. Emissions from ships. Science 278:823-824.

Councell TB, Duckenfield KU, Landa ER, Callender E. 2004. Tire-Wear Particles as a Source of Zinc to the Environment. Environ. Sci. Technol 38 (15): 4206–4214.

Dales R, Wheeler A, Mahmud M, Frescura AM, Smith-Doiron M, Nethery E, Liu L. 2008. The influence of living near roadways on spirometry and exhaled nitric oxide in elementary schoolchildren. Environ Health Perspect 116(10):1423-7.

DeMiguel E, Llamas J, Chacon E, Berg T, Larssen S, Royset O, Vadset M. 1997. Origin and patterns of distribution of trace elements in street dust; unleaded petrol and urban lead. Atmospheric Env 31: 2733-2740.

Duggan ST, Mudway IS, Invernizzi G, Ruprecht AA, Kelly FJ. 2006. A comparison of the oxidative activity of environmental tobacco smoke and ambient traffic-related fine particulate matter. Eur Respir J. 2006. 800s,4634

Fauser P. 1999. Particulate air pollution with emphasis on traffic generated aerosols. Riso-R-1053(EN), Risa National Laboratory, Roskilde, Denmark.

Forsberg B, Hansson HC, Johansson C, Areskoug H, Persson K, Järvholm B. 2005. Comparative health impact assessment of local and regional particulate air pollutants in Scandinavia, Ambio 34: 11–19

Fuller G, Green D. 2006. Evidence for increasing concentrations of primary PM10 in London, Atmospheric Environment 40: 6134–6145.

Garg BD, Cadle SH, Mulawa PA, Groblicki PJ, Laroo C, Parr G. 2000. Brake Wear Particulate Matter Emissions. Environ Sci Technol 34(21): 4463-4469.

Gauderman WJ, Avol E, Gilliland F, Vora H, Thomas D, Berhane K, McConnell R, Kuenzli N, Lurmann F, Rappaport E, Margolis H, Bates D, Peters J. 2004. The effect of air pollution on lung development from 10 to 18 years of age. N Engl J Med 351(11):1057-67.

Gauderman WJ, Avol E, Lurmann F, Kuenzli N, Gilliland F, Peters J, McConnell R. 2005.Childhood asthma and exposure to traffic and nitrogen dioxide. Epidemiology16(6):737-43.

Gilliland FD, McConnell R, Peters J, Gong HJ. 1999. A theoretical basis for investigating ambient air pollution and children's respiratory health. Environ Health Perspect 107 Suppl 3:403-7.

Gilmour PS, Beswick PH, Brown DM, Donaldson K. 1995. Detection of surface free radical activity of respirable industrial fibres using supercoiled phi X174 RF1 plasmid DNA. Carcinogenesis 16(12):2973-9.

Harrison RM, Yin J, Mark D, Stedman J, Appleby RS, Booker J, Moorcroft S. 2001. Studies of the coarse particle (2.5–10 μm) component in UK urban atmospheres. Atmospheric Environment 35 (21): 3667-3679.

Harrison RM, Stedman J, Derwent D. 2008. New Directions: Why are PM10 concentrations in Europe not falling? Atmospheric Environment 42 (3): 603-606

Ingle ST, Pachpande BG, Wagh ND, Patel VS, Attarde SB. 2005. Exposure to vehicular pollution and respiratory impairment of traffic policemen in Jalgaon City, India. Ind Health 43(4):656-62.

Iriyama K, Yoshiura M, Iwamoto T, Ozaki Y. 1984. Simultaneous determination of uric and ascorbic acids in human serum by reversed-phase high-performance liquid chromatography with electrochemical detection. Anal Biochem 141(1): 238-43.

Isaksen I, Persson TA, Selin Lindgren E. 2001. Identification and assessment of ship emissions and their e!ects in the harbour of Goteborg,Sweden. Atmos Environ 35:3659-3666.

Janssen NA, Schwartz J, Zanobetti A, Suh HH. 2002. Air conditioning and source-specific particles as modifiers of the effect of PM(10) on hospital admissions for heart and lung disease. Environ Health Perspect 110:43-9.

Janssen NA, Brunekreef B, van Vliet P, Aarts F, Meliefste K, Harssema H, Fischer P. 2003. The relationship between air pollution from heavy traffic and allergic sensitization,

bronchial hyperresponsiveness, and respiratory symptoms in Dutch schoolchildren. Environ Health Perspect 111(12):1512-8.

Katsouyanni K, Touloumi G, Samoli E, Gryparis A, Le Tertre A, Monopolis Y, Rossi G, Zmirou D, Ballester F, Boumghar A, Anderson HR, Wojtyniak B, Paldy A, Braunstein R, Pekkanen J, Schindler C, Schwartz J. 2001. Confounding and effect modification in the short-term effects of ambient particles on total mortality: results from 29 European cities within the APHEA2 project. Epidemiology 12:521-31.

Kaur H, Halliwell B. 1990. Action of biologically-relevant oxidizing species upon uric acid. Identification of uric acid oxidation products. Chem Biol Interact 73(2-3):235-47.

Kelly FJ, Tetley TD. 1997. Nitrogen dioxide depletes uric acid and ascorbic acid but not glutathione from lung lining fluid. Biochem J. 325 (Pt 1):95-9.

Kelly FJ. 2003. Oxidative stress: its role in air pollution and adverse health effects. Occup Environ Med 60(8):612-6.

Kelly FJ, Kelly J; HEI London Consortium. An Assessment of the Impact of the Congestion Charging Scheme on Air Quality in London - Part 2. Res Rep Health Eff Inst. (due for publication 2010).

Kim JJ, Huen K, Adams S, Smorodinsky S, Hoats A, Malig B, Lipsett M, Ostro B. 2008.Residential traffic and children's respiratory health. Environ Health Perspect 116(9):1274-9.

Kumagai Y, Koide S, Taguchi K, Endo A, Nakai Y, Yoshikawa T, Shimojo N. 2002. Oxidation of proximal protein sulfhydryls by phenanthraquinone, a component of diesel exhaust particles. Chem Res Toxicol 15(4):483-9.

Kunzli N, Mudway IS, Gotschi T, Shi T, Kelly FJ, Cook S, Burney P, Forsberg B, Gauderman JW, Hazenkamp ME, Heinrich J, Jarvis D, Norback D, Payo-Losa F, Poli A, Sunyer J, Borm PJ. 2006. Comparison of oxidative properties, light absorbance, total and elemental mass concentration of ambient PM2.5 collected at 20 European sites. Environ Health Perspect 114(5):684-90.

Laschober C, Limbeck A, Rendl J, Puxbaum H. 2004. Particulate emissions from on-road vehicles in the Kaisermuhlen-Tunnel (Vienna, Austria). Atmospheric Env 38: 2187-2195.

Legret M, Pagotto C. 1999. Evaluation of pollutant loadings in the runoff waters from a major rural highway. Sci Total Environ 235(1-3):143-50.

Lenschow P, Abraham HJ, Kutzner K, Lutz M, Preuß JD, Reichenbächer W. 2001. Some ideas about the sources of PM10. Atmospheric Environment 35 (Supplement 1): 23-33.

Li N, Kim S, Wang M, Froines J, Sioutas C, Nel A. 2002. Use of a stratified oxidative stress model to study the biological effects of ambient concentrated and diesel exhaust particulate matter. Inhal Toxicol 14:459-86.

Li N, Sioutas C, Cho A, Schmitz D, Misra C, Sempf J, Wang M, Oberley T, Froines J, Nel A. 2003. Ultrafine particulate pollutants induce oxidative stress and mitochondrial damage. Environ Health Perspect 111:455-60.

Lukewille A, Bertok I, Amann M, Cofala J, Gyarfas F, /Heyes C, Karvosenoja N, Kilmont Z, Schopp W. 2001. A framework to estimate the potential and costs for the control of fine particulate emissions in Europe. IIASA Interim Report IR-01-023. International

Manoli E, Voutsa D, Samara C. 2002. Chemical characterization and source identification – appointment of fine and coarse air particles in Thessaloniki, Greece. Atmospheric Env. 36; 949-961.

McCreanor J, Cullinan P, Nieuwenhuijsen MJ, Stewart-Evans J, Malliarou E, Jarup L, Harrington R, Svartengren M, Han IK, Ohman-Strickland P, Chung KF, Zhang J. 2007. Respiratory effects of exposure to diesel traffic in persons with asthma. N Engl J Med 357(23):2348-58.

Migliore E, Berti G, Galassi C, Pearce N, Forastiere F, Calabrese R, Armenio L, Biggeri A, Bisanti L, Bugiani M, Cadum E, Chellini E, Dell'orco V, Giannella G, Sestini P, Corbo G, Pistelli R, Viegi G, Ciccone G; SIDRIA-2 Collaborative Group. 2009. Respiratory symptoms in children living near busy roads and their relationship to vehicular traffic: results of an Italian multicenter study (SIDRIA 2). Environ Health 18;8:27.

Miller CA, Linak WP, King C, Wendt JOL. 1998. Fine particle emissions from heavy fual oil combustion in a firetube package boiler. Combust. Sci. and Tech 134: 477-502.

Mills NL, Törnqvist H, Gonzalez MC, Vink E, Robinson SD, Söderberg S, Boon NA, Donaldson K, Sandström T, Blomberg A, Newby DE. 2007. Ischemic and thrombotic effects of dilute diesel-exhaust inhalation in men with coronary heart disease. N Engl J Med 357(11):1075-82.

Monn C, Naef R, Koller T. 2003. Reactions of macrophages exposed to particles <10 microm.Environ Res 91(1): 35-44.

Morgenstern V, Zutavern A, Cyrys J, Brockow I, Koletzko S, Krämer U, Behrendt H, Herbarth O, von Berg A, Bauer CP, Wichmann HE, Heinrich J; GINI Study Group; LISA Study Group. 2008. Atopic diseases, allergic sensitization, and exposure to traffic-related air pollution in children. Am J Respir Crit Care MeD 177(12):1331-7.

Mudway IS, Duggan ST, Kelly FJ. 2005. Ligand mobilisable iron on the surface of ambient particles predicts their oxidative activity. Free Rad Res 39 (supplement 1): S70, PP42.

Mudway IS, Duggan ST, Venkataraman C, Habib G, Kelly FJ, Grigg J. 2005. Combustion of dried animal dung as biofuel results in the generation of highly redox active fine particulates. Part Fibre Toxicol 4(2):6

Mudway IS, Kelly FJ. 1998. Modeling the interactions of ozone with pulmonary epithelial lining fluid antioxidants. Toxicol Appl Pharmacol 148(1):91-100.

Mudway IS, Stenfors N, Duggan ST, Roxborough H, Zielinski H, Marklund SL, Blomberg A, Frew AJ, Sandstrom T, Kelly FJ. 2004. An in vitro and in vivo investigation of the effects of diesel exhaust on human airway lining fluid antioxidants. Arch Biochem Biophys 423:200-12.

Nel A. 2005. ATMOSPHERE: Enhanced: Air Pollution-Related Illness: Effects of Particles. Science 308:804-806.

Nel AE, Diaz-Sanchez D, Li N. 2001. The role of particulate pollutants in pulmonary inflammation and asthma: evidence for the involvement of organic chemicals and oxidative stress. Curr Opin Pulm Med 7:20-6.

Nicolai T, Carr D, Weiland SK, Duhme H, von Ehrenstein O, Wagner C, von Mutius E. 2003. Urban traffic and pollutant exposure related to respiratory outcomes and atopy in a large sample of children. Eur Respir J 21(6):956-63.

Oberdörster G, Maynard A, Donaldson K, Castranova V, Fitzpatrick J, Ausman K, Carter J, Karn B, Kreyling W, Lai D, Olin S, Monteiro-Riviere N, Warheit D, Yang H; ILSI Research Foundation/Risk Science Institute Nanomaterial Toxicity Screening Working Group. 2005.Principles for characterizing the potential human health effects from exposure to nanomaterials: elements of a screening strategy. Part Fibre Toxicol 6;2:8.

Oftedal B, Brunekreef B, Nystad W, Madsen C, Walker SE, Nafstad P. 2008. Residential outdoor air pollution and lung function in schoolchildren. Epidemiology 19(1):129-37.

Omstedt G, Bringfelt B, Johansson C. 2005. A model for vehicle-induced non-tailpipe emissions of particles along Swedish roads. Atmospheric Environment 39 (33):6088-6097.

Onianwa PC. 2001. Monitoring atmospheric metal pollution: a review of the use of mosses as indicators. Environmental Monitoring and Assesment 71: 13-50.

Osborne JW, Costello AB. 2004. Sample size and subject to item ratio in principal components analysis. Practical Assessment, Research & Evaluation, 9 (11)

Pakkanen TA, Kerminen V-M, Loukkola K, Hillamo RE, Aarnio P, Koskentalo T, Maenhaut W. 2003. Size distributions of mass and chemical components in street-level and rooftop PM1 particles in Helsink Atmos Environ 37:1673-1690.

Paolicchi A, Dominici S, Pieri L, Maellaro E, Pompella A. 2002. Glutathione catabolism as a signaling mechanism. Biochem Pharmacol 64(5-6):1027-35.

Pourazar J, Mudway IS, Samet JM, Helleday R, Blomberg A, Wilson SJ, Frew AJ, Kelly FJ, Sandström T. 2005. Diesel exhaust activates redox-sensitive transcription factors and kinases in human airways. Am J Physiol Lung Cell Mol Physiol 289(5):L724-30.

Querol X, Alastuey A, Rodríguez S, Viana MM, Artíñano B, Salvador P, Mantilla E, García do Santos S, Fernandez Patier R, de La Rosa J, Sanchez de la Campa A, Menéndez M, Gil JJ. 2004. Levels of particulate matter in rural, urban and industrial sites in Spain.Sci Total Environ 334-335:359-76.

Roginsky VA, Barsukova TK, Stegmann HB. 1999. Kinetics of redox interaction between substituted quinones and ascorbate under aerobic conditions. Chem Biol Interact 121(2):177-97.

Salvi S, Blomberg A, Rudell B, Kelly F, Sandström T, Holgate ST, Frew A. 1999. Acute inflammatory responses in the airways and peripheral blood after short-term exposure to diesel exhaust in healthy human volunteers. Am J Respir Crit Care Med 159(3):702-9.

Samet JM, Dominici F, Curriero FC, Coursac I, Zeger SL. 2000. Fine particulate air pollution and mortality in 20 U.S. cities, 1987- 1994. N Engl J Med 343:1742-9.

Scaperdas A, Colvile RN. 1999. Assessing the representativeness of monitoring data from an urban intersection site in central London, UK. Atmospheric Environment 33 (4): 661-674.

Schauer JJ, Lough GC, Shafer MM, Christensen WF, Arndt MF, DeMinter JT, Park JS.2006. Characterization of metals emitted from motor vehicles. Res Rep Health Eff Inst 133):1-76.

Sekine K, Shima M, Nitta Y, Adachi M. 2004. Long term effects of exposure to automobile exhaust on the pulmonary function of female adults in Tokyo, Japan. Occup Environ Med 61(4):350-7.

Shi T, Duffin R, Borm PJ, Li H, Weishaupt C, Schins RP. 2006.Hydroxyl-radical-dependent DNA damage by ambient particulate matter from contrasting sampling locations Environ Res 101(1):18-24.

Shi T, Schins RP, Knaapen AM, Kuhlbusch T, Pitz M, Heinrich J, Borm PJ. 2003. Hydroxyl radical generation by electron paramagnetic resonance as a new method to monitor ambient particulate matter composition. J Environ Monit 5(4):550-6.

Sjöberg L, Eriksen TE, Révész L. 1982. The reaction of the hydroxyl radical with glutathione in neutral and alkaline aqueous solution Radiat Res. 89(2):255-63.

Soukup JM, Becker S. 2001. Human alveolar macrophage responses to air pollution particulates are associated with insoluble components of coarse material, including particulate endotoxin.Toxicol Appl Pharmacol 171(1):20-6.

Squadrito GL, Cueto R, Dellinger B, Pryor WA. 2001. Quinoid redox cycling as a mechanism for sustained free radical generation by inhaled airborne particulate matter.Free Radic Biol Med 31(9): 1132-8.

Stenfors N, Pourazar J, Blomberg A, Krishna MT, Mudway I, Helleday R, Kelly FJ, Frew AJ, Sandström T. 2002. Effect of ozone on bronchial mucosal inflammation in asthmatic and healthy subjects. Respir Med 96(5):352-8.

Sternbeck J, Åke Sjödin A, Andréasson K. 2002. Metal emissions from road traffic and the influence of resuspension—results from two tunnel studies. Atmospheric Environment 36 (30): 4735-4744.

Thorpe A, Harrison RM. 2008. Sources and properties of non-exhaust particulate matter from road traffic: a review. Sci Total Environ 400(1-3):270-82.

van Vliet P, Knape M, de Hartog J, Janssen N, Harssema H, Brunekreef B. 1997. Motor vehicle exhaust and chronic respiratory symptoms in children living near freeways.Environ Res 74(2):122-32.

Viana M, Kuhlbusch TAJ , Querol X, Alastuey A, Harrison RM, Hopke PK, Winiwarter W, Vallius M, Szidat S, Prévôt ASH, Hueglin C, Bloemen H, Wåhlin P, Vecchi R, Miranda AI, Kasper-Giebl A, Maenhaut W, Hitzenberger R. 2008. Source apportionment of particulate matter in Europe: A review of methods and results. Journal of Aerosol Science 39(10):827-849.

Valko M, Morris H, Cronin MT. 2005. Metals, toxicity and oxidative stress. Curr Med Chem 12(10):1161-208.

Weckwerth G. 2001. Verification of traffic-emitted aerosol components in the ambient air of Cologne (Germany). Atmospheric Env 35: 5525-5536.

Winiwarter W, Kuhlbusch TAJ, Viana M, Hitzenberger R. 2009. Quality considerations of European PM emission inventories. Atmospheric Environment 43(25): 3819-3828.

Wjst M, Reitmeir P, Dold S, Wulff A, Nicolai T, von Loeffelholz-Colberg EF, von Mutius E. 1993. Road traffic and adverse effects on respiratory health in children. BMJ 307(6904):596-600.

Xia T, Korge P, Weiss JN, Li N, Venkatesen MI, Sioutas C, Nel A. 2004. Quinones and aromatic chemical compounds in particulate matter induce mitochondrial dysfunction: implications for ultrafine particle toxicity. Environ Health Perspect 112:1347-58.

Xia T, Kovochich M, Nel A. 2006. The role of reactive oxygen species and oxidative stress in mediating particulate matter injury. Clin Occup Environ Med 5(4):817-36.

Zanobetti A, Schwartz J, Samoli E, Gryparis A, Touloumi G, Atkinson R, Le Tertre A, Bobros J, Celko M, Goren A, Forsberg B, Michelozzi P, Rabczenko D, Aranguez Ruiz E, Katsouyanni K. 2002. The temporal pattern of mortality responses to air pollution: a multicity assessment of mortality displacement. Epidemiology 13:87-93.

Zechmeister HG, Hohenwallner D, Riss A, Hanus-Illnar A. 2005. Estimation of element deposition derived from road traffic sources by using mosses. Environ Pollut 138(2):238-49.

Zielinski H, Mudway IS, Berube KA, Murphy S, Richards R, Kelly FJ. 1999. Modeling the interactions of particulates with epithelial lining fluid antioxidants. Am J Physiol. 277(4 Pt 1):L719-26.